Mehbub-Ur Rahman

Optimization of In-line Defect Detection by Eddy Current Techniques

kassel university press

Mehbub-Ur Rahman

Optimization of In-line Defect Detection by Eddy Current Techniques

kassel university press

This work has been accepted by the faculty of Electrical Engineering and Computer Science of the University of Kassel as a thesis for acquiring the academic degree of Doktor der Ingenieurwissenschaften (Dr.-Ing.).

Supervisor: Prof. Dr. rer. nat. Karl.J. Langenberg
Co-Supervisor: PD Dr.-Ing. René Marklein

Defense day: 28th October 2010

Bibliographic information published by Deutsche Nationalbibliothek
The Deutsche Nationalbibliothek lists this publication in the Deutsche Nationalbibliografie; detailed bibliographic data is available in the Internet at http://dnb.d-nb.de.

Zugl.: Kassel, Univ., Diss. 2010
ISBN print: 978-3-86219-168-0
ISBN online: 978-3-86219-169-7
URN: http://nbn-resolving.de/urn:nbn:de:0002-31698

Printed by: Unidruckerei, University of Kassel
Printed in Germany

Acknowledgments

The key to the successful completion of any task is motivation. This thesis is the result of four years of hard work. During this period I have been supported and motivated by a number of people. It would be a pleasure for me to show my gratitude to all of them.

I am very grateful to Prof. Dr. rer. nat. Karl-Jörg Langenberg and PD Dr.-Ing. René Marklein for giving me the opportunity to do my Ph.D. thesis in the department of Electromagnetic Theory, presently known as Computational Electronics and Photonics. My principal advisor PD Dr.-Ing. René Marklein has played a very important role in my thesis by guiding me during my research work and by motivating me for better results. I would like to thank him personally for his support and enthusiastic role in this scientific work. I also like to thank Dr.-Ing. Klaus Mayer, Prof. Dr. sc.techn. Bernd Witzigmann, Mrs. Regina Brylla and Dipl.-Ing. Yanna Mikhilina for their cooperation and help on conceptual and software aspects during this thesis.

I would like to thank my friends Dr.-Ing. Shohrab Hossain, Nasir Uddin, M.Sc., Md. Iftekhar Alam, M.Sc. and Dominik Klaus for their continuous motivation and to my colleagues P. Kumar Chinta, M.Sc., Dipl.-Ing. Gregor Ballier and Dipl.-Ing. Ugur Akcakoca for accompanying me during my work.

At the end, I would like to thank my parents and sister for their constant support during this Ph.D. program.

Kassel, Germany
July 1, 2010 Mehbub-Ur Rahman

Contents

Summary

This thesis presents innovative and advanced electromagnetic techniques for the in-line inspection of hot wire steel. The hot wire inspection procedure is performed with the eddy current (EC) sensor technique. Any type of crack on the upper surface of the steel wire disturbs the eddy current distribution which can be detected by the eddy current sensors. However, the eddy current distribution is only weakly influenced by cracks which are parallel to the wire, so-called longitudinal cracks. The conventional eddy current sensors cannot detect these cracks properly. To detect such longitudinal cracks a number of new EC sensors have been developed and successfully tested.

The modeling of the EC sensors and inspection techniques are numerically performed by setting up the governing equations for eddy current problems and then the differential, as well as the integral equations are solved with a suitable numerical method. A proper selection of the numerical technique plays an important role in successful simulation of the eddy current inspection procedure. Different numerical methods - the finite integration technique (FIT), the finite element method (FEM) and the boundary element method (BEM) are used to model this NDT (non-destructive testing) situation. The presented work is a part of the so-called INCOSTEEL project which is sponsored by the European Commission through the Research Fund for Coal and Steel (INCOSTEEL: In-line quality control of hot wire steel - Towards innovative contactless solutions and data fusion).

Every numerical method has its own advantages and disadvantages that need to be considered before using them to model a certain eddy current problem. FIT, FEM and BEM are discussed elaborately in this thesis for this purpose. A FIT based numerical tool MQSFIT is developed as a part of the scientific work. Two other simulation tools, based on FEM and BEM, along with MQSFIT, are used to model and optimize the eddy current sensors developed in INCOSTEEL project. However, the numerical results have to be validated against analytical and published results to prove the accuracy and reliability of the simulations. As a part of that, analytical solutions for a simple eddy current problem are discussed in the work. A comparison of all the numerical methods to the analytical solutions is also presented.

The numerical modeling, optimization and feedback modeling have met the demands of the INCOSTEEL project and thus led to the successful completion of the project in December 2008. The obtained results have opened the door for further future research and innovative ideas.

Chapter 1

Introduction to Eddy Current Sensors and Modeling Techniques

1.1 Statement of the Problem of Hot Wire Steel Inspection

The production of long steel products like steel wires, rods and bars within the steel market is subjected to very strict specifications with regard to quality and reliability as well as in terms of increasing productivity. Product quality along the different production processes has a high impact on the quality of the end component. Nondestructive testing (NDT) techniques are widely used for quality assurance in steel manufacturing, e.g., for the detection and evaluation of all potential types of internal and surface defects. The principal goal is to develop a sensor system to optimize the in-line detection of transversal and longitudinal defects produced in the manufacturing process of hot wire steel. Existing NDT systems have some limitations regarding detection and characterization of several types of common defects.

The aim of this thesis is to discuss the electromagnetic modeling techniques in order to analyze the eddy current inspection techniques. Hot wire stainless steel (Fig. 1.1a) of a diameter $D = 6 - 42$ mm is considered, driven by a guiding system through the sensor coils at a temperature of $1000° - 1200°$ C above the Curie point with a rolling speed up to $v_c = 120$ m/s depending on the diameter of the wire. Typical longitudinal and transversal cracks in the hot wire steel are shown in Fig. 1.1b and 1.1c, respectively. In a parameter study we use cracks with the shortest length of $l = 5$ mm, the lowest width of $w = 0.2$ mm, and a minimum depth of $d = 0.2$ mm.

1.2 Numerical Modeling and Simulation of the Inspection Technique

In Chapter 1 we define the problem of hot wire inspection and give an outline of the applied sensors. A brief description of the numerical tools to model the inspection technique numerically is also presented in Chapter 1. The mathematical background, this means the governing equations of the applied sensor types, are given in Chapter 2. In Chapter 3 we discuss the finite integration technique (FIT) to discretize the magnetic diffusion equation in integral form. The discretizetion is performed in cartesian as well as in cylindrical coordinate

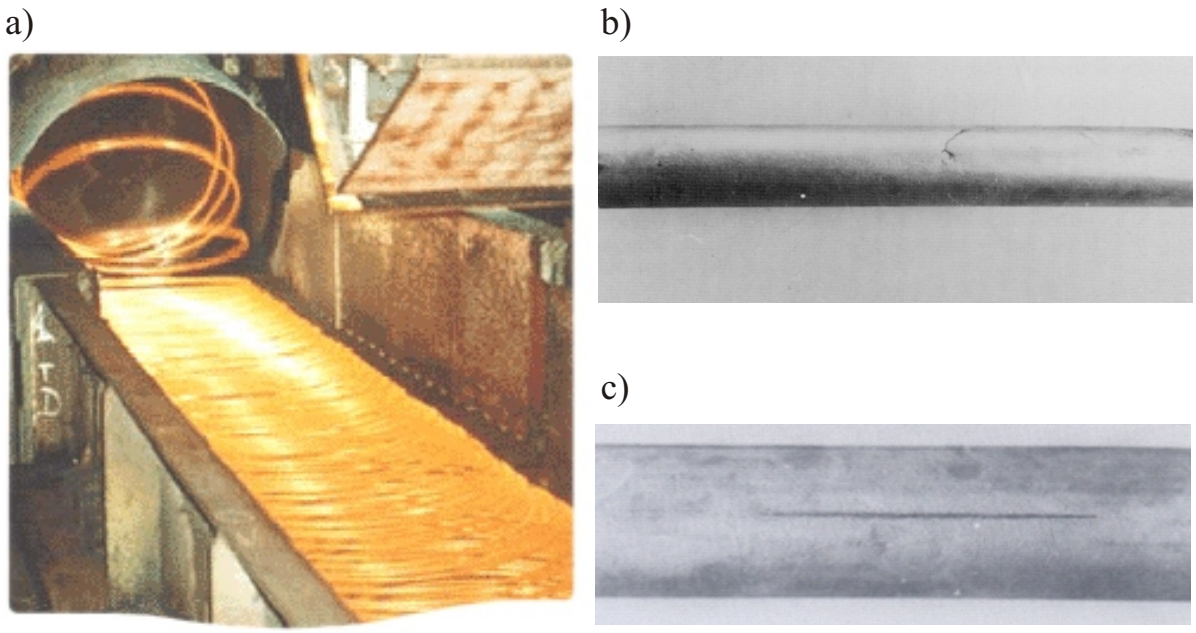

Figure 1.1: a) Hot wire steel in the production line, b) a typical transversal and c) a typical longitudinal crack.

system. The finite element method (FEM) to solve the eddy current problem is discussed in Chapter 4. Both FIT and FEM based simulation tools are used to simulate two dimensional (2-D) problems.

However, all the eddy current sensors cannot be modeled in 2-D and hence, a suitable numerical tool is chosen for 3-D modeling, which is based on the method of moments (MoM), also known as the boundary element method (BEM). The formulation of the so called electric field integral equation (EFIE) and magnetic field integral equation (MFIE) are important for discretization in BEM and are discussed in Chapter 5.

The numerical results need to be validated against the analytical solutions to prove the accuracy and reliability of the modeling. We discuss the analytical solutions of a typical eddy current problem in chapter 6. A comparison of the numerical results with the analytical solutions is also presented. The simulation results using developed eddy current (EC) sensors, along with the performance analysis of the sensors are presented in Chapter 7. At the end, we conclude the scientific work with the final outcome of the eddy current simulations together with the innovative ideas for future research.

To fulfil the demands of the INCOSTEEL project we need to detect transversal and longitudinal cracks with high precision, which includes proper identification of the geometry as well as the location of the crack in the hot wire. Five types of eddy current sensors are developed during this project. A brief description of these sensors is presented in Table 1.1. The encircling coil sensors are modeled by the finite integration technique. As the geometry of the modeled region contains a rotational symmetry, a 3-D eddy current problem is reduced to a 2-D problem in cylindrical coordinates. A FIT based simulation tool is developed to solve such a 2-D problem. Furthermore, we also present numerical modeling of encircling coil sensors with the finite element method. The point coil sensors, i.e., 3-coils sensor, 4-coils sensor, D-coils sensor and pot core sensor are modeled by the boundary element method.

Type of Sensor	Characteristics
Encircling Coil	Consists of four encircling coils Good performance for detecting transversal cracks
3-coils Sensor	Consists of three coils Designed to detect the longitudinal cracks mainly
D-coils Sensor	Designed to detect the longitudinal cracks Limited performance
4-coils Sensor	Modified version of the 3-coils sensor Designed for better detection of the longitudinal cracks
Pot core sensor	Modified version of the D-coils sensor Good performance in detecting longitudinal cracks

Table 1.1: List of developed eddy current sensors.

1.3 Modeling Tools

Selected numerical modeling tools to simulate eddy current (EC) sensors are:

- MQSFIT (*Marklein*, 2002) based on Finite Integration technique (FIT)
- Opera-2d 10.5 (*Opera*, 10.5) based on Finite Element Method (FEM)
- Faraday 6.3 (*Faraday*, 6.1) based on Boundary Element Method (BEM)

1.3.1 MQSFIT

Magnetoquasistatic Finite Integration Technique (MQSFIT) is a software tool, developed for modeling and characterization of the EC sensors during the INCOSTEEL project in 2008. MQSFIT is a frequency domain solver for a monochromatic impressed current excitation and is programmed in MATLAB. The basic geometry is embedded in the code, whereas the geometry details can be changed with a script file easily. The integral form of the magnetoquasistatic equation is discretized using the staggered grid system in cylindrical coordinates. The obtained matrices are then reformulated to generate band matrices which are quite sparse and therefore, are compressed to save memory and computational time. The resulting linear matrix equation is then solved with the conjugate gradient (CG) method. The simulation results, obtained from MQSFIT, are validated against analytical as well as measured results.

1.3.2 Opera

OPERA-2d is a finite element program, developed by Vector Fields Software to analyze electrical engineering designs in two dimensions. It includes a pre and post-Processor environment and analysis modules. The 2-D version of Opera is used here to simulate a rotational

symmetric EC problem. However, Opera-2D consists of a number of different modules. The used modules to solve the EC problems are:

- AC Module (steady state)
- LM module (linear motion)

The steady state module, along with FIT based MQSFIT, are used to observe the effect of cracks in magnetic flux density and electric current density distribution in the test area. The linear motion module is useful to observe the effect of velocity on eddy current distribution on the surface of the steel wire.

1.3.3 Faraday 6.1

Faraday is an easy-to-use 3D eddy current field solver, developed by the Integrated Engineering Software. Using the boundary element method (BEM) Faraday is suitable for applications requiring large open region analysis, exact modeling of boundaries and problems where dealing with small skin depths are critical. The parametric solvers of this tool allow automatically vary and experiment with geometry, materials and sources and thus reduce the tedious, repetitive task of fine-tuning multiple design parameters. The obtained simulation results are saved in text format and a separate MATLAB program is developed to read and plot the results.

1.3.4 Other Tools

Interpretation of the simulation results plays an important role to understand and analyze the performance of the sensors, as well as the effect of different parameters in detection of cracks. The best way to do that is to develop a movie which shows the A-scan of the sensor together with the complete test procedure. The commercial simulation tools, however, do not prepare such a movie. A movie making tool is developed using MATLAB which shows the A-scan obtained from the differential signal on the top and the eddy current test procedure along with the induced current density on the hot wire at the bottom. Snapshots of such movies are included in Chapter 7 to present the simulation results.

Chapter 2

Governing Equations for Magnetoquasistatic Problem

2.1 Maxwell's Equations for Macroscopic Non-moving Medium

Maxwell's equations are a set of equations that govern all macroscopic electromagnetic phenomena. The equations can be written in both differential and integral form. For general time-varying fields and in case of a non-moving medium, Maxwell's equations in integral form are given by *Langenberg* (2003) and *Rothwell & Cloud* (2001):

$$\oint_{C=\partial S} \underline{\mathbf{E}}(\underline{\mathbf{R}},t)\cdot\underline{\mathbf{dR}} = -\iint_S \frac{\partial}{\partial t}\underline{\mathbf{B}}(\underline{\mathbf{R}},t)\cdot\underline{\mathbf{dS}} - \iint_S \underline{\mathbf{J}}_{\mathrm{m}}(\underline{\mathbf{R}},t)\cdot\underline{\mathbf{dS}} \tag{2.1}$$

$$\oint_{C=\partial S} \underline{\mathbf{H}}(\underline{\mathbf{R}},t)\cdot\underline{\mathbf{dR}} = \iint_S \frac{\partial}{\partial t}\underline{\mathbf{D}}(\underline{\mathbf{R}},t)\cdot\underline{\mathbf{dS}} + \iint_S \underline{\mathbf{J}}_{\mathrm{e}}(\underline{\mathbf{R}},t)\cdot\underline{\mathbf{dS}} \tag{2.2}$$

$$\oiint_{S=\partial V} \underline{\mathbf{D}}(\underline{\mathbf{R}},t)\cdot\underline{\mathbf{dS}} = \iiint_V \varrho_{\mathrm{e}}\ \mathrm{d}V \tag{2.3}$$

$$\oiint_{S=\partial V} \underline{\mathbf{B}}(\underline{\mathbf{R}},t)\cdot\underline{\mathbf{dS}} = \iiint_V \varrho_{\mathrm{m}}\ \mathrm{d}V\,, \tag{2.4}$$

with the field quantities

$$\begin{aligned}
\underline{\mathbf{E}} &= \text{electric field strength (V/m)}\\
\underline{\mathbf{D}} &= \text{electric flux density (As/m}^2\text{)}\\
\underline{\mathbf{H}} &= \text{magnetic field strength (A/m)}\\
\underline{\mathbf{B}} &= \text{magnetic flux density (Vs/m}^2\text{)}
\end{aligned}$$

and the source quantities

$$\begin{aligned}
\underline{\mathbf{J}}_{\mathrm{e}} &= \text{electric current density (A/m}^2\text{)}\\
\underline{\mathbf{J}}_{\mathrm{m}} &= \text{magnetic current density (V/m}^2\text{)}\\
\varrho_{\mathrm{e}} &= \text{electric volume charge density (As/m}^3\text{)}\\
\varrho_{\mathrm{m}} &= \text{magnetic volume charge density (Vs/m}^3\text{)}
\end{aligned}$$

Maxwell's equations in differential form can be derived from Eqs. (2.1)-(2.4) by using Gauss' and Stoke's theorems. Let us consider a point in space where all the field quantities and their derivatives are continuous. If we apply Gauss's and Stoke's theorems to Eqs. (2.1)-(2.4), we obtain

$$\boldsymbol{\nabla}\times\underline{\mathbf{E}}(\underline{\mathbf{R}},t) = -\frac{\partial}{\partial t}\underline{\mathbf{B}}(\underline{\mathbf{R}},t) - \underline{\mathbf{J}}_{\mathrm{m}}(\underline{\mathbf{R}},t) \tag{2.5}$$

$$\boldsymbol{\nabla}\times\underline{\mathbf{H}}(\underline{\mathbf{R}},t) = \frac{\partial}{\partial t}\underline{\mathbf{D}}(\underline{\mathbf{R}},t) + \underline{\mathbf{J}}_{\mathrm{e}}(\underline{\mathbf{R}},t) \tag{2.6}$$

$$\boldsymbol{\nabla}\cdot\underline{\mathbf{B}}(\underline{\mathbf{R}},t) = \varrho_{\mathrm{m}}(\underline{\mathbf{R}},t) \tag{2.7}$$

$$\boldsymbol{\nabla}\cdot\underline{\mathbf{D}}(\underline{\mathbf{R}},t) = \varrho_{\mathrm{e}}(\underline{\mathbf{R}},t)\,. \tag{2.8}$$

Here $\underline{\mathbf{E}}$, $\underline{\mathbf{H}}$, $\underline{\mathbf{B}}$ and $\underline{\mathbf{D}}$ stand for electric field strength, magnetic field strength, magnetic field and electric flux density respectively. The continuity equation is given by

$$\boldsymbol{\nabla}\cdot\underline{\mathbf{J}}_{\mathrm{e}}(\underline{\mathbf{R}},t) = -\frac{\partial}{\partial t}\varrho_{\mathrm{e}}(\underline{\mathbf{R}},t)\,. \tag{2.9}$$

Here ϱ_{e} and $\underline{\mathbf{J}}_{\mathrm{e}}$ stand for electric charge density and electric current density respectively. The constitutive equations for vacuum are:

$$\underline{\mathbf{B}}(\underline{\mathbf{R}},t) = \mu_0\underline{\mathbf{H}}(\underline{\mathbf{R}},t) \tag{2.10}$$

$$\underline{\mathbf{D}}(\underline{\mathbf{R}},t) = \varepsilon_0\underline{\mathbf{E}}(\underline{\mathbf{R}},t)\,, \tag{2.11}$$

where μ_0 and ε_0 represent permeability and permittivity of free space. For an inhomogeneous, linear, isotropic and instantaneously reacting medium having the relative permeability μ_{r} and relative permittivity ε_{r} we rewrite Eq. (2.10)-(2.11) as

$$\underline{\mathbf{B}}(\underline{\mathbf{R}},t) = \mu(\underline{\mathbf{R}})\ \underline{\mathbf{H}}(\underline{\mathbf{R}},t) = \mu_0\ \mu_{\mathrm{r}}(\underline{\mathbf{R}})\ \underline{\mathbf{H}}(\underline{\mathbf{R}},t) \tag{2.12}$$

$$\underline{\mathbf{D}}(\underline{\mathbf{R}},t) = \varepsilon(\underline{\mathbf{R}})\ \underline{\mathbf{E}}(\underline{\mathbf{R}},t) = \varepsilon_0\ \varepsilon_{\mathrm{r}}(\underline{\mathbf{R}})\ \underline{\mathbf{E}}(\underline{\mathbf{R}},t)\,. \tag{2.13}$$

However, the electric current density $\underline{\mathbf{J}}_{\mathrm{e}}(\underline{\mathbf{R}},t)$ on the right hand side of Eq. (2.6) has two parts:

$$\underline{\mathbf{J}}_{\mathrm{e}}(\underline{\mathbf{R}},t) = \underline{\mathbf{J}}_{\mathrm{e}}^{\mathrm{con}}(\underline{\mathbf{R}},t) + \underline{\mathbf{J}}_{\mathrm{e}}^{\mathrm{imp}}(\underline{\mathbf{R}},t)\,. \tag{2.14}$$

Here $\underline{\mathbf{J}}_{\mathrm{e}}^{\mathrm{con}}$ and $\underline{\mathbf{J}}_{\mathrm{e}}^{\mathrm{imp}}$ represent the electric current density of the conductor and the external current source respectively. Using Ohm's law of field quantities the conducting part, i.e. the electric current density of the conductor $\underline{\mathbf{J}}_{\mathrm{e}}^{\mathrm{con}}$ is associated with the electric field strength $\underline{\mathbf{E}}(\underline{\mathbf{R}},t)$ by

$$\underline{\mathbf{J}}_{\mathrm{e}}^{\mathrm{con}}(\underline{\mathbf{R}},t) = \sigma_{\mathrm{e}}(\underline{\mathbf{R}})\ \underline{\mathbf{E}}(\underline{\mathbf{R}},t)\,, \tag{2.15}$$

where $\sigma_{\mathrm{e}}(\underline{\mathbf{R}})$ stands for electric conductivity of an inhomogeneous medium. Inserting Eq. (2.15) into Eq. (2.14) yields

$$\underline{\mathbf{J}}_{\mathrm{e}}(\underline{\mathbf{R}},t) = \sigma_{\mathrm{e}}(\underline{\mathbf{R}})\ \underline{\mathbf{E}}(\underline{\mathbf{R}},t) + \underline{\mathbf{J}}_{\mathrm{e}}^{\mathrm{imp}}(\underline{\mathbf{R}},t)\,. \tag{2.16}$$

With the help of this expression of electric current density $\underline{\mathbf{J}}_{\mathrm{e}}(\underline{\mathbf{R}},t)$ we rewrite Eq. (2.6) as

$$\boldsymbol{\nabla}\times\underline{\mathbf{H}}(\underline{\mathbf{R}},t) = \frac{\partial}{\partial t}\underline{\mathbf{D}}(\underline{\mathbf{R}},t) + \sigma_{\mathrm{e}}(\underline{\mathbf{R}})\ \underline{\mathbf{E}}(\underline{\mathbf{R}},t) + \underline{\mathbf{J}}_{\mathrm{e}}^{\mathrm{imp}}(\underline{\mathbf{R}},t)\,. \tag{2.17}$$

2.2 Transition and Boundary Conditions

The electric and magnetic field components satisfy the transition conditions at the interface between two media (see Fig. 2.1a), whereas the boundary conditions need to be fulfilled at the boundary of a perfect electrically conducting (PEC) material (see Fig. 2.1b).

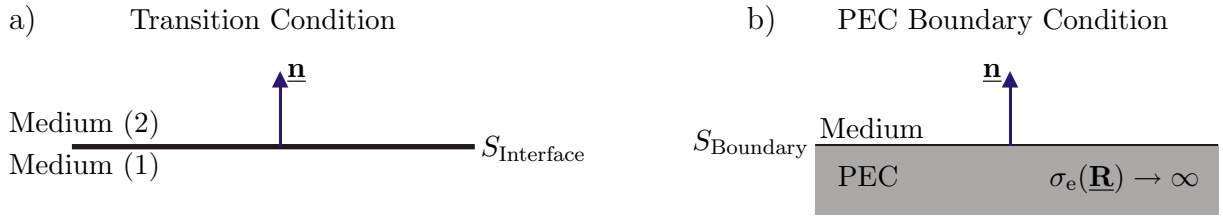

Figure 2.1: a) Transition interface between two materials and b) boundary surface.

2.2.1 Transition Conditions

At the transition surface, the jump at the normal component of the electric flux density $\underline{\mathbf{D}}(\underline{\mathbf{R}}, t)$ is defined by the surface electric charge density $\eta_{\text{e}}(\underline{\mathbf{R}}, t)$ (*Langenberg*, 2003; *EFT II*, 2009). Using Eq. (2.8) we show that

$$\underline{\mathbf{n}} \cdot \left[\underline{\mathbf{D}}^{(2)}(\underline{\mathbf{R}}, t) - \underline{\mathbf{D}}^{(1)}(\underline{\mathbf{R}}, t)\right] = \begin{cases} \eta_{\text{e}}(\underline{\mathbf{R}}, t) & \text{with source} \\ 0 & \text{source-free} \end{cases} \; ; \; \underline{\mathbf{R}} \in \mathrm{S}_{\text{Interface}} \; . \tag{2.18}$$

Here $\underline{\mathbf{n}}$ represents the normal vector on the interface defined in Fig. 2.1a. The tangential component of the electric field strength at the interface follows

$$\underline{\mathbf{n}} \times \left[\underline{\mathbf{E}}^{(2)}(\underline{\mathbf{R}}, t) - \underline{\mathbf{E}}^{(1)}(\underline{\mathbf{R}}, t)\right] = \begin{cases} -\underline{\mathbf{K}}_{\text{m}}(\underline{\mathbf{R}}, t) & \text{with source} \\ \underline{\mathbf{0}} & \text{source-free} \, . \end{cases} \tag{2.19}$$

A jump in the tangential component of the electric field strength represents magnetic current density $\underline{\mathbf{K}}_{\text{m}}(\underline{\mathbf{R}}, t)$ at the transition surface. Again, for the magnetic flux density we define the jump in the normal component by magnetic charge density $\eta_{\text{m}}(\underline{\mathbf{R}}, t)$ at the transition surface.

$$\underline{\mathbf{n}} \cdot \left[\underline{\mathbf{B}}^{(2)}(\underline{\mathbf{R}}, t) - \underline{\mathbf{B}}^{(1)}(\underline{\mathbf{R}}, t)\right] = \begin{cases} \eta_{\text{m}}(\underline{\mathbf{R}}, t) & \text{with source} \\ 0 & \text{source-free} \, . \end{cases} \tag{2.20}$$

The tangential component of the magnetic field strength jumps at the transition surface causes a surface electric current density $\underline{\mathbf{K}}_{\text{e}}(\underline{\mathbf{R}}, t)$

$$\underline{\mathbf{n}} \times \left[\underline{\mathbf{H}}^{(2)}(\underline{\mathbf{R}}, t) - \underline{\mathbf{H}}^{(1)}(\underline{\mathbf{R}}, t)\right] = \begin{cases} \underline{\mathbf{K}}_{\text{e}}(\underline{\mathbf{R}}, t) & \text{with source} \\ \underline{\mathbf{0}} & \text{source-free} \, . \end{cases} \tag{2.21}$$

Now, using the constitutive equations described in Eq. (2.12)-(2.13) we formulate equations Eq. (2.18)-(2.21) as

$$\underline{\mathbf{n}} \cdot \left[\varepsilon^{(2)} \, \underline{\mathbf{E}}^{(2)}(\underline{\mathbf{R}}, t) - \varepsilon^{(1)} \, \underline{\mathbf{E}}^{(1)}(\underline{\mathbf{R}}, t)\right] = \begin{cases} \eta_{\text{e}}(\underline{\mathbf{R}}, t) & \text{with source} \\ 0 & \text{source-free} \end{cases} \tag{2.22}$$

$$\underline{\mathbf{n}} \times \left[\frac{1}{\varepsilon^{(2)}} \, \underline{\mathbf{D}}^{(2)}(\underline{\mathbf{R}}, t) - \frac{1}{\varepsilon^{(1)}} \, \underline{\mathbf{D}}^{(1)}(\underline{\mathbf{R}}, t) \right] = \begin{cases} -\underline{\mathbf{K}}_{\mathrm{m}}(\underline{\mathbf{R}}, t) & \text{with source} \\ \underline{\mathbf{0}} & \text{source-free} \end{cases} \tag{2.23}$$

$$\underline{\mathbf{n}} \cdot \left[\mu^{(2)} \, \underline{\mathbf{B}}^{(2)}(\underline{\mathbf{R}}, t) - \mu^{(1)} \, \underline{\mathbf{B}}^{(1)}(\underline{\mathbf{R}}, t) \right] = \begin{cases} \eta_{\mathrm{m}}(\underline{\mathbf{R}}, t) & \text{with source} \\ 0 & \text{source-free} \end{cases} \tag{2.24}$$

$$\underline{\mathbf{n}} \times \left[\frac{1}{\mu^{(2)}} \, \underline{\mathbf{B}}^{(2)}(\underline{\mathbf{R}}, t) - \frac{1}{\mu^{(1)}} \, \underline{\mathbf{B}}^{(1)}(\underline{\mathbf{R}}, t) \right] = \begin{cases} \underline{\mathbf{K}}_{\mathrm{e}}(\underline{\mathbf{R}}, t) & \text{with source} \\ \underline{\mathbf{0}} & \text{source-free}\,. \end{cases} \tag{2.25}$$

2.2.2 Boundary Conditions

For a perfectly electrically conducting (PEC) boundary, the electric conductivity inside the PEC material is expressed by $\sigma_{\mathrm{e}} \to \infty$ (*EFT I*, 2009). In Fig. 2.1b medium (2) is a PEC material, where the surface S_{Boundary} denotes the boundary. As a result, the tangential component of the electric field strength and the normal component of magnetic flux density at the boundary becomes zero, i.e.,

$$\underline{\mathbf{n}} \times \underline{\mathbf{E}}(\underline{\mathbf{R}}, t) = \underline{\mathbf{0}} \tag{2.26}$$

$$\underline{\mathbf{n}} \cdot \underline{\mathbf{B}}(\underline{\mathbf{R}}, t) = 0\,. \tag{2.27}$$

Furthermore, the normal component of the electric flux density $\underline{\mathbf{D}}(\underline{\mathbf{R}}, t)$ is expressed by the electric charge density $\eta_{\mathrm{e}}(\underline{\mathbf{R}}, t)$ on the boundary surface and therefore, we obtain

$$\underline{\mathbf{n}} \cdot \underline{\mathbf{D}}(\underline{\mathbf{R}}, t) = \eta_{\mathrm{e}}(\underline{\mathbf{R}}, t) \tag{2.28}$$

and using the constitutive equation we write

$$\underline{\mathbf{n}} \cdot \underline{\mathbf{E}}(\underline{\mathbf{R}}, t) = \frac{1}{\varepsilon} \, \eta_{\mathrm{e}}(\underline{\mathbf{R}}, t)\,. \tag{2.29}$$

The tangential component of the magnetic field strength $\underline{\mathbf{H}}(\underline{\mathbf{R}}, t)$ is determined by the surface electric current density $\underline{\mathbf{K}}_{\mathrm{e}}(\underline{\mathbf{R}}, t)$ at the boundary surface S_{Boundary}, which leads to

$$\underline{\mathbf{n}} \times \underline{\mathbf{H}}(\underline{\mathbf{R}}, t) = \underline{\mathbf{K}}_{\mathrm{e}}(\underline{\mathbf{R}}, t) \tag{2.30}$$

and is written using constitutive equation as

$$\underline{\mathbf{n}} \times \underline{\mathbf{B}}(\underline{\mathbf{R}}, t) = \mu \, \underline{\mathbf{K}}_{\mathrm{e}}(\underline{\mathbf{R}}, t)\,. \tag{2.31}$$

2.3 Field Equations in the Frequency Domain

The eddy current problem can be solved in the time domain as well as in the frequency domain. The time domain technique is often used in case of pulsed eddy current system. In case of excitation pulse of a single frequency the static solution of the eddy current problem can easily be obtained in the frequency domain. Therefore, it is necessary to transform the

governing equations of the previous section into frequency domain using Fourier transformation. For a function $f(t)$ we define the fourier transformed $F(\omega)$ as

$$F(\omega) = \int_{-\infty}^{\infty} f(t)\ \mathrm{e}^{\mathrm{j}\,\omega t}\ \mathrm{d}t\,, \tag{2.32}$$

where ω represents the angular frequency. Again, for a function $F(\omega)$ the inverse Fourier transformation is defined by

$$f(t) = \frac{1}{2\pi} \int_{-\infty}^{\infty} F(\omega)\ \mathrm{e}^{-\mathrm{j}\,\omega t}\ \mathrm{d}\omega\,. \tag{2.33}$$

According to the definition of the Fourier integrals in Eq. (2.32) we obtain the following Fourier transforms:

$$\begin{aligned}
\frac{\partial}{\partial t} \quad &\circ\!\!-\!\!\bullet \quad -\mathrm{j}\,\omega \\
\underline{\mathbf{E}}(\underline{\mathbf{R}}, t) \quad &\circ\!\!-\!\!\bullet \quad \underline{\mathbf{E}}(\underline{\mathbf{R}}, \omega) \\
\underline{\mathbf{B}}(\underline{\mathbf{R}}, t) \quad &\circ\!\!-\!\!\bullet \quad \underline{\mathbf{B}}(\underline{\mathbf{R}}, \omega) \\
\underline{\mathbf{A}}_{\mathrm{m}}(\underline{\mathbf{R}}, t) \quad &\circ\!\!-\!\!\bullet \quad \underline{\mathbf{A}}_{\mathrm{m}}(\underline{\mathbf{R}}, \omega) \\
\underline{\mathbf{J}}_{\mathrm{e}}^{\mathrm{imp}}(\underline{\mathbf{R}}, t) \quad &\circ\!\!-\!\!\bullet \quad \underline{\mathbf{J}}_{\mathrm{e}}^{\mathrm{imp}}(\underline{\mathbf{R}}, \omega)\,.
\end{aligned}$$

Using these identities Maxwell's equations described by Eq. (2.5)-(2.8) are expressed in frequency domain by

$$\boldsymbol{\nabla} \times \underline{\mathbf{E}}(\underline{\mathbf{R}}, \omega) = \quad \mathrm{j}\,\omega \underline{\mathbf{B}}(\underline{\mathbf{R}}, \omega) - \underline{\mathbf{J}}_{\mathrm{m}}(\underline{\mathbf{R}}, \omega) \tag{2.34}$$

$$\begin{aligned}
\boldsymbol{\nabla} \times \underline{\mathbf{H}}(\underline{\mathbf{R}}, \omega) &= -\mathrm{j}\,\omega \underline{\mathbf{D}}(\underline{\mathbf{R}}, \omega) + \underline{\mathbf{J}}_{\mathrm{e}}(\underline{\mathbf{R}}, \omega) \\
&= -\mathrm{j}\,\omega \underline{\mathbf{D}}(\underline{\mathbf{R}}, \omega) + \sigma_{\mathrm{e}}(\underline{\mathbf{R}})\ \underline{\mathbf{E}}(\underline{\mathbf{R}}, \omega) + \underline{\mathbf{J}}_{\mathrm{e}}^{\mathrm{imp}}(\underline{\mathbf{R}}, \omega)
\end{aligned} \tag{2.35}$$

$$\boldsymbol{\nabla} \cdot \underline{\mathbf{B}}(\underline{\mathbf{R}}, \omega) = \quad \varrho_{\mathrm{m}}(\underline{\mathbf{R}}, \omega) \tag{2.36}$$

$$\boldsymbol{\nabla} \cdot \underline{\mathbf{D}}(\underline{\mathbf{R}}, \omega) = \quad \varrho_{\mathrm{e}}(\underline{\mathbf{R}}, \omega) \tag{2.37}$$

and for a medium having the relative permeability μ_r and relative permittivity ε_r the constitutive equations in frequency domain are formulated as

$$\underline{\mathbf{B}}(\underline{\mathbf{R}}, \omega) = \mu(\underline{\mathbf{R}})\ \underline{\mathbf{H}}(\underline{\mathbf{R}}, \omega) = \mu_0\ \mu_{\mathrm{r}}(\underline{\mathbf{R}})\ \underline{\mathbf{H}}(\underline{\mathbf{R}}, \omega) \tag{2.38}$$

$$\underline{\mathbf{D}}(\underline{\mathbf{R}}, \omega) = \varepsilon(\underline{\mathbf{R}})\ \underline{\mathbf{E}}(\underline{\mathbf{R}}, \omega) = \varepsilon_0\ \varepsilon_{\mathrm{r}}(\underline{\mathbf{R}})\ \underline{\mathbf{E}}(\underline{\mathbf{R}}, \omega)\,. \tag{2.39}$$

2.4 Inhomogeneous Helmholtz Equations

The inhomogeneous Helmholtz equations describe the wave propagation in the frequency domain for the electric field strength $\underline{\mathbf{E}}(\underline{\mathbf{R}}, \omega)$ and the magnetic field strength $\underline{\mathbf{H}}(\underline{\mathbf{R}}, \omega)$.

2.4.1 Inhomogeneous Helmholtz Equation for the Electric Field

Maxwell's first equation in differential form in the frequency domain states

$$\boldsymbol{\nabla}\times\underline{\mathbf{E}}(\underline{\mathbf{R}},\omega) = \mathrm{j}\,\omega\underline{\mathbf{B}}(\underline{\mathbf{R}},\omega) \;-\; \underline{\mathbf{J}}_{\mathrm{m}}(\underline{\mathbf{R}},\omega)\,. \tag{2.40}$$

Taking the curl of this equation results

$$\boldsymbol{\nabla}\times\boldsymbol{\nabla}\times\underline{\mathbf{E}}(\underline{\mathbf{R}},\omega) = \mathrm{j}\,\omega\boldsymbol{\nabla}\times\underline{\mathbf{B}}(\underline{\mathbf{R}},\omega) \;-\; \boldsymbol{\nabla}\times\underline{\mathbf{J}}_{\mathrm{m}}(\underline{\mathbf{R}},\omega)\,, \tag{2.41}$$

which is reformulated using the constitutive equation Eq. (2.38) as

$$\boldsymbol{\nabla}\times\boldsymbol{\nabla}\times\underline{\mathbf{E}}(\underline{\mathbf{R}},\omega) = \mathrm{j}\,\omega\boldsymbol{\nabla}\times\left[\mu(\underline{\mathbf{R}})\;\underline{\mathbf{H}}(\underline{\mathbf{R}},\omega)\right] \;-\; \boldsymbol{\nabla}\times\underline{\mathbf{J}}_{\mathrm{m}}(\underline{\mathbf{R}},\omega)\,. \tag{2.42}$$

Simplifying Eq. (2.42) for a medium of homogeneous μ yields

$$\boldsymbol{\nabla}\times\boldsymbol{\nabla}\times\underline{\mathbf{E}}(\underline{\mathbf{R}},\omega) = \mathrm{j}\,\omega\mu\;\boldsymbol{\nabla}\times\underline{\mathbf{H}}(\underline{\mathbf{R}},\omega) \;-\; \boldsymbol{\nabla}\times\underline{\mathbf{J}}_{\mathrm{m}}(\underline{\mathbf{R}},\omega)\,, \tag{2.43}$$

Using Maxwell's second equation Eq. (2.35) we obtain

$$\begin{aligned}
&\boldsymbol{\nabla}\times\boldsymbol{\nabla}\times\underline{\mathbf{E}}(\underline{\mathbf{R}},\omega)\\
&\quad= \;\mathrm{j}\,\omega\mu\left[-\mathrm{j}\,\omega\underline{\mathbf{D}}(\underline{\mathbf{R}},\omega) + \sigma_{\mathrm{e}}(\underline{\mathbf{R}})\;\underline{\mathbf{E}}(\underline{\mathbf{R}},\omega) + \underline{\mathbf{J}}_{\mathrm{e}}^{\mathrm{imp}}(\underline{\mathbf{R}},\omega)\right] \;-\; \boldsymbol{\nabla}\times\underline{\mathbf{J}}_{\mathrm{m}}(\underline{\mathbf{R}},\omega)\\
&\quad= \;\omega^2\mu\;\underline{\mathbf{D}}(\underline{\mathbf{R}},\omega) \;+\; \mathrm{j}\,\omega\mu\sigma_{\mathrm{e}}(\underline{\mathbf{R}})\;\underline{\mathbf{E}}(\underline{\mathbf{R}},\omega) + \;\mathrm{j}\,\omega\mu\;\underline{\mathbf{J}}_{\mathrm{e}}^{\mathrm{imp}}(\underline{\mathbf{R}},\omega) \;-\; \boldsymbol{\nabla}\times\underline{\mathbf{J}}_{\mathrm{m}}(\underline{\mathbf{R}},\omega)\,.
\end{aligned} \tag{2.44}$$

The $\boldsymbol{\nabla}\times\boldsymbol{\nabla}\times$ operator on the left side of Eq. (2.44) is expressed by

$$\boldsymbol{\nabla}\times\boldsymbol{\nabla}\times\underline{\mathbf{E}}(\underline{\mathbf{R}},\omega) = \boldsymbol{\nabla}\boldsymbol{\nabla}\cdot\underline{\mathbf{E}}(\underline{\mathbf{R}},\omega) \;-\; \Delta\underline{\mathbf{E}}(\underline{\mathbf{R}},\omega)\,. \tag{2.45}$$

For a medium of homogeneous electric permittivity, $\varepsilon(\underline{\mathbf{R}}) = \varepsilon$ and therefore, Using the constitutive equation Eq. (2.39) we write

$$\boldsymbol{\nabla}\times\boldsymbol{\nabla}\times\underline{\mathbf{E}}(\underline{\mathbf{R}},\omega) = \frac{1}{\varepsilon}\boldsymbol{\nabla}\boldsymbol{\nabla}\cdot\underline{\mathbf{D}}(\underline{\mathbf{R}},\omega) \;-\; \Delta\underline{\mathbf{E}}(\underline{\mathbf{R}},\omega)\,, \tag{2.46}$$

which is reformulated using Maxwell's fourth equation Eq. (2.37) as

$$\boldsymbol{\nabla}\times\boldsymbol{\nabla}\times\underline{\mathbf{E}}(\underline{\mathbf{R}},\omega) = \frac{1}{\varepsilon}\boldsymbol{\nabla}\varrho_{\mathrm{e}}(\underline{\mathbf{R}},\omega) \;-\; \Delta\underline{\mathbf{E}}(\underline{\mathbf{R}},\omega)\,, \tag{2.47}$$

Inserting Eq. (2.47) in Eq. (2.44) and replacing $\underline{\mathbf{D}}(\underline{\mathbf{R}},\omega)$ with $\varepsilon\underline{\mathbf{E}}(\underline{\mathbf{R}},\omega)$ results

$$\begin{aligned}
&\Delta\underline{\mathbf{E}}(\underline{\mathbf{R}},\omega) \;+\; \omega^2\mu\varepsilon\;\underline{\mathbf{E}}(\underline{\mathbf{R}},\omega) \;+\; \mathrm{j}\,\omega\mu\sigma_{\mathrm{e}}(\underline{\mathbf{R}})\;\underline{\mathbf{E}}(\underline{\mathbf{R}},\omega)\\
&\qquad= -\,\mathrm{j}\,\omega\mu\;\underline{\mathbf{J}}_{\mathrm{e}}^{\mathrm{imp}}(\underline{\mathbf{R}},\omega) \;+\; \frac{1}{\varepsilon}\boldsymbol{\nabla}\varrho_{\mathrm{e}}(\underline{\mathbf{R}},\omega) \;+\; \boldsymbol{\nabla}\times\underline{\mathbf{J}}_{\mathrm{m}}(\underline{\mathbf{R}},\omega)
\end{aligned} \tag{2.48}$$

and for a conductive medium of homogeneous electric conductivity, we write $\sigma_{\mathrm{e}}(\underline{\mathbf{R}}) = \sigma_{\mathrm{e}}$ and thus we obtain

$$\begin{aligned}
&\Delta\underline{\mathbf{E}}(\underline{\mathbf{R}},\omega) \;+\; \omega^2\mu\varepsilon\;\underline{\mathbf{E}}(\underline{\mathbf{R}},\omega) \;+\; \mathrm{j}\,\omega\mu\sigma_{\mathrm{e}}\;\underline{\mathbf{E}}(\underline{\mathbf{R}},\omega)\\
&\quad= -\,\mathrm{j}\,\omega\mu\;\underline{\mathbf{J}}_{\mathrm{e}}^{\mathrm{imp}}(\underline{\mathbf{R}},\omega) \;+\; \frac{1}{\varepsilon}\boldsymbol{\nabla}\varrho_{\mathrm{e}}(\underline{\mathbf{R}},\omega) \;+\; \boldsymbol{\nabla}\times\underline{\mathbf{J}}_{\mathrm{m}}(\underline{\mathbf{R}},\omega)
\end{aligned}$$

$$\Rightarrow\quad \Delta\underline{\mathbf{E}}(\underline{\mathbf{R}},\omega) + k_{\mathrm{c}}^2\;\underline{\mathbf{E}}(\underline{\mathbf{R}},\omega) \;= -\,\mathrm{j}\,\omega\mu\;\underline{\mathbf{J}}_{\mathrm{e}}^{\mathrm{imp}}(\underline{\mathbf{R}},\omega) + \frac{1}{\varepsilon}\boldsymbol{\nabla}\varrho_{\mathrm{e}}(\underline{\mathbf{R}},\omega) + \boldsymbol{\nabla}\times\underline{\mathbf{J}}_{\mathrm{m}}(\underline{\mathbf{R}},\omega)\,, \tag{2.49}$$

where k_{c} is the complex wave number and is expressed by

$$k_{\mathrm{c}} = \sqrt{\omega^2\mu\varepsilon + \mathrm{j}\,\omega\mu\sigma_{\mathrm{e}}}\;. \tag{2.50}$$

2.4.2 Inhomogeneous Helmholtz Equation for the Magnetic Field

We recall Maxwell's second equation in differential form in frequency domain

$$\boldsymbol{\nabla}\times\underline{\mathbf{H}}(\underline{\mathbf{R}},\omega) = -\,\mathrm{j}\,\omega\underline{\mathbf{D}}(\underline{\mathbf{R}},\omega) + \sigma_\mathrm{e}(\underline{\mathbf{R}})\;\underline{\mathbf{E}}(\underline{\mathbf{R}},\omega) + \underline{\mathbf{J}}_\mathrm{e}^\mathrm{imp}(\underline{\mathbf{R}},\omega)\,. \tag{2.51}$$

Let us introduce a curl operator ($\boldsymbol{\nabla}\times$) on both sides

$$\boldsymbol{\nabla}\times\boldsymbol{\nabla}\times\underline{\mathbf{H}}(\underline{\mathbf{R}},\omega) = \boldsymbol{\nabla}\times\left[-\,\mathrm{j}\,\omega\underline{\mathbf{D}}(\underline{\mathbf{R}},\omega) + \sigma_\mathrm{e}(\underline{\mathbf{R}})\;\underline{\mathbf{E}}(\underline{\mathbf{R}},\omega) + \underline{\mathbf{J}}_\mathrm{e}^\mathrm{imp}(\underline{\mathbf{R}},\omega)\right]\,. \tag{2.52}$$

Using the constitutive equation Eq. (2.39) for a medium of homogeneous electric permittivity we obtain

$$\boldsymbol{\nabla}\times\boldsymbol{\nabla}\times\underline{\mathbf{H}}(\underline{\mathbf{R}},\omega) \;=\; -\,\mathrm{j}\,\omega\varepsilon\boldsymbol{\nabla}\times\underline{\mathbf{E}}(\underline{\mathbf{R}},\omega) \;+\; \boldsymbol{\nabla}\times\left[\sigma_\mathrm{e}(\underline{\mathbf{R}})\;\underline{\mathbf{E}}(\underline{\mathbf{R}},\omega)\right] + \boldsymbol{\nabla}\times\underline{\mathbf{J}}_\mathrm{e}^\mathrm{imp}(\underline{\mathbf{R}},\omega)\,. \tag{2.53}$$

Rearranging Eq. (2.53) results

$$\begin{aligned}&\boldsymbol{\nabla}\times\boldsymbol{\nabla}\times\underline{\mathbf{H}}(\underline{\mathbf{R}},\omega)\\ &\quad= \left[-\,\mathrm{j}\,\omega\varepsilon + \;\sigma_\mathrm{e}(\underline{\mathbf{R}})\right]\boldsymbol{\nabla}\times\underline{\mathbf{E}}(\underline{\mathbf{R}},\omega) \;-\; \underline{\mathbf{E}}(\underline{\mathbf{R}},\omega)\times\boldsymbol{\nabla}\sigma_\mathrm{e}(\underline{\mathbf{R}}) \;+\; \boldsymbol{\nabla}\times\underline{\mathbf{J}}_\mathrm{e}^\mathrm{imp}(\underline{\mathbf{R}},\omega)\,.\end{aligned} \tag{2.54}$$

The $\boldsymbol{\nabla}\times\boldsymbol{\nabla}\times$ operator of Eq. (2.54) is given by

$$\boldsymbol{\nabla}\times\boldsymbol{\nabla}\times\underline{\mathbf{H}}(\underline{\mathbf{R}},\omega) = \boldsymbol{\nabla}\boldsymbol{\nabla}\cdot\underline{\mathbf{H}}(\underline{\mathbf{R}},\omega) \;-\; \Delta\underline{\mathbf{H}}(\underline{\mathbf{R}},\omega)\,. \tag{2.55}$$

Using the constitutive equation Eq. (2.38) we show that

$$\boldsymbol{\nabla}\times\boldsymbol{\nabla}\times\underline{\mathbf{H}}(\underline{\mathbf{R}},\omega) = \boldsymbol{\nabla}\boldsymbol{\nabla}\cdot\frac{1}{\mu(\underline{\mathbf{R}})}\underline{\mathbf{B}}(\underline{\mathbf{R}},\omega) \;-\; \Delta\underline{\mathbf{H}}(\underline{\mathbf{R}},\omega)\,. \tag{2.56}$$

For a medium of homogeneous magnetic permeability, it is assumed that $\mu(\underline{\mathbf{R}}) = \mu$, which leads to

$$\boldsymbol{\nabla}\times\boldsymbol{\nabla}\times\underline{\mathbf{H}}(\underline{\mathbf{R}},\omega) = \frac{1}{\mu}\boldsymbol{\nabla}\boldsymbol{\nabla}\cdot\underline{\mathbf{B}}(\underline{\mathbf{R}},\omega) \;-\; \Delta\underline{\mathbf{H}}(\underline{\mathbf{R}},\omega)\,. \tag{2.57}$$

Using Maxwell's third equation Eq. (2.36) in Eq. (2.57) results

$$\boldsymbol{\nabla}\times\boldsymbol{\nabla}\times\underline{\mathbf{H}}(\underline{\mathbf{R}},\omega) = \frac{1}{\mu}\boldsymbol{\nabla}\varrho_\mathrm{m}(\underline{\mathbf{R}},\omega) \;-\; \Delta\underline{\mathbf{H}}(\underline{\mathbf{R}},\omega)\,. \tag{2.58}$$

Inserting Eq. (2.58) in Eq. (2.53) yields

$$\begin{aligned}&\frac{1}{\mu}\boldsymbol{\nabla}\varrho_\mathrm{m}(\underline{\mathbf{R}},\omega) - \Delta\underline{\mathbf{H}}(\underline{\mathbf{R}},\omega)\\ &\quad= \left[-\,\mathrm{j}\,\omega\varepsilon + \;\sigma_\mathrm{e}(\underline{\mathbf{R}})\right]\boldsymbol{\nabla}\times\underline{\mathbf{E}}(\underline{\mathbf{R}},\omega) \;-\; \underline{\mathbf{E}}(\underline{\mathbf{R}},\omega)\times\boldsymbol{\nabla}\sigma_\mathrm{e}(\underline{\mathbf{R}}) \;+\; \boldsymbol{\nabla}\times\underline{\mathbf{J}}_\mathrm{e}^\mathrm{imp}(\underline{\mathbf{R}},\omega)\,.\end{aligned} \tag{2.59}$$

Replacing $\boldsymbol{\nabla}\times\underline{\mathbf{E}}(\underline{\mathbf{R}},\omega)$ according to the Maxwell's first equation Eq. (2.34) we obtain

$$\begin{aligned}&\frac{1}{\mu}\boldsymbol{\nabla}\varrho_\mathrm{m}(\underline{\mathbf{R}},\omega) - \Delta\underline{\mathbf{H}}(\underline{\mathbf{R}},\omega)\\ &= \left[-\,\mathrm{j}\,\omega\varepsilon + \;\sigma_\mathrm{e}(\underline{\mathbf{R}})\right]\left[\,\mathrm{j}\,\omega\underline{\mathbf{B}}(\underline{\mathbf{R}},\omega) - \underline{\mathbf{J}}_\mathrm{m}(\underline{\mathbf{R}},\omega)\right] \;-\; \underline{\mathbf{E}}(\underline{\mathbf{R}},\omega)\times\boldsymbol{\nabla}\sigma_\mathrm{e}(\underline{\mathbf{R}}) \;+\; \boldsymbol{\nabla}\times\underline{\mathbf{J}}_\mathrm{e}^\mathrm{imp}(\underline{\mathbf{R}},\omega)\end{aligned} \tag{2.60}$$

and we rearrange by using the constitutive equation Eq. (2.38) to obtain

$$\begin{aligned}\Delta\underline{\mathbf{H}}(\underline{\mathbf{R}},\omega) \;+\; \omega^2\varepsilon\mu\;\underline{\mathbf{H}}(\underline{\mathbf{R}},\omega) \;+\; \mathrm{j}\,\omega\sigma_\mathrm{e}(\underline{\mathbf{R}})\mu\;\underline{\mathbf{H}}(\underline{\mathbf{R}},\omega) \;-\; \underline{\mathbf{E}}(\underline{\mathbf{R}},\omega)\times\boldsymbol{\nabla}\sigma_\mathrm{e}(\underline{\mathbf{R}})\\ = -\,\mathrm{j}\,\omega\varepsilon\underline{\mathbf{J}}_\mathrm{m}(\underline{\mathbf{R}},\omega) \;+\; \sigma_\mathrm{e}(\underline{\mathbf{R}})\underline{\mathbf{J}}_\mathrm{m}(\underline{\mathbf{R}},\omega) \;+\; \frac{1}{\mu}\boldsymbol{\nabla}\varrho_\mathrm{m}(\underline{\mathbf{R}},\omega) \;-\; \boldsymbol{\nabla}\times\underline{\mathbf{J}}_\mathrm{e}^\mathrm{imp}(\underline{\mathbf{R}},\omega)\,. \qquad (2.61)\end{aligned}$$

For a medium of homogeneous electric conductivity σ_e we neglect the term $\underline{\mathbf{E}}(\underline{\mathbf{R}},\omega)\times\boldsymbol{\nabla}\sigma_\mathrm{e}(\underline{\mathbf{R}})$, and hence, Eq. (2.61) is simplified to

$$\begin{aligned}\Delta\underline{\mathbf{H}}(\underline{\mathbf{R}},\omega) \;+\; \omega^2\mu\varepsilon\;\underline{\mathbf{H}}(\underline{\mathbf{R}},\omega) \;+\; \mathrm{j}\,\omega\mu\sigma_\mathrm{e}\;\underline{\mathbf{H}}(\underline{\mathbf{R}},\omega)\\ = -\,\mathrm{j}\,\omega\varepsilon\underline{\mathbf{J}}_\mathrm{m}(\underline{\mathbf{R}},\omega) \;+\; \sigma_\mathrm{e}\;\underline{\mathbf{J}}_\mathrm{m}(\underline{\mathbf{R}},\omega) \;+\; \frac{1}{\mu}\boldsymbol{\nabla}\varrho_\mathrm{m}(\underline{\mathbf{R}},\omega) \;-\; \boldsymbol{\nabla}\times\underline{\mathbf{J}}_\mathrm{e}^\mathrm{imp}(\underline{\mathbf{R}},\omega)\,, \qquad (2.62)\end{aligned}$$

which can be formulated as

$$\begin{aligned}\Delta\underline{\mathbf{H}}(\underline{\mathbf{R}},\omega) \;+\; k_\mathrm{c}^2\;\underline{\mathbf{H}}(\underline{\mathbf{R}},\omega)\\ = -\,\mathrm{j}\,\omega\varepsilon\underline{\mathbf{J}}_\mathrm{m}(\underline{\mathbf{R}},\omega) \;+\; \sigma_\mathrm{e}\;\underline{\mathbf{J}}_\mathrm{m}(\underline{\mathbf{R}},\omega) \;+\; \frac{1}{\mu}\boldsymbol{\nabla}\varrho_\mathrm{m}(\underline{\mathbf{R}},\omega) \;-\; \boldsymbol{\nabla}\times\underline{\mathbf{J}}_\mathrm{e}^\mathrm{imp}(\underline{\mathbf{R}},\omega)\,, \qquad (2.63)\end{aligned}$$

where

$$k_\mathrm{c} = \sqrt{\omega^2\mu\varepsilon + \mathrm{j}\,\omega\mu\sigma_\mathrm{e}}\,. \qquad (2.64)$$

2.5 Electromagnetic Potentials of an Electrically Conducting Material

Firstly, we derive the potential representation for the electric and magnetic field strength using electric and magnetic scalar and vector potentials for the source-free case. Using these expressions we derive the the potential representation with source in the second part.

2.5.1 Electromagnetic Potentials in Source-Free Case

The Maxwell's equations in frequency domain, described by Eq. (2.34)-(2.37) are written in source-free case as

$$\boldsymbol{\nabla}\times\underline{\mathbf{E}}(\underline{\mathbf{R}},\omega) = \mathrm{j}\,\omega\underline{\mathbf{B}}(\underline{\mathbf{R}},\omega) \qquad (2.65)$$

$$\boldsymbol{\nabla}\times\underline{\mathbf{H}}(\underline{\mathbf{R}},\omega) = -\,\mathrm{j}\,\omega\underline{\mathbf{D}}(\underline{\mathbf{R}},\omega) + \sigma_\mathrm{e}\;\underline{\mathbf{E}}(\underline{\mathbf{R}},\omega) \qquad (2.66)$$

$$\boldsymbol{\nabla}\cdot\underline{\mathbf{D}}(\underline{\mathbf{R}},\omega) = 0 \qquad (2.67)$$

$$\boldsymbol{\nabla}\cdot\underline{\mathbf{B}}(\underline{\mathbf{R}},\omega) = 0\,. \qquad (2.68)$$

2.5.1.1 Derivation of the Potential Representation using Magnetic Vector Potential and Electric Scalar Potential

We know from the vector algebra that the curl of divergence produces also zero, i.e, for a vector $\underline{\mathbf{A}}_\mathrm{m}(\underline{\mathbf{R}},\omega)$ we obtain

$$\boldsymbol{\nabla}\cdot[\boldsymbol{\nabla}\times\underline{\mathbf{A}}_\mathrm{m}(\underline{\mathbf{R}},\omega)] = 0\,. \qquad (2.69)$$

From the equations Eq. (2.68) and Eq. (2.69) the magnetic flux density $\underline{\mathbf{B}}(\underline{\mathbf{R}},\omega)$ is given by

$$\underline{\mathbf{B}}(\underline{\mathbf{R}},\omega) = \boldsymbol{\nabla}\times\underline{\mathbf{A}}_{\mathrm{m}}(\underline{\mathbf{R}},\omega)\,, \tag{2.70}$$

where $\underline{\mathbf{A}}_{\mathrm{m}}(\underline{\mathbf{R}},\omega)$ is called magnetic vector potential, because it is related to the magnetic flux density $\underline{\mathbf{B}}(\underline{\mathbf{R}},\omega)$ through differentiation. The first Maxwell's equation (Eq. (2.65)), also known as Faraday's law of induction in source-free case, is written using magnetic vector potential $\underline{\mathbf{A}}_{\mathrm{m}}(\underline{\mathbf{R}},\omega)$ as

$$\begin{aligned} \boldsymbol{\nabla}\times\underline{\mathbf{E}}(\underline{\mathbf{R}},\omega) &= \mathrm{j}\,\omega\boldsymbol{\nabla}\times\underline{\mathbf{A}}_{\mathrm{m}}(\underline{\mathbf{R}},\omega) \\ \Rightarrow\quad \boldsymbol{\nabla}\times\underbrace{\left[\underline{\mathbf{E}}(\underline{\mathbf{R}},\omega) - \mathrm{j}\,\omega\underline{\mathbf{A}}_{\mathrm{m}}(\underline{\mathbf{R}},\omega)\right]}_{=\,\boldsymbol{\nabla}\Phi_{\mathrm{e}}(\underline{\mathbf{R}},\omega)} &= \underline{\mathbf{0}}\,, \end{aligned} \tag{2.71}$$

which leads to the electric scalar potential $\Phi_{\mathrm{e}}(\underline{\mathbf{R}},\omega)$ because of the vector identity

$$\boldsymbol{\nabla}\times\left[\boldsymbol{\nabla}\Phi_{\mathrm{e}}(\underline{\mathbf{R}},\omega)\right] = \underline{\mathbf{0}}\,. \tag{2.72}$$

Rewriting Eq. (2.71) results

$$\underline{\mathbf{E}}(\underline{\mathbf{R}},\omega) - \mathrm{j}\,\omega\underline{\mathbf{A}}_{\mathrm{m}}(\underline{\mathbf{R}},\omega) = -\boldsymbol{\nabla}\Phi_{\mathrm{e}}(\underline{\mathbf{R}},\omega)\,, \tag{2.73}$$

where $\Phi_{\mathrm{e}}(\underline{\mathbf{R}},\omega)$ is called electric scalar potential. The negative sign on the right-hand side is introduced because of the historical convention (*Langenberg*, 2003) and it defines the sign of the electrical voltage in static case. Rearranging Eq. (2.73) yields

$$\underline{\mathbf{E}}(\underline{\mathbf{R}},\omega) = -\boldsymbol{\nabla}\Phi_{\mathrm{e}}(\underline{\mathbf{R}},\omega) + \mathrm{j}\,\omega\underline{\mathbf{A}}_{\mathrm{m}}(\underline{\mathbf{R}},\omega)\,. \tag{2.74}$$

2.5.1.2 Derivation of the Potential Representation using Magnetic Scalar Potential and Electric Vector Potential

For a vector $\underline{\mathbf{A}}_{\mathrm{e}}(\underline{\mathbf{R}},\omega)$ we know from vector identity that

$$\boldsymbol{\nabla}\cdot\left[\boldsymbol{\nabla}\times\underline{\mathbf{A}}_{\mathrm{e}}(\underline{\mathbf{R}},\omega)\right] = 0\,. \tag{2.75}$$

From the equations Eq. (2.68) and Eq. (2.75) the electric flux density $\underline{\mathbf{D}}(\underline{\mathbf{R}},\omega)$ is defined by

$$\underline{\mathbf{D}}(\underline{\mathbf{R}},\omega) = -\boldsymbol{\nabla}\times\underline{\mathbf{A}}_{\mathrm{e}}(\underline{\mathbf{R}},\omega)\,, \tag{2.76}$$

where $\underline{\mathbf{A}}_{\mathrm{e}}(\underline{\mathbf{R}},\omega)$ is called electric vector potential and it is related to the electric flux density $\underline{\mathbf{D}}(\underline{\mathbf{R}},\omega)$ through differentiation. The negative sign on the right-hand side is introduced according to the historical convention. Maxwell's second equation (Eq. (2.66)), also known as Ampère-Maxwell circuital law of induction is reformulated in source-free case using the constitutive equation Eq. (2.39) as

$$\boldsymbol{\nabla}\times\underline{\mathbf{H}}(\underline{\mathbf{R}},\omega) = -\mathrm{j}\,\omega\underline{\mathbf{D}}(\underline{\mathbf{R}},\omega) + \frac{\sigma_{\mathrm{e}}}{\varepsilon}\underline{\mathbf{D}}(\underline{\mathbf{R}},\omega)\,. \tag{2.77}$$

Using electric vector potential $\underline{\mathbf{A}}_{\mathrm{e}}(\underline{\mathbf{R}},\omega)$ we obtain

$$\begin{aligned} \boldsymbol{\nabla}\times\underline{\mathbf{H}}(\underline{\mathbf{R}},\omega) &= -\mathrm{j}\,\omega\left[-\boldsymbol{\nabla}\times\underline{\mathbf{A}}_{\mathrm{e}}(\underline{\mathbf{R}},\omega)\right] + \frac{\sigma_{\mathrm{e}}}{\varepsilon}\left[-\boldsymbol{\nabla}\times\underline{\mathbf{A}}_{\mathrm{e}}(\underline{\mathbf{R}},\omega)\right] \\ \Rightarrow\quad \boldsymbol{\nabla}\times\underline{\mathbf{H}}(\underline{\mathbf{R}},\omega) &= \mathrm{j}\,\omega\boldsymbol{\nabla}\times\underline{\mathbf{A}}_{\mathrm{e}} - \frac{\sigma_{\mathrm{e}}}{\varepsilon}\boldsymbol{\nabla}\times\underline{\mathbf{A}}_{\mathrm{e}}(\underline{\mathbf{R}},\omega) \\ \Rightarrow\quad \boldsymbol{\nabla}\times\left[\underline{\mathbf{H}}(\underline{\mathbf{R}},\omega) - \mathrm{j}\,\omega\underline{\mathbf{A}}_{\mathrm{e}}(\underline{\mathbf{R}},\omega) + \frac{\sigma_{\mathrm{e}}}{\varepsilon}\underline{\mathbf{A}}_{\mathrm{e}}(\underline{\mathbf{R}},\omega)\right] &= \underline{\mathbf{0}}\,. \end{aligned} \tag{2.78}$$

For a scalar potential $\Phi_{\mathrm{m}}(\underline{\mathbf{R}},\omega)$

$$\boldsymbol{\nabla}\times\left[\boldsymbol{\nabla}\Phi_{\mathrm{m}}(\underline{\mathbf{R}},\omega)\right]=\underline{\mathbf{0}}\,. \tag{2.79}$$

Comparing Eq. (2.79) to Eq. (2.78) leads to

$$\underline{\mathbf{H}}(\underline{\mathbf{R}},\omega)-\,\mathrm{j}\,\omega\underline{\mathbf{A}}_{\mathrm{e}}(\underline{\mathbf{R}},\omega)+\frac{\sigma_{\mathrm{e}}}{\varepsilon}\underline{\mathbf{A}}_{\mathrm{e}}(\underline{\mathbf{R}},\omega)=-\boldsymbol{\nabla}\Phi_{\mathrm{m}}(\underline{\mathbf{R}},\omega)\,, \tag{2.80}$$

where $\Phi_{\mathrm{m}}(\underline{\mathbf{R}},\omega)$ is called magnetic scalar potential and the negative sign on the right-hand side is introduced because of the historical convention. Rearranging Eq. (2.80) results

$$\underline{\mathbf{H}}(\underline{\mathbf{R}},\omega)=-\boldsymbol{\nabla}\Phi_{\mathrm{m}}(\underline{\mathbf{R}},\omega)+\,\mathrm{j}\,\omega\underline{\mathbf{A}}_{\mathrm{e}}(\underline{\mathbf{R}},\omega)-\frac{\sigma_{\mathrm{e}}}{\varepsilon}\underline{\mathbf{A}}_{\mathrm{e}}(\underline{\mathbf{R}},\omega)\,. \tag{2.81}$$

2.5.2 Electromagnetic Potentials in Case with Electric and Magnetic Sources

The electric and magnetic fields in terms of the potentials in source-free case are described by equations (2.70), (2.74), (2.76) and (2.81). In case of electric and magnetic sources for an electrically conducting media using superposition theorem we reformulate these equations as

$$\underline{\mathbf{E}}(\underline{\mathbf{R}},\omega)=-\boldsymbol{\nabla}\Phi_{\mathrm{e}}(\underline{\mathbf{R}},\omega)+\,\mathrm{j}\,\omega\underline{\mathbf{A}}_{\mathrm{m}}(\underline{\mathbf{R}},\omega)-\frac{1}{\varepsilon}\boldsymbol{\nabla}\times\underline{\mathbf{A}}_{\mathrm{e}}(\underline{\mathbf{R}},\omega) \tag{2.82}$$

$$\underline{\mathbf{H}}(\underline{\mathbf{R}},\omega)=-\boldsymbol{\nabla}\Phi_{\mathrm{m}}(\underline{\mathbf{R}},\omega)+\,\mathrm{j}\,\omega\underline{\mathbf{A}}_{\mathrm{e}}(\underline{\mathbf{R}},\omega)-\frac{\sigma_{\mathrm{e}}}{\varepsilon}\underline{\mathbf{A}}_{\mathrm{e}}(\underline{\mathbf{R}},\omega)+\frac{1}{\mu}\boldsymbol{\nabla}\times\underline{\mathbf{A}}_{\mathrm{m}}(\underline{\mathbf{R}},\omega) \tag{2.83}$$

$$\underline{\mathbf{B}}(\underline{\mathbf{R}},\omega)=-\mu\boldsymbol{\nabla}\Phi_{\mathrm{m}}(\underline{\mathbf{R}},\omega)+\,\mathrm{j}\,\omega\mu\underline{\mathbf{A}}_{\mathrm{e}}(\underline{\mathbf{R}},\omega)-\frac{\mu\sigma_{\mathrm{e}}}{\varepsilon}\underline{\mathbf{A}}_{\mathrm{e}}(\underline{\mathbf{R}},\omega)+\boldsymbol{\nabla}\times\underline{\mathbf{A}}_{\mathrm{m}}(\underline{\mathbf{R}},\omega) \tag{2.84}$$

$$\underline{\mathbf{D}}(\underline{\mathbf{R}},\omega)=-\varepsilon\boldsymbol{\nabla}\Phi_{\mathrm{e}}(\underline{\mathbf{R}},\omega)+\,\mathrm{j}\,\omega\varepsilon\underline{\mathbf{A}}_{\mathrm{m}}(\underline{\mathbf{R}},\omega)-\boldsymbol{\nabla}\times\underline{\mathbf{A}}_{\mathrm{e}}(\underline{\mathbf{R}},\omega)\,. \tag{2.85}$$

2.6 Decoupling of Maxwell's Equations by Electromagnetic Potentials

Maxwell's equations represent a coupled system where the electric and magnetic fields are physically coupled through induction and magnetomotive force. Mathematically we observe the coupling of the fields through divergence and curl operators. However, the electric and magnetic fields can be decoupled using magnetic and electric scalar and vector potentials.

2.6.1 Expression of the Magnetic Vector Potential in the Frequency Domain

We start with the Ampère-Maxwell circuital law in frequency domain and recall Eq. (2.35)

$$\boldsymbol{\nabla}\times\underline{\mathbf{H}}(\underline{\mathbf{R}},\omega)=(-\,\mathrm{j}\,\omega\varepsilon+\sigma_{\mathrm{e}})\,\underline{\mathbf{E}}(\underline{\mathbf{R}},\omega)+\underline{\mathbf{J}}_{\mathrm{e}}^{\mathrm{imp}}(\underline{\mathbf{R}},\omega)\,. \tag{2.86}$$

The magnetic field strength $\underline{\mathbf{H}}(\underline{\mathbf{R}},\omega)$ and electric field strength $\underline{\mathbf{E}}(\underline{\mathbf{R}},\omega)$ are represented by the potentials according to Eqs. (2.82)-(2.83) and therefore, we rewrite Eq. (2.86) as

$$\begin{aligned}\boldsymbol{\nabla}\times&\left[-\boldsymbol{\nabla}\Phi_{\mathrm{m}}(\underline{\mathbf{R}},\omega)+\,\mathrm{j}\,\omega\underline{\mathbf{A}}_{\mathrm{e}}(\underline{\mathbf{R}},\omega)-\frac{\sigma_{\mathrm{e}}}{\varepsilon}\underline{\mathbf{A}}_{\mathrm{e}}(\underline{\mathbf{R}},\omega)+\frac{1}{\mu}\boldsymbol{\nabla}\times\underline{\mathbf{A}}_{\mathrm{m}}(\underline{\mathbf{R}},\omega)\right]\\&=(-\,\mathrm{j}\,\omega\varepsilon+\sigma_{\mathrm{e}})\,\left[-\boldsymbol{\nabla}\Phi_{\mathrm{e}}+\,\mathrm{j}\,\omega\underline{\mathbf{A}}_{\mathrm{m}}-\frac{1}{\varepsilon}\boldsymbol{\nabla}\times\underline{\mathbf{A}}_{\mathrm{e}}\right]+\underline{\mathbf{J}}_{\mathrm{e}}^{\mathrm{imp}}(\underline{\mathbf{R}},\omega)\,.\end{aligned} \tag{2.87}$$

Rearranging Eq. (2.87) yields

$$-\mu \underbrace{\boldsymbol{\nabla}\times\boldsymbol{\nabla}\Phi_{\mathrm{m}}(\underline{\mathbf{R}},\omega)}_{=\underline{\mathbf{0}}} + \mathrm{j}\,\omega\mu\boldsymbol{\nabla}\times\underline{\mathbf{A}}_{\mathrm{e}}(\underline{\mathbf{R}},\omega) - \frac{\mu\sigma_{\mathrm{e}}}{\varepsilon}\underline{\mathbf{A}}_{\mathrm{e}}(\underline{\mathbf{R}},\omega) + \boldsymbol{\nabla}\times\boldsymbol{\nabla}\times\underline{\mathbf{A}}_{\mathrm{m}}(\underline{\mathbf{R}},\omega)$$
$$= \mathrm{j}\,\omega\mu\varepsilon\boldsymbol{\nabla}\Phi_{\mathrm{e}}(\underline{\mathbf{R}},\omega) + \omega^2\mu\varepsilon\ \underline{\mathbf{A}}_{\mathrm{m}}(\underline{\mathbf{R}},\omega) + \mathrm{j}\,\omega\mu\boldsymbol{\nabla}\times\underline{\mathbf{A}}_{\mathrm{e}}(\underline{\mathbf{R}},\omega) - \mu\sigma_{\mathrm{e}}\boldsymbol{\nabla}\Phi_{\mathrm{e}}(\underline{\mathbf{R}},\omega)$$
$$+ \mathrm{j}\,\omega\mu\sigma_{\mathrm{e}}\ \underline{\mathbf{A}}_{\mathrm{m}}(\underline{\mathbf{R}},\omega) - \frac{\mu\sigma_{\mathrm{e}}}{\varepsilon}\underline{\mathbf{A}}_{\mathrm{e}}(\underline{\mathbf{R}},\omega) + \mu\ \underline{\mathbf{J}}_{\mathrm{e}}^{\mathrm{imp}}(\underline{\mathbf{R}},\omega)\,. \tag{2.88}$$

Canceling the common parts from both sides we obtain

$$\boldsymbol{\nabla}\times\boldsymbol{\nabla}\times\underline{\mathbf{A}}_{\mathrm{m}}(\underline{\mathbf{R}},\omega) = \mathrm{j}\,\omega\mu\varepsilon\boldsymbol{\nabla}\Phi_{\mathrm{e}}(\underline{\mathbf{R}},\omega) + \omega^2\mu\varepsilon\ \underline{\mathbf{A}}_{\mathrm{m}}(\underline{\mathbf{R}},\omega) - \mu\sigma_{\mathrm{e}}\boldsymbol{\nabla}\Phi_{\mathrm{e}}(\underline{\mathbf{R}},\omega)$$
$$+ \mathrm{j}\,\omega\mu\sigma_{\mathrm{e}}\ \underline{\mathbf{A}}_{\mathrm{m}}(\underline{\mathbf{R}},\omega) + \mu\ \underline{\mathbf{J}}_{\mathrm{e}}^{\mathrm{imp}}(\underline{\mathbf{R}},\omega)\,. \tag{2.89}$$

The $\boldsymbol{\nabla}\times\boldsymbol{\nabla}\times$ operator can be replaced by $\boldsymbol{\nabla}\boldsymbol{\nabla}\cdot - \boldsymbol{\nabla}\cdot\boldsymbol{\nabla}$, which leads to

$$\boldsymbol{\nabla}\cdot\boldsymbol{\nabla}\underline{\mathbf{A}}_{\mathrm{m}}(\underline{\mathbf{R}},\omega) + \omega^2\mu\varepsilon\ \underline{\mathbf{A}}_{\mathrm{m}}(\underline{\mathbf{R}},\omega) + \mathrm{j}\,\omega\mu\sigma_{\mathrm{e}}\underline{\mathbf{A}}_{\mathrm{m}}(\underline{\mathbf{R}},\omega)$$
$$= \mu\underline{\mathbf{J}}_{\mathrm{e}}^{\mathrm{imp}}(\underline{\mathbf{R}},\omega) + \boldsymbol{\nabla}\boldsymbol{\nabla}\cdot\underline{\mathbf{A}}_{\mathrm{m}}(\underline{\mathbf{R}},\omega) + \mathrm{j}\,\omega\mu\varepsilon\boldsymbol{\nabla}\Phi_{\mathrm{e}}(\underline{\mathbf{R}},\omega) - \mu\sigma_{\mathrm{e}}\boldsymbol{\nabla}\Phi_{\mathrm{e}}(\underline{\mathbf{R}},\omega)$$
$$\Rightarrow\quad \Delta\underline{\mathbf{A}}_{\mathrm{m}}(\underline{\mathbf{R}},\omega) + k_{\mathrm{c}}^2\ \underline{\mathbf{A}}_{\mathrm{m}}(\underline{\mathbf{R}},\omega)$$
$$= -\mu\underline{\mathbf{J}}_{\mathrm{e}}^{\mathrm{imp}}(\underline{\mathbf{R}},\omega) + \boldsymbol{\nabla}\left[\boldsymbol{\nabla}\cdot\underline{\mathbf{A}}_{\mathrm{m}}(\underline{\mathbf{R}},\omega) - \mathrm{j}\,\omega\mu\varepsilon\Phi_{\mathrm{e}}(\underline{\mathbf{R}},\omega) + \mu\sigma_{\mathrm{e}}\Phi_{\mathrm{e}}(\underline{\mathbf{R}},\omega)\right]\,. \tag{2.90}$$

With the Lorenz gauge

$$\boldsymbol{\nabla}\cdot\underline{\mathbf{A}}_{\mathrm{m}}(\underline{\mathbf{R}},\omega) - \mathrm{j}\,\omega\mu\varepsilon\Phi_{\mathrm{e}}(\underline{\mathbf{R}},\omega) + \mu\sigma_{\mathrm{e}}\Phi_{\mathrm{e}}(\underline{\mathbf{R}},\omega) = 0 \tag{2.91}$$

we obtain from Eq. (2.90)

$$\Delta\underline{\mathbf{A}}_{\mathrm{m}}(\underline{\mathbf{R}},\omega) + k_{\mathrm{c}}^2\ \underline{\mathbf{A}}_{\mathrm{m}}(\underline{\mathbf{R}},\omega) = -\mu\underline{\mathbf{J}}_{\mathrm{e}}^{\mathrm{imp}}(\underline{\mathbf{R}},\omega)\ . \tag{2.92}$$

2.6.2 Expression of the Electric Scalar Potential in the Frequency Domain

Let us recall Maxwell's fourth equation in frequency domain

$$\boldsymbol{\nabla}\cdot\underline{\mathbf{D}}(\underline{\mathbf{R}},\omega) = \varrho_{\mathrm{e}}(\underline{\mathbf{R}},\omega)\,. \tag{2.93}$$

Using the expression of the electric flux density $\underline{\mathbf{D}}(\underline{\mathbf{R}},\omega)$ by the potentials according to Eq. (2.85) results

$$\boldsymbol{\nabla}\cdot\left[-\varepsilon\boldsymbol{\nabla}\Phi_{\mathrm{e}}(\underline{\mathbf{R}},\omega) + \mathrm{j}\,\omega\varepsilon\underline{\mathbf{A}}_{\mathrm{m}}(\underline{\mathbf{R}},\omega) - \boldsymbol{\nabla}\times\underline{\mathbf{A}}_{\mathrm{e}}(\underline{\mathbf{R}},\omega)\right] = \varrho_{\mathrm{e}}(\underline{\mathbf{R}},\omega)\,, \tag{2.94}$$

which is rearranged as

$$-\varepsilon\boldsymbol{\nabla}\cdot\boldsymbol{\nabla}\Phi_{\mathrm{e}}(\underline{\mathbf{R}},\omega) + \mathrm{j}\,\omega\varepsilon\boldsymbol{\nabla}\cdot\underline{\mathbf{A}}_{\mathrm{m}}(\underline{\mathbf{R}},\omega) - \underbrace{\boldsymbol{\nabla}\cdot\boldsymbol{\nabla}\times\underline{\mathbf{A}}_{\mathrm{e}}(\underline{\mathbf{R}},\omega)}_{=\underline{\mathbf{0}}} = \varrho_{\mathrm{e}}(\underline{\mathbf{R}},\omega)$$
$$\Rightarrow\quad \Delta\Phi_{\mathrm{e}}(\underline{\mathbf{R}},\omega) = -\frac{1}{\varepsilon}\varrho_{\mathrm{e}}(\underline{\mathbf{R}},\omega) + \mathrm{j}\,\omega\boldsymbol{\nabla}\cdot\underline{\mathbf{A}}_{\mathrm{m}}(\underline{\mathbf{R}},\omega)\ . \tag{2.95}$$

Now we add on both sides of Eq. (2.95) the term $(\omega^2\mu\varepsilon + \mathrm{j}\,\omega\mu\sigma_\mathrm{e})\,\Phi_\mathrm{e}(\underline{\mathbf{R}},\omega)$ and thus we obtain the PDE for $\Phi_\mathrm{e}(\underline{\mathbf{R}},\omega)$

$$\begin{aligned}
&\Delta\Phi_\mathrm{e}(\underline{\mathbf{R}},\omega) + \left(\omega^2\varepsilon\mu + \mathrm{j}\,\omega\mu\sigma_\mathrm{e}\right)\Phi_\mathrm{e}(\underline{\mathbf{R}},\omega)\\
&\quad = -\frac{1}{\varepsilon}\varrho_\mathrm{e}(\underline{\mathbf{R}},\omega) + \mathrm{j}\,\omega\boldsymbol{\nabla}\cdot\underline{\mathbf{A}}_\mathrm{m}(\underline{\mathbf{R}},\omega) + \omega^2\mu\varepsilon\Phi_\mathrm{e}(\underline{\mathbf{R}},\omega) + \mathrm{j}\,\omega\mu\sigma_\mathrm{e}\Phi_\mathrm{e}(\underline{\mathbf{R}},\omega)\\
\Rightarrow\quad &\Delta\Phi_\mathrm{e}(\underline{\mathbf{R}},\omega) + k_\mathrm{c}^2\;\Phi_\mathrm{e}(\underline{\mathbf{R}},\omega)\\
&\quad = -\frac{1}{\varepsilon}\varrho_\mathrm{e}(\underline{\mathbf{R}},\omega) + \mathrm{j}\,\omega\left[\boldsymbol{\nabla}\cdot\underline{\mathbf{A}}_\mathrm{m}(\underline{\mathbf{R}},\omega) - \mathrm{j}\,\omega\mu\varepsilon\Phi_\mathrm{e}(\underline{\mathbf{R}},\omega) + \mathrm{j}\,\omega\mu\sigma_\mathrm{e}\Phi_\mathrm{e}(\underline{\mathbf{R}},\omega)\right]\,, \qquad (2.96)
\end{aligned}$$

which is comparable to the PDE for $\underline{\mathbf{A}}_\mathrm{m}(\underline{\mathbf{R}},\omega)$ in Eq. (2.89). With the Lorenz gauge (Eq. (2.91)) we simplify Eq. (2.96) to

$$\Delta\Phi_\mathrm{e}(\underline{\mathbf{R}},\omega) + k_\mathrm{c}^2\;\Phi_\mathrm{e}(\underline{\mathbf{R}},\omega) = -\frac{1}{\varepsilon}\varrho_\mathrm{e}(\underline{\mathbf{R}},\omega)\;. \qquad (2.97)$$

2.6.3 Expression of the Electric Vector Potential in the Frequency Domain

Faraday's law of induction in frequency domain states

$$\boldsymbol{\nabla}\times\underline{\mathbf{E}}(\underline{\mathbf{R}},\omega) = \mathrm{j}\,\omega\underline{\mathbf{B}}(\underline{\mathbf{R}},\omega) - \underline{\mathbf{J}}_\mathrm{m}(\underline{\mathbf{R}},\omega)\,. \qquad (2.98)$$

Inserting the representation of magnetic field strength $\underline{\mathbf{E}}(\underline{\mathbf{R}},\omega)$ and magnetic flux density strength $\underline{\mathbf{B}}(\underline{\mathbf{R}},\omega)$ by the potentials according to Eq. (2.82) and Eq. (2.84) we find

$$\begin{aligned}
&\boldsymbol{\nabla}\times\left[-\boldsymbol{\nabla}\Phi_\mathrm{e}(\underline{\mathbf{R}},\omega) + \mathrm{j}\,\omega\underline{\mathbf{A}}_\mathrm{m}(\underline{\mathbf{R}},\omega) - \frac{1}{\varepsilon}\boldsymbol{\nabla}\times\underline{\mathbf{A}}_\mathrm{e}(\underline{\mathbf{R}},\omega)\right]\\
&\quad = \mathrm{j}\,\omega\left[-\mu\boldsymbol{\nabla}\Phi_\mathrm{m}(\underline{\mathbf{R}},\omega) + \mathrm{j}\,\omega\mu\underline{\mathbf{A}}_\mathrm{e}(\underline{\mathbf{R}},\omega) - \frac{\mu\sigma_\mathrm{e}}{\varepsilon}\underline{\mathbf{A}}_\mathrm{e}(\underline{\mathbf{R}},\omega) + \boldsymbol{\nabla}\times\underline{\mathbf{A}}_\mathrm{m}(\underline{\mathbf{R}},\omega)\right] - \underline{\mathbf{J}}_\mathrm{m}(\underline{\mathbf{R}},\omega)\,.
\end{aligned} \qquad (2.99)$$

Rearranging Eq. (2.99) results

$$\begin{aligned}
&-\underbrace{\boldsymbol{\nabla}\times\boldsymbol{\nabla}\Phi_\mathrm{e}(\underline{\mathbf{R}},\omega)}_{=\underline{\mathbf{0}}} + \mathrm{j}\,\omega\boldsymbol{\nabla}\times\underline{\mathbf{A}}_\mathrm{m}(\underline{\mathbf{R}},\omega) - \frac{1}{\varepsilon}\boldsymbol{\nabla}\times\boldsymbol{\nabla}\times\underline{\mathbf{A}}_\mathrm{e}(\underline{\mathbf{R}},\omega)\\
&\quad = -\mathrm{j}\,\omega\mu\boldsymbol{\nabla}\Phi_\mathrm{m}(\underline{\mathbf{R}},\omega) - \omega^2\mu\;\underline{\mathbf{A}}_\mathrm{e}(\underline{\mathbf{R}},\omega) - \mathrm{j}\,\omega\frac{\mu\sigma_\mathrm{e}}{\varepsilon}\;\underline{\mathbf{A}}_\mathrm{e}(\underline{\mathbf{R}},\omega) + \mathrm{j}\,\omega\boldsymbol{\nabla}\times\underline{\mathbf{A}}_\mathrm{m}(\underline{\mathbf{R}},\omega)\\
&\qquad - \underline{\mathbf{J}}_\mathrm{m}(\underline{\mathbf{R}},\omega)\,.
\end{aligned} \qquad (2.100)$$

We cancel the common parts from both sides and rewrite Eq. (2.100) as

$$\begin{aligned}
&\Delta\underline{\mathbf{A}}_\mathrm{e}(\underline{\mathbf{R}},\omega) + \omega^2\mu\varepsilon\;\underline{\mathbf{A}}_\mathrm{e}(\underline{\mathbf{R}},\omega) + \mathrm{j}\,\omega\mu\sigma_\mathrm{e}\;\underline{\mathbf{A}}_\mathrm{e}(\underline{\mathbf{R}},\omega)\\
&\quad = -\varepsilon\underline{\mathbf{J}}_\mathrm{m}(\underline{\mathbf{R}},\omega) + \boldsymbol{\nabla}\boldsymbol{\nabla}\cdot\underline{\mathbf{A}}_\mathrm{e}(\underline{\mathbf{R}},\omega) - \mathrm{j}\,\omega\mu\varepsilon\boldsymbol{\nabla}\Phi_\mathrm{m}(\underline{\mathbf{R}},\omega)\\
\Rightarrow\quad &\Delta\underline{\mathbf{A}}_\mathrm{e}(\underline{\mathbf{R}},\omega) + k_\mathrm{c}^2\;\underline{\mathbf{A}}_\mathrm{e}(\underline{\mathbf{R}},\omega)\\
&\quad = -\varepsilon\underline{\mathbf{J}}_\mathrm{m}(\underline{\mathbf{R}},\omega) + \boldsymbol{\nabla}\left[\boldsymbol{\nabla}\cdot\underline{\mathbf{A}}_\mathrm{e}(\underline{\mathbf{R}},\omega) - \mathrm{j}\,\omega\mu\varepsilon\Phi_\mathrm{m}(\underline{\mathbf{R}},\omega)\right]\;. \qquad (2.101)
\end{aligned}$$

With the Lorenz gauge

$$\boldsymbol{\nabla} \cdot \underline{\mathbf{A}}_{\mathrm{e}}(\underline{\mathbf{R}}, \omega) - \mathrm{j}\,\omega\mu\varepsilon\Phi_{\mathrm{m}}(\underline{\mathbf{R}}, \omega) = 0 \tag{2.102}$$

we obtain from Eq. (2.101)

$$\Delta\underline{\mathbf{A}}_{\mathrm{e}}(\underline{\mathbf{R}}, \omega) + k_{\mathrm{c}}^2\ \underline{\mathbf{A}}_{\mathrm{e}}(\underline{\mathbf{R}}, \omega) = -\varepsilon\underline{\mathbf{J}}_{\mathrm{m}}(\underline{\mathbf{R}}, \omega)\ . \tag{2.103}$$

2.6.4 Expression of the Magnetic Scalar Potential in the Frequency Domain

We recall Maxwell's third equation in frequency domain Eq. (2.36)

$$\boldsymbol{\nabla} \cdot \underline{\mathbf{B}}(\underline{\mathbf{R}}, \omega) = \varrho_{\mathrm{m}}(\underline{\mathbf{R}}, \omega)\,. \tag{2.104}$$

Using the expression electric flux density $\underline{\mathbf{D}}(\underline{\mathbf{R}}, \omega)$ by the potentials according to Eq. (2.85) we obtain

$$\boldsymbol{\nabla} \cdot \left[-\mu\boldsymbol{\nabla}\Phi_{\mathrm{m}}(\underline{\mathbf{R}}, \omega) + \mathrm{j}\,\omega\mu\underline{\mathbf{A}}_{\mathrm{e}}(\underline{\mathbf{R}}, \omega) - \frac{\mu\sigma_{\mathrm{e}}}{\varepsilon}\underline{\mathbf{A}}_{\mathrm{e}}(\underline{\mathbf{R}}, \omega) + \boldsymbol{\nabla}\times\underline{\mathbf{A}}_{\mathrm{m}}(\underline{\mathbf{R}}, \omega)\right] = \varrho_{\mathrm{m}}(\underline{\mathbf{R}}, \omega)\,, \tag{2.105}$$

which is rearranged as

$$\begin{aligned} -\mu\boldsymbol{\nabla}\cdot\boldsymbol{\nabla}\Phi_{\mathrm{m}}(\underline{\mathbf{R}}, \omega) + \mathrm{j}\,\omega\mu\boldsymbol{\nabla}\cdot\underline{\mathbf{A}}_{\mathrm{e}}(\underline{\mathbf{R}}, \omega) - \frac{\mu\sigma_{\mathrm{e}}}{\varepsilon}\boldsymbol{\nabla}\cdot\underline{\mathbf{A}}_{\mathrm{e}}(\underline{\mathbf{R}}, \omega) - \underbrace{\boldsymbol{\nabla}\cdot\boldsymbol{\nabla}\times\underline{\mathbf{A}}_{\mathrm{m}}(\underline{\mathbf{R}}, \omega)}_{=\,\underline{\mathbf{0}}} \\ = \varrho_{\mathrm{m}}(\underline{\mathbf{R}}, \omega) \end{aligned}$$

$$\Rightarrow\quad \Delta\Phi_{\mathrm{m}}(\underline{\mathbf{R}}, \omega) = -\frac{1}{\mu}\varrho_{\mathrm{m}}(\underline{\mathbf{R}}, \omega) + \mathrm{j}\,\omega\boldsymbol{\nabla}\cdot\underline{\mathbf{A}}_{\mathrm{e}}(\underline{\mathbf{R}}, \omega) - \frac{\sigma_{\mathrm{e}}}{\varepsilon}\boldsymbol{\nabla}\cdot\underline{\mathbf{A}}_{\mathrm{e}}(\underline{\mathbf{R}}, \omega)\ . \tag{2.106}$$

Adding on both sides of Eq. (2.106) the term $(\omega^2\mu\varepsilon + \mathrm{j}\,\omega\mu\sigma_{\mathrm{e}})\,\Phi_{\mathrm{m}}(\underline{\mathbf{R}}, \omega)$ results

$$\begin{aligned} &\Delta\Phi_{\mathrm{m}}(\underline{\mathbf{R}}, \omega) + \left(\omega^2\varepsilon\mu + \mathrm{j}\,\omega\mu\sigma_{\mathrm{e}}\right)\Phi_{\mathrm{m}}(\underline{\mathbf{R}}, \omega) \\ &\quad = -\frac{1}{\mu}\varrho_{\mathrm{m}}(\underline{\mathbf{R}}, \omega) + \mathrm{j}\,\omega\boldsymbol{\nabla}\cdot\underline{\mathbf{A}}_{\mathrm{e}}(\underline{\mathbf{R}}, \omega) - \frac{\sigma_{\mathrm{e}}}{\varepsilon}\boldsymbol{\nabla}\cdot\underline{\mathbf{A}}_{\mathrm{e}}(\underline{\mathbf{R}}, \omega) + \omega^2\mu\varepsilon\Phi_{\mathrm{m}}(\underline{\mathbf{R}}, \omega) \\ &\qquad + \mathrm{j}\,\omega\mu\sigma_{\mathrm{e}}\Phi_{\mathrm{m}}(\underline{\mathbf{R}}, \omega)\ . \end{aligned} \tag{2.107}$$

Following Lorenz gauge Eq. (2.102) we show that

$$\begin{aligned} &\boldsymbol{\nabla}\cdot\underline{\mathbf{A}}_{\mathrm{e}}(\underline{\mathbf{R}}, \omega) - \mathrm{j}\,\omega\mu\varepsilon\Phi_{\mathrm{m}}(\underline{\mathbf{R}}, \omega) = 0 \\ \Rightarrow\quad &\boldsymbol{\nabla}\cdot\underline{\mathbf{A}}_{\mathrm{e}}(\underline{\mathbf{R}}, \omega) = \mathrm{j}\,\omega\mu\varepsilon\Phi_{\mathrm{m}}(\underline{\mathbf{R}}, \omega)\ . \end{aligned} \tag{2.108}$$

Inserting Eq. (2.108) into Eq. (2.107) yields

$$\begin{aligned} &\Delta\Phi_{\mathrm{m}}(\underline{\mathbf{R}}, \omega) + \left(\omega^2\varepsilon\mu + \mathrm{j}\,\omega\mu\sigma_{\mathrm{e}}\right)\Phi_{\mathrm{m}}(\underline{\mathbf{R}}, \omega) \\ &\quad = -\frac{1}{\mu}\varrho_{\mathrm{m}}(\underline{\mathbf{R}}, \omega) + \mathrm{j}\,\omega\boldsymbol{\nabla}\cdot\underline{\mathbf{A}}_{\mathrm{e}}(\underline{\mathbf{R}}, \omega) - \mathrm{j}\,\omega\mu\sigma_{\mathrm{e}}\Phi_{\mathrm{m}}(\underline{\mathbf{R}}, \omega) + \omega^2\mu\varepsilon\Phi_{\mathrm{m}}(\underline{\mathbf{R}}, \omega) \\ &\qquad + \mathrm{j}\,\omega\mu\sigma_{\mathrm{e}}\Phi_{\mathrm{m}}(\underline{\mathbf{R}}, \omega) \end{aligned}$$

$$\Rightarrow\quad \Delta\Phi_{\mathrm{m}}(\underline{\mathbf{R}}, \omega) + k_{\mathrm{c}}^2\ \Phi_{\mathrm{m}}(\underline{\mathbf{R}}, \omega) = -\frac{1}{\mu}\varrho_{\mathrm{m}}(\underline{\mathbf{R}}, \omega) + \mathrm{j}\,\omega\left[\boldsymbol{\nabla}\cdot\underline{\mathbf{A}}_{\mathrm{e}}(\underline{\mathbf{R}}, \omega) - \mathrm{j}\,\omega\mu\varepsilon\Phi_{\mathrm{m}}(\underline{\mathbf{R}}, \omega)\right]\ . \tag{2.109}$$

With the Lorenz gauge Eq. (2.102) we obtain

$$\Delta\Phi_{\mathrm{m}}(\underline{\mathbf{R}},\omega) + k_{\mathrm{c}}^2\ \Phi_{\mathrm{m}}(\underline{\mathbf{R}},\omega) = -\frac{1}{\mu}\varrho_{\mathrm{m}}(\underline{\mathbf{R}},\omega)\ . \tag{2.110}$$

2.6.5 Summary of Electromagnetic Potentials in the Frequency Domain

The final expressions for the electric and magnetic vector and scalar potentials are listed from Eq. (2.92), Eq. (2.97), Eq. (2.103) and Eq. (2.110) as

$$\Delta\underline{\mathbf{A}}_{\mathrm{m}}(\underline{\mathbf{R}},\omega) + k_{\mathrm{c}}^2\ \underline{\mathbf{A}}_{\mathrm{m}}(\underline{\mathbf{R}},\omega) = -\mu\underline{\mathbf{J}}_{\mathrm{e}}^{\mathrm{imp}}(\underline{\mathbf{R}},\omega) \tag{2.111}$$

$$\Delta\Phi_{\mathrm{e}}(\underline{\mathbf{R}},\omega) + k_{\mathrm{c}}^2\ \Phi_{\mathrm{e}}(\underline{\mathbf{R}},\omega) = -\frac{1}{\varepsilon}\varrho_{\mathrm{e}}(\underline{\mathbf{R}},\omega) \tag{2.112}$$

$$\Delta\underline{\mathbf{A}}_{\mathrm{e}}(\underline{\mathbf{R}},\omega) + k_{\mathrm{c}}^2\ \underline{\mathbf{A}}_{\mathrm{e}}(\underline{\mathbf{R}},\omega) = -\varepsilon\underline{\mathbf{J}}_{\mathrm{m}}(\underline{\mathbf{R}},\omega) \tag{2.113}$$

$$\Delta\Phi_{\mathrm{m}}(\underline{\mathbf{R}},\omega) + k_{\mathrm{c}}^2\ \Phi_{\mathrm{m}}(\underline{\mathbf{R}},\omega) = -\frac{1}{\mu}\varrho_{\mathrm{m}}(\underline{\mathbf{R}},\omega)\ . \tag{2.114}$$

2.7 Magnetoquasistatic Field

The magnetoquasistatic (MQS) field is defined by using a simple rule of thumb: Lower the time rate of change (frequency) of the driving source so the fields become static (*Haus & Melcher*, 1989). If the electric field vanishes in this process, the field is MQS. As we have discussed earlier, the complex wave number is given by

$$k_{\mathrm{c}} = \sqrt{\omega^2\mu\varepsilon + \mathrm{j}\,\omega\mu\sigma_{\mathrm{e}}}\,. \tag{2.115}$$

For a medium of large electric conductivity σ_{e} we assume

$$\omega\mu\sigma_{\mathrm{e}} \gg \omega^2\mu\varepsilon \qquad \Rightarrow \quad \sigma_{\mathrm{e}} \gg \omega\varepsilon\,, \tag{2.116}$$

which results

$$k_{\mathrm{c}} \approx \sqrt{\mathrm{j}\,\omega\mu\sigma_{\mathrm{e}}}\,. \tag{2.117}$$

However, the real part of the wave number is originated from the diffusion current of the Ampère-Maxwell circuital law and hence, the diffusion part on the right hand side of Eq. (2.35) is approximated as zero, i.e.

$$\mathrm{j}\,\omega\underline{\mathbf{D}}(\underline{\mathbf{R}},\omega) \ \approx\ 0 \tag{2.118}$$

and thus we obtain from Eq. (2.35)

$$\begin{aligned}\boldsymbol{\nabla}\times\underline{\mathbf{H}}(\underline{\mathbf{R}},\omega) &= \sigma_{\mathrm{e}}(\underline{\mathbf{R}})\ \underline{\mathbf{E}}(\underline{\mathbf{R}},\omega) + \underline{\mathbf{J}}_{\mathrm{e}}^{\mathrm{imp}}(\underline{\mathbf{R}},\omega)\\ \boldsymbol{\nabla}\times\left[\frac{1}{\mu(\underline{\mathbf{R}})}\underline{\mathbf{B}}(\underline{\mathbf{R}},\omega)\right] &= \sigma_{\mathrm{e}}(\underline{\mathbf{R}})\ \underline{\mathbf{E}}(\underline{\mathbf{R}},\omega) + \underline{\mathbf{J}}_{\mathrm{e}}^{\mathrm{imp}}(\underline{\mathbf{R}},\omega)\,.\end{aligned} \tag{2.119}$$

Using the magnetoquasistatic approximation the inhomogeneous Helmholtz equation for electric field strength is written using Eq. (2.49) as

$$\Delta\underline{\mathbf{E}}(\underline{\mathbf{R}},\omega) + \mathrm{j}\,\omega\mu\sigma_{\mathrm{e}}\ \underline{\mathbf{E}}(\underline{\mathbf{R}},\omega) = -\,\mathrm{j}\,\omega\mu\ \underline{\mathbf{J}}_{\mathrm{e}}^{\mathrm{imp}}(\underline{\mathbf{R}},\omega) + \frac{1}{\varepsilon}\boldsymbol{\nabla}\varrho_{\mathrm{e}}(\underline{\mathbf{R}},\omega) + \boldsymbol{\nabla}\times\underline{\mathbf{J}}_{\mathrm{m}}(\underline{\mathbf{R}},\omega)$$

$$\Rightarrow\quad \Delta\underline{\mathbf{E}}(\underline{\mathbf{R}},\omega) + k_{\mathrm{c}}^2\ \underline{\mathbf{E}}(\underline{\mathbf{R}},\omega) = -\,\mathrm{j}\,\omega\mu\ \underline{\mathbf{J}}_{\mathrm{e}}^{\mathrm{imp}}(\underline{\mathbf{R}},\omega) + \frac{1}{\varepsilon}\boldsymbol{\nabla}\varrho_{\mathrm{e}}(\underline{\mathbf{R}},\omega) + \boldsymbol{\nabla}\times\underline{\mathbf{J}}_{\mathrm{m}}(\underline{\mathbf{R}},\omega) \tag{2.120}$$

and the expression for magnetic field strength is obtained from Eq. (2.63) by neglecting the term $\mathrm{j}\,\omega\varepsilon\underline{\mathbf{J}}_{\mathrm{m}}(\underline{\mathbf{R}},\omega)$ according to Eq. (2.116) as

$$\Delta\underline{\mathbf{H}}(\underline{\mathbf{R}},\omega) + \mathrm{j}\,\omega\mu\sigma_{\mathrm{e}}\;\underline{\mathbf{H}}(\underline{\mathbf{R}},\omega) = \sigma_{\mathrm{e}}\;\underline{\mathbf{J}}_{\mathrm{m}}(\underline{\mathbf{R}},\omega) + \frac{1}{\mu}\boldsymbol{\nabla}\varrho_{\mathrm{m}}(\underline{\mathbf{R}},\omega) - \boldsymbol{\nabla}\times\underline{\mathbf{J}}_{\mathrm{e}}^{\mathrm{imp}}(\underline{\mathbf{R}},\omega)$$

$$\Rightarrow\quad \Delta\underline{\mathbf{H}}(\underline{\mathbf{R}},\omega) + k_{\mathrm{c}}^2\;\underline{\mathbf{H}}(\underline{\mathbf{R}},\omega) = \sigma_{\mathrm{e}}\;\underline{\mathbf{J}}_{\mathrm{m}}(\underline{\mathbf{R}},\omega) + \frac{1}{\mu}\boldsymbol{\nabla}\varrho_{\mathrm{m}}(\underline{\mathbf{R}},\omega) - \boldsymbol{\nabla}\times\underline{\mathbf{J}}_{\mathrm{e}}^{\mathrm{imp}}(\underline{\mathbf{R}},\omega)\,, \quad (2.121)$$

where

$$k_{\mathrm{c}} = \sqrt{\mathrm{j}\,\omega\mu\sigma_{\mathrm{e}}} \;=\; \sqrt{\mathrm{j}}\,\sqrt{\omega\mu\sigma_{\mathrm{e}}}\,. \quad (2.122)$$

For the square-root of the imaginary unit j we compute

$$\begin{aligned}\sqrt{\mathrm{j}} = \sqrt{\mathrm{e}^{\mathrm{j}\frac{\pi}{2}}} \;&=\; \left(\mathrm{e}^{\mathrm{j}\frac{\pi}{2}}\right)^{\frac{1}{2}} \;=\; \mathrm{e}^{\mathrm{j}\frac{\pi}{4}} \\ &= \cos\frac{\pi}{4} \;+\; \mathrm{j}\,\sin\frac{\pi}{4} \;=\; \frac{1}{\sqrt{2}} \;+\mathrm{j}\,\frac{1}{\sqrt{2}}\;. \end{aligned} \quad (2.123)$$

It follows for the complex wave number

$$\begin{aligned} k_{\mathrm{c}} &= \left(\frac{1}{\sqrt{2}} \;+\; \mathrm{j}\,\frac{1}{\sqrt{2}}\right)\;\sqrt{\omega\mu\sigma_{\mathrm{e}}} \\ &= \sqrt{\frac{\omega\mu\sigma_{\mathrm{e}}}{2}} \;+\; \mathrm{j}\sqrt{\frac{\omega\mu\sigma_{\mathrm{e}}}{2}} \;=\; \Re\{k_{\mathrm{c}}\} \;+\; \mathrm{j}\,\Im\{k_{\mathrm{c}}\}\;. \end{aligned} \quad (2.124)$$

The real part $\Re\{k_{\mathrm{c}}\}$ represents wave propagation and the imaginary part $\Im\{k_{\mathrm{c}}\}$ stands for the attenuation of the electromagnetic waves in conductive medium, whereas Eq. (2.124) states that in magnetoquasistatic case the real part and imaginary part of the complex wave number k_{c} are the same. Again, the electric and magnetic field strength are represented using electric and magnetic scalar and vector potentials are described by Eq. (2.82) and Eq. (2.83). In magnetoquasistatic case, using the approximation Eq. (2.118) we neglect the term $\mathrm{j}\,\omega\underline{\mathbf{A}}_{\mathrm{e}}(\underline{\mathbf{R}},\omega)$ of Eq. (2.83) and thus we obtain

$$\underline{\mathbf{E}}(\underline{\mathbf{R}},\omega) = -\boldsymbol{\nabla}\Phi_{\mathrm{e}}(\underline{\mathbf{R}},\omega) + \mathrm{j}\,\omega\underline{\mathbf{A}}_{\mathrm{m}}(\underline{\mathbf{R}},\omega) - \frac{1}{\varepsilon}\boldsymbol{\nabla}\times\underline{\mathbf{A}}_{\mathrm{e}}(\underline{\mathbf{R}},\omega) \quad (2.125)$$

$$\underline{\mathbf{H}}(\underline{\mathbf{R}},\omega) = -\boldsymbol{\nabla}\Phi_{\mathrm{m}}(\underline{\mathbf{R}},\omega) - \frac{\sigma_{\mathrm{e}}}{\varepsilon}\underline{\mathbf{A}}_{\mathrm{e}}(\underline{\mathbf{R}},\omega) + \frac{1}{\mu}\boldsymbol{\nabla}\times\underline{\mathbf{A}}_{\mathrm{m}}(\underline{\mathbf{R}},\omega)\,. \quad (2.126)$$

2.8 Magnetoquasistatic Field Equations with Magnetic Vector Potential

The magnetic vector potential $\underline{\mathbf{A}}_{\mathrm{m}}(\underline{\mathbf{R}},\omega)$ can be related to the electric field strength $\underline{\mathbf{E}}(\underline{\mathbf{R}},\omega)$ in frequency domain using Eq. (2.125). Neglecting the magnetic sources we find

$$\underline{\mathbf{E}}(\underline{\mathbf{R}},\omega) = \mathrm{j}\,\omega\underline{\mathbf{A}}_{\mathrm{m}}(\underline{\mathbf{R}},\omega) \;-\; \boldsymbol{\nabla}\Phi_{\mathrm{e}}(\underline{\mathbf{R}},\omega)\,, \quad (2.127)$$

which shows the relationship between the electric field strength $\underline{\mathbf{E}}(\underline{\mathbf{R}},\omega)$ with the magnetic vector potential $\underline{\mathbf{A}}_{\mathrm{m}}(\underline{\mathbf{R}},\omega)$. In non-moving conductor case the electric scalar potential term of Eq. (2.127) can be approximated as zero and hence

$$\underline{\mathbf{E}}(\underline{\mathbf{R}},\omega) = \mathrm{j}\,\omega\underline{\mathbf{A}}_{\mathrm{m}}(\underline{\mathbf{R}},\omega)\,. \quad (2.128)$$

Using magnetic vector potential $\underline{\mathbf{A}}_{\mathrm{m}}(\underline{\mathbf{R}},\omega)$ we rewrite Eq. (2.119) as

$$\boldsymbol{\nabla}\times\left[\nu(\underline{\mathbf{R}})\boldsymbol{\nabla}\times\underline{\mathbf{A}}_{\mathrm{m}}(\underline{\mathbf{R}},\omega)\right]-\,\mathrm{j}\,\omega\sigma_{\mathrm{e}}(\underline{\mathbf{R}})\;\underline{\mathbf{A}}_{\mathrm{m}}(\underline{\mathbf{R}},\omega)=\underline{\mathbf{J}}_{\mathrm{e}}^{\mathrm{imp}}(\underline{\mathbf{R}},\omega)\,, \tag{2.129}$$

where $\nu(\underline{\mathbf{R}})=1/\mu(\underline{\mathbf{R}})$. Eq. (2.129) represents the magnetic diffusion equation in frequency domain with magnetic vector potential for a medium of inhomogeneous permeability $\mu(\underline{\mathbf{R}})$ and electric conductivity $\sigma_{\mathrm{e}}(\underline{\mathbf{R}})$, whereas Eq. (2.111) describes magnetic vector potential for a medium of homogeneous $\mu(\underline{\mathbf{R}})$ and $\sigma_{\mathrm{e}}(\underline{\mathbf{R}})$. Rewriting Eq. (2.129) in integral form results

$$\iint\limits_{S}\boldsymbol{\nabla}\times\left[\nu(\underline{\mathbf{R}})\;\boldsymbol{\nabla}\times\underline{\mathbf{A}}_{\mathrm{m}}(\underline{\mathbf{R}},\omega)\right]\cdot\underline{\mathbf{dS}}-\iint\limits_{S}\mathrm{j}\,\omega\sigma_{\mathrm{e}}(\underline{\mathbf{R}})\;\underline{\mathbf{A}}_{\mathrm{m}}(\underline{\mathbf{R}},\omega)\cdot\underline{\mathbf{dS}}\;=\;\iint\limits_{S}\underline{\mathbf{J}}_{\mathrm{e}}^{\mathrm{imp}}(\underline{\mathbf{R}},\omega)\cdot\underline{\mathbf{dS}}\,. \tag{2.130}$$

Let us apply the Stoke's Theorem on the double Curl term of Eq. (2.130) and thus we obtain

$$\oint\limits_{C=\partial S}\left[\nu(\underline{\mathbf{R}})\;\boldsymbol{\nabla}\times\underline{\mathbf{A}}_{\mathrm{m}}(\underline{\mathbf{R}},\omega)\right]\cdot\underline{\mathbf{dR}}-\iint\limits_{S}\mathrm{j}\,\omega\sigma_{\mathrm{e}}(\underline{\mathbf{R}})\;\underline{\mathbf{A}}_{\mathrm{m}}(\underline{\mathbf{R}},\omega)\cdot\underline{\mathbf{dS}}\;=\;\iint\limits_{S}\underline{\mathbf{J}}_{\mathrm{e}}^{\mathrm{imp}}(\underline{\mathbf{R}},\omega)\cdot\underline{\mathbf{dS}}\,, \tag{2.131}$$

which describes the magnetoquasistatic problem in the frequency domain with magnetic vector potential. Eq. (2.131) is considered as the governing equation for the solution of the eddy current problem by the finite integration technique (FIT) in chapter 3 and by the finite element method (FEM) in chapter 4, where we determine the unknown values of the magnetic vector potential $\underline{\mathbf{A}}_{\mathrm{m}}(\underline{\mathbf{R}},\omega)$ to solve the magnetoquasistatic problem.

2.9 Transition and Boundary Conditions for the Magnetic Vector Potential

The transition and boundary conditions have to be considered while discretizing the governing equation Eq. (2.131) by FIT or FEM for unknown values of $\underline{\mathbf{A}}_{\mathrm{m}}(\underline{\mathbf{R}},\omega)$. For the magnetic vector potential the Coulomb gauge states that

$$\boldsymbol{\nabla}\cdot\underline{\mathbf{A}}_{\mathrm{m}}(\underline{\mathbf{R}},t)=0\,, \tag{2.132}$$

which is written in integral form as

$$\oiint\limits_{S=\partial V}\underline{\mathbf{A}}_{\mathrm{m}}(\underline{\mathbf{R}},t)\cdot\underline{\mathbf{dS}}=0\,. \tag{2.133}$$

We solve the integral for an elementary surface ΔS and thus we obtain

$$\begin{aligned}&\left[\underline{\mathbf{A}}_{\mathrm{m}}^{(2)}(\underline{\mathbf{R}},t)-\underline{\mathbf{A}}_{\mathrm{m}}^{(1)}(\underline{\mathbf{R}},t)\right]\cdot\underline{\mathbf{n}}\;\Delta S=0\\ &\Rightarrow\underline{\mathbf{n}}\cdot\left[\underline{\mathbf{A}}_{\mathrm{m}}^{(2)}(\underline{\mathbf{R}},t)-\underline{\mathbf{A}}_{\mathrm{m}}^{(1)}(\underline{\mathbf{R}},t)\right]=0\end{aligned} \tag{2.134}$$

and in the frequency domain:

$$\underline{\mathbf{n}}\cdot\left[\underline{\mathbf{A}}_{\mathrm{m}}^{(2)}(\underline{\mathbf{R}},\omega)-\underline{\mathbf{A}}_{\mathrm{m}}^{(1)}(\underline{\mathbf{R}},\omega)\right]=0\,, \tag{2.135}$$

which means the normal component of the magnetic vector potential $\underline{\mathbf{A}}_{\mathrm{m}}(\underline{\mathbf{R}}, t)$ is continuous at the transition interface. Again, for a source free transition interface, rewriting Eq. (2.19) in the frequency domain results

$$\underline{\mathbf{n}} \times \left[\underline{\mathbf{E}}^{(2)}(\underline{\mathbf{R}}, \omega) - \underline{\mathbf{E}}^{(1)}(\underline{\mathbf{R}}, \omega) \right] = \underline{\mathbf{0}} \,. \tag{2.136}$$

Inserting Eq. (2.128) in Eq. (2.136) yields

$$\begin{aligned} \underline{\mathbf{n}} \times \left\{ \mathrm{j}\,\omega \left[\underline{\mathbf{A}}_{\mathrm{m}}^{(2)}(\underline{\mathbf{R}}, \omega) - \underline{\mathbf{A}}_{\mathrm{m}}^{(1)}(\underline{\mathbf{R}}, \omega) \right] \right\} &= \underline{\mathbf{0}} \\ \Rightarrow \underline{\mathbf{n}} \times \left[\underline{\mathbf{A}}_{\mathrm{m}}^{(2)}(\underline{\mathbf{R}}, \omega) - \underline{\mathbf{A}}_{\mathrm{m}}^{(1)}(\underline{\mathbf{R}}, \omega) \right] &= \underline{\mathbf{0}} \,, \end{aligned} \tag{2.137}$$

which states that the tangential component of the magnetic vector potential $\underline{\mathbf{A}}_{\mathrm{m}}(\underline{\mathbf{R}}, \omega)$ is continuous at the transition interface.

To define the PEC boundary condition for the magnetic vector potential we set $\underline{\mathbf{A}}_{\mathrm{m}}^{(1)}(\underline{\mathbf{R}}, \omega) = \underline{\mathbf{0}}$ in Eq. (2.143) which results

$$\underline{\mathbf{n}} \cdot \left[\underline{\mathbf{A}}_{\mathrm{m}}^{(2)}(\underline{\mathbf{R}}, \omega) \right] = 0 \qquad \text{i.e.,} \qquad \underline{\mathbf{n}} \cdot \underline{\mathbf{A}}_{\mathrm{m}}(\underline{\mathbf{R}}, \omega) = 0 \tag{2.138}$$

and from Eq. (2.137) we obtain

$$\underline{\mathbf{n}} \times \underline{\mathbf{A}}_{\mathrm{m}}(\underline{\mathbf{R}}, t) = \underline{\mathbf{0}} \,. \tag{2.139}$$

We sum up from Eq. (2.138) and Eq. (2.139) that the tangential and normal components of the magnetic vector potential diminish at the PEC boundary. The transition and boundary conditions of the magnetic vector potential will be discussed further in chapter 3 and 4 for FIT and FEM, respectively.

2.10 Field Equations for a Moving Conductor

Maxwell's equations in their differential and integral form are valid for any stationary media. However, Maxwell's third and fourth equation are not affected by the motion of the medium (*Poljak & Brebbia*, 2005). On the other hand, the extension of the law of induction, expressed by Maxwell's first equation for a moving medium, requires considerable care. The governing equations for the modeling of an eddy current sensor in a moving conductor are Maxwell's equations for a moving medium, where the first one read (*Rothwell & Cloud*, 2001)

$$\boldsymbol{\nabla} \times \underline{\mathbf{E}}(\underline{\mathbf{R}}, t) = -\frac{\partial}{\partial t} \underline{\mathbf{B}}(\underline{\mathbf{R}}, t) - \underline{\mathbf{J}}_{\mathrm{m}}(\underline{\mathbf{R}}, t) + \boldsymbol{\nabla} \times \left[\underline{\mathbf{v}}_{\mathrm{c}}(\underline{\mathbf{R}}, t) \times \underline{\mathbf{B}}(\underline{\mathbf{R}}, t) \right] \,, \tag{2.140}$$

which is derived from Maxwell's equations in integral form by using the Helmholtz transport theorem (*Rothwell & Cloud*, 2001; *Tai*, 1997). Neglecting the magnetic current density $\underline{\mathbf{J}}_{\mathrm{m}}(\underline{\mathbf{R}}, t)$ results

$$\boldsymbol{\nabla} \times \underline{\mathbf{E}}(\underline{\mathbf{R}}, t) = -\frac{\partial}{\partial t} \underline{\mathbf{B}}(\underline{\mathbf{R}}, t) + \boldsymbol{\nabla} \times \left[\underline{\mathbf{v}}_{\mathrm{c}}(\underline{\mathbf{R}}, t) \times \underline{\mathbf{B}}(\underline{\mathbf{R}}, t) \right] \,. \tag{2.141}$$

Using magnetic vector potential $\underline{\mathbf{A}}_{\mathrm{m}}(\underline{\mathbf{R}},t)$ we rewrite Eq. (2.141) as

$$\begin{aligned}
&\boldsymbol{\nabla}\times\underline{\mathbf{E}}(\underline{\mathbf{R}},t) = -\frac{\partial}{\partial t}\left[\boldsymbol{\nabla}\times\underline{\mathbf{A}}_{\mathrm{m}}(\underline{\mathbf{R}},t)\right] + \boldsymbol{\nabla}\times\left[\underline{\mathbf{v}}_{\mathrm{c}}(\underline{\mathbf{R}},t)\times\boldsymbol{\nabla}\times\underline{\mathbf{A}}_{\mathrm{m}}(\underline{\mathbf{R}},t)\right] \\
\Rightarrow\quad &\boldsymbol{\nabla}\times\underbrace{\left[\underline{\mathbf{E}}(\underline{\mathbf{R}},t) + \frac{\partial\underline{\mathbf{A}}_{\mathrm{m}}(\underline{\mathbf{R}},t)}{\partial t} - \underline{\mathbf{v}}_{\mathrm{c}}(\underline{\mathbf{R}},t)\times\boldsymbol{\nabla}\times\underline{\mathbf{A}}_{\mathrm{m}}(\underline{\mathbf{R}},t)\right]}_{=-\boldsymbol{\nabla}\Phi_{\mathrm{e}}(\underline{\mathbf{R}},t)} = \underline{\mathbf{0}}\,. \qquad (2.142)
\end{aligned}$$

Using electric scalar potential $\Phi_{\mathrm{e}}(\underline{\mathbf{R}},t)$ we obtain

$$\begin{aligned}
&\underline{\mathbf{E}}(\underline{\mathbf{R}},t) + \frac{\partial\underline{\mathbf{A}}_{\mathrm{m}}(\underline{\mathbf{R}},t)}{\partial t} - \underline{\mathbf{v}}_{\mathrm{c}}(\underline{\mathbf{R}},t)\times\boldsymbol{\nabla}\times\underline{\mathbf{A}}_{\mathrm{m}}(\underline{\mathbf{R}},t) = -\boldsymbol{\nabla}\Phi_{\mathrm{e}}(\underline{\mathbf{R}},t) \\
\Rightarrow\quad &\underline{\mathbf{E}}(\underline{\mathbf{R}},t) = -\frac{\partial\underline{\mathbf{A}}_{\mathrm{m}}(\underline{\mathbf{R}},t)}{\partial t} + \underline{\mathbf{v}}_{\mathrm{c}}(\underline{\mathbf{R}},t)\times\boldsymbol{\nabla}\times\underline{\mathbf{A}}_{\mathrm{m}}(\underline{\mathbf{R}},t) - \boldsymbol{\nabla}\Phi_{\mathrm{e}}(\underline{\mathbf{R}},t)\,. \qquad (2.143)
\end{aligned}$$

Formulating Eq. (2.143) in frequency domain yields

$$\underline{\mathbf{E}}(\underline{\mathbf{R}},\omega) = \mathrm{j}\,\omega\underline{\mathbf{A}}_{\mathrm{m}}(\underline{\mathbf{R}},\omega) + \underline{\mathbf{v}}_{\mathrm{c}}\times\boldsymbol{\nabla}\times\underline{\mathbf{A}}_{\mathrm{m}}(\underline{\mathbf{R}},\omega) - \boldsymbol{\nabla}\Phi_{\mathrm{e}}(\underline{\mathbf{R}},\omega)\,. \qquad (2.144)$$

Using equation Eq. (2.131) we arrive at the magnetic diffusion equation for a moving conductor

$$\begin{aligned}
&\boldsymbol{\nabla}\times\left[\nu(\underline{\mathbf{R}})\boldsymbol{\nabla}\times\underline{\mathbf{A}}_{\mathrm{m}}(\underline{\mathbf{R}},\omega)\right] - \sigma_{\mathrm{e}}(\underline{\mathbf{R}})\left[\mathrm{j}\,\omega\ \underline{\mathbf{A}}_{\mathrm{m}}(\underline{\mathbf{R}},\omega) + \underline{\mathbf{v}}_{\mathrm{c}}\times\boldsymbol{\nabla}\times\underline{\mathbf{A}}_{\mathrm{m}}(\underline{\mathbf{R}},\omega) - \boldsymbol{\nabla}\Phi_{\mathrm{e}}(\underline{\mathbf{R}},\omega)\right] \\
&\qquad = \underline{\mathbf{J}}_{\mathrm{e}}^{\mathrm{imp}}(\underline{\mathbf{R}},\omega)\,. \qquad (2.145)
\end{aligned}$$

For a medium of homogeneous μ Eq. (2.145) is simplified to

$$\begin{aligned}
&\Delta\underline{\mathbf{A}}_{\mathrm{m}}(\underline{\mathbf{R}},\omega) + \mu\sigma_{\mathrm{e}}(\underline{\mathbf{R}})\left[\mathrm{j}\,\omega\ \underline{\mathbf{A}}_{\mathrm{m}}(\underline{\mathbf{R}},\omega) + \underline{\mathbf{v}}_{\mathrm{c}}\times\boldsymbol{\nabla}\times\underline{\mathbf{A}}_{\mathrm{m}}(\underline{\mathbf{R}},\omega) - \boldsymbol{\nabla}\Phi_{\mathrm{e}}(\underline{\mathbf{R}},\omega)\right] \\
&\qquad = -\mu\underline{\mathbf{J}}_{\mathrm{e}}^{\mathrm{imp}}(\underline{\mathbf{R}},\omega)\,. \qquad (2.146)
\end{aligned}$$

Chapter 3

Finite Integration Technique (FIT)

Historically, the finite integration technique (FIT) was first applied to the full sets of Maxwell's equations in integral form (*Weiland*, 1977). The method uses all six vector components of electric field strength and magnetic flux density on a dual grid system (*Marklein*, 2002). In our case, FIT is used for the direct discretisation of the governing equation of magnetoquasistatics. As described eddy current sensors are driven by a monochromatic excitation pulse, it is easier to solve the magnetoquasistaic problem in the frequency domain than in the time domain. The governing equations in integral form are then discretized on a staggered voxel grid in space. The allocation of the vector components satisfies the transition conditions "automatically", if the inhomogeneous material is discretised (*Marklein*, 1997, 2002). The following steps should be followed to solve a magnetoquasistaic problem using FIT:

- Discretization of electromagnetic medium in space (Sec. 3.1)
- Allocation of the discrete field quantities (Sec. 3.2)
- Setting up the discrete field quantities and derivation of the grid equation in cartesian coordinates (Sec. 3.3-3.4)
- Derivation of the grid equation in cylindrical coordinates (Sec. 3.5-3.6)
- Implementation of the boundary condition (Sec. 3.7)
- Formation of a band matrix (Sec. 3.8)

3.1 Discretization of the Electromagnetic Medium in Space

The governing equation of a magnetoquasistatic problem in the frequency domain can be recalled from Chapter 2 as

$$\oint\limits_{C=\partial S} [\nu(\underline{\mathbf{R}})\ \boldsymbol{\nabla}\times\underline{\mathbf{A}}_{\mathrm{m}}(\underline{\mathbf{R}},\omega)]\cdot\underline{\mathbf{dR}}\ -\ \iint\limits_{S} \mathrm{j}\,\omega\ \sigma_{\mathrm{e}}(\underline{\mathbf{R}})\ \underline{\mathbf{A}}_{\mathrm{m}}(\underline{\mathbf{R}},\omega)\cdot\underline{\mathbf{dS}}\ =\ \iint\limits_{S}\underline{\mathbf{J}}_{\mathrm{e}}^{\mathrm{imp}}(\underline{\mathbf{R}},\omega)\cdot\underline{\mathbf{dS}}\ . \tag{3.1}$$

Before we start with the discretization of the governing equation, we have to define the discretization of the medium in material cells. The discretization of the electromagnetic medium $\mathcal{M}_{\mathrm{em}}$ is defined as follows:

- The material cells $m^{(n)}$ of the material grid M has a constant material filling and coincides with the grid cells $g^{(n)}$ of the grid G, i. e.

$$m^{(n)} = g^{(n)} .$$

- the material cells $m^{(n)}$ is addressed with the grid node n in the center point of the grid cell $g^{(n)}$ of the grid G

$$\{\underline{\underline{\boldsymbol{\mu}}}(\underline{\mathbf{R}}), \underline{\underline{\boldsymbol{\sigma}}}_{\mathrm{e}}(\underline{\mathbf{R}})\} , \underline{\mathbf{R}} \in \mathbb{R}^3 \quad \Rightarrow \quad \{\underline{\underline{\boldsymbol{\mu}}}^{(n)}, \underline{\underline{\boldsymbol{\sigma}}}_{\mathrm{e}}^{(n)}\} , n \in \mathbb{R}^N ,$$

where all material tensors have the form

$$\underline{\underline{\boldsymbol{\mu}}} = \mu_{ii} \, \underline{\mathbf{e}}_i \underline{\mathbf{e}}_i .$$

3.2 Allocation of the Discrete Field Quantities in Cartesian Coordinates

The governing equation, along with the transition and boundary conditions, prescribe the allocation of the discrete electromagnetic field components. Instead of deriving the allocation while discretizing the governing equations, we define the allocation of the discrete electromagnetic field components as it follows. The allocation of the discrete field components has to be performed in that way, that only continuous field component are allocated at the boundary $\partial m^{(n)}$ of next nairbour material cells $m^{(n)}$, in order to ensure the transition conditions, which read for a source–free interface

$$\underline{\mathbf{n}} \cdot \underline{\mathbf{B}}(\underline{\mathbf{R}}, \omega) = \text{continous} \tag{3.2}$$

and using the Coulomb gauge we write the transition condition for the magnetic vector potential $\underline{\mathbf{A}}_{\mathrm{m}}(\underline{\mathbf{R}}, \omega)$ from Eq. (2.134) as

$$\underline{\mathbf{n}} \cdot \underline{\mathbf{A}}_{\mathrm{m}}(\underline{\mathbf{R}}, \omega) = \text{continous} . \tag{3.3}$$

For a source-free interface the tangential component of the electric field strength and the normal component of the magnetic flux density must be continuous. We define the allocation of the discrete electromagnetic field quantities as follows:

- the three Cartesian components of the magnetic vector potential vector $\mathrm{A}_i^{(n)}$ are positioned at the center of the edges of the material cell $m^{(n)}$ and each Cartesian component points in positive coordinate direction.

- the three Cartesian components of the magnetic flux density vector $\mathrm{B}_i^{(n)}$ are positioned at the center of the edges of the facet with the normal vector $\underline{\mathbf{n}} = \underline{\mathbf{e}}_i$ of the material cell $m^{(n)}$ and points in positive coordinate direction.

- the three Cartesian components $\mathrm{J}_{\mathrm{m},i}^{(n)}$– and $\mathrm{H}_i^{(n)}$ coincide with the $\mathrm{B}_i^{(n)}$ components.

- the three Cartesian components $\mathrm{J}_{\mathrm{e},i}^{(n)}$–, and $\mathrm{D}_i^{(n)}$ components coincide with the $\mathrm{A}_i^{(n)}$ components.

Fig. 3.1 shows the allocation of the discrete electromagnetic field components assigned to the global grid node n. This allocation ensures that only normal components of the magnetic flux density and only tangential components of the electric field strength are positioned at the interface between material cells with different material properties. The transition conditions Eqs. (3.2)-(3.3) are ensured in a natural way.

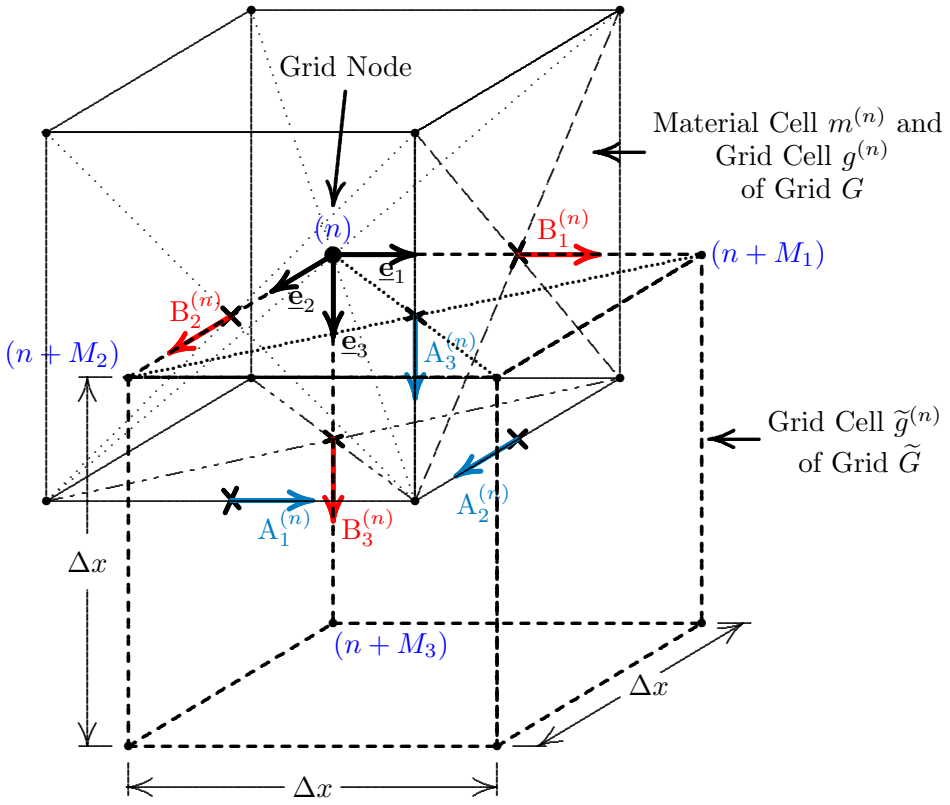

Figure 3.1: Allocation of the discrete magnetic field components $\mathrm{A}_1^{(n)}$, $\mathrm{A}_2^{(n)}$, $\mathrm{A}_3^{(n)}$, $\mathrm{B}_1^{(n)}$, $\mathrm{B}_2^{(n)}$, and $\mathrm{B}_3^{(n)}$ assigned to the global grid node (n)

3.3 Discrete Field Quantities in Cartesian Coordinates in 2-D case

We have discussed in Chapter 2 that the encircling coil sensors can be simulated using the rotational symmetry and therefore, a 3-D magnetoquasistatic problem can be reduced into a 2-D problem in cylindrical coordinates. As the first step, the discrete field quantities will be discussed in cartesian coordinates in this section. Fig. 3.1 can be reduced to Fig. 3.2 for 2-D case, which shows the integration cell $I_{A_y}^{(n)}$. We define the allocation of the discrete field quantities as follows:

- The y component of magnetic vector potential A_y is positioned at the corners of the material cells, as for example, $A_y^{(n)}$ is positioned at the common node of the four material cells $m^{(n)}$, $m^{(n+M_x)}$, $m^{(n+M_z)}$, and $m^{(n+M_x+M_z)}$ and it points the normal direction of the xz plane.

- The x and z components of the magnetic flux density vector $B_x^{(n)}$, $B_z^{(n)}$, $B_x^{(n+M_z)}$, and $B_z^{(n+M_x)}$ are positioned at the center of the edges of the facet and each component points the tangential directions to the surface.

- The y component of electric current density $J_{ey}^{(n)}$ is positioned at the center of the material cell $m^{(n)}$. Similarly, $J_{ey}^{(n+M_x)}$, $J_{ey}^{(n+M_z)}$, and $J_{ey}^{(n+M_x+M_z)}$ are positioned at the center of corresponding material cells.

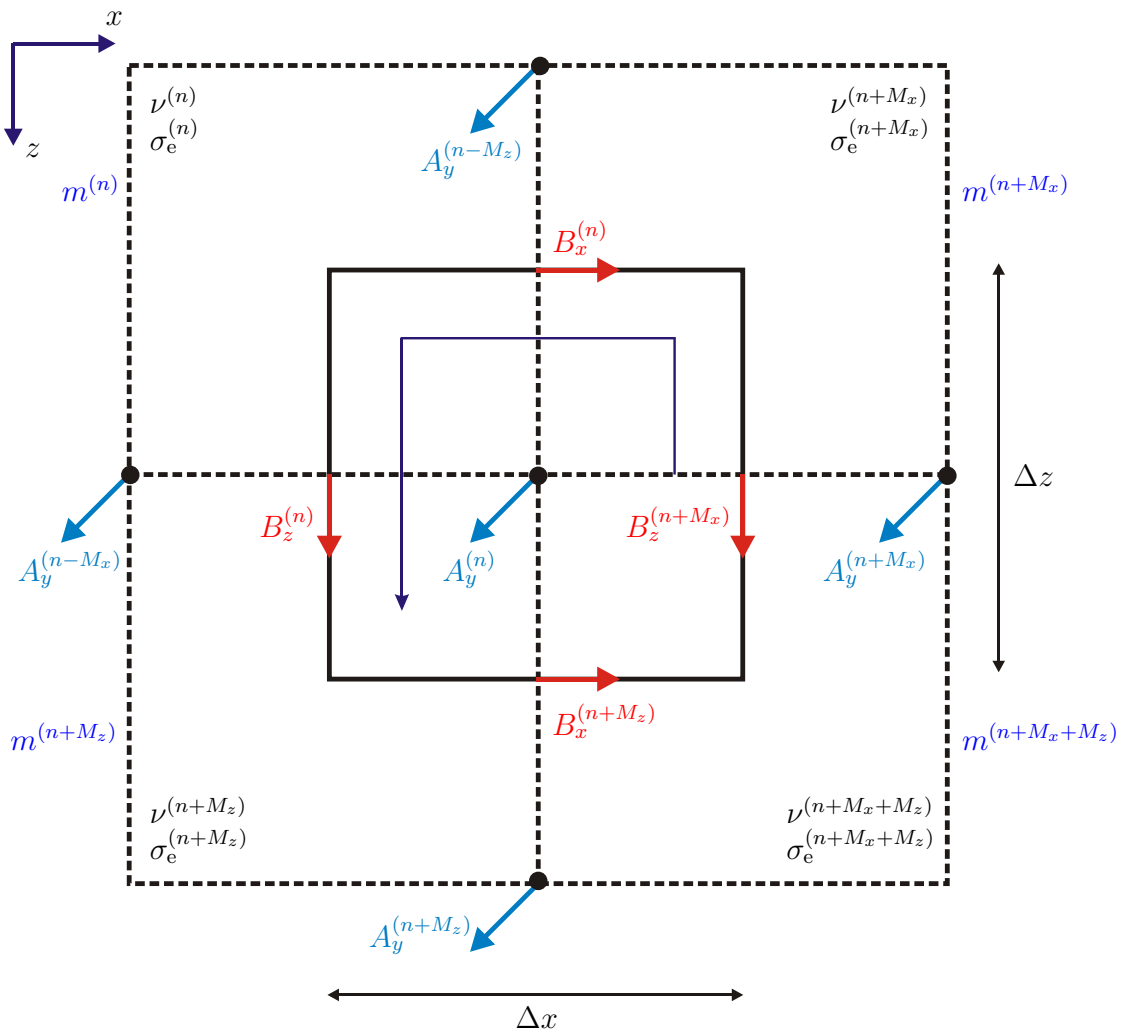

Figure 3.2: Allocation of the discrete electromagnetic field components B_x, B_z, and A_y assigned to the global grid node (n) in 2-D case in cartesian coordinates.

3.4 Derivation of the Discrete Grid Equation in Cartesian Coordinates in 2-D case

The discrete grid equation in cartesian coordinates can be computed by discretizing the governing equation Eq. (3.1) using the following steps:

1. The line integral contains a curl operator which can be computed in the cartesian coordinates as:

$$\nabla \times \underline{\mathbf{A}}_m(\underline{\mathbf{R}}, \omega) = \left[\frac{\partial A_z(\omega)}{\partial y} - \frac{\partial A_y(\omega)}{\partial z}\right] \underline{\mathbf{e}}_x + \left[\frac{\partial A_x(\omega)}{\partial z} - \frac{\partial A_z(\omega)}{\partial x}\right] \underline{\mathbf{e}}_y + \left[\frac{\partial A_y(\omega)}{\partial x} - \frac{\partial A_x(\omega)}{\partial y}\right] \underline{\mathbf{e}}_z \ . \tag{3.4}$$

As we are computing in xz plane and are considering only the y component of magnetic vector potential, The curl operator can be reduced to

$$\nabla \times \underline{\mathbf{A}}_m(\underline{\mathbf{R}}, \omega) = -\frac{\partial A_y(\omega)}{\partial z} \underline{\mathbf{e}}_x + \frac{\partial A_y(\omega)}{\partial x} \underline{\mathbf{e}}_z \ . \tag{3.5}$$

2. Furthermore, the line integral can be divided into four parts, named as: 'Up', 'down', 'Left', and 'Right' integral, which results

$$\int\limits_{C^{(u)}} [\nu(\underline{\mathbf{R}})\boldsymbol{\nabla}\times\underline{\mathbf{A}}_{\mathrm{m}}(\underline{\mathbf{R}},\omega)] \cdot \underline{\mathbf{dR}} = \int\limits_{C^{(u)}} \nu^{(u)} \left[-\frac{\partial A_y(\omega)}{\partial z}\underline{\mathbf{e}}_x + \frac{\partial A_y(\omega)}{\partial x}\underline{\mathbf{e}}_z\right] \cdot \underline{\mathbf{e}}_x \mathrm{d}x$$

$$\Rightarrow \int\limits_{C^{(u)}} [\nu(\underline{\mathbf{R}})\ \underline{\mathbf{B}}(\underline{\mathbf{R}},\omega)] \cdot \underline{\mathbf{dR}} = \int\limits_{C^{(u)}} \nu^{(u)} \left[-\frac{\partial A_y(\omega)}{\partial z}\right] \mathrm{d}x \ . \tag{3.6}$$

$$\int\limits_{C^{(d)}} [\nu(\underline{\mathbf{R}})\boldsymbol{\nabla}\times\underline{\mathbf{A}}_{\mathrm{m}}(\underline{\mathbf{R}},\omega)] \cdot \underline{\mathbf{dR}} = \int\limits_{C^{(d)}} \nu^{(d)} \left[-\frac{\partial A_y(\omega)}{\partial z}\underline{\mathbf{e}}_x + \frac{\partial A_y(\omega)}{\partial x}\underline{\mathbf{e}}_z\right] \cdot \underline{\mathbf{e}}_x \mathrm{d}x$$

$$\Rightarrow \int\limits_{C^{(d)}} [\nu(\underline{\mathbf{R}})\ \underline{\mathbf{B}}(\underline{\mathbf{R}},\omega)] \cdot \underline{\mathbf{dR}} = \int\limits_{C^{(d)}} \nu^{(d)} \left[-\frac{\partial A_y(\omega)}{\partial z}\right] \mathrm{d}x \ . \tag{3.7}$$

$$\int\limits_{C^{(l)}} [\nu(\underline{\mathbf{R}})\boldsymbol{\nabla}\times\underline{\mathbf{A}}_{\mathrm{m}}(\underline{\mathbf{R}},\omega)] \cdot \underline{\mathbf{dR}} = \int\limits_{C^{(l)}} \nu^{(l)} \left[-\frac{\partial A_y(\omega)}{\partial z}\underline{\mathbf{e}}_x + \frac{\partial A_y(\omega)}{\partial x}\underline{\mathbf{e}}_z\right] \cdot \underline{\mathbf{e}}_z \mathrm{d}z$$

$$\Rightarrow \int\limits_{C^{(l)}} [\nu(\underline{\mathbf{R}})\ \underline{\mathbf{B}}(\underline{\mathbf{R}},\omega)] \cdot \underline{\mathbf{dR}} = \int\limits_{C^{(l)}} \nu^{(l)} \left[+\frac{\partial A_y(\omega)}{\partial x}\right] \mathrm{d}z \ . \tag{3.8}$$

$$\int\limits_{C^{(r)}} [\nu(\underline{\mathbf{R}})\boldsymbol{\nabla}\times\underline{\mathbf{A}}_{\mathrm{m}}(\underline{\mathbf{R}},\omega)] \cdot \underline{\mathbf{dR}} = \int\limits_{C^{(r)}} \nu^{(r)} \left[-\frac{\partial A_y(\omega)}{\partial z}\underline{\mathbf{e}}_x + \frac{\partial A_y(\omega)}{\partial x}\underline{\mathbf{e}}_z\right] \cdot \underline{\mathbf{e}}_z \mathrm{d}z$$

$$\Rightarrow \int\limits_{C^{(r)}} [\nu(\underline{\mathbf{R}})\ \underline{\mathbf{B}}(\underline{\mathbf{R}},\omega)] \cdot \underline{\mathbf{dR}} = \int\limits_{C^{(r)}} \nu^{(r)} \left[+\frac{\partial A_y(\omega)}{\partial x}\right] \mathrm{d}z \ . \tag{3.9}$$

3. The component $A_y^{(n)}$ is positioned in the center of the integration cell $I_{A_y}^{(n)}$. By using the right-hand rule, the line integral can be shown as a sum of these four integrals as

$$\begin{aligned}
&\oint\limits_{C=\partial S} [\nu(\underline{\mathbf{R}})\boldsymbol{\nabla}\times\underline{\mathbf{A}}_{\mathrm{m}}((\underline{\mathbf{R}},\omega)] \cdot \underline{\mathbf{dR}} \\
&\quad = \int\limits_{C^{(d)}} [\nu(\underline{\mathbf{R}})\ \underline{\mathbf{B}}(\underline{\mathbf{R}},\omega)] \cdot \underline{\mathbf{dR}} \ - \int\limits_{C^{(u)}} [\nu(\underline{\mathbf{R}})\ \underline{\mathbf{B}}(\underline{\mathbf{R}},\omega)] \cdot \underline{\mathbf{dR}} \\
&\quad + \int\limits_{C^{(l)}} [\nu(\underline{\mathbf{R}})\ \underline{\mathbf{B}}(\underline{\mathbf{R}},\omega)] \cdot \underline{\mathbf{dR}} \ - \int\limits_{C^{(r)}} [\nu(\underline{\mathbf{R}})\ \underline{\mathbf{B}}(\underline{\mathbf{R}},\omega)] \cdot \underline{\mathbf{dR}} \\
&\quad = \int\limits_{C^{(d)}} \nu^{(d)}\mathrm{B}_x^{(d)}(\omega)\,\mathrm{d}x - \int\limits_{C^{(u)}} \nu^{(u)}\mathrm{B}_x^{(u)}(\omega)\,\mathrm{d}x + \int\limits_{C^{(l)}} \nu^{(l)}\mathrm{B}_z^{(l)}(\omega)\,\mathrm{d}z - \int\limits_{C^{(r)}} \nu^{(r)}\mathrm{B}_z^{(r)}(\omega)\,\mathrm{d}z \ .
\end{aligned} \tag{3.10}$$

4. The cells are considered to be quadratic and therefore, $\Delta z = \Delta x$.

5. The other two integrals of Eq. (3.1) are surface integrals and can be computed directly.

6. Average values of material parameters $\nu(\underline{\mathbf{R}})$ and $\sigma_{\mathrm{e}}(\underline{\mathbf{R}})$ should be taken while computing the integrals.

Up: Fig. 3.3a shows the upper part of the integration cell $I_{A_y}^{(n)}$. We can write from Eq. (3.6) that

$$\begin{aligned}
\int\limits_{C^{(u)}} \nu^{(u)} B_x^{(u)}(\omega)\,\mathrm{d}x &= \int\limits_{C^{(u)}} \frac{\nu^{(n)}+\nu^{(n+M_x)}}{2} B_x^{(n)}(\omega)\,\mathrm{d}x \\
&= \frac{\nu^{(n)}+\nu^{(n+M_x)}}{2}\left[\frac{A_y^{(n-M_z)}(\omega)-A_y^{(n)}(\omega)}{\Delta z^{(n)}}\right]\Delta x^{(n)} + \mathcal{O}\left[(\Delta x)^3\right] \\
&\approx \frac{\nu^{(n)}+\nu^{(n+M_x)}}{2}\left[A_y^{(n-M_z)}(\omega)-A_y^{(n)}(\omega)\right]\frac{\Delta x}{\Delta z} \\
&= \nu_{\mathrm{H}_x}^{(n)}\left[A_y^{(n-M_z)}(\omega)-A_y^{(n)}(\omega)\right] \quad , \qquad (3.11)
\end{aligned}$$

where $\nu_{\mathrm{H}_x}^{(n)}$ will be computed by averaging the magnetic impermeability of the cells $m^{(n)}$ and $m^{(n+M_x)}$ as

$$\nu_{\mathrm{H}_x}^{(n)} = \frac{\nu^{(n)}+\nu^{(n+M_x)}}{2} \quad . \qquad (3.12)$$

Down: The lower part of the integration cell $I_{A_y}^{(n)}$ (Fig. 3.3b) will be considered here.

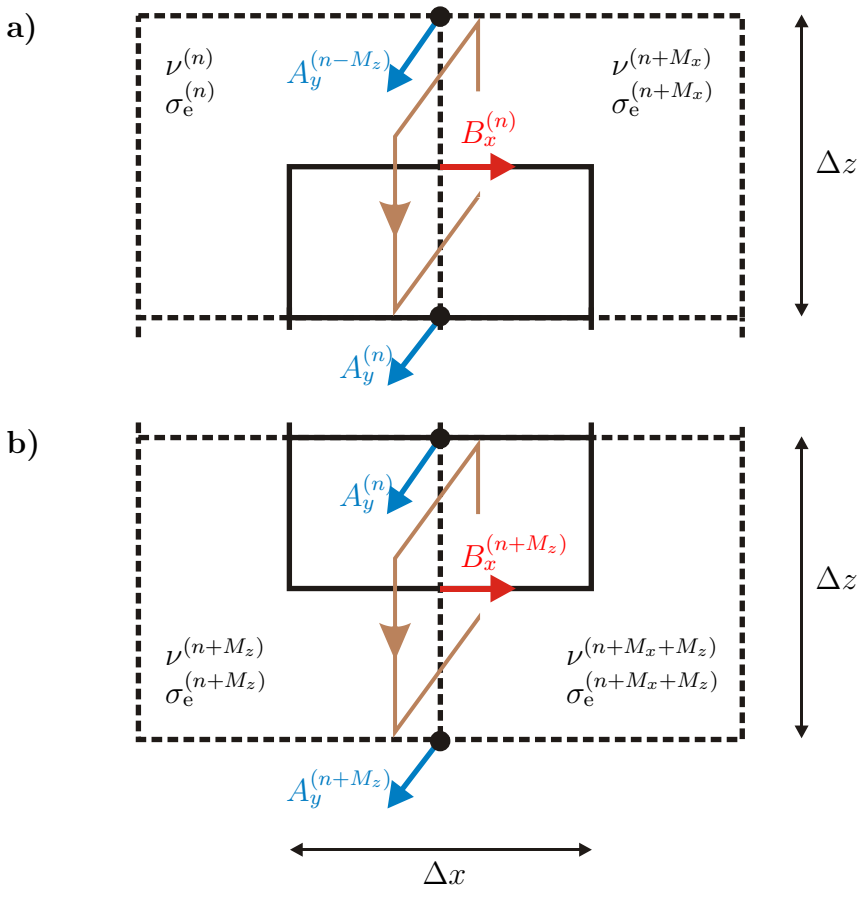

Figure 3.3: a) Upper part and b) lower part of the integration cell $I_{A_y}^{(n)}$.

Eq. (3.7) can be re-written as

$$\begin{aligned}
\int\limits_{C^{(d)}} \nu^{(d)} B_x^{(d)}(\omega)\,\mathrm{d}x &= \int\limits_{C^{(d)}} \frac{\nu^{(n+M_z)} + \nu^{(n+M_x+M_z)}}{2}\, B_x^{(n+M_z)}(\omega)\,\mathrm{d}x \\
&= \frac{\nu^{(n+M_z)} + \nu^{(n+M_x+M_z)}}{2} \left[\frac{A_y^{(n)}(\omega) - A_y^{(n+M_z)}(\omega)}{\Delta z^{(n+M_z)}}\right] \Delta x^{(n+M_z)} + \mathcal{O}\left[(\Delta x)^3\right] \\
&\approx \frac{\nu^{(n+M_z)} + \nu^{(n+M_x+M_z)}}{2} \left[A_y^{(n)}(\omega) - A_y^{(n+M_z)}(\omega)\right] \frac{\Delta x}{\Delta z} \\
&= \nu_{\mathrm{H}_x}^{(n+M_z)} \left[A_y^{(n)}(\omega) - A_y^{(n+M_z)}(\omega)\right] \quad , \qquad (3.13)
\end{aligned}$$

where the magnetic impermeability of the cells $m^{(n+M_z)}$ and $m^{(n+M_x+M_z)}$ will be averaged to compute $\nu_{\mathrm{H}_x}^{(n+M_z)}$ as

$$\nu_{\mathrm{H}_x}^{(n+M_z)} \;=\; \frac{\nu^{(n+M_z)} + \nu^{(n+M_x+M_z)}}{2} \quad . \qquad (3.14)$$

Left: Let us now consider the left part of the integration cell (Fig. 3.4a). We can show from Eq. (3.8) that

$$\begin{aligned}
\int\limits_{C^{(l)}} \nu^{(l)} \mathrm{B}_z^{(l)}(\omega)\,\mathrm{d}z &= \int\limits_{C^{(l)}} \frac{\nu^{(n)} + \nu^{(n+M_z)}}{2}\, \mathrm{B}_z^{(n)}(\omega)\,\mathrm{d}z \\
&= \frac{\nu^{(n)} + \nu^{(n+M_z)}}{2} \left[\frac{A_y^{(n)}(\omega) - A_y^{(n-M_x)}(\omega)}{\Delta x^{(n)}}\right] \Delta z^{(n)} + \mathcal{O}\left[(\Delta z)^3\right] \\
&\approx \frac{\nu^{(n)} + \nu^{(n+M_z)}}{2} \left[A_y^{(n)}(\omega) - A_y^{(n-M_x)}(\omega)\right] \frac{\Delta z}{\Delta x} \\
&= \nu_{\mathrm{H}_z}^{(n)} \left[A_y^{(n)}(\omega) - A_y^{(n-M_x)}(\omega)\right] \quad , \qquad (3.15)
\end{aligned}$$

where $\nu_{\mathrm{H}_z}^{(n)}$ will be computed by averaging the magnetic impermeability of the cells $m^{(n)}$ and $m^{(n+M_z)}$ as

$$\nu_{\mathrm{H}_z}^{(n)} \;=\; \frac{\nu^{(n)} + \nu^{(n+M_z)}}{2} \quad . \qquad (3.16)$$

Right: The right part of the line integral can be realized from Fig. 3.4b. Rearranging Eq. (3.9) yields

$$\begin{aligned}
\int\limits_{C^{(r)}} \nu^{(r)} \mathrm{B}_z^{(r)}(\omega)\,\mathrm{d}z &= \int\limits_{C^{(r)}} \frac{\nu^{(n+M_x)} + \nu^{(n+M_x+M_z)}}{2}\, B_z^{(n+M_x)}(\omega)\,\mathrm{d}z \\
&= \frac{\nu^{(n+M_x)} + \nu^{(n+M_x+M_z)}}{2} \left[\frac{A_y^{(n+M_x)}(\omega) - A_y^{(n)}(\omega)}{\Delta x^{(n+M_x)}}\right] \Delta z^{(n+M_x)} + \mathcal{O}\left[(\Delta z)^3\right] \\
&\approx \frac{\nu^{(n+M_x)} + \nu^{(n+M_x+M_z)}}{2} \left[A_y^{(n+M_x)}(\omega) - A_y^{(n)}(\omega)\right] \frac{\Delta x}{\Delta z} \\
&= \nu_{\mathrm{H}_z}^{(n+M_x)} \left[A_y^{(n+M_x)}(\omega) - A_y^{(n)}(\omega)\right] \quad , \qquad (3.17)
\end{aligned}$$

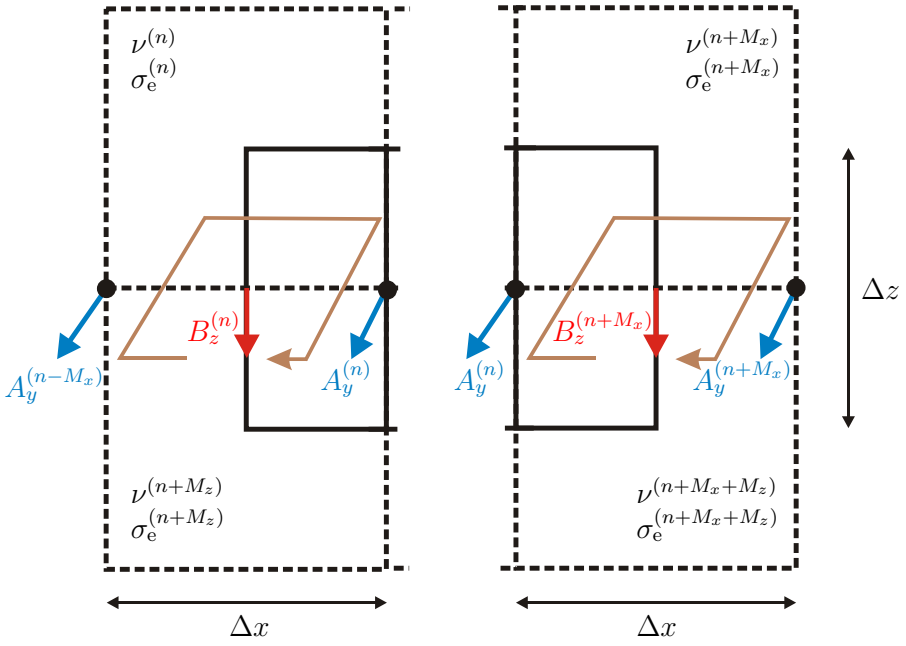

Figure 3.4: a) Left part and b) right part of the integration cell $I_{A_y}^{(n)}$.

where the magnetic impermeability of the cells $m^{(n+M_x)}$ and $m^{(n+M_x+M_z)}$ will be averaged to compute $\nu_{\mathrm{H}_z}^{(n+M_x)}$ as

$$\nu_{\mathrm{H}_z}^{(n+M_x)} = \frac{\nu^{(n+M_x)} + \nu^{(n+M_x+M_z)}}{2} \quad . \tag{3.18}$$

Using Eq. (3.10) we can sum up all the parts to compute the local grid equation for the integration cell $I_{A_y}^{(n)}$ as:

$$\begin{aligned}
&\oint_{C=\partial S} [\nu(\underline{\mathbf{R}})\boldsymbol{\nabla}\times\underline{\mathbf{A}}_{\mathrm{m}}(\underline{\mathbf{R}},\omega)] \cdot \underline{\mathbf{dR}} \\
&= \int_{C^{(d)}} \nu^{(d)}\mathrm{B}_x^{(d)}(\omega)\,dx - \int_{C^{(u)}} \nu^{(u)}\mathrm{B}_x^{(u)}(\omega)\,dx + \int_{C^{(l)}} \nu^{(l)}\mathrm{B}_z^{(l)}(\omega)\,dz - \int_{C^{(r)}} \nu^{(r)}\mathrm{B}_z^{(r)}(\omega)\,dz \\
&= \nu_{\mathrm{H}_x}^{(n+M_z)}\left[A_y^{(n)}(\omega) - A_y^{(n+M_z)}(\omega)\right] - \nu_{\mathrm{H}_x}^{(n)}\left[A_y^{(n-M_z)}(\omega) - A_y^{(n)}(\omega)\right] \\
&\quad + \nu_{\mathrm{H}_z}^{(n)}\left[A_y^{(n)}(\omega) - A_y^{(n-M_x)}(\omega)\right] - \nu_{\mathrm{H}_z}^{(n+M_x)}\left[A_y^{(n+M_x)}(\omega) - A_y^{(n)}(\omega)\right] \\
&= -\nu_{\mathrm{H}_x}^{(n)}A_y^{(n-M_z)}(\omega) - \nu_{\mathrm{H}_z}^{(n)}A_y^{(n-M_x)}(\omega) - \nu_{\mathrm{H}_z}^{(n+M_x)}A_y^{(n+M_x)}(\omega) - \nu_{\mathrm{H}_x}^{(n+M_z)}A_y^{(n+M_z)}(\omega) \\
&\quad + \left[\nu_{\mathrm{H}_x}^{(n)} + \nu_{\mathrm{H}_x}^{(n+M_z)} + \nu_{\mathrm{H}_z}^{(n)} + \nu_{\mathrm{H}_z}^{(n+M_x)}\right] A_y^{(n)}(\omega) \quad .
\end{aligned} \tag{3.19}$$

Now let us compute the first surface integral. The electric conductivity at node n will be computed by averaging the values of surrounding cells as:

$$\widetilde{\sigma}^{(n)} = \frac{1}{4}\left[\sigma^{(n)} + \sigma^{(n+M_x)} + \sigma^{(n+M_z)} + \sigma^{(n+M_x+M_z)}\right] \quad . \tag{3.20}$$

Using the average electric conductivity $\widetilde{\sigma}^{(n)}$ the first surface integral of Eq. (3.1) can be written as:

$$\begin{aligned}\iint\limits_S \mathrm{j}\,\omega\;\sigma_\mathrm{e}(\underline{\mathbf{R}})\;\underline{\mathbf{A}}_\mathrm{m}(\underline{\mathbf{R}},\omega)\cdot\underline{\mathbf{dS}} \;&=\; \mathrm{j}\,\omega\iint\limits_S \widetilde{\sigma}^{(n)}A_y^{(n)}(\omega)\;\underline{\mathbf{e}}_y\cdot\underline{\mathbf{e}}_y\;\mathrm{d}S\\ &=\; \mathrm{j}\,\omega\;\widetilde{\sigma}^{(n)}A_y^{(n)}(\omega)\,\Delta x\,\Delta z\;+\mathcal{O}\left[(\Delta x)^3\Delta z+(\Delta z)^3\Delta x\right]\\ &\approx\; \mathrm{j}\,\omega\;\widetilde{\sigma}^{(n)}A_y^{(n)}(\omega)\,(\Delta x)^2\;\;, \end{aligned}\tag{3.21}$$

by assuming $\Delta x=\Delta z$ which results $\mathrm{d}S=(\Delta x)^2$. The second surface integral of Eq. (3.1) can be computed in the similar way.

$$\begin{aligned}\iint\limits_S \underline{\mathbf{J}}_\mathrm{e}^\mathrm{imp}(\underline{\mathbf{R}},\omega)\cdot\underline{\mathbf{dS}} \;=\; \iint\limits_S J_{ey}^{(n)}(\omega)\;\underline{\mathbf{e}}_y\cdot\underline{\mathbf{e}}_y\;\mathrm{d}S \;&=\; J_{ey}^{(n)}(\omega)\,\Delta x\,\Delta z+\mathcal{O}\left[(\Delta x)^3\Delta z+(\Delta z)^3\Delta x\right]\\ &\approx\; J_{ey}^{(n)}(\omega)\,(\Delta x)^2\;\;. \end{aligned}\tag{3.22}$$

Inserting Eqs. (3.19)-(3.22) in Eq. (3.1) yields,

$$\begin{aligned}&-\nu_{\mathrm{H}_x}^{(n)}\,A_y^{(n-M_z)}-\nu_{\mathrm{H}_z}^{(n)}\,A_y^{(n-M_x)}-\nu_{\mathrm{H}_z}^{(n+M_x)}\,A_y^{(n+M_x)}-\nu_{\mathrm{H}_x}^{(n+M_z)}\,A_y^{(n+M_z)}\\ &\quad+\left[\nu_{\mathrm{H}_x}^{(n)}+\nu_{\mathrm{H}_x}^{(n+M_z)}+\nu_{\mathrm{H}_z}^{(n)}+\nu_{\mathrm{H}_z}^{(n+M_x)}\right]A_y^{(n)}-\mathrm{j}\,\omega\;\widetilde{\sigma}^{(n)}A_y^{(n)}\,(\Delta x)^2 \;=\; J_{ey}^{(n)}\,(\Delta x)^2\,. \end{aligned}\tag{3.23}$$

Rearranging Eq. (3.23) delivers

$$\begin{aligned}&-\nu_{\mathrm{H}_x}^{(n)}\,A_y^{(n-M_z)}-\nu_{\mathrm{H}_z}^{(n)}\,A_y^{(n-M_x)}+\left[\nu_{\mathrm{H}_x}^{(n)}+\nu_{\mathrm{H}_x}^{(n+M_z)}+\nu_{\mathrm{H}_z}^{(n)}+\nu_{\mathrm{H}_z}^{(n+M_x)}\right.\\ &\qquad\left.-\mathrm{j}\,\omega\;\widetilde{\sigma}^{(n)}(\Delta x)^2\right]A_y^{(n)}-\nu_{\mathrm{H}_z}^{(n+M_x)}\,A_y^{(n+M_x)}-\nu_{\mathrm{H}_x}^{(n+M_z)}\,A_y^{(n+M_z)} \;=\; J_{ey}^{(n)}\,(\Delta x)^2\,. \end{aligned}\tag{3.24}$$

Introducing the shift operator $\mathcal{S}_{\pm M_i}$ and the identity operator $\mathcal{I}$ we obtain

$$\begin{aligned}\Big\{&-\nu_{\mathrm{H}_x}^{(n)}\mathcal{S}_{-M_z}-\nu_{\mathrm{H}_z}^{(n)}\mathcal{S}_{-M_x}+\left[\nu_{\mathrm{H}_x}^{(n)}+\nu_{\mathrm{H}_x}^{(n+M_z)}+\nu_{\mathrm{H}_z}^{(n)}+\nu_{\mathrm{H}_z}^{(n+M_x)}-\mathrm{j}\,\omega\;\widetilde{\sigma}^{(n)}(\Delta x)^2\right]\mathcal{I}\\ &\qquad-\nu_{\mathrm{H}_z}^{(n+M_x)}\mathcal{S}_{M_x}-\nu_{\mathrm{H}_x}^{(n+M_z)}\mathcal{S}_{M_z}\Big\}A_y^{(n)} \;=\; J_{ey}^{(n)}(\Delta x)^2\,. \end{aligned}\tag{3.25}$$

The final equation can be written in the form

$$\left\{\mathtt{t1}^{(n)}\,\mathcal{S}_{-M_z}+\mathtt{s1}^{(n)}\,\mathcal{S}_{-M_x}+\left[\mathtt{d1}^{(n)}+\mathtt{d2}^{(n)}\right]\mathcal{I}+\mathtt{s2}^{(n)}\,\mathcal{S}_{+M_x}+\mathtt{t2}^{(n)}\,\mathcal{S}_{+M_z}\right\}\mathtt{x}^{(n)} \;=\; \mathtt{b}^{(n)}\,,\tag{3.26}$$

with the coefficients

$$\mathtt{t1}^{(n)} = -\nu_{\mathrm{H}_x}^{(n)} \tag{3.27}$$

$$\mathtt{s1}^{(n)} = -\nu_{\mathrm{H}_z}^{(n)} \tag{3.28}$$

$$\mathtt{d1}^{(n)} = \nu_{\mathrm{H}_x}^{(n)} + \nu_{\mathrm{H}_x}^{(n+M_z)} + \nu_{\mathrm{H}_z}^{(n)} + \nu_{\mathrm{H}_z}^{(n+M_x)} \tag{3.29}$$

$$\mathtt{d2}^{(n)} = -\,\mathrm{j}\,\omega\,\widetilde{\sigma}^{(n)}(\Delta x)^2 \tag{3.30}$$

$$\mathtt{s2}^{(n)} = -\nu_{\mathrm{H}_z}^{(n+M_x)} \tag{3.31}$$

$$\mathtt{t2}^{(n)} = -\nu_{\mathrm{H}_x}^{(n+M_z)} \tag{3.32}$$

$$\mathtt{x}^{(n)} = A_y^{(n)} \tag{3.33}$$

$$\mathtt{b}^{(n)} = J_{\mathrm{e}y}^{(n)}(\Delta x)^2\,. \tag{3.34}$$

3.5 Discrete Field Quantities in Cylindrical Coordinates in 2-D case

The discrete field quantities in cylindrical coordinates can be computed in the similar way as in cartesian coordinates. We have to consider the following few changes in this case:

- The simulation will be performed in rz plane, instead of xz plane.
- The unknown field quantity is A_φ.
- The left and right integrals of Eq. (3.15) and Eq. (3.17) will contain extra coefficients, as the curl operator in cylindrical coordinates differs from that in the cartesian coordinates.

Fig. 3.5 shows the integration cell $I_{A_\varphi}^{(n)}$ for 2-D case. The allocation of the field quantities is listed below:

- The φ component of magnetic vector potential A_φ is positioned at the corners of the material cells and point the normal direction of the rz plane.
- The r and z components of the magnetic flux density vector $B_r^{(n)}$, $B_z^{(n)}$, $B_r^{(n+M_z)}$, and $B_z^{(n+M_r)}$ are positioned at the center of the edges of the facet and each component points the tangential directions to the surface.
- The φ component of electric current density $J_{\mathrm{e}\varphi}^{(n)}$ is positioned at the center of the material cell $m^{(n)}$.

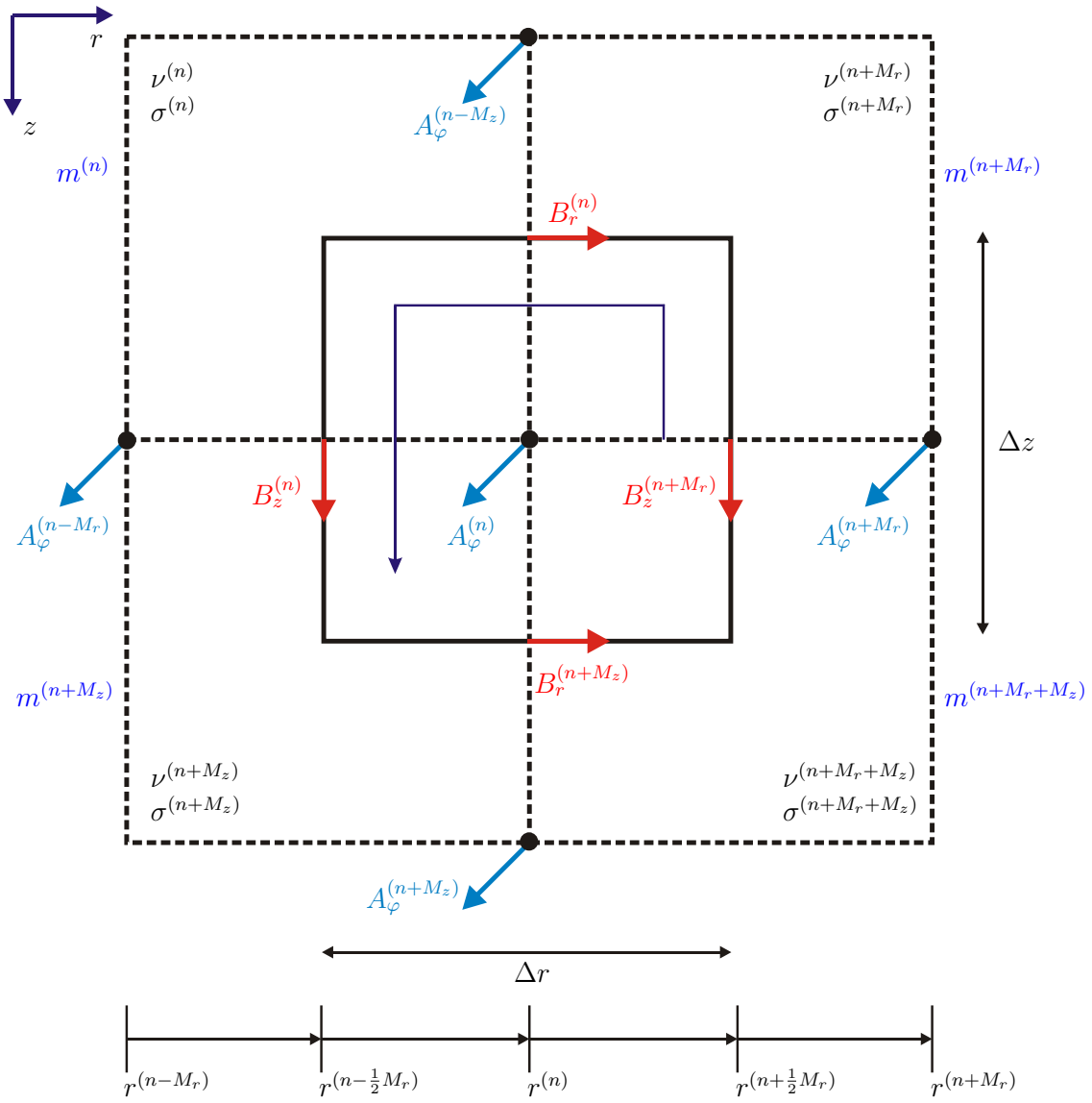

Figure 3.5: Allocation of the discrete electromagnetic field components B_r, B_z, and A_φ assigned to the global grid node (n) in 2-D case in cylindrical coordinates.

3.6 Derivation of the Discrete Grid Equation in Cylindrical Coordinates in 2-D case

We can determine the discrete grid equation in cylindrical coordinates by discretizing the governing equation Eq. (3.1) using the following steps:

1. The curl operator of the line integral can be computed in the cylindrical coordinates as:

$$\nabla\times\underline{\mathbf{A}}_{\mathrm{m}}(\underline{\mathbf{R}},\omega) = \left[\frac{1}{r}\frac{\partial A_z(\omega)}{\partial\varphi}-\frac{\partial A_\varphi(\omega)}{\partial z}\right]\underline{\mathbf{e}}_r+\left[\frac{\partial A_r(\omega)}{\partial z}-\frac{\partial A_z(\omega)}{\partial r}\right]\underline{\mathbf{e}}_\varphi + \frac{1}{r}\left[\frac{\partial(r\,A_\varphi(\omega))}{\partial r}-\frac{\partial A_r(\omega)}{\partial\varphi}\right]\underline{\mathbf{e}}_z \quad . \tag{3.35}$$

As the rz plane is the computation plane, magnetic vector potential has only the φ

component and therefore, the curl operator can be reduced to

$$\boldsymbol{\nabla}\times\underline{\mathbf{A}}_{\mathrm{m}}(\underline{\mathbf{R}},\omega) \;=\; -\,\frac{\partial A_\varphi(\omega)}{\partial z}\underline{\mathbf{e}}_r + \;\frac{1}{r}\frac{\partial(r\,A_\varphi(\omega))}{\partial r}\underline{\mathbf{e}}_z \;. \tag{3.36}$$

2. The line integral of of Eq. (3.1) can be divided into 'Up', 'Down', 'Left', and 'Right' integrals, that results

$$\int\limits_{C^{(u)}} [\nu(\underline{\mathbf{R}})\boldsymbol{\nabla}\times\underline{\mathbf{A}}_{\mathrm{m}}(\underline{\mathbf{R}},\omega)]\cdot\underline{\mathbf{dR}} = \int\limits_{C^{(u)}} \nu^{(u)}\left[-\,\frac{\partial A_\varphi(\omega)}{\partial z}\underline{\mathbf{e}}_r + \;\frac{1}{r}\frac{\partial(r\,A_\varphi(\omega))}{\partial r}\underline{\mathbf{e}}_z\right]\cdot\underline{\mathbf{e}}_r\;\mathrm{d}r$$

$$\Rightarrow \int\limits_{C^{(u)}} [\nu(\underline{\mathbf{R}})\;\underline{\mathbf{B}}(\underline{\mathbf{R}},\omega)]\cdot\underline{\mathbf{dR}} = \int\limits_{C^{(u)}} \nu^{(u)}\left[-\,\frac{\partial A_\varphi(\omega)}{\partial z}\right]\mathrm{d}r \;. \tag{3.37}$$

$$\int\limits_{C^{(d)}} [\nu(\underline{\mathbf{R}})\boldsymbol{\nabla}\times\underline{\mathbf{A}}_{\mathrm{m}}(\underline{\mathbf{R}},\omega)]\cdot\underline{\mathbf{dR}} = \int\limits_{C^{(d)}} \nu^{(d)}\left[-\,\frac{\partial A_\varphi(\omega)}{\partial z}\underline{\mathbf{e}}_r + \;\frac{1}{r}\frac{\partial(r\,A_\varphi(\omega))}{\partial r}\underline{\mathbf{e}}_z\right]\cdot\underline{\mathbf{e}}_r\;\mathrm{d}r$$

$$\Rightarrow \int\limits_{C^{(d)}} [\nu(\underline{\mathbf{R}})\;\underline{\mathbf{B}}(\underline{\mathbf{R}},\omega)]\cdot\underline{\mathbf{dR}} = \int\limits_{C^{(d)}} \nu^{(d)}\left[-\,\frac{\partial A_\varphi(\omega)}{\partial z}\right]\mathrm{d}r \;. \tag{3.38}$$

$$\int\limits_{C^{(l)}} [\nu(\underline{\mathbf{R}})\boldsymbol{\nabla}\times\underline{\mathbf{A}}_{\mathrm{m}}(\underline{\mathbf{R}},\omega)]\cdot\underline{\mathbf{dR}} = \int\limits_{C^{(l)}} \nu^{(l)}\left[-\,\frac{\partial A_\varphi(\omega)}{\partial z}\underline{\mathbf{e}}_r + \;\frac{1}{r}\frac{\partial(r\,A_\varphi(\omega))}{\partial r}\underline{\mathbf{e}}_z\right]\cdot\underline{\mathbf{e}}_z\;\mathrm{d}z$$

$$\Rightarrow \int\limits_{C^{(l)}} [\nu(\underline{\mathbf{R}})\;\underline{\mathbf{B}}(\underline{\mathbf{R}},\omega)]\cdot\underline{\mathbf{dR}} = \int\limits_{C^{(l)}} \nu^{(l)}\left[\frac{1}{r}\frac{\partial(r\,A_\varphi(\omega))}{\partial r}\right]\mathrm{d}z \;. \tag{3.39}$$

$$\int\limits_{C^{(r)}} [\nu(\underline{\mathbf{R}})\boldsymbol{\nabla}\times\underline{\mathbf{A}}_{\mathrm{m}}(\underline{\mathbf{R}},\omega)]\cdot\underline{\mathbf{dR}} = \int\limits_{C^{(r)}} \nu^{(r)}\left[-\,\frac{\partial A_\varphi(\omega)}{\partial z}\underline{\mathbf{e}}_r + \;\frac{1}{r}\frac{\partial(r\,A_\varphi(\omega))}{\partial r}\underline{\mathbf{e}}_z\right]\cdot\underline{\mathbf{e}}_z\;\mathrm{d}z$$

$$\Rightarrow \int\limits_{C^{(r)}} [\nu(\underline{\mathbf{R}})\;\underline{\mathbf{B}}(\underline{\mathbf{R}},\omega)]\cdot\underline{\mathbf{dR}} = \int\limits_{C^{(r)}} \nu^{(r)}\left[\frac{1}{r}\frac{\partial(r\,A_\varphi(\omega))}{\partial r}\right]\mathrm{d}z \;. \tag{3.40}$$

3. $A_\varphi^{(n)}$ is positioned in the center of the integration cell $I_{A_\varphi}^{(n)}$. The line integral of Eq. (3.1) can be computed as a sum of these four integrals as

$$\begin{aligned}
&\oint\limits_{C=\partial S} [\nu(\underline{\mathbf{R}})\boldsymbol{\nabla}\times\underline{\mathbf{A}}_{\mathrm{m}}((\underline{\mathbf{R}},\omega)]\cdot\underline{\mathbf{dR}} \\
&\quad= \int\limits_{C^{(d)}} [\nu(\underline{\mathbf{R}})\;\underline{\mathbf{B}}(\underline{\mathbf{R}},\omega)]\cdot\underline{\mathbf{dR}} \;-\int\limits_{C^{(u)}} [\nu(\underline{\mathbf{R}})\;\underline{\mathbf{B}}(\underline{\mathbf{R}},\omega)]\cdot\underline{\mathbf{dR}} \\
&\quad\;+\int\limits_{C^{(l)}} [\nu(\underline{\mathbf{R}})\;\underline{\mathbf{B}}(\underline{\mathbf{R}},\omega)]\cdot\underline{\mathbf{dR}} \;-\int\limits_{C^{(r)}} [\nu(\underline{\mathbf{R}})\;\underline{\mathbf{B}}(\underline{\mathbf{R}},\omega)]\cdot\underline{\mathbf{dR}} \\
&\quad= \int\limits_{C^{(d)}} \nu^{(d)}\mathrm{B}_r^{(d)}(\omega)\,\mathrm{d}r - \int\limits_{C^{(u)}} \nu^{(u)}\mathrm{B}_r^{(u)}(\omega)\,\mathrm{d}r + \int\limits_{C^{(l)}} \nu^{(l)}\mathrm{B}_z^{(l)}(\omega)\,\mathrm{d}z - \int\limits_{C^{(r)}} \nu^{(r)}\mathrm{B}_z^{(r)}(\omega)\,\mathrm{d}z \;.
\end{aligned} \tag{3.41}$$

4. Quadratic cells are taken here for ease of discretization, i.e., $\Delta z = \Delta r$.

5. The surface integrals of Eq. (3.1) can be computed directly.

6. Average values of material parameters $\nu(\underline{\mathbf{R}})$ and $\sigma_{\mathrm{e}}(\underline{\mathbf{R}})$ should be taken while computing the integrals.

Up: The upper part can be computed by rearranging Eq. (3.37) as

$$\begin{aligned}
\int\limits_{C^{(u)}} \nu^{(u)} B_r^{(u)}(\omega)\,\mathrm{d}r &= \int\limits_{C^{(u)}} \frac{\nu^{(n)} + \nu^{(n+M_r)}}{2} \left[-\frac{\partial A_\varphi(\omega)}{\partial z} \right] \mathrm{d}r \\
&= \frac{\nu^{(n)} + \nu^{(n+M_r)}}{2} \left[\frac{A_\varphi^{(n-M_z)}(\omega) - A_\varphi^{(n)}(\omega)}{\Delta z^{(n)}} \right] \Delta r^{(n)} + \mathcal{O}\left[(\Delta r)^3\right] \\
&\approx \frac{\nu^{(n)} + \nu^{(n+M_r)}}{2} \left[A_\varphi^{(n-M_z)}(\omega) - A_\varphi^{(n)}(\omega) \right] \frac{\Delta r}{\Delta z} \\
&= \nu_{\mathrm{H}_r}^{(n)} \left[A_\varphi^{(n-M_z)}(\omega) - A_\varphi^{(n)}(\omega) \right] \quad , \qquad (3.42)
\end{aligned}$$

where $\nu_{\mathrm{H}_r}^{(n)}$ will be computed by averaging the magnetic impermeability of the cells $m^{(n)}$ and $m^{(n+M_r)}$ as

$$\nu_{\mathrm{H}_r}^{(n)} \;=\; \frac{\nu^{(n)} + \nu^{(n+M_r)}}{2} \quad . \qquad (3.43)$$

Down: The lower part of the integration cell $I_{A_\varphi}^{(n)}$ can be computed using Eq. (3.38) as

$$\begin{aligned}
\int\limits_{C^{(d)}} \nu^{(d)} B_r^{(d)}(\omega)\,\mathrm{d}r &= \int\limits_{C^{(d)}} \frac{\nu^{(n+M_z)} + \nu^{(n+M_r+M_z)}}{2} \left[-\frac{\partial A_\varphi(\omega)}{\partial z} \right] \mathrm{d}r \\
&= \frac{\nu^{(n+M_z)} + \nu^{(n+M_r+M_z)}}{2} \left[\frac{A_\varphi^{(n)}(\omega) - A_\varphi^{(n+M_z)}(\omega)}{\Delta z^{(n+M_z)}} \right] \Delta r^{(n+M_z)} + \mathcal{O}\left[(\Delta r)^3\right] \\
&\approx \frac{\nu^{(n+M_z)} + \nu^{(n+M_r+M_z)}}{2} \left[A_\varphi^{(n)}(\omega) - A_\varphi^{(n+M_z)}(\omega) \right] \frac{\Delta r}{\Delta z} \\
&= \nu_{\mathrm{H}_r}^{(n+M_z)} \left[A_\varphi^{(n)}(\omega) - A_\varphi^{(n+M_z)}(\omega) \right] \quad , \qquad (3.44)
\end{aligned}$$

where the magnetic impermeability of the cells $m^{(n+M_z)}$ and $m^{(n+M_r+M_z)}$ will be averaged to compute $\nu_{\mathrm{H}_r}^{(n+M_z)}$ as

$$\nu_{\mathrm{H}_x}^{(n+M_z)} \;=\; \frac{\nu^{(n+M_z)} + \nu^{(n+M_r+M_z)}}{2} \quad . \qquad (3.45)$$

Left: Let us now rearrange Eq. (3.39) to compute the left part as

$$\begin{aligned}
\int\limits_{C^{(l)}} \nu^{(l)} \mathrm{B}_z^{(l)}(\omega)\,\mathrm{d}z &= \int\limits_{C^{(l)}} \frac{\nu^{(n)}+\nu^{(n+M_z)}}{2}\left[\frac{1}{r}\frac{\partial(r\,A_\varphi(\omega))}{\partial r}\right]\mathrm{d}z \\
&= \frac{\nu^{(n)}+\nu^{(n+M_z)}}{2\,r^{(n-\frac{1}{2}M_r)}}\left[\frac{r^{(n)}A_\varphi^{(n)}(\omega)-r^{(n-M_r)}A_\varphi^{(n-M_r)}(\omega)}{\Delta r^{(n)}}\right]\Delta z^{(n)}+\mathcal{O}\left[(\Delta z)^3\right] \\
&\approx \nu_{\mathrm{H}_z}^{(n)}\left[\frac{r^{(n)}}{r^{(n-\frac{1}{2}M_r)}}A_\varphi^{(n)}(\omega)-\frac{r^{(n-M_r)}}{r^{(n-\frac{1}{2}M_r)}}A_\varphi^{(n-M_r)}(\omega)\right]\frac{\Delta z}{\Delta r} \\
&= \nu_{\mathrm{H}_z}^{(n)}\left[\frac{r^{(n)}}{r^{(n-\frac{1}{2}M_r)}}A_\varphi^{(n)}(\omega)-\frac{r^{(n-M_r)}}{r^{(n-\frac{1}{2}M_r)}}A_\varphi^{(n-M_r)}(\omega)\right]\quad, \qquad (3.46)
\end{aligned}$$

where $\nu_{\mathrm{H}_z}^{(n)}$ will be computed by averaging the magnetic impermeability of the cells $m^{(n)}$ and $m^{(n+M_z)}$ as

$$\nu_{\mathrm{H}_z}^{(n)} \;=\; \frac{\nu^{(n)}+\nu^{(n+M_z)}}{2}\quad. \qquad (3.47)$$

Right: The right part of the line integral can be computed using Eq. (3.40) as

$$\begin{aligned}
\int\limits_{C^{(r)}} \nu^{(r)} \mathrm{B}_z^{(r)}(\omega)\,\mathrm{d}z &= \int\limits_{C^{(r)}} \frac{\nu^{(n+M_r)}+\nu^{(n+M_r+M_z)}}{2}\left[\frac{1}{r}\frac{\partial(r\,A_\varphi(\omega))}{\partial r}\right]\mathrm{d}z \\
&= \frac{\nu^{(n+M_r)}+\nu^{(n+M_r+M_z)}}{2\,r^{(n+\frac{1}{2}M_r)}}\left[\frac{r^{(n+M_r)}A_\varphi^{(n+M_r)}(\omega)-r^{(n)}A_\varphi^{(n)}(\omega)}{\Delta r^{(n+M_r)}}\right]\Delta z^{(n+M_r)} \\
&\qquad +\mathcal{O}\left[(\Delta z)^3\right] \\
&\approx \nu_{\mathrm{H}_z}^{(n+M_r)}\left[\frac{r^{(n+M_r)}}{r^{(n+\frac{1}{2}M_r)}}A_\varphi^{(n+M_r)}(\omega)-\frac{r^{(n)}}{r^{(n+\frac{1}{2}M_r)}}A_\varphi^{(n)}(\omega)\right]\frac{\Delta z}{\Delta r} \\
&= \nu_{\mathrm{H}_z}^{(n+M_r)}\left[\frac{r^{(n+M_r)}}{r^{(n+\frac{1}{2}M_r)}}A_\varphi^{(n+M_r)}(\omega)-\frac{r^{(n)}}{r^{(n+\frac{1}{2}M_r)}}A_\varphi^{(n)}(\omega)\right]\quad, \qquad (3.48)
\end{aligned}$$

where the magnetic impermeability of the cells $m^{(n+M_r)}$ and $m^{(n+M_r+M_z)}$ will be averaged to compute $\nu_{\mathrm{H}_z}^{(n+M_r)}$ as

$$\nu_{\mathrm{H}_z}^{(n+M_r)} \;=\; \frac{\nu^{(n+M_r)}+\nu^{(n+M_r+M_z)}}{2}\quad. \qquad (3.49)$$

Using Eq. (3.41) we can sum up all the parts to compute the line integral for the integration cell $I_{A_\varphi}^{(n)}$ as:

$$
\begin{aligned}
&\oint_{C=\partial S} \left[\nu(\underline{\mathbf{R}})\boldsymbol{\nabla}\times\underline{\mathbf{A}}_{\mathrm{m}}(\underline{\mathbf{R}},\omega)\right]\cdot\underline{\mathbf{dR}} \\
&\quad= \int_{C^{(d)}} \nu^{(d)}\mathrm{B}_r^{(d)}(\omega)\,dr - \int_{C^{(u)}} \nu^{(u)}\mathrm{B}_r^{(u)}(\omega)\,dr + \int_{C^{(l)}} \nu^{(l)}\mathrm{B}_z^{(l)}(\omega)\,dz - \int_{C^{(r)}} \nu^{(r)}\mathrm{B}_z^{(r)}(\omega)\,dz \\
&\quad= \nu_{\mathrm{H}_r}^{(n+M_z)}\left[A_\varphi^{(n)}(\omega) - A_\varphi^{(n+M_z)}(\omega)\right] - \nu_{\mathrm{H}_r}^{(n)}\left[A_\varphi^{(n-M_z)}(\omega) - A_\varphi^{(n)}(\omega)\right] \\
&\qquad+ \nu_{\mathrm{H}_z}^{(n)}\left[\frac{r^{(n)}}{r^{(n-\frac{1}{2}M_r)}}A_\varphi^{(n)}(\omega) - \frac{r^{(n-M_r)}}{r^{(n-\frac{1}{2}M_r)}}A_\varphi^{(n-M_r)}(\omega)\right] \\
&\qquad- \nu_{\mathrm{H}_z}^{(n+M_r)}\left[\frac{r^{(n+M_r)}}{r^{(n+\frac{1}{2}M_r)}}A_\varphi^{(n+M_r)}(\omega) - \frac{r^{(n)}}{r^{(n+\frac{1}{2}M_r)}}A_\varphi^{(n)}(\omega)\right] \\
&\quad= -\nu_{\mathrm{H}_r}^{(n)}A_\varphi^{(n-M_z)}(\omega) - \nu_{\mathrm{H}_z}^{(n)}\frac{r^{(n-M_r)}}{r^{(n-\frac{1}{2}M_r)}}A_\varphi^{(n-M_r)}(\omega) \\
&\qquad- \nu_{\mathrm{H}_z}^{(n+M_r)}\frac{r^{(n+M_r)}}{r^{(n+\frac{1}{2}M_r)}}A_\varphi^{(n+M_r)}(\omega) - \nu_{\mathrm{H}_r}^{(n+M_z)}A_\varphi^{(n+M_z)}(\omega) \\
&\qquad+ \left[\nu_{\mathrm{H}_r}^{(n)} + \nu_{\mathrm{H}_r}^{(n+M_z)} + \nu_{\mathrm{H}_z}^{(n)}\frac{r^{(n)}}{r^{(n-\frac{1}{2}M_r)}} + \nu_{\mathrm{H}_z}^{(n+M_r)}\frac{r^{(n)}}{r^{(n+\frac{1}{2}M_r)}}\right]A_\varphi^{(n)}(\omega)\ . \qquad (3.50)
\end{aligned}
$$

The first surface integral of Eq. (3.1) contains electric conductivity σ_{e}, which will be computed at node n by averaging the values of surrounding cells as:

$$
\widetilde{\sigma}^{(n)} = \frac{1}{4}\left[\sigma^{(n)} + \sigma^{(n+M_r)} + \sigma^{(n+M_z)} + \sigma^{(n+M_r+M_z)}\right]\ . \qquad (3.51)
$$

Using the average electric conductivity $\widetilde{\sigma}^{(n)}$ we can compute the first surface integral as:

$$
\begin{aligned}
\iint_S \mathrm{j}\,\omega\ \sigma_{\mathrm{e}}(\underline{\mathbf{R}})\ \underline{\mathbf{A}}_{\mathrm{m}}(\underline{\mathbf{R}},\omega)\cdot\underline{\mathbf{dS}} &= \mathrm{j}\,\omega \iint_S \widetilde{\sigma}^{(n)}A_\varphi^{(n)}(\omega)\ \underline{\mathbf{e}}_\varphi\cdot\underline{\mathbf{e}}_\varphi\ \mathrm{d}S \\
&= \mathrm{j}\,\omega\ \widetilde{\sigma}^{(n)}A_\varphi^{(n)}(\omega)\,\Delta r\,\Delta z + \mathcal{O}\left[(\Delta r)^3\Delta z + (\Delta z)^3\Delta r\right] \\
&\approx \mathrm{j}\,\omega\ \widetilde{\sigma}^{(n)}A_\varphi^{(n)}(\omega)\,(\Delta r)^2\ , \qquad (3.52)
\end{aligned}
$$

where the grid cells are assumed to be quadratic, that results $\Delta r = \Delta z$ and $\mathrm{d}S = (\Delta r)^2$. The second surface integral of Eq. (3.1) can be computed in the similar way.

$$
\begin{aligned}
\iint_S \underline{\mathbf{J}}_{\mathrm{e}}^{\mathrm{imp}}(\underline{\mathbf{R}},\omega)\cdot\underline{\mathbf{dS}} &= \iint_S J_{\mathrm{e}\varphi}^{(n)}(\omega)\ \underline{\mathbf{e}}_\varphi\cdot\underline{\mathbf{e}}_\varphi\ \mathrm{d}S = J_{\mathrm{e}\varphi}^{(n)}(\omega)\,\Delta r\,\Delta z + \mathcal{O}\left[(\Delta r)^3\Delta z + (\Delta z)^3\Delta r\right] \\
&\approx J_{\mathrm{e}\varphi}^{(n)}(\omega)\,(\Delta r)^2\ . \qquad (3.53)
\end{aligned}
$$

Inserting Eqs. (3.50)-(3.53) in Eq. (3.1) yields,

$$
\begin{aligned}
&- \nu_{\mathrm{H}_r}^{(n)} A_{\varphi}^{(n-M_z)} - \nu_{\mathrm{H}_z}^{(n)} \frac{r^{(n-M_r)}}{r^{(n-\frac{1}{2}M_r)}} A_{\varphi}^{(n-M_r)} - \nu_{\mathrm{H}_z}^{(n+M_r)} \frac{r^{(n+M_r)}}{r^{(n+\frac{1}{2}M_r)}} A_{\varphi}^{(n+M_r)} \\
&- \nu_{\mathrm{H}_r}^{(n+M_z)} A_{\varphi}^{(n+M_z)} + \left[\nu_{\mathrm{H}_r}^{(n)} + \nu_{\mathrm{H}_r}^{(n+M_z)} + \nu_{\mathrm{H}_z}^{(n)} \frac{r^{(n)}}{r^{(n-\frac{1}{2}M_r)}} + \nu_{\mathrm{H}_z}^{(n+M_r)} \frac{r^{(n)}}{r^{(n+\frac{1}{2}M_r)}} \right] A_{\varphi}^{(n)} \\
&- \mathrm{j}\,\omega\, \widetilde{\sigma}^{(n)} A_{\varphi}^{(n)} (\Delta x)^2 = J_{\mathrm{e}\varphi}^{(n)} (\Delta r)^2 . \qquad (3.54)
\end{aligned}
$$

Eq. (3.54) can be rewritten as

$$
\begin{aligned}
&- \nu_{\mathrm{H}_r}^{(n)} A_{\varphi}^{(n-M_z)} - \nu_{\mathrm{H}_z}^{(n)} \frac{r^{(n-M_r)}}{r^{(n-\frac{1}{2}M_r)}} A_{\varphi}^{(n-M_r)} \\
&+ \left[\nu_{\mathrm{H}_r}^{(n)} + \nu_{\mathrm{H}_r}^{(n+M_z)} + \nu_{\mathrm{H}_z}^{(n)} \frac{r^{(n)}}{r^{(n-\frac{1}{2}M_r)}} + \nu_{\mathrm{H}_z}^{(n+M_r)} \frac{r^{(n)}}{r^{(n+\frac{1}{2}M_r)}} - \mathrm{j}\,\omega\, \widetilde{\sigma}^{(n)} (\Delta x)^2 \right] A_{\varphi}^{(n)} \\
&- \nu_{\mathrm{H}_z}^{(n+M_r)} \frac{r^{(n+M_r)}}{r^{(n+\frac{1}{2}M_r)}} A_{\varphi}^{(n+M_r)} - \nu_{\mathrm{H}_r}^{(n+M_z)} A_{\varphi}^{(n+M_z)} = J_{\mathrm{e}\varphi}^{(n)} (\Delta r)^2 . \qquad (3.55)
\end{aligned}
$$

Using the shift operator $\mathcal{S}_{\pm M_i}$ and the identity operator $\mathcal{I}$ we can rearrange Eqs. (3.55) as following

$$
\begin{aligned}
&\Bigg\{ - \nu_{\mathrm{H}_r}^{(n)} \mathcal{S}_{-M_z} - \nu_{\mathrm{H}_z}^{(n)} \frac{r^{(n-M_r)}}{r^{(n-\frac{1}{2}M_r)}} \mathcal{S}_{-M_r} \\
&+ \left[\nu_{\mathrm{H}_r}^{(n)} + \nu_{\mathrm{H}_r}^{(n+M_z)} + \nu_{\mathrm{H}_z}^{(n)} \frac{r^{(n)}}{r^{(n-\frac{1}{2}M_r)}} + \nu_{\mathrm{H}_z}^{(n+M_r)} \frac{r^{(n)}}{r^{(n+\frac{1}{2}M_r)}} - \mathrm{j}\,\omega\, \widetilde{\sigma}^{(n)} (\Delta x)^2 \right] \mathcal{I} \\
&- \nu_{\mathrm{H}_z}^{(n+M_r)} \frac{r^{(n+M_r)}}{r^{(n+\frac{1}{2}M_r)}} \mathcal{S}_{+M_r} - \nu_{\mathrm{H}_r}^{(n+M_z)} \mathcal{S}_{+M_z} \Bigg\} A_{\varphi}^{(n)} = J_{\mathrm{e}\varphi}^{(n)} (\Delta r)^2 . \qquad (3.56)
\end{aligned}
$$

The final grid equation can be written in the form

$$
\left\{ \mathtt{t1}^{(n)} \mathcal{S}_{-M_z} + \mathtt{s1}^{(n)} \mathcal{S}_{-M_r} + \left[\mathtt{d1}^{(n)} + \mathtt{d2}^{(n)} \right] \mathcal{I} + \mathtt{s2}^{(n)} \mathcal{S}_{+M_r} + \mathtt{t2}^{(n)} \mathcal{S}_{+M_z} \right\} \mathtt{x}^{(n)} = \mathtt{b}^{(n)} , \qquad (3.57)
$$

where the coefficients can be computed as following

$$
\mathtt{t1}^{(n)} = -\nu_{\mathrm{H}_r}^{(n)} \qquad (3.58)
$$

$$
\mathtt{s1}^{(n)} = -\nu_{\mathrm{H}_z}^{(n)} \frac{r^{(n-M_r)}}{r^{(n-\frac{1}{2}M_r)}} \qquad (3.59)
$$

$$
\mathtt{d1}^{(n)} = \nu_{\mathrm{H}_r}^{(n)} + \nu_{\mathrm{H}_r}^{(n+M_z)} + \nu_{\mathrm{H}_z}^{(n)} \frac{r^{(n)}}{r^{(n-\frac{1}{2}M_r)}} + \nu_{\mathrm{H}_z}^{(n+M_r)} \frac{r^{(n)}}{r^{(n+\frac{1}{2}M_r)}} \qquad (3.60)
$$

$$\mathtt{d2}^{(n)} = -\,\mathrm{j}\,\omega\;\widetilde{\sigma}^{(n)}(\Delta r)^2 \tag{3.61}$$

$$\mathtt{s2}^{(n)} = -\nu_{\mathrm{H}_z}^{(n+M_r)}\,\frac{r^{(n+M_r)}}{r^{(n+\frac{1}{2}M_r)}} \tag{3.62}$$

$$\mathtt{t2}^{(n)} = -\nu_{\mathrm{H}_r}^{(n+M_z)} \tag{3.63}$$

$$\mathtt{x}^{(n)} = \;\; A_{\varphi}^{(n)} \tag{3.64}$$

$$\mathtt{b}^{(n)} = \;\; J_{\mathrm{e}\varphi}^{(n)}(\Delta r)^2\,. \tag{3.65}$$

3.7 Boundary Conditions

Fig. 3.6 shows the simulation plane rz in cylindrical coordinates, which is discretized by $N_r \times N_z$ nodes. The coefficients $t1$, $t2$, $s1$, $s2$, $d1$ and $d2$ are computed at each node of the simulation plane using Eqs. (3.58)-(3.63). Before forming a band matrix from these

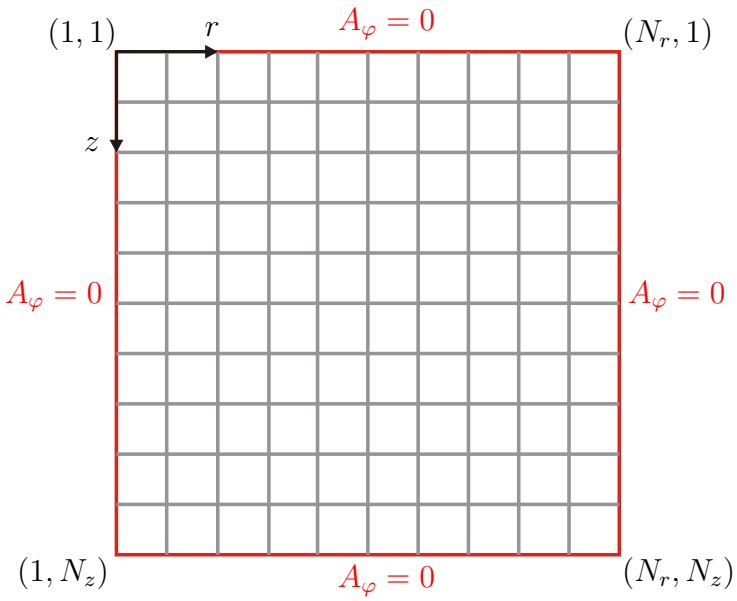

Figure 3.6: PEC boundary condition on a FIT cell.

coefficients to solve the final grid equation, the boundary condition should be implemented which can be

- perfectly electric conducting (PEC)
- perfectly matched layer (PML)

The perfectly electric conducting (PEC) boundary condition is considered here. From the transition condition described in Eq. (3.3) we know that

$$\underline{\mathbf{n}} \cdot \underline{\mathbf{A}}_{\mathrm{m}}(\underline{\mathbf{R}}, \omega) = \text{continuous}$$

$$\Rightarrow \;\; \underline{\mathbf{n}} \cdot \left[\underline{\mathbf{A}}_{\mathrm{m}}^{(2)}(\underline{\mathbf{R}}, \omega) - \underline{\mathbf{A}}_{\mathrm{m}}^{(1)}(\underline{\mathbf{R}}, \omega)\right] = 0\,. \tag{3.66}$$

At the material boundary Eq. (3.66) can be rewritten as

$$\underline{\mathbf{n}} \cdot [\boldsymbol{\nabla} \times \underline{\mathbf{A}}_{\mathrm{m}}(\underline{\mathbf{R}}, \omega)] = 0\,. \tag{3.67}$$

As our simulation domain resides in rz plane, the normal vector $\underline{\mathbf{n}} = \underline{\mathbf{e}}_{\varphi}$ and hence,

$$\begin{aligned} \underline{\mathbf{e}}_{\varphi} \times \underline{\mathbf{A}}_{\mathrm{m}}(\underline{\mathbf{R}}, \omega) &= 0 \\ \Rightarrow A_{\varphi}(\underline{\mathbf{R}}, \omega) &= 0\,, \end{aligned} \tag{3.68}$$

The PEC boundary condition is applied to the outermost nodes (marked red), and therefore, the computation region will be reduced to $(N_r - 1) \times (N_z - 1)$. Let us now discuss the top, bottom, left and right boundaries individually.

Top Boundary: Fig. 3.7a shows the top side of the simulation domain. As $A\varphi^{(n_r,1)} = 0$,

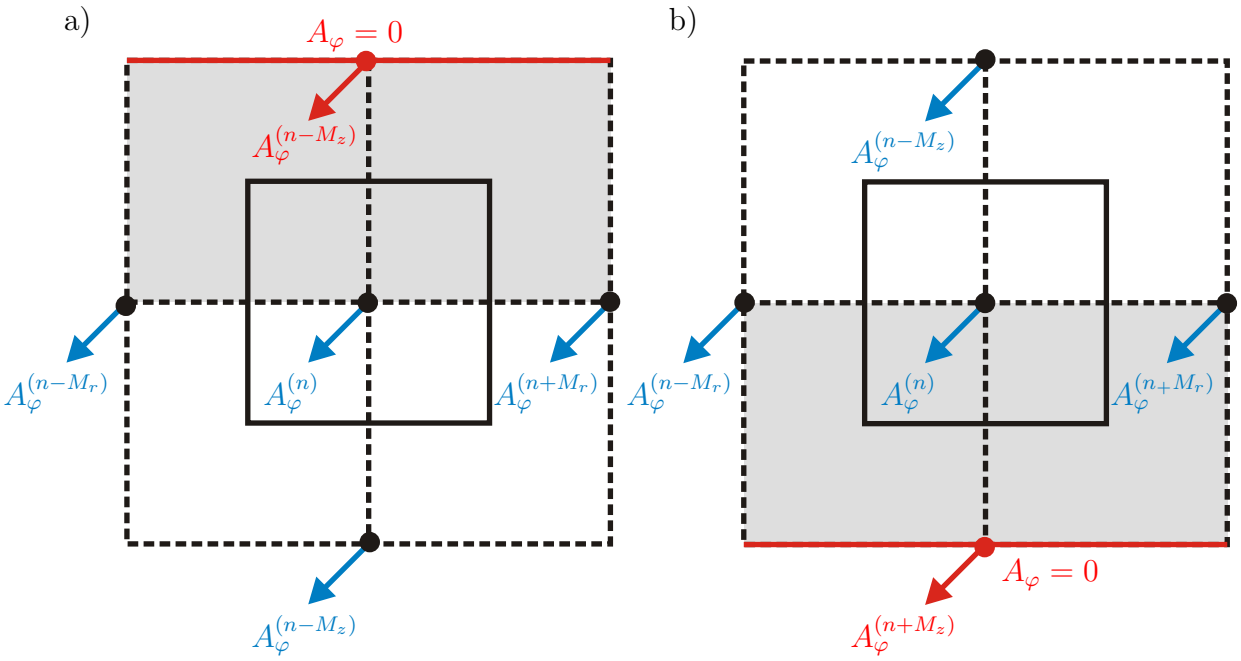

Figure 3.7: PEC boundary condition on the a) top and b) bottom of the simulation domain.

the discrete grid equation (Eq. (3.55)) can be rewritten by setting $A\varphi^{(n-M_z)} = 0$ as

$$\begin{aligned} -\,\nu_{\mathrm{H}_z}^{(n)} \frac{r^{(n-M_r)}}{r^{(n-\frac{1}{2}M_r)}} A_{\varphi}^{(n-M_r)} + \Bigg[\nu_{\mathrm{H}_r}^{(n)} + \nu_{\mathrm{H}_r}^{(n+M_z)} + \nu_{\mathrm{H}_z}^{(n)} \frac{r^{(n)}}{r^{(n-\frac{1}{2}M_r)}} + \nu_{\mathrm{H}_z}^{(n+M_r)} \frac{r^{(n)}}{r^{(n+\frac{1}{2}M_r)}} \\ -\,\mathrm{j}\,\omega\,\widetilde{\sigma}^{(n)}\,(\Delta x)^2 \Bigg] A_{\varphi}^{(n)} - \nu_{\mathrm{H}_z}^{(n+M_r)} \frac{r^{(n+M_r)}}{r^{(n+\frac{1}{2}M_r)}} A_{\varphi}^{(n+M_r)} - \nu_{\mathrm{H}_r}^{(n+M_z)} A_{\varphi}^{(n+M_z)} = J_{\mathrm{e}\varphi}^{(n)}\,(\Delta r)^2 \end{aligned} \tag{3.69}$$

$$\Rightarrow \left\{ \mathtt{s1}^{(n)}\,\mathcal{S}_{-M_r} + \left[\mathtt{d1}^{(n)} + \mathtt{d2}^{(n)} \right] \mathcal{I} + \mathtt{s2}^{(n)}\,\mathcal{S}_{+M_r} + \mathtt{t2}^{(n)}\,\mathcal{S}_{+M_z} \right\} \mathtt{x}^{(n)} = \mathtt{b}^{(n)}\,. \tag{3.70}$$

The coefficients can be computed using Eqs. (3.59)-(3.65) as mentioned in Sec. 3.6.

Bottom Boundary: The bottom side of the simulation domain is shown in Fig. 3.7b. The boundary condition leads to $A\varphi^{(n_r,N_z)} = 0$ and therefore, the discrete grid equation (Eq. (3.55)) can be rewritten by setting $A\varphi^{(n+M_z)} = 0$ as

$$-\nu_{\mathrm{H}_r}^{(n)} A_\varphi^{(n-M_z)} - \nu_{\mathrm{H}_z}^{(n)} \frac{r^{(n-M_r)}}{r^{(n-\frac{1}{2}M_r)}} A_\varphi^{(n-M_r)} + \Bigg[\nu_{\mathrm{H}_r}^{(n)} + \nu_{\mathrm{H}_r}^{(n+M_z)} + \nu_{\mathrm{H}_z}^{(n)} \frac{r^{(n)}}{r^{(n-\frac{1}{2}M_r)}} + \nu_{\mathrm{H}_z}^{(n+M_r)} \frac{r^{(n)}}{r^{(n+\frac{1}{2}M_r)}} - \mathrm{j}\,\omega\,\widetilde{\sigma}^{(n)}\,(\Delta x)^2 \Bigg] A_\varphi^{(n)} - \nu_{\mathrm{H}_z}^{(n+M_r)} \frac{r^{(n+M_r)}}{r^{(n+\frac{1}{2}M_r)}} A_\varphi^{(n+M_r)} = J_{\mathrm{e}\varphi}^{(n)}\,(\Delta r)^2 \tag{3.71}$$

$$\Rightarrow \left\{ \mathtt{t1}^{(n)}\,\mathcal{S}_{-M_z} + \mathtt{s1}^{(n)}\,\mathcal{S}_{-M_r} + \left[\mathtt{d1}^{(n)} + \mathtt{d2}^{(n)}\right] \mathcal{I} + \mathtt{s2}^{(n)}\,\mathcal{S}_{+M_r} \right\} \mathtt{x}^{(n)} = \mathtt{b}^{(n)}\,. \tag{3.72}$$

Left Boundary: The effect of PEC boundary condition at the left side of the simulation

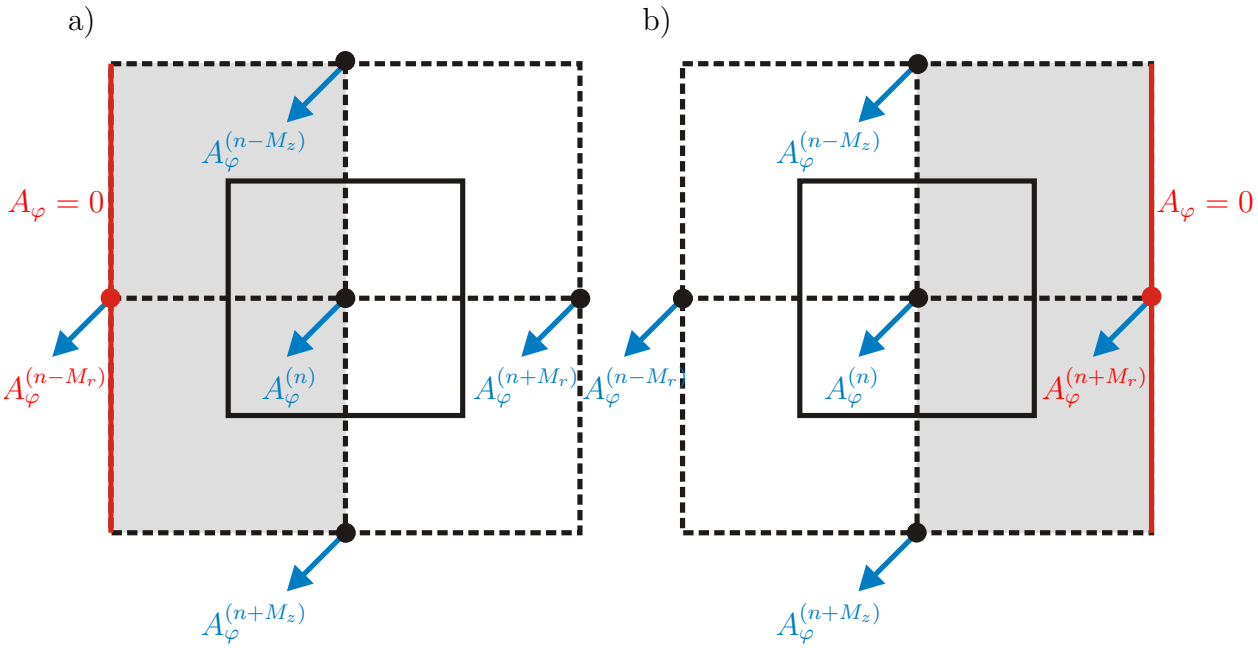

Figure 3.8: PEC boundary condition on the a) left side and b) right side of the simulation domain.

domain is shown in Fig. 3.8a. On the left boundary $A_\varphi(1, n_z) = 0$ and therefore, the discrete grid equation (Eq. (3.55)) can be rewritten by setting $A\varphi^{(n-M_r)} = 0$ as

$$-\nu_{\mathrm{H}_r}^{(n)} A_\varphi^{(n-M_z)} + \Bigg[\nu_{\mathrm{H}_r}^{(n)} + \nu_{\mathrm{H}_r}^{(n+M_z)} + \nu_{\mathrm{H}_z}^{(n)} \frac{r^{(n)}}{r^{(n-\frac{1}{2}M_r)}} + \nu_{\mathrm{H}_z}^{(n+M_r)} \frac{r^{(n)}}{r^{(n+\frac{1}{2}M_r)}} - \mathrm{j}\,\omega\,\widetilde{\sigma}^{(n)}\,(\Delta x)^2 \Bigg] A_\varphi^{(n)} - \nu_{\mathrm{H}_z}^{(n+M_r)} \frac{r^{(n+M_r)}}{r^{(n+\frac{1}{2}M_r)}} A_\varphi^{(n+M_r)} - \nu_{\mathrm{H}_r}^{(n+M_z)} A_\varphi^{(n+M_z)} = J_{\mathrm{e}\varphi}^{(n)}\,(\Delta r)^2 \tag{3.73}$$

$$\Rightarrow \left\{ \mathtt{t1}^{(n)}\,\mathcal{S}_{-M_z} + \left[\mathtt{d1}^{(n)} + \mathtt{d2}^{(n)}\right] \mathcal{I} + \mathtt{s2}^{(n)}\,\mathcal{S}_{+M_r} + \mathtt{t2}^{(n)}\,\mathcal{S}_{+M_z} \right\} \mathtt{x}^{(n)} = \mathtt{b}^{(n)}\,. \tag{3.74}$$

Right Boundary: The right side of the simulation domain is shown in Fig. 3.8b. The boundary condition results $A\varphi^{(N_r,n_z)} = 0$ and therefore, the discrete grid equation (Eq. (3.55)) can be rewritten by setting $A\varphi^{(n+M_r)} = 0$ as

$$-\ \nu_{\mathrm{H}_r}^{(n)} A_\varphi^{(n-M_z)} - \ \nu_{\mathrm{H}_z}^{(n)} \frac{r^{(n-M_r)}}{r^{(n-\frac{1}{2}M_r)}} A_\varphi^{(n-M_r)} + \Bigg[\ \nu_{\mathrm{H}_r}^{(n)} + \ \nu_{\mathrm{H}_r}^{(n+M_z)} + \ \nu_{\mathrm{H}_z}^{(n)} \frac{r^{(n)}}{r^{(n-\frac{1}{2}M_r)}} + \nu_{\mathrm{H}_z}^{(n+M_r)} \frac{r^{(n)}}{r^{(n+\frac{1}{2}M_r)}} - \mathrm{j}\,\omega\ \widetilde{\sigma}^{(n)}\,(\Delta x)^2 \Bigg] A_\varphi^{(n)} - \ \nu_{\mathrm{H}_r}^{(n+M_z)} A_\varphi^{(n+M_z)} \ = \ J_{\mathrm{e}\varphi}^{(n)}\,(\Delta r)^2 \tag{3.75}$$

$$\Rightarrow \left\{ \mathtt{t1}^{(n)}\,\mathcal{S}_{-M_z} + \mathtt{s1}^{(n)}\,\mathcal{S}_{-M_r} + \left[\mathtt{d1}^{(n)} + \mathtt{d2}^{(n)} \right] \mathcal{I} + \mathtt{t2}^{(n)}\,\mathcal{S}_{+M_z} \right\} \mathtt{x}^{(n)} \ = \ \mathtt{b}^{(n)}\,. \tag{3.76}$$

3.8 Formation of a Band Matrix

A typical LU decomposition is showed in Fig. 3.9. Now let us take the final grid equation in

$$[\mathbf{A}] = \begin{bmatrix} & [\mathbf{U}] & \\ [\mathbf{D}] & & \\ [\mathbf{L}] & & \end{bmatrix} = [\mathbf{L}] + [\mathbf{D}] + [\mathbf{U}]$$

$[\mathbf{L}]$: lower matrix
$[\mathbf{D}]$: diagonal matrix
$[\mathbf{U}]$: upper matrix

Figure 3.9: 2-D case in the rz plane: decomposition of the matrix $[\mathbf{A}]$ into 5 bands

cylindrical coordinates. Using the shift operator $\mathcal{S}_{\pm M_i}$ and the identity operator $\mathcal{I}$, we can form a band matrix from Eq. (3.57) by taking the following steps:

- The computation region is $(N_r - 1) \times (N_z - 1)$. The coefficients t1, t2, s1, s2, d1, d2 and b are computed for each node.

- The main diagonal of $[\mathbf{A}]$ correspond to the coefficients d1 and d2 with identity operator $\mathcal{I}$, and therefore, it contains $N' = (N_r - 1) \times (N_z - 1)$ values.

- t1 and t2 correspond to the first lower band LM1 and the second lower band LM2 respectively. The shift operator $\mathcal{S}_{\pm M_r} = 1$ and $\mathcal{S}_{\pm M_z} = N_r$. Using these values of the shift operators LM1 and LM2 are positioned as shown in Fig. 3.10, where LM1 and LM2 have $N' - 1$ and $N' - N_r$ components respectively.

- Similarly s1 and s2 correspond to the first upper band UM1 and the second upper band UM2 respectively. UM1 and UM2 contain $N' - 1$ and $N' - N_r$ components respectively, and are positioned as shown in Fig. 3.10.

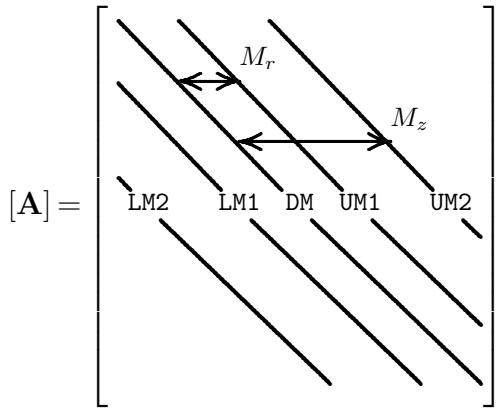

LM2	:	2nd lower band
LM1	:	1st lower band
DM	:	diagonal band
UM1	:	1st upper band
UM2	:	2nd upper band

Figure 3.10: 2-D case in the rz plane: formation of bandmatrx

We can rewrite Eq. (3.57) following these steps as

$$\left\{\mathtt{LM2}^{(n)}\,\mathcal{S}_{-M_z} + \mathtt{LM1}^{(n)}\,\mathcal{S}_{-M_r} + \mathtt{DM}^{(n)}\,\mathcal{I} + \mathtt{UM1}^{(n)}\,\mathcal{S}_{M_r} + \mathtt{UM2}^{(n)}\,\mathcal{S}_{M_z}\right\}\mathtt{x}^{(n)} = \mathtt{b}^{(n)} \quad , \tag{3.77}$$

with the normalized coefficients

$$\mathtt{DM}^{(n)} = \frac{\mathtt{d1}^{(n)} + \mathtt{d2}^{(n)}}{\mathtt{d1}^{(n)} + \mathtt{d2}^{(n)}} \;=\; 1 \quad . \tag{3.78}$$

$$\mathtt{LM2}^{(n)} = \frac{\mathtt{t1}^{(n)}}{\mathtt{t1}^{(n)} + \mathtt{s1}^{(n)} + \mathtt{s2}^{(n)} + \mathtt{t2}^{(n)} + \mathtt{d2}^{(n)}} \quad . \tag{3.79}$$

$$\mathtt{LM1}^{(n)} = \frac{\mathtt{s1}^{(n)}}{\mathtt{t1}^{(n)} + \mathtt{s1}^{(n)} + \mathtt{s2}^{(n)} + \mathtt{t2}^{(n)} + \mathtt{d2}^{(n)}} \quad . \tag{3.80}$$

$$\mathtt{UM1}^{(n)} = \frac{\mathtt{s2}^{(n)}}{\mathtt{t1}^{(n)} + \mathtt{s1}^{(n)} + \mathtt{s2}^{(n)} + \mathtt{t2}^{(n)} + \mathtt{d2}^{(n)}} \quad . \tag{3.81}$$

$$\mathtt{UM2}^{(n)} = \frac{\mathtt{t2}^{(n)}}{\mathtt{t1}^{(n)} + \mathtt{s1}^{(n)} + \mathtt{s2}^{(n)} + \mathtt{t2}^{(n)} + \mathtt{d2}^{(n)}} \quad . \tag{3.82}$$

$$\mathtt{x}^{(n)} = A_{\varphi}^{(n)} \quad . \tag{3.83}$$

$$\mathtt{b}^{(n)} = -\frac{J_{\mathrm{e}\varphi}^{(n)}\,(\Delta r)^2}{\mathtt{t1}^{(n)} + \mathtt{s1}^{(n)} + \mathtt{s2}^{(n)} + \mathtt{t2}^{(n)} + \mathtt{d2}^{(n)}} \quad . \tag{3.84}$$

We can write Eq. (3.77) in the general form

$$[\mathbf{A}]\,\{\mathbf{x}\} = \{\mathbf{b}\}\,, \tag{3.85}$$

which is a linear matrix equation and a suitable linear matrix solver will be used to solve this equation by determining the unknown values of $\{\mathbf{x}\}$.

3.9 Computation of Induced Electric Voltage

The electric field strength $\underline{\mathbf{E}}(\underline{\mathbf{R}},\omega)$ is then computed from the magnetic vector potential $\underline{\mathbf{A}}_{\mathrm{m}}(\underline{\mathbf{R}},\omega)$ in the second step using Eq. (2.128) which can be recalled from Chapter 2 as

$$\underline{\mathbf{E}}(\underline{\mathbf{R}},\omega) = \mathrm{j}\,\omega\underline{\mathbf{A}}_{\mathrm{m}}(\underline{\mathbf{R}},\omega)\,. \tag{3.86}$$

The induced electric voltage $V_{\mathrm{e}}(\omega)$ for each conductor of the receiving coil is then calculated from the electric field strength by

$$V_{\mathrm{e}}(\omega) = \oint \underline{\mathbf{E}}(\underline{\mathbf{R}}, \omega) \cdot \underline{\mathbf{dR}} \,. \tag{3.87}$$

The total induced electric voltage of the receiving coil is then computed as

$$V_{\mathrm{e}}^{\mathrm{tot}}(\omega) = N_t \; V_{\mathrm{e}}(\omega) \,, \tag{3.88}$$

where the receiving coil consists of N_t turns of copper wire. The modelling of the receiving coils will be discussed in detail in Chapter 7.

Chapter 4

Finite Element Method (FEM)

The finite element method (FEM) is a numerical technique for obtaining approximate solutions to boundary-value problems of mathematical physics. The basis of the modern finite element method consists of Ritz variational method and Galerkin's method. The principle of this method is to replace an entire continuous domain by a number of subdomains in which the unknown function is represented by interpolation functions with unknown coefficients and thus, the solution of the entire domain is approximated by a finite number of unknown coefficients. A system of algebraic equations is then obtained by applying the Ritz variational or Galerkin procedure (*Kost*, 1994; *Jin*, 2002). The system of equations are solved to determine the unknown coefficients. The following steps will be followed to solve a magnetoquasistatic problem using FEM:

- Formulation of the magnetoquasistatic governing equation (Sec. 4.1)
- Discretization of the domain in space (Sec. 4.2)
- Node-based elemental interpolation (Sec. 4.3)
- Formulation by Galerkin's method (Sec. 4.4)
- Formulation of the system of equations (Sec. 4.5)
- Implementation of the boundary conditions (Sec. 4.6)

4.1 Formulation of the Magnetoquasistatic Governing Equation

As we have discussed earlier, the described eddy current sensors are driven by a monochromatic excitation pulse, it is easier to solve the magnetoquasistatic problem in the frequency domain than in the time domain. Let us recall the governing equation of the magnetoquasistatic problem in the frequency domain from Chapter 2 as

$$\boldsymbol{\nabla}\times\left[\nu(\underline{\mathbf{R}})\boldsymbol{\nabla}\times\underline{\mathbf{A}}_{\mathrm{m}}(\underline{\mathbf{R}},\omega)\right]-\,\mathrm{j}\,\omega\sigma_{\mathrm{e}}(\underline{\mathbf{R}})\;\underline{\mathbf{A}}_{\mathrm{m}}(\underline{\mathbf{R}},\omega)=\underline{\mathbf{J}}_{\mathrm{e}}^{\mathrm{imp}}(\underline{\mathbf{R}},\omega)\;\;. \tag{4.1}$$

The developed encircling coil sensors are simulated using the rotational symmetry and hence, a 3-D magnetoquasistatic problem is reduced into a 2-D problem in cylindrical coordinates. As the first step, the discrete field quantities will be discussed in Cartesian coordinates.

4.1.1 2-D Formulation in Cartesian Coordinates

The Curl Operator of Eq. (4.1) is computed in Cartesian coordinates as:

$$\boldsymbol{\nabla}\times\underline{\mathbf{A}}_{\mathrm{m}}(\underline{\mathbf{R}},\omega) \;=\; \left[\frac{\partial A_z(x,z,\omega)}{\partial y}-\frac{\partial A_y(x,z,\omega)}{\partial z}\right]\underline{\mathbf{e}}_x+\left[\frac{\partial A_x(x,z,\omega)}{\partial z}-\frac{\partial A_z(x,z,\omega)}{\partial x}\right]\underline{\mathbf{e}}_y + \left[\frac{\partial A_y(x,z,\omega)}{\partial x}-\frac{\partial A_x(x,z,\omega)}{\partial y}\right]\underline{\mathbf{e}}_z \;. \quad (4.2)$$

Let us consider that our simulation domain Ω lies in xz plane and therefore, we have to consider only the y component of magnetic vector potential. As a result, the curl operator is reduced to

$$\boldsymbol{\nabla}\times\underline{\mathbf{A}}_{\mathrm{m}}(\underline{\mathbf{R}},\omega) = -\;\frac{\partial A_y(x,z,\omega)}{\partial z}\;\underline{\mathbf{e}}_x+\;\frac{\partial A_y(x,z,\omega)}{\partial x}\;\underline{\mathbf{e}}_z \;. \quad (4.3)$$

The left-hand side of Eq. (4.1) can be computed as

$$\begin{aligned}&\boldsymbol{\nabla}\times\left[\nu(\underline{\mathbf{R}})\boldsymbol{\nabla}\times\underline{\mathbf{A}}_{\mathrm{m}}(\underline{\mathbf{R}},\omega)\right]\\ &=\left[\underline{\mathbf{e}}_x\frac{\partial}{\partial x}\;+\;\underline{\mathbf{e}}_y\frac{\partial}{\partial y}\;+\;\underline{\mathbf{e}}_z\frac{\partial}{\partial z}\right]\times\left[-\;\nu(x,z)\frac{\partial A_y(x,z,\omega)}{\partial z}\underline{\mathbf{e}}_x+\;\nu(x,z)\frac{\partial A_y(x,z,\omega)}{\partial x}\underline{\mathbf{e}}_z\right].\end{aligned} \quad (4.4)$$

The electric current density $\underline{\mathbf{J}}_{\mathrm{e}}^{\mathrm{imp}}(\underline{\mathbf{R}},\omega)$ has only the y component and therefore, we have to consider only the coefficients of $\underline{\mathbf{e}}_y$, which results

$$\boldsymbol{\nabla}\times\left[\nu(\underline{\mathbf{R}})\boldsymbol{\nabla}\times\underline{\mathbf{A}}_{\mathrm{m}}(\underline{\mathbf{R}},\omega)\right] \;=\; -\;\frac{\partial}{\partial x}\left[\nu(x,z)\frac{\partial A_y(x,z,\omega)}{\partial x}\right]\underline{\mathbf{e}}_y-\;\frac{\partial}{\partial z}\left[\nu(x,z)\frac{\partial A_y(x,z,\omega)}{\partial z}\right]\underline{\mathbf{e}}_y\,. \quad (4.5)$$

Inserting Eq. (4.5) in Eq. (4.1) and replacing $\underline{\mathbf{A}}_{\mathrm{m}}(\underline{\mathbf{R}},\omega)$ with $A_y(x,z,\omega)\underline{\mathbf{e}}_y$ results

$$-\;\frac{\partial}{\partial x}\left[\nu(x,z)\frac{\partial A_y(x,z,\omega)}{\partial x}\right]\underline{\mathbf{e}}_y-\;\frac{\partial}{\partial z}\left[\nu(x,z)\frac{\partial A_y(x,z,\omega)}{\partial z}\right]\underline{\mathbf{e}}_y - \;\mathrm{j}\,\omega\sigma_{\mathrm{e}}(x,z)A_y(x,z,\omega)\underline{\mathbf{e}}_y = J_{\mathrm{e}y}(x,z,\omega)\underline{\mathbf{e}}_y\,, \quad (4.6)$$

which is rewritten as

$$-\;\frac{\partial}{\partial x}\left[\nu(x,z)\frac{\partial A_y(x,z,\omega)}{\partial x}\right]-\;\frac{\partial}{\partial z}\left[\nu(x,z)\frac{\partial A_y(x,z,\omega)}{\partial z}\right] - \;\mathrm{j}\,\omega\sigma_{\mathrm{e}}(x,z)A_y(x,z,\omega) = J_{\mathrm{e}y}(x,z,\omega)\;. \quad (4.7)$$

The Dirichlet and Neumann conditions are common boundary conditions for the magnetic vector potential. We write the Dirichlet boundary condition as

$$A_y(x,z,\omega) = \text{constant}\,. \quad (4.8)$$

At the interface between the two medium having different magnetic impermeability ν, the magnetic vector potential satisfies the continuity conditions

$$A_y^{(1)}(x,z,\omega) = A_y^{(2)}(x,z,\omega) \quad (4.9)$$

$$\nu^{(1)}\frac{\partial A_y^{(1)}(x,z,\omega)}{\partial n} = \nu^{(2)}\frac{\partial A_y^{(2)}(x,z,\omega)}{\partial n}\;. \quad (4.10)$$

4.1.2 2-D Formulation in Cylindrical Coordinates

We can compute the Curl Operator of Eq. (4.1) in cylindrical coordinates as:

$$\boldsymbol{\nabla}\times\underline{\mathbf{A}}_{\mathrm{m}}(\underline{\mathbf{R}},\omega) = \left[\frac{1}{r}\frac{\partial A_z(r,z,\omega)}{\partial\varphi} - \frac{\partial A_\varphi(r,z,\omega)}{\partial z}\right]\underline{\mathbf{e}}_r + \left[\frac{\partial A_r(r,z,\omega)}{\partial z} - \frac{\partial A_z(r,z,\omega)}{\partial r}\right]\underline{\mathbf{e}}_\varphi + \frac{1}{r}\left[\frac{\partial(r\,A_\varphi(r,z,\omega))}{\partial r} - \frac{\partial A_r(r,z,\omega)}{\partial\varphi}\right]\underline{\mathbf{e}}_z \ . \tag{4.11}$$

Let us consider the rz plane as the computation plane, therefore, the magnetic vector potential contains only the φ component. The curl operator of Eq. (4.11) is reduced to

$$\boldsymbol{\nabla}\times\underline{\mathbf{A}}_{\mathrm{m}}(\underline{\mathbf{R}},\omega) = -\frac{\partial A_\varphi(r,z,\omega)}{\partial z}\underline{\mathbf{e}}_r + \frac{1}{r}\frac{\partial(r\,A_\varphi(r,z,\omega))}{\partial r}\underline{\mathbf{e}}_z \ . \tag{4.12}$$

Assuming that the electric current density $\underline{\mathbf{J}}_{\mathrm{e}}^{\mathrm{imp}}(\underline{\mathbf{R}},\omega)$ has only the φ component, we consider only the coefficients of $\underline{\mathbf{e}}_\varphi$, which results

$$\boldsymbol{\nabla}\times\left[\nu(\underline{\mathbf{R}})\boldsymbol{\nabla}\times\underline{\mathbf{A}}_{\mathrm{m}}(\underline{\mathbf{R}},\omega)\right] = -\frac{\partial}{\partial r}\left[\frac{\nu(r,z)}{r}\frac{\partial A_\varphi(r,z,\omega)}{\partial r}\right]\underline{\mathbf{e}}_\varphi - \frac{\partial}{\partial z}\left[\nu(r,z)\frac{\partial A_\varphi(r,z,\omega)}{\partial z}\right]\underline{\mathbf{e}}_\varphi \, . \tag{4.13}$$

Inserting Eq. (4.13) in Eq. (4.1) and replacing $\underline{\mathbf{A}}_{\mathrm{m}}(\underline{\mathbf{R}},\omega)$ with $A_\varphi(r,z,\omega)\underline{\mathbf{e}}_\varphi$ results

$$-\frac{\partial}{\partial r}\left[\frac{1}{r}\nu(r,z)\frac{\partial A_\varphi(r,z,\omega)}{\partial r}\right]\underline{\mathbf{e}}_\varphi - \frac{\partial}{\partial z}\left[\nu(r,z)\frac{\partial A_\varphi(r,z,\omega)}{\partial z}\right]\underline{\mathbf{e}}_\varphi - \mathrm{j}\,\omega\sigma_{\mathrm{e}}(r,z)A_\varphi(r,z,\omega)\underline{\mathbf{e}}_\varphi = J_{\mathrm{e}\varphi}(r,z,\omega)\underline{\mathbf{e}}_\varphi \, , \tag{4.14}$$

which is rearranged as

$$-\frac{\partial}{\partial r}\left[\frac{1}{r}\nu(\underline{\mathbf{R}})\frac{\partial A_\varphi(r,z,\omega)}{\partial r}\right] - \frac{\partial}{\partial z}\left[\nu(r,z)\frac{\partial A_\varphi(r,z,\omega)}{\partial z}\right] - \mathrm{j}\,\omega\sigma_{\mathrm{e}}(r,z)A_\varphi(r,z,\omega) = J_{\mathrm{e}\varphi}(r,z,\omega) \ . \tag{4.15}$$

Before we employ the finite element formulation for a solution of the problem, we check the continuity conditions for rA_φ at the interface of medium 1 and 2.

$$r^{(1)}A_\varphi^{(1)}(r,z,\omega) = r^{(2)}A_\varphi^{(2)}(r,z,\omega) \tag{4.16}$$

$$\frac{1}{r^{(1)}\nu^{(1)}}\frac{\partial}{\partial n}\left[r^{(1)}A_\varphi^{(1)}(r,z,\omega)\right] = \frac{1}{r^{(2)}\nu^{(2)}}\frac{\partial}{\partial n}\left[r^{(2)}A_\varphi^{(2)}(r,z,\omega)\right] \ . \tag{4.17}$$

4.2 Discretization of the Domain in 2-D Space

We have to discretize the simulation domain before we start with the discretization of the governing equation. FEM is based on the spatial discretization of the solution domain, where a given finite element is associated to its physical dimensions in space (*Ida*, 1995). Therefore, the first step of a finite element analysis is to divide the domain Ω in a finite

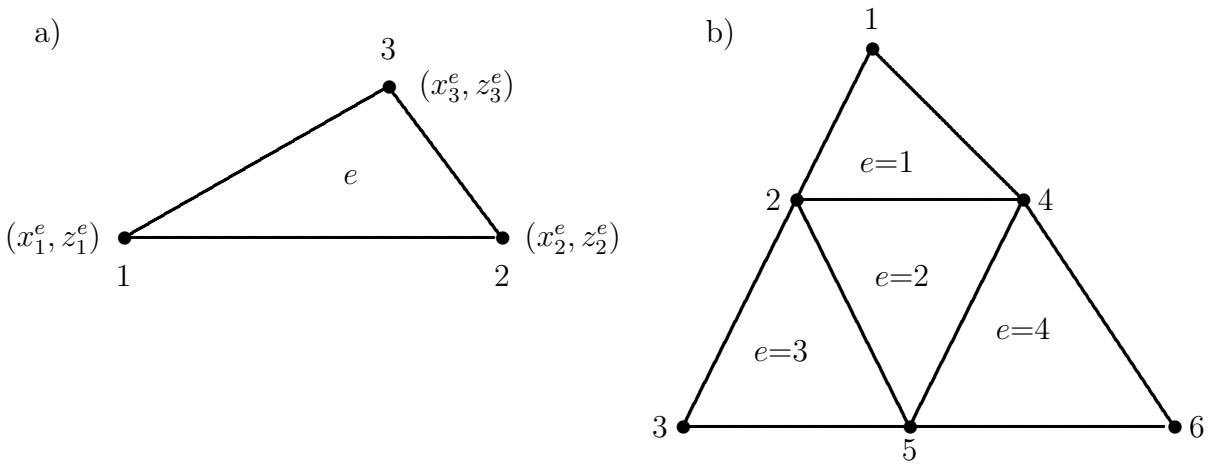

Figure 4.1: a) 2-D triangular element and b) 2-D discretization with four elements.

number of elements, in our case, a finite number of two-dimensional elements. Furthermore, the elements should be connected by their vertices, i.e., a vertex of an element can only be the vertex of the neighboring element. We have taken linear triangular elements to discretize the domain. A typical triangular element is shown in Fig. 4.1a. The nodes and elements can be labeled with separate sets of integers for identification. Since each element is related to three nodes, a node is assigned a local label in the associated element, in addition to its global label relative to the entire system. Fig. 4.1b shows a typical FEM discretization with four elements.

4.3 Node-Based Elemental Interpolation

After discretizing the simulation domain we have to approximate the unknown function A_y in case of the cartesian coordinates. For linear triangular elements the unknown function A_y within each element can be approximated as

$$A_y^e(x,z) = a^e + b^e x + c^e z \ , \tag{4.18}$$

where a^e, b^e and c^e are constant coefficients to be determined for each element e. Fig. 4.1a shows a linear triangular element with three nodes, where the nodes are numbered counter-clockwise by numerals 1, 2 and 3, with the corresponding values of A_y denoted by A_{y1}^e, A_{y2}^e and A_{y3}^e. Using Eq. (4.18) at the three nodes results

$$A_{y1}^e(x,z) = a^e + b^e x_1 + c^e z_1 \tag{4.19}$$

$$A_{y2}^e(x,z) = a^e + b^e x_2 + c^e z_2 \tag{4.20}$$

$$A_{y3}^e(x,z) = a^e + b^e x_3 + c^e z_3 \ , \tag{4.21}$$

where x_j^e and z_j^e represents the coordinates of the j-th node in the e-th element for $j = 1, 2, 3$. Eqs. (4.19)-(4.21) can be rewritten as

$$\begin{bmatrix} A_{y1}^e \\ A_{y2}^e \\ A_{y3}^e \end{bmatrix} = \begin{bmatrix} 1 & x_1 & z_1 \\ 1 & x_2 & z_2 \\ 1 & x_3 & z_3 \end{bmatrix} \begin{bmatrix} a \\ b \\ c \end{bmatrix} \ . \tag{4.22}$$

Solving for the coefficients a^e, b^e und c^e as functions of A^e_{yj} results

$$\begin{bmatrix} a \\ b \\ c \end{bmatrix} = \begin{bmatrix} 1 & x_1 & z_1 \\ 1 & x_2 & z_2 \\ 1 & x_3 & z_3 \end{bmatrix}^{-1} \begin{bmatrix} A^e_{y1} \\ A^e_{y2} \\ A^e_{y3} \end{bmatrix} . \tag{4.23}$$

Inserting Eq. (4.23) in Eq. (4.18) yields

$$A^e_y(x,z) = \begin{bmatrix} 1 & x & z \end{bmatrix} \begin{bmatrix} 1 & x_1 & z_1 \\ 1 & x_2 & z_2 \\ 1 & x_3 & z_3 \end{bmatrix}^{-1} \begin{bmatrix} A^e_{y1} \\ A^e_{y2} \\ A^e_{y3} \end{bmatrix} , \tag{4.24}$$

which can be written in the form (*Silvester & Ferrari*, 1983)

$$A^e_y(x,z) = \sum_{j=1}^{3} N^e_j(x,z)\ A^e_{yj} \ , \tag{4.25}$$

where N^e_j are the interpolation or expansion functions, also known as basis functions, which can be denoted as

$$N^e_j(x,z) = \frac{1}{2\Delta^e}(a^e_j + b^e_j x + c^e_j z) \ , \tag{4.26}$$

in which

$$\begin{aligned} a^e_1 &= x^e_2 z^e_3 - x^e_3 z^e_2; \quad & b^e_1 &= z^e_2 - z^e_3; \quad & c^e_1 &= x^e_3 - x^e_2 \\ a^e_2 &= x^e_3 z^e_1 - x^e_1 z^e_3; \quad & b^e_2 &= z^e_3 - z^e_1; \quad & c^e_2 &= x^e_1 - x^e_3 \\ a^e_3 &= x^e_1 z^e_2 - x^e_2 z^e_1; \quad & b^e_3 &= z^e_1 - z^e_2; \quad & c^e_3 &= x^e_2 - x^e_1 \end{aligned} \tag{4.27}$$

and Δ^e represents the area of the e-th element as

$$\Delta^e = \frac{1}{2} \begin{vmatrix} 1 & x^e_1 & z^e_1 \\ 1 & x^e_2 & z^e_2 \\ 1 & x^e_3 & z^e_3 \end{vmatrix} = \frac{1}{2}\left(b^e_1 c^e_2 - b^e_2 c^e_1\right) . \tag{4.28}$$

4.4 Formulation by Galerkin's Method

Galerkin's method belongs to the family of weighted residual methods, which seeks the solution by weighting the residual of the differential equation. When applying Galerkin's testing procedure, the testing function is identical to the expansion function (*Volakis et al.*, 1998).

4.4.1 Formulation in Cartesian Coordinates

The residual associated with Eq. (4.7) is computed as

$$\begin{aligned} r = &- \frac{\partial}{\partial x}\left[\nu(x,z)\frac{\partial A_y(x,z,\omega)}{\partial x}\right] - \frac{\partial}{\partial z}\left[\nu(x,z)\frac{\partial A_y(x,z,\omega)}{\partial z}\right] - \mathrm{j}\,\omega\sigma_{\mathrm{e}}(x,z)A_y(x,z,\omega) \\ &- J_{\mathrm{e}y}(x,z,\omega) . \end{aligned} \tag{4.29}$$

For simplicity let us replace $A_y(x,z,\omega)$ with A_y and for element e we rearrange Eq. (4.29) as

$$r^e = -\frac{\partial}{\partial x}\left[\nu^e \frac{\partial A_y}{\partial x}\right] - \frac{\partial}{\partial z}\left[\nu^e \frac{\partial A_y}{\partial z}\right] - \mathrm{j}\,\omega\sigma^e A_y - J_{ey} \tag{4.30}$$

and the weighted residual for element e is formulated as

$$R_i^e = \iint\limits_{\Omega^e} N_i^e \; r \; \mathrm{d}x \; \mathrm{d}z \qquad ; \; i = 1,2,3 \; . \tag{4.31}$$

Inserting Eq. (4.30) in Eq. (4.31) yields

$$R_i^e = \iint\limits_{\Omega^e} N_i^e \left[-\frac{\partial}{\partial x}\left(\nu^e \frac{\partial A_y}{\partial x}\right) - \frac{\partial}{\partial z}\left(\nu^e \frac{\partial A_y}{\partial z}\right) - \mathrm{j}\,\omega\sigma^e A_y - J_{ey}\right] \mathrm{d}x \; \mathrm{d}z \; , \tag{4.32}$$

which is written as

$$\begin{aligned} R_i^e \;=\; & -\iint\limits_{\Omega^e} N_i^e \frac{\partial}{\partial x}\left(\nu^e \frac{\partial A_y}{\partial x}\right) \mathrm{d}x \; \mathrm{d}z - \iint\limits_{\Omega^e} N_i^e \frac{\partial}{\partial z}\left(\nu^e \frac{\partial A_y}{\partial z}\right) \mathrm{d}x \; \mathrm{d}z \\ & -\mathrm{j}\,\omega \iint\limits_{\Omega^e} N_i^e \sigma^e A_y \; \mathrm{d}x \; \mathrm{d}z - \iint\limits_{\Omega^e} N_i^e J_{ey} \; \mathrm{d}x \; \mathrm{d}z \; . \end{aligned} \tag{4.33}$$

We formulate the first integral of Eq. (4.33) as

$$-\iint\limits_{\Omega^e} N_i^e \frac{\partial}{\partial x}\left(\nu^e \frac{\partial A_y}{\partial x}\right) \mathrm{d}x \; \mathrm{d}z \;=\; -\iint\limits_{\Omega^e} \left[-\frac{\partial N_i^e}{\partial x}\,\nu^e \frac{\partial A_y}{\partial x} + \frac{\partial}{\partial x}\left(N_i^e\,\nu^e \frac{\partial A_y}{\partial x}\right)\right] \mathrm{d}x \; \mathrm{d}z \tag{4.34}$$

and we rewrite the second integral of Eq. (4.33) as

$$-\iint\limits_{\Omega^e} N_i^e \frac{\partial}{\partial z}\left(\nu^e \frac{\partial A_y}{\partial z}\right) \mathrm{d}x \; \mathrm{d}z \;=\; -\iint\limits_{\Omega^e} \left[-\frac{\partial N_i^e}{\partial z}\,\nu^e \frac{\partial A_y}{\partial z} + \frac{\partial}{\partial z}\left(N_i^e\,\nu^e \frac{\partial A_y}{\partial z}\right)\right] \mathrm{d}x \; \mathrm{d}z \; . \tag{4.35}$$

Using Eqs. (4.34)-(4.35) we rearrange Eq. (4.33) as

$$\begin{aligned} R_i^e \;=\; & -\iint\limits_{\Omega^e} \left[-\frac{\partial N_i^e}{\partial x}\,\nu^e \frac{\partial A_y}{\partial x} + \frac{\partial}{\partial x}\left(N_i^e\,\nu^e \frac{\partial A_y}{\partial x}\right)\right] \mathrm{d}x \; \mathrm{d}z \\ & -\iint\limits_{\Omega^e} \left[-\frac{\partial N_i^e}{\partial z}\,\nu^e \frac{\partial A_y}{\partial z} + \frac{\partial}{\partial z}\left(N_i^e\,\nu^e \frac{\partial A_y}{\partial z}\right)\right] \mathrm{d}x \; \mathrm{d}z \\ & -\mathrm{j}\,\omega \iint\limits_{\Omega^e} N_i^e \sigma^e A_y \; \mathrm{d}x \; \mathrm{d}z - \iint\limits_{\Omega^e} N_i^e J_{ey} \; \mathrm{d}x \; \mathrm{d}z \\ \Rightarrow R_i^e \;=\; & \iint\limits_{\Omega^e} \left[\frac{\partial N_i^e}{\partial x}\,\nu^e \frac{\partial A_y}{\partial x} + \frac{\partial N_i^e}{\partial z}\,\nu^e \frac{\partial A_y}{\partial z}\right] \mathrm{d}x \; \mathrm{d}z \\ & -\iint\limits_{\Omega^e} \left[\frac{\partial}{\partial x}\left(N_i^e\,\nu^e \frac{\partial A_y}{\partial x}\right) + \frac{\partial}{\partial z}\left(N_i^e\,\nu^e \frac{\partial A_y}{\partial z}\right)\right] \mathrm{d}x \; \mathrm{d}z \\ & -\mathrm{j}\,\omega \iint\limits_{\Omega^e} N_i^e \sigma^e A_y \; \mathrm{d}x \; \mathrm{d}z - \iint\limits_{\Omega^e} N_i^e J_{ey} \; \mathrm{d}x \; \mathrm{d}z \; . \end{aligned} \tag{4.36}$$

The second integral of Eq. (4.36) is rewritten as

$$
\begin{aligned}
&-\iint\limits_{\Omega^e}\left[\frac{\partial}{\partial x}\left(N_i^e\,\nu^e\,\frac{\partial A_y}{\partial x}\right)+\frac{\partial}{\partial z}\left(N_i^e\,\nu^e\,\frac{\partial A_y}{\partial z}\right)\right]\mathrm{d}x\;\mathrm{d}z\\
&\qquad=-\iint\limits_{\Omega^e}\left[\frac{\partial U(x,z)}{\partial x}+\frac{\partial V(x,z)}{\partial z}\right]\mathrm{d}S\\
&\qquad=-\iint\limits_{\Omega^e}\boldsymbol{\nabla}\cdot\left[U(x,z)\underline{\mathbf{e}}_x+V(x,z)\underline{\mathbf{e}}_z\right]\mathrm{d}S\;\;, \qquad (4.37)
\end{aligned}
$$

where

$$U(x,z)=N_i^e\,\nu^e\,\frac{\partial A_y}{\partial x} \qquad (4.38)$$

$$V(x,z)=N_i^e\,\nu^e\,\frac{\partial A_y}{\partial z}\;\;. \qquad (4.39)$$

Using Gauss' theorem on the right-side of Eq. (4.37) yields

$$-\iint\limits_{\Omega^e}\boldsymbol{\nabla}\cdot\left[U(x,z)\underline{\mathbf{e}}_x+V(x,z)\underline{\mathbf{e}}_z\right]\mathrm{d}S=-\oint\limits_{C=\partial S}\left[U(x,z)\underline{\mathbf{e}}_x+V(x,z)\underline{\mathbf{e}}_z\right]\cdot\underline{\mathbf{dR}}\;\;, \qquad (4.40)$$

which results

$$
\begin{aligned}
&-\iint\limits_{\Omega^e}\left[\frac{\partial}{\partial x}\left(N_i^e\,\nu^e\,\frac{\partial A_y}{\partial x}\right)+\frac{\partial}{\partial z}\left(N_i^e\,\nu^e\,\frac{\partial A_y}{\partial z}\right)\right]\mathrm{d}x\;\mathrm{d}z\\
&\qquad=-\oint\limits_{C=\partial S}\left\{\left[N_i^e\,\nu^e\,\frac{\partial A_y}{\partial x}\right]\underline{\mathbf{e}}_x+\left[N_i^e\,\nu^e\,\frac{\partial A_y}{\partial z}\right]\underline{\mathbf{e}}_z\right\}\cdot\underline{\mathbf{dR}}\;\;. \qquad (4.41)
\end{aligned}
$$

Inserting Eq. (4.41) in Eq. (4.36) results

$$
\begin{aligned}
R_i^e \;=\;&\iint\limits_{\Omega^e}\left[\frac{\partial N_i^e}{\partial x}\,\nu^e\,\frac{\partial A_y}{\partial x}+\frac{\partial N_i^e}{\partial z}\,\nu^e\,\frac{\partial A_y}{\partial z}\right]\mathrm{d}x\;\mathrm{d}z\\
&-\oint\limits_{C=\partial S}\left\{\left[N_i^e\,\nu^e\,\frac{\partial A_y}{\partial x}\right]\underline{\mathbf{e}}_x+\left[N_i^e\,\nu^e\,\frac{\partial A_y}{\partial z}\right]\underline{\mathbf{e}}_z\right\}\cdot\underline{\mathbf{dR}}\\
&-\mathrm{j}\,\omega\iint\limits_{\Omega^e}N_i^e\sigma^e A_y\;\mathrm{d}x\;\mathrm{d}z-\iint\limits_{\Omega^e}N_i^e J_{\mathrm{e}y}\;\mathrm{d}x\;\mathrm{d}z\;\;. \qquad (4.42)
\end{aligned}
$$

The unknown function A_y is written with basis functions using Eq. (4.25) as

$$A_y^e\,(x,z)=\sum_{j=1}^{3}N_j^e\,(x,z)\;A_{yj}^e \qquad (4.43)$$

and the first order derivatives of A_y is expressed as

$$\frac{\partial}{\partial x}A_y^e\,(x,z)=\sum_{j=1}^{3}A_{yj}^e\frac{\partial N_j^e\,(x,z)}{\partial x} \qquad (4.44)$$

$$\frac{\partial}{\partial z}A_y^e\,(x,z)=\sum_{j=1}^{3}A_{yj}^e\frac{\partial N_j^e\,(x,z)}{\partial z}\;\;. \qquad (4.45)$$

Using Eqs. (4.43)-(4.45) we rewrite Eq. (4.42) as

$$\begin{aligned} R_i \;=\; & \sum_{j=1}^{3} A_{yj}^e \iint\limits_{\Omega^e} \nu^e \left[\frac{\partial N_i^e}{\partial x} \frac{\partial N_j^e}{\partial x} + \frac{\partial N_i^e}{\partial z} \frac{\partial N_j^e}{\partial z} \right] \mathrm{d}x \; \mathrm{d}z \\ & - \mathrm{j}\,\omega \sum_{j=1}^{3} A_{yj}^e \iint\limits_{\Omega^e} \sigma^e \, N_i^e N_j^e \, \mathrm{d}x \; \mathrm{d}z - \iint\limits_{\Omega^e} N_i^e J_{ey} \; \mathrm{d}x \; \mathrm{d}z \\ & - \oint\limits_{C=\partial S} \left\{ \left[N_i^e \, \nu^e \, \frac{\partial A_y}{\partial x} \right] \underline{\mathbf{e}}_x + \left[N_i^e \, \nu^e \, \frac{\partial A_y}{\partial z} \right] \underline{\mathbf{e}}_z \right\} \cdot \underline{\mathbf{dR}} \;, \end{aligned} \tag{4.46}$$

which is written in matrix form

$$[\mathbf{S}]\,\{\mathbf{A}\} - \mathrm{j}\,\omega\,[\mathbf{T}]\,\{\mathbf{A}\} - \{\mathbf{b}\} + \{\mathbf{g}\} = 0 \;. \tag{4.47}$$

Rearranging Eq. (4.47) results

$$[\mathbf{S}]\,\{\mathbf{A}\} - \mathrm{j}\,\omega\,[\mathbf{T}]\,\{\mathbf{A}\} = \{\mathbf{b}\} - \{\mathbf{g}\} \;, \tag{4.48}$$

with the coefficients in local form

$$S_{ij}^e = \iint\limits_{\Omega^e} \nu^e \left[\frac{\partial N_i^e}{\partial x} \frac{\partial N_j^e}{\partial x} + \frac{\partial N_i^e}{\partial z} \frac{\partial N_j^e}{\partial z} \right] \mathrm{d}x \; \mathrm{d}z \tag{4.49}$$

$$T_{ij}^e = \iint\limits_{\Omega^e} \sigma^e \, N_i^e N_j^e \, \mathrm{d}x \; \mathrm{d}z \tag{4.50}$$

$$b_i^e = \iint\limits_{\Omega^e} N_i^e J_{ey} \; \mathrm{d}x \; \mathrm{d}z \tag{4.51}$$

$$g_i^e = \oint\limits_{C=\partial S} \left\{ \left[N_i^e \, \nu^e \, \frac{\partial A_y}{\partial x} \right] \underline{\mathbf{e}}_x + \left[N_i^e \, \nu^e \, \frac{\partial A_y}{\partial z} \right] \underline{\mathbf{e}}_z \right\} \cdot \underline{\mathbf{dR}} \tag{4.52}$$

$$A^e = A_y^e(x, z, \omega) \;. \tag{4.53}$$

In our case, there is no source at the boundary and therefore, we set $\{\mathbf{g}\} = 0$ and simplify Eq. (4.48) as

$$[\mathbf{S}]\,\{\mathbf{A}\} - \mathrm{j}\,\omega\,[\mathbf{T}]\,\{\mathbf{A}\} = \{\mathbf{b}\} \;. \tag{4.54}$$

4.4.2 Formulation in Cylindrical Coordinates

The magnetoquasistatic governing equation in cylindrical coordinates is described by Eq. (4.14). The residual associated with this equation is computed as

$$\begin{aligned} r = & - \frac{\partial}{\partial r} \left[\frac{1}{r} \nu(r,z) \frac{\partial A_\varphi(r,z,\omega)}{\partial r} \right] - \frac{\partial}{\partial z} \left[\nu(r,z) \frac{\partial A_\varphi(r,z,\omega)}{\partial z} \right] - \mathrm{j}\,\omega \sigma_\mathrm{e}(r,z) A_\varphi(r,z,\omega) \\ & - J_{\mathrm{e}\varphi}(r,z,\omega) \,. \end{aligned} \tag{4.55}$$

If we follow the same steps as for the cartesian coordinates, we shall obtain the matrix equation of similar form

$$[\mathbf{S}]\,\{\mathbf{A}\} - \mathrm{j}\,\omega\,[\mathbf{T}]\,\{\mathbf{A}\} = \{\mathbf{b}\}\ , \tag{4.56}$$

where the coefficients are denoted as

$$S_{ij}^e = \iint\limits_{\Omega^e} \frac{\nu^e}{r}\left[\frac{\partial N_i^e}{\partial r}\,\frac{\partial N_j^e}{\partial r} + \frac{\partial N_i^e}{\partial z}\,\frac{\partial N_j^e}{\partial z}\right] \mathrm{d}r\ \mathrm{d}z \tag{4.57}$$

$$T_{ij}^e = \iint\limits_{\Omega^e} \sigma^e\, N_i^e N_j^e\, \mathrm{d}r\ \mathrm{d}z \tag{4.58}$$

$$b_i^e = \iint\limits_{\Omega^e} N_i^e J_{\mathrm{e}\varphi}\ \mathrm{d}r\ \mathrm{d}z \tag{4.59}$$

$$g_i^e = \oint\limits_{C=\partial S} \left\{\left[N_i^e\,\nu^e\,\frac{\partial A_\varphi}{\partial r}\right]\underline{\mathbf{e}}_r + \left[N_i^e\,\nu^e\,\frac{\partial A_\varphi}{\partial z}\right]\underline{\mathbf{e}}_z\right\}\cdot\underline{\mathbf{dR}} \tag{4.60}$$

$$A^e = r\,A_\varphi^e(r,z,\omega)\ . \tag{4.61}$$

4.5 Formulation of the System of Equations

Let us consider the 2-D formulation in cartesian coordinates. The global matrices [**T**], [**S**] and {**b**} described in Eq. (4.54) can be computed using the following steps:

- Computation of the local coefficients S_{ij}^e, T_{ij}^e and b_i^e for each element
- Relating the local nodes of the elements to the global nodes
- Arrangement of the local coefficients in global matrices

4.5.1 Computation of the Local Coefficients

The local T-matrix is described in Eq. (4.50) as

$$T_{ij}^e = \iint\limits_{\Omega^e} \sigma^e\, N_i^e N_j^e\, \mathrm{d}x\ \mathrm{d}z\ , \tag{4.62}$$

which is computed as (see *Ida*, 1995, p. 316)

$$[T^e] = \frac{\Delta^e}{12}\,\sigma^e \begin{bmatrix} 2 & 1 & 1 \\ 1 & 2 & 1 \\ 1 & 1 & 2 \end{bmatrix}\ . \tag{4.63}$$

Furthermore, the S-Matrix is denoted by Eq. (4.49)

$$S_{ij}^e = \iint\limits_{\Omega^e} \nu^e \left[\frac{\partial N_i^e}{\partial x}\,\frac{\partial N_j^e}{\partial x} + \frac{\partial N_i^e}{\partial z}\,\frac{\partial N_j^e}{\partial z}\right] \mathrm{d}x\ \mathrm{d}z\ , \tag{4.64}$$

which is evaluated as (see *Ida*, 1995, p. 323)

$$[S^e] = \frac{\nu^e}{4\,\Delta^e} \begin{bmatrix} (b_1^e)^2 + (c_1^e)^2 & b_1^e\,b_2^e + c_1^e\,c_2^e & b_1^e\,b_3^e + c_1^e\,c_3^e \\ b_2^e\,b_1^e + c_2^e\,c_1^e & (b_2^e)^2 + (c_2^e)^2 & b_2^e\,b_3^e + c_2^e\,c_3^e \\ b_3^e\,b_1^e + c_3^e\,c_1^e & b_3^e\,b_2^e + c_3^e\,c_2^e & (b_3^e)^2 + (c_3^e)^2 \end{bmatrix} . \tag{4.65}$$

The local b-vector in cartesian coordinates is described by

$$b_i^e = \iint\limits_{\Omega^e} N_i^e J_{ey}\ \mathrm{d}x\ \mathrm{d}z \tag{4.66}$$

and is formulated as (see *Jin*, 2002, p. 98)

$$b_i^e = \frac{\Delta^e}{3} J_{ey}\ . \tag{4.67}$$

4.5.2 Relating the Local Nodes of the Elements to the Global Nodes

A typical 2-D discretizing scheme is shown in Fig. 4.2, where the global node numbers are marked in blue and the local node numbers in black. Each element has three nodes who can be identified by their local as well as global numbers. A relationship between these two numbers is presented in Table 4.1. On the left side, the elements are described with global numbers associated to the corresponding nodes. As for example, an arbitrary element $e = 7$ contains three nodes with the global numbers $n(1,7) = 5$, $n(2,7) = 6$ and $n(3,7) = 9$. The coordinates of the global nodes are listed on the right side.

e	n(1,e)	n(2,e)	n(3,e)
1	1	2	5
2	2	6	5
3	2	3	6
4	3	7	6
5	3	4	7
6	4	8	7
7	5	6	9
8	6	10	9
9	6	7	10
10	7	11	10
11	7	8	11
12	8	12	11
13	9	10	13
14	10	14	13
15	10	11	14
16	11	15	14
17	11	12	15
18	12	16	15

Global node	x	z
1	0	0
2	0.5	0
3	1.0	0
4	1.5	0
5	0	0.5
6	0.5	0.5
7	1.0	0.5
8	1.5	0.5
9	0	1.0
10	0.5	1.0
11	1.0	1.0
12	1.5	1.0
13	0	1.5
14	0.5	1.5
15	1.0	1.5
16	1.5	1.5

Table 4.1: Left: 2-D global node number and right: coordinates of the global nodes.

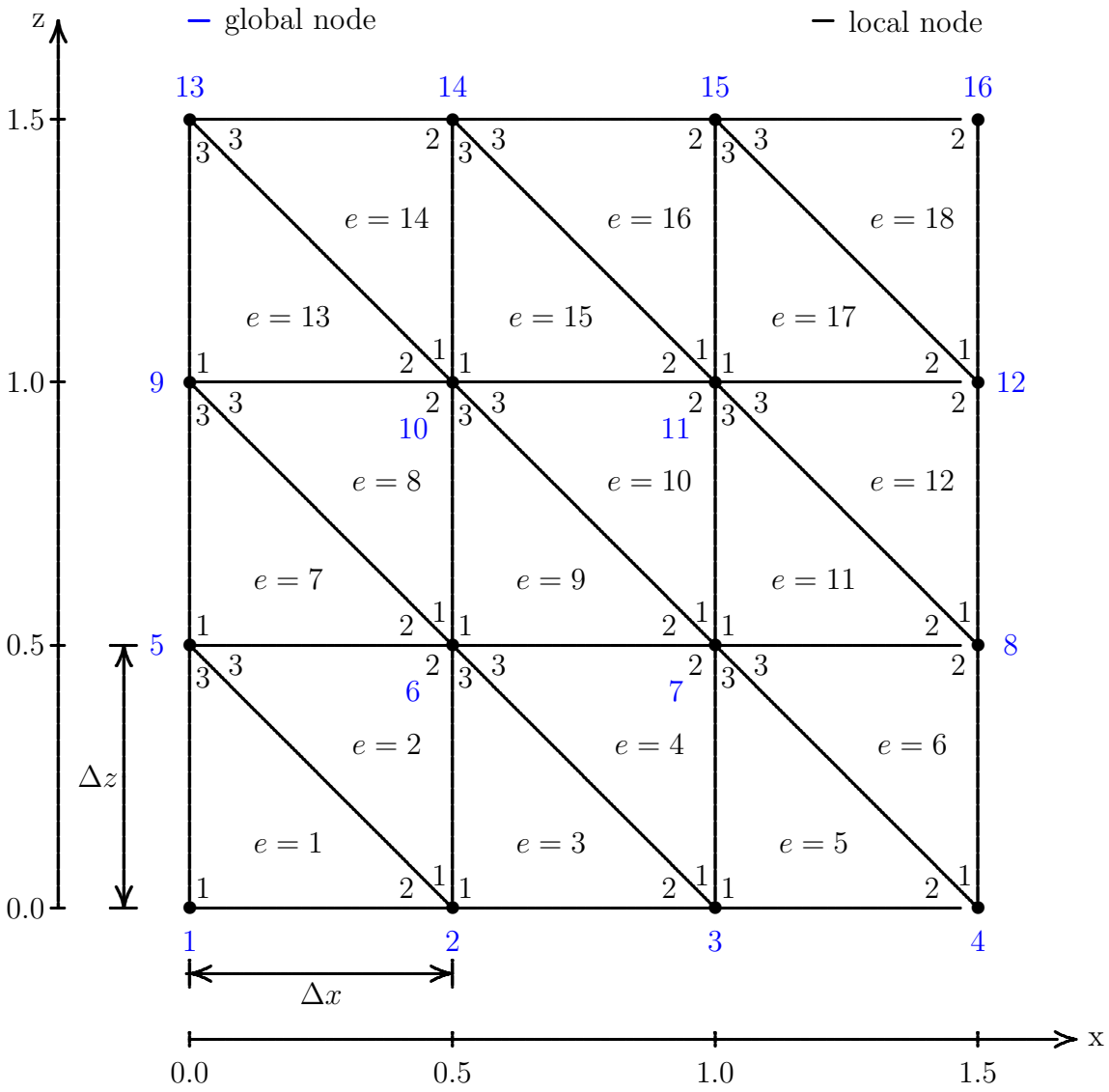

Figure 4.2: 2-D discretization with linear triangular elements.

4.5.3 Arrangement of the local coefficients in global matrices

The local coefficients S_{ij}^e, T_{ij}^e and b_i^e are computed in cartesian coordinates using Eqs. (4.63), (4.65) and (4.67) for each element. T_{ij}^e and S_{ij}^e can be included in the global matrices [**T**] and [**S**] by

$$T_{ij}^e = T_{n(i,e),\,n(j,e)} \tag{4.68}$$

$$S_{ij}^e = S_{n(i,e),\,n(j,e)} \quad , \tag{4.69}$$

which means, the local coefficients T_{ij}^e and S_{ij}^e for e-th element should be placed in the global [**T**] and [**S**] matrices, respectively, with the corresponding row and column numbers $n(i,e), n(j,e)$. The dimension of the generated [**T**] and [**S**] matrices depend on the number of global nodes, and therefore, on the number of elements. Table 4.1 shows an example with $e = 18$ elements and $n = 16$ global nodes. The resulting [**T**] and [**S**] matrices have the dimensions of $n \times n = 16 \times 16$.

As a second example, Eqs. (4.70)-(4.71) show the construction of [**T**] and [**S**] matrices respectively for $e = 6$ elements (see Fig. 4.1b), where the number of global nodes is $n = 8$ and hence, the size of the matrices becomes $n \times n = 8 \times 8$ (*Akcakoca*, 2009).

$$\sum_{e=1}^{6}[T^e] \;=\; [\mathbf{T}] \;= \tag{4.70}$$

$$\begin{bmatrix}
T_{11}^{(1)} & T_{12}^{(1)} & 0 & 0 & T_{13}^{(1)} & 0 & 0 & 0 \\
T_{21}^{(1)} & (T_{22}^{(1)} + T_{11}^{(2)} + T_{11}^{(3)}) & T_{12}^{(3)} & 0 & (T_{23}^{(1)} + T_{13}^{(2)}) & (T_{12}^{(2)} + T_{13}^{(3)}) & 0 & 0 \\
0 & T_{21}^{(3)} & (T_{22}^{(3)} + T_{11}^{(4)} + T_{11}^{(5)}) & T_{12}^{(5)} & 0 & (T_{23}^{(3)} + T_{13}^{(4)}) & (T_{12}^{(4)} + T_{13}^{(5)}) & 0 \\
0 & 0 & T_{21}^{(5)} & (T_{22}^{(5)} + T_{11}^{(6)}) & 0 & 0 & (T_{23}^{(5)} + T_{13}^{(6)}) & T_{12}^{(6)} \\
T_{31}^{(1)} & (T_{32}^{(1)} + T_{31}^{(2)}) & 0 & 0 & (T_{33}^{(1)} + T_{33}^{(2)}) & T_{32}^{(2)} & 0 & 0 \\
0 & (T_{21}^{(2)} + T_{31}^{(3)}) & (T_{32}^{(3)} + T_{31}^{(4)}) & 0 & T_{23}^{(2)} & (T_{22}^{(2)} + T_{33}^{(3)} + T_{33}^{(4)}) & T_{32}^{(4)} & 0 \\
0 & 0 & (T_{21}^{(4)} + T_{31}^{(5)}) & (T_{32}^{(5)} + T_{31}^{(6)}) & 0 & T_{23}^{(4)} & (T_{22}^{(4)} + T_{33}^{(5)} + T_{33}^{(6)}) & T_{32}^{(6)} \\
0 & 0 & 0 & T_{21}^{(6)} & 0 & 0 & T_{23}^{(6)} & T_{22}^{(6)}
\end{bmatrix}$$

$$\sum_{e=1}^{6}[S^e] \;=\; [\mathbf{S}] \;= \tag{4.71}$$

$$\begin{bmatrix}
S_{11}^{(1)} & S_{12}^{(1)} & 0 & 0 & S_{13}^{(1)} & 0 & 0 & 0 \\
S_{21}^{(1)} & (S_{22}^{(1)} + S_{11}^{(2)} + S_{11}^{(3)}) & S_{12}^{(3)} & 0 & (S_{23}^{(1)} + S_{13}^{(2)}) & (S_{12}^{(2)} + S_{13}^{(3)}) & 0 & 0 \\
0 & S_{21}^{(3)} & (S_{22}^{(3)} + S_{11}^{(4)} + S_{11}^{(5)}) & S_{12}^{(5)} & 0 & (S_{23}^{(3)} + S_{13}^{(4)}) & (S_{12}^{(4)} + S_{13}^{(5)}) & 0 \\
0 & 0 & S_{21}^{(5)} & (S_{22}^{(5)} + S_{11}^{(6)}) & 0 & 0 & (S_{23}^{(5)} + S_{13}^{(6)}) & S_{12}^{(6)} \\
S_{31}^{(1)} & (S_{32}^{(1)} + S_{31}^{(2)}) & 0 & 0 & (S_{33}^{(1)} + S_{33}^{(2)}) & S_{32}^{(2)} & 0 & 0 \\
0 & (S_{21}^{(2)} + S_{31}^{(3)}) & (S_{32}^{(3)} + S_{31}^{(4)}) & 0 & S_{23}^{(2)} & (S_{22}^{(2)} + S_{33}^{(3)} + S_{33}^{(4)}) & S_{32}^{(4)} & 0 \\
0 & 0 & (S_{21}^{(4)} + S_{31}^{(5)}) & (S_{32}^{(5)} + S_{31}^{(6)}) & 0 & S_{23}^{(4)} & (S_{22}^{(4)} + S_{33}^{(5)} + S_{33}^{(6)}) & S_{32}^{(6)} \\
0 & 0 & 0 & S_{21}^{(6)} & 0 & 0 & S_{23}^{(6)} & S_{22}^{(6)}
\end{bmatrix}.$$

Similarly, b_i^e can be included in $\{\mathbf{b}\}$ vector by

$$b_i^e = b_{\,n(i,e)} \;\;, \tag{4.72}$$

which means, the local coefficients b_i^e for e-th element should be positioned in the global $\{\mathbf{b}\}$ vector with the corresponding row number $n(i, e)$. As an example, the construction of $\{\mathbf{b}\}$

vector for $e = 6$ elements is shown in Eq. (4.73).

$$\sum_{e=1}^{6}[b^e] \;=\; \{\mathbf{b}\} \;=\; \left\{ \begin{array}{c} b_1^{(1)} \\ b_2^{(1)} + b_1^{(2)} + b_1^{(3)} + b_1^{(4)} \\ b_2^{(3)} + b_1^{(5)} + b_1^{(6)} \\ b_2^{(5)} \\ b_3^{(1)} + b_3^{(2)} \\ b_2^{(2)} + b_3^{(4)} \\ b_3^{(3)} + b_2^{(4)} + b_3^{(6)} \\ b_3^{(5)} + b_2^{(6)} \end{array} \right\} \;. \tag{4.73}$$

The boundary conditions should be applied before we solve the generated linear matrix equation Eq. (4.54).

4.6 Implementation of the Boundary Conditions

In this section, the Dirichlet boundary conditions will be discussed. Let us consider Fig. 4.1b and assume that the nodes $n = 3$, $n = 5$ and $n = 6$ lie on the boundary (see Fig. 4.3), where A_y is constant, i.e.

$$A_{yn} \;=\; p_n \;=\; p \qquad ;\; n = 3, 5, 6 \;. \tag{4.74}$$

The linear matrix equation described in Eq. (4.54) is rewritten as

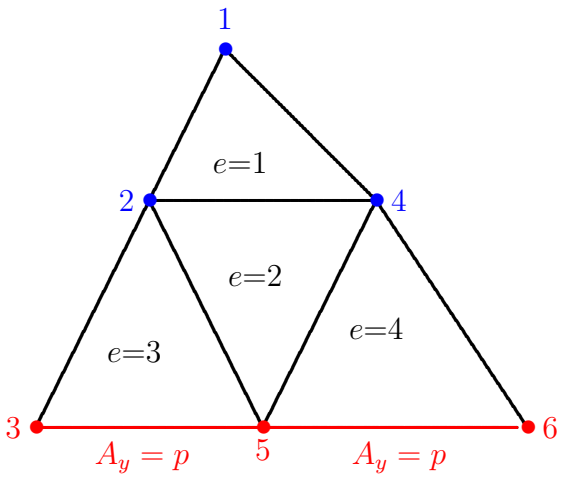

Figure 4.3: Dirichlet boundary condition on the simulation domain Ω.

$$\begin{aligned} &[\mathbf{S}] - \mathrm{j}\,\omega\,[\mathbf{T}]\{\mathbf{A}\} = \{\mathbf{b}\} \\ &\Rightarrow\; [\mathbf{K}]\{\mathbf{A}\} = \{\mathbf{b}\} \;, \end{aligned} \tag{4.75}$$

where

$$[\mathbf{K}] \;=\; [\mathbf{S}] - \mathrm{j}\,\omega\,[\mathbf{T}] \;=\; \begin{bmatrix} K_{11} & K_{12} & K_{13} & K_{14} & K_{15} & K_{16} \\ K_{21} & K_{22} & K_{23} & K_{24} & K_{25} & K_{26} \\ K_{31} & K_{32} & K_{33} & K_{34} & K_{35} & K_{36} \\ K_{41} & K_{42} & K_{43} & K_{44} & K_{45} & K_{46} \\ K_{51} & K_{52} & K_{53} & K_{54} & K_{55} & K_{56} \\ K_{61} & K_{62} & K_{63} & K_{64} & K_{65} & K_{66} \end{bmatrix} \tag{4.76}$$

and using this expression $[\mathbf{K}]$ we rewrite Eq. (4.75) as

$$\begin{bmatrix} K_{11} & K_{12} & K_{13} & K_{14} & K_{15} & K_{16} \\ K_{21} & K_{22} & K_{23} & K_{24} & K_{25} & K_{26} \\ K_{31} & K_{32} & K_{33} & K_{34} & K_{35} & K_{36} \\ K_{41} & K_{42} & K_{43} & K_{44} & K_{45} & K_{46} \\ K_{51} & K_{52} & K_{53} & K_{54} & K_{55} & K_{56} \\ K_{61} & K_{62} & K_{63} & K_{64} & K_{65} & K_{66} \end{bmatrix} \begin{Bmatrix} A_{y1} \\ A_{y2} \\ A_{y3} \\ A_{y4} \\ A_{y5} \\ A_{y6} \end{Bmatrix} \;=\; \begin{Bmatrix} b_1 \\ b_2 \\ b_3 \\ b_4 \\ b_5 \\ b_6 \end{Bmatrix} \;. \tag{4.77}$$

To impose the conditions described by Eq. (4.74), we simply set

$$b_3 \;=\; b_5 \;=\; b_6 \;=\; p \;, \tag{4.78}$$

which results

$$K_{33} \;=\; K_{55} \;=\; K_{66} \;=\; 1 \tag{4.79}$$

and

$$K_{3i} \;=\; K_{5i} \;=\; K_{6i} \;=\; 0 \qquad ;\; i = 1,2,3,4,5,6 \;. \tag{4.80}$$

However, imposing boundary conditions in such a way destroys the symmetry of the matrix $[\mathbf{K}]$. To restore this property the $[\mathbf{K}]$ matrix has to be modified by setting

$$K_{i3} \;=\; K_{i5} \;=\; K_{i6} \;=\; 0 \qquad ;\; i = 1,2,3,4,5,6 \;, \tag{4.81}$$

which causes a modification of the $\{\mathbf{b}\}$ vector as

$$b_i \;\leftarrow b_i - K_{i3}p - K_{i5}p - K_{i6}p \qquad ;\; i = 1,2,4\,. \tag{4.82}$$

Using Eq. (4.78)-(4.82) the matrix $[\mathbf{K}]$ becomes

$$[\mathbf{K}] \;=\; \begin{bmatrix} K_{11} & K_{12} & 0 & K_{14} & 0 & 0 \\ K_{21} & K_{22} & 0 & K_{24} & 0 & 0 \\ 0 & 0 & 1 & K_{34} & 0 & 0 \\ K_{41} & K_{42} & 0 & K_{44} & 0 & 0 \\ 0 & 0 & 0 & 0 & 1 & 0 \\ 0 & 0 & 0 & 0 & 0 & 1 \end{bmatrix} \tag{4.83}$$

and the vector $\{\mathbf{b}\}$ becomes

$$\{\mathbf{b}\} = \begin{Bmatrix} b_1 - K_{13}p - K_{15}p - K_{16}p \\ b_2 - K_{23}p - K_{25}p - K_{26}p \\ p \\ b_4 - K_{43}p - K_{45}p - K_{46}p \\ p \\ p \end{Bmatrix} . \tag{4.84}$$

We can, however, delete the third, fifth and sixth equation from the system, which will not change the solution. Thus, the final system of equations will be written as

$$\begin{bmatrix} K_{11} & K_{12} & K_{14} \\ K_{21} & K_{22} & K_{24} \\ K_{41} & K_{42} & K_{44} \end{bmatrix} \begin{Bmatrix} A_{y1} \\ A_{y2} \\ A_{y4} \end{Bmatrix} = \begin{Bmatrix} b_1 - K_{13}p - K_{15}p - K_{16}p \\ b_2 - K_{23}p - K_{25}p - K_{26}p \\ b_4 - K_{43}p - K_{45}p - K_{46}p \end{Bmatrix} , \tag{4.85}$$

which will be solved by a linear matrix solver to determine the unknown values of A_y.

However, it is possible to impose the Dirichlet boundary conditions following a second approach. Let us consider the same boundary problem described in Fig. 4.3. Instead of imposing the conditions (4.78)-(4.81) directly, we choose a very large number, e.g., 10^{99} and thus we obtain

$$K_{33} = K_{55} = K_{66} = 10^{99} \tag{4.86}$$

and therefore,

$$b_3 = b_5 = b_6 = p \times 10^{99} . \tag{4.87}$$

As a result, the system of equation becomes

$$\begin{bmatrix} K_{11} & K_{12} & K_{13} & K_{14} & K_{15} & K_{16} \\ K_{21} & K_{22} & K_{23} & K_{24} & K_{25} & K_{26} \\ K_{31} & K_{32} & 10^{99} & K_{34} & K_{35} & K_{36} \\ K_{41} & K_{42} & K_{43} & K_{44} & K_{45} & K_{46} \\ K_{51} & K_{52} & K_{53} & K_{54} & 10^{99} & K_{56} \\ K_{61} & K_{62} & K_{63} & K_{64} & K_{65} & 10^{99} \end{bmatrix} \begin{Bmatrix} A_{y1} \\ A_{y2} \\ A_{y3} \\ A_{y4} \\ A_{y5} \\ A_{y6} \end{Bmatrix} = \begin{Bmatrix} b_1 \\ b_2 \\ p \times 10^{99} \\ b_4 \\ p \times 10^{99} \\ p \times 10^{99} \end{Bmatrix} . \tag{4.88}$$

We observe from Eq. (4.88) that the symmetry of the $[\mathbf{K}]$ matrix is retained and we do not require any additional steps. This approach is therefore much simpler than the first approach and it needs only two operations two impose boundary conditions: one on the diagonal element and the other on the known source vector. Additionally, this technique is suitable for the sparse matrices, stored in a compact form. However, all the equations associated with the boundary nodes exist and hence, a reduction of the size of the matrices is not permitted here, which is the major disadvantage of this approach (*Jin*, 2002).

Chapter 5

Boundary Element Method (BEM)

The boundary element method (BEM), also known as the method of moments (MoM), approaches the eddy current problem by solving the underlying boundary integral equations (BIE), based on quasi-variational principles, for the equivalent sources, i.e., for the equivalent electric and magnetic current density and the electric and magnetic charge density. BEM is applicable to problems for which Green's functions can be calculated, which usually involve fields in linear homogeneous media. This places considerable restrictions on the range and generality of problems to which boundary elements can usefully be applied (*Gibson*, 2007; *Harrington*, 1993). The boundary integral equation approach leads to the development of so-called week formulations, which permit the approximate satisfaction of the different equations or conditions (*Poljak & Brebbia*, 2005). The use of approximate functions for the variables under consideration in these week formulations introduce errors that are minimized using the weighted residual techniques, such as, Galerkin's method.

BEM offers a number of advantages over the other numerical methods, such as:

- Dimensions of the problems are effectively reduced by one.
- The simulation domain is extended to infinity without the need to discretize a large portion of the body.
- BEM requires meshes, which can be easily varied without the need to satisfy the type of continuity requirements, which is essential in FEM.
- More accurate weighting functions are applied in BEM, such as, Green's functions.

Because of these advantages BEM becomes a more suitable candidate than the domain type methods in eddy current analysis with high conductivity or at high frequency. However, there are some difficulties in analyzing eddy current problems with BEM (*Zhang*, 1997), which can be mentioned as:

- The vector nature of problems results in a very large number of unknowns.
- Loose coupling between electric and magnetic fields in the air at low frequency makes it difficult to satisfy the interface conditions and to obtain a unique solution in conjunction with an appropriate choice of Gauge condition.
- Highly singular kernels in boundary integral equations require expensive numerical integration to obtain accurate solutions.

A magnetoquasistatic problem is solved by the boundary element method using the following steps:

- Formulation of the magnetoquasistatic governing equation (Sec. 5.1)
- Integral equation formulation (Sec. 5.2 and 5.3)
- Boundary element discretization and formulation of the system of equations (Sec. 5.4)

5.1 Formulation of the Magnetoquasistatic Governing Equation

In our case, the simulated hot wire has a temperature of $1000° - 1200°$ C, which is well above Curie point and therefore, the relative permeability μ_r can be considered to be 1 and $\mu(\underline{\mathbf{R}}) = \mu_0$. Similarly, we can consider that the relative permittivity $\varepsilon_\mathrm{e} = 1$, which results $\varepsilon = \varepsilon_0$. As a result, the hot wire can be represented by a linear, isotropic and homogeneous conducting material region V_{σ_e}, which is embedded in free space V_0. The region V_{σ_e} is bounded by the surface S_{σ_e} with the outward unit normal $\underline{\mathbf{n}}_{\sigma_\mathrm{e}}$ and is characterized by magnetic permeability $\mu(\underline{\mathbf{R}}) = \mu_0$ and electric conductivity σ_e, as shown in Fig. 5.1.

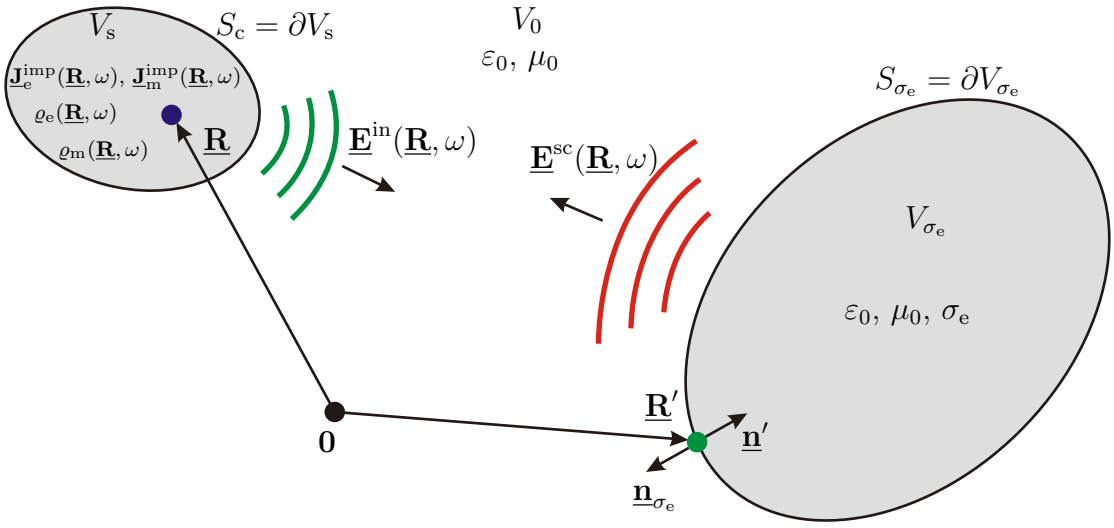

Figure 5.1: Geometry for applying Green's functions.

5.1.1 Formulation for the Conducting Region

Using Eq. (2.120) and Eq. (2.121) we write the inhomogeneous Helmholtz equations in magnetoquasistatic case for the conducting region V_{σ_e} as

$$\Delta\underline{\mathbf{E}}(\underline{\mathbf{R}},\omega) + k_\mathrm{c}^2\ \underline{\mathbf{E}}(\underline{\mathbf{R}},\omega) = -\,\mathrm{j}\,\omega\mu_0\ \underline{\mathbf{J}}_\mathrm{e}^\mathrm{imp}(\underline{\mathbf{R}},\omega) + \frac{1}{\varepsilon_0}\boldsymbol{\nabla}\varrho_\mathrm{e}(\underline{\mathbf{R}},\omega) + \boldsymbol{\nabla}\times\underline{\mathbf{J}}_\mathrm{m}(\underline{\mathbf{R}},\omega) \tag{5.1}$$

$$\Delta\underline{\mathbf{H}}(\underline{\mathbf{R}},\omega) + k_\mathrm{c}^2\ \underline{\mathbf{H}}(\underline{\mathbf{R}},\omega) = \sigma_\mathrm{e}\ \underline{\mathbf{J}}_\mathrm{m}(\underline{\mathbf{R}},\omega) + \frac{1}{\mu_0}\boldsymbol{\nabla}\varrho_\mathrm{m}(\underline{\mathbf{R}},\omega) - \boldsymbol{\nabla}\times\underline{\mathbf{J}}_\mathrm{e}^\mathrm{imp}(\underline{\mathbf{R}},\omega)\ , \tag{5.2}$$

where k_c is the complex wave number and is given by

$$k_c = \sqrt{j\,\omega\mu\sigma_e}\ . \tag{5.3}$$

We express the electric field strength $\underline{\mathbf{E}}(\underline{\mathbf{R}},\omega)$ and magnetic field strength $\underline{\mathbf{H}}(\underline{\mathbf{R}},\omega)$ by the electric and magnetic scalar and vector potentials from Eq. (2.125) and Eq. (2.126) as

$$\underline{\mathbf{E}}(\underline{\mathbf{R}},\omega) = -\boldsymbol{\nabla}\Phi_e(\underline{\mathbf{R}},\omega) + j\,\omega\ \underline{\mathbf{A}}_m(\underline{\mathbf{R}},\omega) - \frac{1}{\varepsilon_0}\boldsymbol{\nabla}\times\underline{\mathbf{A}}_e(\underline{\mathbf{R}},\omega) \tag{5.4}$$

$$\underline{\mathbf{H}}(\underline{\mathbf{R}},\omega) = -\boldsymbol{\nabla}\Phi_m(\underline{\mathbf{R}},\omega) - \frac{\sigma_e}{\varepsilon}\underline{\mathbf{A}}_e(\underline{\mathbf{R}},\omega) + \frac{1}{\mu_0}\boldsymbol{\nabla}\times\underline{\mathbf{A}}_m(\underline{\mathbf{R}},\omega)\,, \tag{5.5}$$

where $\underline{\mathbf{A}}_m(\underline{\mathbf{R}},\omega)$, $\underline{\mathbf{A}}_e(\underline{\mathbf{R}},\omega)$, $\Phi_e(\underline{\mathbf{R}},\omega)$ and $\Phi_m(\underline{\mathbf{R}},\omega)$ represent magnetic vector potential, electric vector potential, electric scalar potential and magnetic scalar potential respectively. Using Lorentz approximation we write the following expressions for the potentials

$$\Delta\Phi_e(\underline{\mathbf{R}},\omega) + k_c^2\Phi_e(\underline{\mathbf{R}},\omega) = -\frac{1}{\varepsilon_0}\varrho_e(\underline{\mathbf{R}},\omega) \tag{5.6}$$

$$\Delta\underline{\mathbf{A}}_m(\underline{\mathbf{R}},\omega) + k_c^2\underline{\mathbf{A}}_m(\underline{\mathbf{R}},\omega) = -\mu_0\underline{\mathbf{J}}_e^{\mathrm{imp}}(\underline{\mathbf{R}},\omega) \tag{5.7}$$

$$\Delta\Phi_m(\underline{\mathbf{R}},\omega) + k_c^2\Phi_m(\underline{\mathbf{R}},\omega) = -\frac{1}{\mu_0}\varrho_m(\underline{\mathbf{R}},\omega) \tag{5.8}$$

$$\Delta\underline{\mathbf{A}}_e(\underline{\mathbf{R}},\omega) + k_c^2\underline{\mathbf{A}}_e(\underline{\mathbf{R}},\omega) = -\varepsilon_0\underline{\mathbf{J}}_m(\underline{\mathbf{R}},\omega)\,. \tag{5.9}$$

Using equations Eq. (5.6)-Eq. (5.9) we need to define a Green's function which satisfies the following differential equation

$$\Delta G_{\sigma_e}(\underline{\mathbf{R}}-\underline{\mathbf{R}}',\omega) + k_c^2 G_{\sigma_e}(\underline{\mathbf{R}}-\underline{\mathbf{R}}',\omega) = -\delta(\underline{\mathbf{R}}-\underline{\mathbf{R}}',\omega)\,, \tag{5.10}$$

where $G_{\sigma_e}(\underline{\mathbf{R}}-\underline{\mathbf{R}}',\omega)$ is the scalar Green's function for the conducting region V_{σ_e} and is defined by

$$G_{\sigma_e}(\underline{\mathbf{R}}-\underline{\mathbf{R}}',\omega) = \frac{e^{j\,k_c|\underline{\mathbf{R}}-\underline{\mathbf{R}}'|}}{4\pi|\underline{\mathbf{R}}-\underline{\mathbf{R}}'|} \tag{5.11}$$

and applying Green's theorem for vector variables boundary integral equations for the field vectors are derived.

5.1.2 Formulation for the Non-Conducting Region

For the non-conducting region V_0, $\sigma_e = 0$ and hence we rewrite Eqs. (5.1)-(5.2) as

$$\Delta\underline{\mathbf{E}}(\underline{\mathbf{R}},\omega) = -\,j\,\omega\mu_0\ \underline{\mathbf{J}}_e^{\mathrm{imp}}(\underline{\mathbf{R}},\omega) + \frac{1}{\varepsilon_0}\boldsymbol{\nabla}\varrho_e(\underline{\mathbf{R}},\omega) + \boldsymbol{\nabla}\times\underline{\mathbf{J}}_m(\underline{\mathbf{R}},\omega) \tag{5.12}$$

$$\Delta\underline{\mathbf{H}}(\underline{\mathbf{R}},\omega) = \frac{1}{\mu_0}\boldsymbol{\nabla}\varrho_m(\underline{\mathbf{R}},\omega) - \boldsymbol{\nabla}\times\underline{\mathbf{J}}_e^{\mathrm{imp}}(\underline{\mathbf{R}},\omega)\,. \tag{5.13}$$

The electric field strength $\underline{\mathbf{E}}(\underline{\mathbf{R}},\omega)$ and magnetic field strength $\underline{\mathbf{H}}(\underline{\mathbf{R}},\omega)$ are expressed by the electric and magnetic scalar and vector potentials by equations Eq. (5.4) and Eq. (5.5).

Again, using Eqs. (5.6)-(5.9) we write the expressions for the potentials as

$$\Delta\Phi_{\mathrm{e}}(\underline{\mathbf{R}},\omega) = -\frac{1}{\varepsilon_0}\varrho_{\mathrm{e}}(\underline{\mathbf{R}},\omega) \tag{5.14}$$

$$\Delta\underline{\mathbf{A}}_{\mathrm{m}}(\underline{\mathbf{R}},\omega) = -\mu_0\underline{\mathbf{J}}_{\mathrm{e}}^{\mathrm{imp}}(\underline{\mathbf{R}},\omega) \tag{5.15}$$

$$\Delta\Phi_{\mathrm{m}}(\underline{\mathbf{R}},\omega) = -\frac{1}{\mu_0}\varrho_{\mathrm{m}}(\underline{\mathbf{R}},\omega) \tag{5.16}$$

$$\Delta\underline{\mathbf{A}}_{\mathrm{e}}(\underline{\mathbf{R}},\omega) = -\varepsilon_0\underline{\mathbf{J}}_{\mathrm{m}}(\underline{\mathbf{R}},\omega)\,. \tag{5.17}$$

We define a Green's function $G_{\mathrm{ms}}(\underline{\mathbf{R}}-\underline{\mathbf{R}}')$ for the non-conducting region V_0 which satisfies the equation

$$\Delta G_{\mathrm{ms}}(\underline{\mathbf{R}}-\underline{\mathbf{R}}') = -\delta(\underline{\mathbf{R}}-\underline{\mathbf{R}}')\,, \tag{5.18}$$

where

$$G_{\mathrm{ms}}(\underline{\mathbf{R}}-\underline{\mathbf{R}}') = \frac{1}{4\pi|\underline{\mathbf{R}}-\underline{\mathbf{R}}'|}\ . \tag{5.19}$$

5.2 Integral Representation of Electrical and Magnetic Field Strength

5.2.1 Integral Representation for Conducting Region

The special solutions of the inhomogeneous Helmholtz equations Eq. (5.1) and Eq. (5.2) in magnetoquasistatic case for the conducting region $V_{\sigma_{\mathrm{e}}}$ are written using the scalar Green's function as

$$\begin{aligned}
\underline{\mathbf{E}}(\underline{\mathbf{R}},\omega) \;=\; & -\frac{1}{\varepsilon_0}\,\boldsymbol{\nabla}\iiint\limits_{V_{\sigma_{\mathrm{e}}}} \varrho_{\mathrm{e}}(\underline{\mathbf{R}}',\omega)\; G_{\sigma_{\mathrm{e}}}(\underline{\mathbf{R}}-\underline{\mathbf{R}}',\omega)\;\mathrm{d}^3\underline{\mathbf{R}}' \\
& + \mathrm{j}\,\omega\mu_0 \iiint\limits_{V_{\sigma_{\mathrm{e}}}} \underline{\mathbf{J}}_{\mathrm{e}}^{\mathrm{imp}}(\underline{\mathbf{R}}',\omega)\; G_{\sigma_{\mathrm{e}}}(\underline{\mathbf{R}}-\underline{\mathbf{R}}',\omega)\;\mathrm{d}^3\underline{\mathbf{R}}' \\
& - \boldsymbol{\nabla}\times\iiint\limits_{V_{\sigma_{\mathrm{e}}}} \underline{\mathbf{J}}_{\mathrm{m}}(\underline{\mathbf{R}}',\omega)\; G_{\sigma_{\mathrm{e}}}(\underline{\mathbf{R}}-\underline{\mathbf{R}}',\omega)\;\mathrm{d}^3\underline{\mathbf{R}}'
\end{aligned} \tag{5.20}$$

$$\begin{aligned}
\underline{\mathbf{H}}(\underline{\mathbf{R}},\omega) \;=\; & -\frac{1}{\mu_0}\,\boldsymbol{\nabla}\iiint\limits_{V_{\sigma_{\mathrm{e}}}} \varrho_{\mathrm{m}}(\underline{\mathbf{R}}',\omega)\; G_{\sigma_{\mathrm{e}}}(\underline{\mathbf{R}}-\underline{\mathbf{R}}',\omega)\;\mathrm{d}^3\underline{\mathbf{R}}' \\
& - \sigma_{\mathrm{e}} \iiint\limits_{V_{\sigma_{\mathrm{e}}}} \underline{\mathbf{J}}_{\mathrm{m}}^{\mathrm{imp}}(\underline{\mathbf{R}}',\omega)\; G_{\sigma_{\mathrm{e}}}(\underline{\mathbf{R}}-\underline{\mathbf{R}}',\omega)\;\mathrm{d}^3\underline{\mathbf{R}}' \\
& + \boldsymbol{\nabla}\times\iiint\limits_{V_{\sigma_{\mathrm{e}}}} \underline{\mathbf{J}}_{\mathrm{e}}(\underline{\mathbf{R}}',\omega)\; G_{\sigma_{\mathrm{e}}}(\underline{\mathbf{R}}-\underline{\mathbf{R}}',\omega)\;\mathrm{d}^3\underline{\mathbf{R}}'\,.
\end{aligned} \tag{5.21}$$

Let us apply Gauss's integral theorem to reduce the volume sources to surface sources, which results

$$\varrho_{\mathrm{e,m}} \;\Rightarrow\; \eta_{\mathrm{e,m}} \tag{5.22}$$

$$\underline{\mathbf{J}}_{\mathrm{e,m}} \;\Rightarrow\; \underline{\mathbf{K}}_{\mathrm{e,m}}\,. \tag{5.23}$$

Using these expressions on the conducting surface S_{σ_e} we formulate the boundary conditions from equations Eq. (2.18)-Eq. (2.21) as

$$\begin{aligned}
\eta_e(\underline{\mathbf{R}}',\omega) &= \varepsilon_0\ \underline{\mathbf{n}}_{\sigma_e}\cdot\underline{\mathbf{E}}(\underline{\mathbf{R}}',\omega) &= -\varepsilon_0\ \underline{\mathbf{n}}'\cdot\underline{\mathbf{E}}(\underline{\mathbf{R}}',\omega) &(5.24)\\
\underline{\mathbf{K}}_e(\underline{\mathbf{R}}',\omega) &= \underline{\mathbf{n}}_{\sigma_e}\times\underline{\mathbf{H}}(\underline{\mathbf{R}}',\omega) &= -\underline{\mathbf{n}}'\times\underline{\mathbf{H}}(\underline{\mathbf{R}}',\omega) &(5.25)\\
\eta_m(\underline{\mathbf{R}}',\omega) &= \mu_0\ \underline{\mathbf{n}}_{\sigma_e}\cdot\underline{\mathbf{H}}(\underline{\mathbf{R}}',\omega) &= -\mu_0\ \underline{\mathbf{n}}'\cdot\underline{\mathbf{H}}(\underline{\mathbf{R}}',\omega) &(5.26)\\
\underline{\mathbf{K}}_m(\underline{\mathbf{R}}',\omega) &= -\underline{\mathbf{n}}_{\sigma_e}\times\underline{\mathbf{E}}(\underline{\mathbf{R}}',\omega) &= \underline{\mathbf{n}}'\times\underline{\mathbf{E}}(\underline{\mathbf{R}}',\omega)\,, &(5.27)
\end{aligned}$$

where $\underline{\mathbf{n}}_{\sigma_e}$ is the normal vector on the conducting surface S_{σ_e} as shown in Fig. 5.1 and $\underline{\mathbf{n}}' = -\underline{\mathbf{n}}_{\sigma_e}$. Using equations (5.22)-(5.27) we replace the volume integrals of Eq. (5.20) and Eq. (5.21) with the closed surface integrals and thus we obtain

$$\begin{aligned}
\underline{\mathbf{E}}(\underline{\mathbf{R}},\omega) = \ & \boldsymbol{\nabla}\oiint_{S_{\sigma_e}}\underline{\mathbf{n}}'\cdot\underline{\mathbf{E}}(\underline{\mathbf{R}}',\omega)\ G_{\sigma_e}(\underline{\mathbf{R}}-\underline{\mathbf{R}}',\omega)\ \mathrm{d}S'\\
& -\mathrm{j}\,\omega\mu_0\oiint_{S_{\sigma_e}}\underline{\mathbf{n}}'\times\underline{\mathbf{H}}(\underline{\mathbf{R}}',\omega)\ G_{\sigma_e}(\underline{\mathbf{R}}-\underline{\mathbf{R}}',\omega)\ \mathrm{d}S'\\
& -\boldsymbol{\nabla}\times\oiint_{S_{\sigma_e}}\underline{\mathbf{n}}'\times\underline{\mathbf{E}}(\underline{\mathbf{R}}',\omega)\ G_{\sigma_e}(\underline{\mathbf{R}}-\underline{\mathbf{R}}',\omega)\ \mathrm{d}S' \qquad (5.28)
\end{aligned}$$

$$\begin{aligned}
\underline{\mathbf{H}}(\underline{\mathbf{R}},\omega) = \ & \boldsymbol{\nabla}\oiint_{S_{\sigma_e}}\underline{\mathbf{n}}'\cdot\underline{\mathbf{H}}(\underline{\mathbf{R}}',\omega)\ G_{\sigma_e}(\underline{\mathbf{R}}-\underline{\mathbf{R}}',\omega)\ \mathrm{d}S'\\
& -\sigma_e\oiint_{S_{\sigma_e}}\underline{\mathbf{n}}'\times\underline{\mathbf{E}}(\underline{\mathbf{R}}',\omega)\ G_{\sigma_e}(\underline{\mathbf{R}}-\underline{\mathbf{R}}',\omega)\ \mathrm{d}S'\\
& -\boldsymbol{\nabla}\times\oiint_{S_{\sigma_e}}\underline{\mathbf{n}}'\times\underline{\mathbf{H}}(\underline{\mathbf{R}}',\omega)\ G_{\sigma_e}(\underline{\mathbf{R}}-\underline{\mathbf{R}}',\omega)\ \mathrm{d}S'\,. \qquad (5.29)
\end{aligned}$$

The $\boldsymbol{\nabla}$-differentiation of $G_{\sigma_e}(\underline{\mathbf{R}}-\underline{\mathbf{R}}',\omega)$ can be performed inside the integral and hence, the $(\underline{\mathbf{R}}-\underline{\mathbf{R}}')$ dependency of G_{σ_e} can be replaced by $-\boldsymbol{\nabla}'$-differentiation, which yields

$$\begin{aligned}
\underline{\mathbf{E}}(\underline{\mathbf{R}},\omega) = \ & -\oiint_{S_{\sigma_e}}\underline{\mathbf{n}}'\cdot\underline{\mathbf{E}}(\underline{\mathbf{R}}',\omega)\ \boldsymbol{\nabla}'G_{\sigma_e}(\underline{\mathbf{R}}-\underline{\mathbf{R}}',\omega)\ \mathrm{d}S'\\
& -\mathrm{j}\,\omega\mu_0\oiint_{S_{\sigma_e}}\underline{\mathbf{n}}'\times\underline{\mathbf{H}}(\underline{\mathbf{R}}',\omega)\ G_{\sigma_e}(\underline{\mathbf{R}}-\underline{\mathbf{R}}',\omega)\ \mathrm{d}S'\\
& -\oiint_{S_{\sigma_e}}[\underline{\mathbf{n}}'\times\underline{\mathbf{E}}(\underline{\mathbf{R}}',\omega)]\times\boldsymbol{\nabla}'G_{\sigma_e}(\underline{\mathbf{R}}-\underline{\mathbf{R}}',\omega)\ \mathrm{d}S' \qquad (5.30)
\end{aligned}$$

$$\underline{\mathbf{H}}(\underline{\mathbf{R}},\omega) = -\oiint_{S_{\sigma_\mathrm{e}}} \underline{\mathbf{n}}' \cdot \underline{\mathbf{H}}(\underline{\mathbf{R}}',\omega)\ \boldsymbol{\nabla}' G_{\sigma_\mathrm{e}}(\underline{\mathbf{R}}-\underline{\mathbf{R}}',\omega)\ \mathrm{d}S'$$

$$-\sigma_\mathrm{e} \oiint_{S_{\sigma_\mathrm{e}}} \underline{\mathbf{n}}' \times \underline{\mathbf{E}}(\underline{\mathbf{R}}',\omega)\ G_{\sigma_\mathrm{e}}(\underline{\mathbf{R}}-\underline{\mathbf{R}}',\omega)\ \mathrm{d}S'$$

$$-\oiint_{S_{\sigma_\mathrm{e}}} [\underline{\mathbf{n}}' \times \underline{\mathbf{H}}(\underline{\mathbf{R}}',\omega)] \times \boldsymbol{\nabla}' G_{\sigma_\mathrm{e}}(\underline{\mathbf{R}}-\underline{\mathbf{R}}',\omega)\ \mathrm{d}S'\,. \tag{5.31}$$

The equations Eq. (5.30) and Eq. (5.31) are called the Stratton-Chu version of the integrals. At the surface of the conducting region using the boundary value of the Helmholtz representation we rewrite Eq. (5.30) and Eq. (5.31) as

$$\frac{1}{2}\underline{\mathbf{E}}_{\sigma_\mathrm{e}}(\underline{\mathbf{R}},\omega) = -\oiint_{S_{\sigma_\mathrm{e}}} \underline{\mathbf{n}}' \cdot \underline{\mathbf{E}}_{\sigma_\mathrm{e}}(\underline{\mathbf{R}}',\omega)\ \boldsymbol{\nabla}' G_{\sigma_\mathrm{e}}(\underline{\mathbf{R}}-\underline{\mathbf{R}}',\omega)\ \mathrm{d}S'$$

$$-\mathrm{j}\,\omega\mu_0 \oiint_{S_{\sigma_\mathrm{e}}} \underline{\mathbf{n}}' \times \underline{\mathbf{H}}_{\sigma_\mathrm{e}}(\underline{\mathbf{R}}',\omega)\ G_{\sigma_\mathrm{e}}(\underline{\mathbf{R}}-\underline{\mathbf{R}}',\omega)\ \mathrm{d}S'$$

$$-\oiint_{S_{\sigma_\mathrm{e}}} \left[\underline{\mathbf{n}}' \times \underline{\mathbf{E}}_{\sigma_\mathrm{e}}(\underline{\mathbf{R}}',\omega)\right] \times \boldsymbol{\nabla}' G_{\sigma_\mathrm{e}}(\underline{\mathbf{R}}-\underline{\mathbf{R}}',\omega)\ \mathrm{d}S' \tag{5.32}$$

$$\frac{1}{2}\underline{\mathbf{H}}_{\sigma_\mathrm{e}}(\underline{\mathbf{R}},\omega) = -\oiint_{S_{\sigma_\mathrm{e}}} \underline{\mathbf{n}}' \cdot \underline{\mathbf{H}}_{\sigma_\mathrm{e}}(\underline{\mathbf{R}}',\omega)\ \boldsymbol{\nabla}' G_{\sigma_\mathrm{e}}(\underline{\mathbf{R}}-\underline{\mathbf{R}}',\omega)\ \mathrm{d}S'$$

$$-\sigma_\mathrm{e} \oiint_{S_{\sigma_\mathrm{e}}} \underline{\mathbf{n}}' \times \underline{\mathbf{E}}_{\sigma_\mathrm{e}}(\underline{\mathbf{R}}',\omega)\ G_{\sigma_\mathrm{e}}(\underline{\mathbf{R}}-\underline{\mathbf{R}}',\omega)\ \mathrm{d}S'$$

$$-\oiint_{S_{\sigma_\mathrm{e}}} \left[\underline{\mathbf{n}}' \times \underline{\mathbf{H}}_{\sigma_\mathrm{e}}(\underline{\mathbf{R}}',\omega)\right] \times \boldsymbol{\nabla}' G_{\sigma_\mathrm{e}}(\underline{\mathbf{R}}-\underline{\mathbf{R}}',\omega)\ \mathrm{d}S'\,, \tag{5.33}$$

where $\underline{\mathbf{E}}_{\sigma_\mathrm{e}}(\underline{\mathbf{R}},\omega)$ and $\underline{\mathbf{H}}_{\sigma_\mathrm{e}}(\underline{\mathbf{R}},\omega)$ represent the electric and magnetic field strength in conducting region, respectively.

5.2.2 Integral Representation for Non-conducting Region

For the non-conducting region we set $\sigma_\mathrm{e} = 0$ in Eqs. (5.30)-(5.31) and thus we obtain the special solutions for the homogeneous Helmholtz equations Eq. (5.12) and Eq. (5.13). We write the electric field strength and magnetic field strength in non-conducting region as $\underline{\mathbf{E}}_0(\underline{\mathbf{R}},\omega)$ and $\underline{\mathbf{H}}_0(\underline{\mathbf{R}},\omega)$, respectively and thus we obtain

$$\underline{\mathbf{E}}_0(\underline{\mathbf{R}},\omega) = -\oiint_{S_0=\partial V_0} \underline{\mathbf{n}}' \cdot \underline{\mathbf{E}}_0(\underline{\mathbf{R}}',\omega)\ \boldsymbol{\nabla}' G_\mathrm{ms}(\underline{\mathbf{R}}-\underline{\mathbf{R}}')\ \mathrm{d}S'$$

$$-\mathrm{j}\,\omega\mu_0 \oiint_{S_0=\partial V_0} \underline{\mathbf{n}}' \times \underline{\mathbf{H}}_0(\underline{\mathbf{R}}',\omega)\ G_\mathrm{ms}(\underline{\mathbf{R}}-\underline{\mathbf{R}}')\ \mathrm{d}S'$$

$$-\oiint_{S_0=\partial V_0} [\underline{\mathbf{n}}' \times \underline{\mathbf{E}}_0(\underline{\mathbf{R}}',\omega)] \times \boldsymbol{\nabla}' G_\mathrm{ms}(\underline{\mathbf{R}}-\underline{\mathbf{R}}')\ \mathrm{d}S' \tag{5.34}$$

$$\underline{\mathbf{H}}_0(\underline{\mathbf{R}},\omega) \;=\; -\oiint\limits_{S_0=\partial V_0} \underline{\mathbf{n}}' \cdot \underline{\mathbf{H}}_0(\underline{\mathbf{R}}',\omega)\; \boldsymbol{\nabla}' G_{\mathrm{ms}}(\underline{\mathbf{R}}-\underline{\mathbf{R}}')\; \mathrm{d}S'$$

$$-\oiint\limits_{S_0=\partial V_0} [\underline{\mathbf{n}}' \times \underline{\mathbf{H}}_0(\underline{\mathbf{R}}',\omega)] \times \boldsymbol{\nabla}' G_{\mathrm{ms}}(\underline{\mathbf{R}}-\underline{\mathbf{R}}')\; \mathrm{d}S' \,. \tag{5.35}$$

However, the external sources are located in the non-conducting region (see Fig. 5.1) and hence, we have to add the source terms on the right side of Eq. (5.34) and Eq. (5.35), which results

$$\underline{\mathbf{E}}_0(\underline{\mathbf{R}},\omega) \;=\; \underline{\mathbf{E}}^{\mathrm{imp}}(\underline{\mathbf{R}},\omega) \;-\oiint\limits_{S_0=\partial V_0} \underline{\mathbf{n}}' \cdot \underline{\mathbf{E}}_0(\underline{\mathbf{R}}',\omega)\; \boldsymbol{\nabla}' G_{\mathrm{ms}}(\underline{\mathbf{R}}-\underline{\mathbf{R}}')\; \mathrm{d}S'$$

$$-\;\mathrm{j}\,\omega\mu_0 \oiint\limits_{S_0=\partial V_0} \underline{\mathbf{n}}' \times \underline{\mathbf{H}}_0(\underline{\mathbf{R}}',\omega)\; G_{\mathrm{ms}}(\underline{\mathbf{R}}-\underline{\mathbf{R}}')\; \mathrm{d}S'$$

$$-\oiint\limits_{S_0=\partial V_0} [\underline{\mathbf{n}}' \times \underline{\mathbf{E}}_0(\underline{\mathbf{R}}',\omega)] \times \boldsymbol{\nabla}' G_{\mathrm{ms}}(\underline{\mathbf{R}}-\underline{\mathbf{R}}')\; \mathrm{d}S' \tag{5.36}$$

$$\underline{\mathbf{H}}_0(\underline{\mathbf{R}},\omega) \;=\; \underline{\mathbf{H}}^{\mathrm{imp}}(\underline{\mathbf{R}},\omega) \;-\oiint\limits_{S_0=\partial V_0} \underline{\mathbf{n}}' \cdot \underline{\mathbf{H}}_0(\underline{\mathbf{R}}',\omega)\; \boldsymbol{\nabla}' G_{\mathrm{ms}}(\underline{\mathbf{R}}-\underline{\mathbf{R}}')\; \mathrm{d}S'$$

$$-\oiint\limits_{S_0=\partial V_0} [\underline{\mathbf{n}}' \times \underline{\mathbf{H}}_0(\underline{\mathbf{R}}',\omega)] \times \boldsymbol{\nabla}' G_{\mathrm{ms}}(\underline{\mathbf{R}}-\underline{\mathbf{R}}')\; \mathrm{d}S' \,. \tag{5.37}$$

Considering the electric surface current density $\underline{\mathbf{K}}_{\mathrm{e}}^{\mathrm{imp}}(\underline{\mathbf{R}}',\omega)$ as the source, we write the expression of incident electric field $\underline{\mathbf{E}}^{\mathrm{imp}}(\underline{\mathbf{R}},\omega)$ using Green's theorem as

$$\underline{\mathbf{E}}^{\mathrm{imp}}(\underline{\mathbf{R}},\omega) = -\,\mathrm{j}\,\omega\mu_0 \oiint\limits_{S_{\mathrm{c}}} \underline{\mathbf{K}}_{\mathrm{e}}^{\mathrm{imp}}(\underline{\mathbf{R}}',\omega)\; G_{\mathrm{ms}}(\underline{\mathbf{R}}-\underline{\mathbf{R}}')\; \mathrm{d}S'$$

$$= -\,\mathrm{j}\,\omega\mu_0 \oiint\limits_{S_{\mathrm{c}}} \underline{\mathbf{n}}' \times \underline{\mathbf{H}}_0(\underline{\mathbf{R}}',\omega)\; G_{\mathrm{ms}}(\underline{\mathbf{R}}-\underline{\mathbf{R}}')\; \mathrm{d}S' \,. \tag{5.38}$$

The expression for incident magnetic field $\underline{\mathbf{H}}^{\mathrm{imp}}(\underline{\mathbf{R}},\omega)$ is written using Maxwell's first equation as

$$\mathrm{j}\,\omega\underline{\mathbf{B}}^{\mathrm{imp}}(\underline{\mathbf{R}},\omega) = \boldsymbol{\nabla}\times\underline{\mathbf{E}}^{\mathrm{imp}}(\underline{\mathbf{R}},\omega) = -\,\mathrm{j}\,\omega\mu_0\boldsymbol{\nabla}\times \oiint\limits_{S_{\mathrm{c}}} \underline{\mathbf{K}}_{\mathrm{e}}^{\mathrm{imp}}(\underline{\mathbf{R}}',\omega)\; G_{\mathrm{ms}}(\underline{\mathbf{R}}-\underline{\mathbf{R}}')\; \mathrm{d}S'$$

$$\Rightarrow\quad \underline{\mathbf{H}}^{\mathrm{imp}}(\underline{\mathbf{R}},\omega) = -\boldsymbol{\nabla}\times \oiint\limits_{S_{\mathrm{c}}} \underline{\mathbf{K}}_{\mathrm{e}}^{\mathrm{imp}}(\underline{\mathbf{R}}',\omega)\; G_{\mathrm{ms}}(\underline{\mathbf{R}}-\underline{\mathbf{R}}')\; \mathrm{d}S' \,. \tag{5.39}$$

5.3 Integral Equation Formulation

Before we derive the boundary integral equations, we have to set the transition conditions for the electric and magnetic field. The transition conditions for the tangential components of the electric and magnetic field strength are described by (*Zhang*, 1997)

$$\underline{\mathbf{n}}' \times \underline{\mathbf{H}}_{\sigma_{\mathrm{e}}}(\underline{\mathbf{R}},\omega) = \underline{\mathbf{n}}' \times \underline{\mathbf{H}}_0(\underline{\mathbf{R}},\omega) = -\underline{\mathbf{K}}_{\mathrm{e}}(\underline{\mathbf{R}},\omega) \tag{5.40}$$

$$\underline{\mathbf{n}}' \times \underline{\mathbf{E}}_{\sigma_{\mathrm{e}}}(\underline{\mathbf{R}},\omega) = \underline{\mathbf{n}}' \times \underline{\mathbf{E}}_0(\underline{\mathbf{R}},\omega) = \underline{\mathbf{K}}_{\mathrm{m}}(\underline{\mathbf{R}},\omega) \,. \tag{5.41}$$

Let us recall the transition condition for magnetic flux density at the source-free transition surface from chapter 2:

$$\underline{\mathbf{n}}' \cdot \left[\underline{\mathbf{B}}_{\sigma_\mathrm{e}}(\underline{\mathbf{R}}, t) - \underline{\mathbf{B}}_0(\underline{\mathbf{R}}, t)\right] = 0\,, \tag{5.42}$$

which is written in frequency domain as

$$\underline{\mathbf{n}}' \cdot \left[\underline{\mathbf{B}}_{\sigma_\mathrm{e}}(\underline{\mathbf{R}}, \omega) - \underline{\mathbf{B}}_0(\underline{\mathbf{R}}, \omega)\right] = 0 \quad \Rightarrow \quad \underline{\mathbf{n}}' \cdot \left[\underline{\mathbf{H}}_{\sigma_\mathrm{e}}(\underline{\mathbf{R}}, \omega) - \underline{\mathbf{H}}_0(\underline{\mathbf{R}}, \omega)\right] = 0\,. \tag{5.43}$$

The normal component of the magnetic flux density is expressed using Maxwell's first equation as

$$\underline{\mathbf{n}}' \cdot \underline{\mathbf{B}}_{\sigma_\mathrm{e}}(\underline{\mathbf{R}}, \omega) = \underline{\mathbf{B}}_0(\underline{\mathbf{R}}, \omega) = \frac{1}{\mathrm{j}\,\omega} \boldsymbol{\nabla} \cdot \left[\underline{\mathbf{n}}' \times \underline{\mathbf{E}}_0(\underline{\mathbf{R}}, \omega)\right] = -\frac{\mathrm{j}}{\omega} \boldsymbol{\nabla} \cdot \underline{\mathbf{K}}_\mathrm{m}(\underline{\mathbf{R}}, \omega)\,. \tag{5.44}$$

The transition condition for the normal component of electric field strength is recalled as

$$\underline{\mathbf{n}}' \cdot \left[\underline{\mathbf{E}}_{\sigma_\mathrm{e}}(\underline{\mathbf{R}}, \omega) - \underline{\mathbf{E}}_0(\underline{\mathbf{R}}, \omega)\right] = -\frac{1}{\varepsilon_0} \eta_\mathrm{e}(\underline{\mathbf{R}}, \omega)\,. \tag{5.45}$$

However, for the low frequency eddy current problems we assume $\omega\varepsilon \approx 0$ and hence, the normal component of electric field strength in conductive medium vanishes which results

$$\underline{\mathbf{n}}' \cdot \underline{\mathbf{E}}_{\sigma_\mathrm{e}}(\underline{\mathbf{R}}, \omega) = 0 \tag{5.46}$$

$$\underline{\mathbf{n}}' \cdot \underline{\mathbf{E}}_0(\underline{\mathbf{R}}, \omega) = -\frac{1}{\varepsilon_0} \eta_\mathrm{e}(\underline{\mathbf{R}}, \omega)\,. \tag{5.47}$$

The integral representations of the electric and magnetic field strength in conductive and non-conductive medium are described in equations (5.32), (5.33), (5.36) and (5.37) and need to be solved to find the equivalent sources. In order to obtain accurate solutions an over determined system has to be solved and the transition conditions described by Eqs. (5.40)-(5.47), need to be satisfied.

5.3.1 Electric Field Integral (EFIE) Formulation

The surface of the conductive region V_{σ_e} acts as a transition surface between the conducting and non-conducting region and hence, both Eq. (5.32) and Eq. (5.36) are valid at this surface.

5.3.1.1 EFIE for Conducting Region

Inserting the transition conditions (5.40)-(5.47) in Eq. (5.32) yields

$$\begin{aligned} \frac{1}{2}\underline{\mathbf{E}}_{\sigma_\mathrm{e}}(\underline{\mathbf{R}}, \omega) \;=\; & \mathrm{j}\,\omega\mu_0 \oiint_{S_{\sigma_\mathrm{e}}} \underline{\mathbf{K}}_\mathrm{e}(\underline{\mathbf{R}}', \omega)\; G_{\sigma_\mathrm{e}}(\underline{\mathbf{R}} - \underline{\mathbf{R}}', \omega)\; \mathrm{d}S' \\ & - \oiint_{S_{\sigma_\mathrm{e}}} \underline{\mathbf{K}}_\mathrm{m}(\underline{\mathbf{R}}', \omega) \times \boldsymbol{\nabla}' G_{\sigma_\mathrm{e}}(\underline{\mathbf{R}} - \underline{\mathbf{R}}', \omega)\; \mathrm{d}S'\,. \end{aligned} \tag{5.48}$$

We compute $\underline{\mathbf{n}}' \times \underline{\mathbf{E}}_{\sigma_\mathrm{e}}(\underline{\mathbf{R}}, \omega)$ and rearrange Eq. (5.48) by using the transition condition Eq. (5.41) as

$$\begin{aligned} \frac{1}{2}\underline{\mathbf{K}}_\mathrm{m}(\underline{\mathbf{R}}, \omega) \;+\; & \underline{\mathbf{n}}' \times \oiint_{S_{\sigma_\mathrm{e}}} \underline{\mathbf{K}}_\mathrm{m}(\underline{\mathbf{R}}', \omega) \times \boldsymbol{\nabla}' G_{\sigma_\mathrm{e}}(\underline{\mathbf{R}} - \underline{\mathbf{R}}', \omega)\; \mathrm{d}S' \\ = \; & \mathrm{j}\,\omega\mu_0\; \underline{\mathbf{n}}' \times \oiint_{S_{\sigma_\mathrm{e}}} \underline{\mathbf{K}}_\mathrm{e}(\underline{\mathbf{R}}', \omega)\; G_{\sigma_\mathrm{e}}(\underline{\mathbf{R}} - \underline{\mathbf{R}}', \omega)\; \mathrm{d}S'\,. \end{aligned} \tag{5.49}$$

Again, we perform the operation $(\underline{\mathbf{n}}' \cdot)$ on both sides of Eq. (5.48) and using the transition conditions Eq. (5.46) we obtain

$$\underline{\mathbf{n}}' \cdot \oiint_{S_{\sigma_\mathrm{e}}} \underline{\mathbf{K}}_\mathrm{m}(\underline{\mathbf{R}}', \omega) \times \boldsymbol{\nabla}' G_{\sigma_\mathrm{e}}(\underline{\mathbf{R}} - \underline{\mathbf{R}}', \omega)\, \mathrm{d}S' = \underline{\mathbf{n}}' \cdot \mathrm{j}\,\omega\mu_0 \oiint_{S_{\sigma_\mathrm{e}}} \underline{\mathbf{K}}_\mathrm{e}(\underline{\mathbf{R}}', \omega)\, G_{\sigma_\mathrm{e}}(\underline{\mathbf{R}} - \underline{\mathbf{R}}', \omega)\, \mathrm{d}S' \,. \tag{5.50}$$

5.3.1.2 EFIE for Non-conducting Region

We insert the transition conditions (5.40)-(5.47) in the integral representation of the electric field strength Eq. (5.36)

$$\begin{aligned} \underline{\mathbf{E}}_0(\underline{\mathbf{R}}, \omega) = {} & \underline{\mathbf{E}}^\mathrm{imp}(\underline{\mathbf{R}}, \omega) + \oiint_{S_{\sigma_\mathrm{e}}} \frac{1}{\varepsilon_0} \eta_\mathrm{e}(\underline{\mathbf{R}}', \omega)\, \boldsymbol{\nabla}' G_\mathrm{ms}(\underline{\mathbf{R}} - \underline{\mathbf{R}}')\, \mathrm{d}S' \\ & + \mathrm{j}\,\omega\mu_0 \oiint_{S_{\sigma_\mathrm{e}}} \underline{\mathbf{K}}_\mathrm{e}(\underline{\mathbf{R}}', \omega)\, G_\mathrm{ms}(\underline{\mathbf{R}} - \underline{\mathbf{R}}')\, \mathrm{d}S' \\ & - \oiint_{S_{\sigma_\mathrm{e}}} \underline{\mathbf{K}}_\mathrm{m}(\underline{\mathbf{R}}', \omega) \times \boldsymbol{\nabla}' G_\mathrm{ms}(\underline{\mathbf{R}} - \underline{\mathbf{R}}')\, \mathrm{d}S' \,. \end{aligned} \tag{5.51}$$

Performing the operation $(\underline{\mathbf{n}}' \times)$ and rearranging Eq. (5.51) yields

$$\begin{aligned} & \underline{\mathbf{K}}_\mathrm{m}(\underline{\mathbf{R}}, \omega) + \underline{\mathbf{n}}' \times \oiint_{S_{\sigma_\mathrm{e}}} \underline{\mathbf{K}}_\mathrm{m}(\underline{\mathbf{R}}', \omega) \times \boldsymbol{\nabla}' G_\mathrm{ms}(\underline{\mathbf{R}} - \underline{\mathbf{R}}')\, \mathrm{d}S' \\ & - \frac{1}{\varepsilon_0}\, \underline{\mathbf{n}}' \times \oiint_{S_{\sigma_\mathrm{e}}} \eta_\mathrm{e}(\underline{\mathbf{R}}', \omega)\, \boldsymbol{\nabla}' G_\mathrm{ms}(\underline{\mathbf{R}} - \underline{\mathbf{R}}')\, \mathrm{d}S' \\ & = \mathrm{j}\,\omega\mu_0\, \underline{\mathbf{n}}' \times \oiint_{S_{\sigma_\mathrm{e}}} \underline{\mathbf{K}}_\mathrm{e}(\underline{\mathbf{R}}', \omega)\, G_\mathrm{ms}(\underline{\mathbf{R}} - \underline{\mathbf{R}}')\, \mathrm{d}S' + \underline{\mathbf{n}}' \times \underline{\mathbf{E}}^\mathrm{imp}(\underline{\mathbf{R}}, \omega) \,. \end{aligned} \tag{5.52}$$

Similarly, performing the operation $(\underline{\mathbf{n}}' \cdot)$ results

$$\begin{aligned} & -\frac{1}{\varepsilon_0} \eta_\mathrm{e}(\underline{\mathbf{R}}, \omega) + \underline{\mathbf{n}}' \cdot \oiint_{\sigma_\mathrm{e}} \underline{\mathbf{K}}_\mathrm{m}(\underline{\mathbf{R}}', \omega) \times \boldsymbol{\nabla}' G_\mathrm{ms}(\underline{\mathbf{R}} - \underline{\mathbf{R}}')\, \mathrm{d}S' \\ & - \frac{1}{\varepsilon_0}\, \underline{\mathbf{n}}' \cdot \oiint_{S_{\sigma_\mathrm{e}}} \eta_\mathrm{e}(\underline{\mathbf{R}}', \omega)\, \boldsymbol{\nabla}' G_\mathrm{ms}(\underline{\mathbf{R}} - \underline{\mathbf{R}}')\, \mathrm{d}S' \\ & = \mathrm{j}\,\omega\mu_0\, \underline{\mathbf{n}}' \cdot \oiint_{S_{\sigma_\mathrm{e}}} \underline{\mathbf{K}}_\mathrm{e}(\underline{\mathbf{R}}', \omega)\, G_\mathrm{ms}(\underline{\mathbf{R}} - \underline{\mathbf{R}}')\, \mathrm{d}S' + \underline{\mathbf{n}}' \cdot \underline{\mathbf{E}}^\mathrm{imp}(\underline{\mathbf{R}}, \omega) \,. \end{aligned} \tag{5.53}$$

We solve the electric field integral equations, described by (5.49), (5.50) (5.52) and (5.53) to find the unknown surface source quantities. However, EFIE has the disadvantage that Fredholm integral equations of the second kind are used for the electric field quantities only, which leads to ill-conditioned equations systems when the complex diffusion constant increases at higher frequencies or higher conductivity (*Rucker et al.*, 1995).

5.3.2 Magnetic Field Integral (MFIE) Formulation

As we have mentioned earlier, the surface S_{σ_e} acts as a transition surface between the conducting and non-conducting region. Thus both Eq. (5.33) and Eq. (5.37) are valid at this surface.

5.3.2.1 MFIE for Conducting Region

Let us insert the transition conditions (5.40)-(5.47) in Eq. (5.33) to obtain

$$\begin{aligned}\frac{1}{2}\underline{\mathbf{H}}_{\sigma_\mathrm{e}}(\underline{\mathbf{R}},\omega) \;=\; & -\oiint_{S_{\sigma_\mathrm{e}}} \frac{\mathrm{j}}{\omega\mu}\; [\boldsymbol{\nabla}'\cdot\underline{\mathbf{K}}_\mathrm{m}(\underline{\mathbf{R}},\omega)]\;\boldsymbol{\nabla}' G_{\sigma_\mathrm{e}}(\underline{\mathbf{R}}-\underline{\mathbf{R}}',\omega)\;\mathrm{d}S' \\ & -\sigma_\mathrm{e}\oiint_{S_{\sigma_\mathrm{e}}} \underline{\mathbf{K}}_\mathrm{m}(\underline{\mathbf{R}}',\omega)\; G_{\sigma_\mathrm{e}}(\underline{\mathbf{R}}-\underline{\mathbf{R}}',\omega)\;\mathrm{d}S' \\ & +\oiint_{S_{\sigma_\mathrm{e}}} \underline{\mathbf{K}}_\mathrm{e}(\underline{\mathbf{R}}',\omega)\times\boldsymbol{\nabla}' G_{\sigma_\mathrm{e}}(\underline{\mathbf{R}}-\underline{\mathbf{R}}',\omega)\;\mathrm{d}S'\,. \end{aligned} \tag{5.54}$$

We compute then $\underline{\mathbf{n}}'\times\underline{\mathbf{H}}_{\sigma_\mathrm{e}}(\underline{\mathbf{R}},\omega)$ and rearrange Eq. (5.54) by using the transition condition Eq. (5.40) as

$$\begin{aligned} -\frac{1}{2}\underline{\mathbf{K}}_\mathrm{e}(\underline{\mathbf{R}},\omega) \;-\; & \underline{\mathbf{n}}'\times\oiint_{S_{\sigma_\mathrm{e}}} \underline{\mathbf{K}}_\mathrm{e}(\underline{\mathbf{R}}',\omega)\times\boldsymbol{\nabla}' G_{\sigma_\mathrm{e}}(\underline{\mathbf{R}}-\underline{\mathbf{R}}',\omega)\;\mathrm{d}S' \\ & +\frac{\mathrm{j}}{\omega\mu}\;\underline{\mathbf{n}}'\times\oiint_{S_{\sigma_\mathrm{e}}} [\boldsymbol{\nabla}'\cdot\underline{\mathbf{K}}_\mathrm{m}(\underline{\mathbf{R}}',\omega)]\;\boldsymbol{\nabla}' G_{\sigma_\mathrm{e}}(\underline{\mathbf{R}}-\underline{\mathbf{R}}',\omega)\;\mathrm{d}S' \\ & =-\sigma_\mathrm{e}\;\underline{\mathbf{n}}'\times\oiint_{S_{\sigma_\mathrm{e}}} \underline{\mathbf{K}}_\mathrm{m}(\underline{\mathbf{R}}',\omega)\; G_{\sigma_\mathrm{e}}(\underline{\mathbf{R}}-\underline{\mathbf{R}}',\omega)\;\mathrm{d}S'\,. \end{aligned} \tag{5.55}$$

Performing the operation $(\underline{\mathbf{n}}'\cdot)$ on both sides of Eq. (5.54) and using the transition conditions Eq. (5.44) yields

$$\begin{aligned} -\frac{1}{2}\frac{\mathrm{j}}{\omega\mu}\boldsymbol{\nabla}\cdot\underline{\mathbf{K}}_\mathrm{m}(\underline{\mathbf{R}},\omega) \;-\; & \underline{\mathbf{n}}'\cdot\oiint_{S_{\sigma_\mathrm{e}}} \underline{\mathbf{K}}_\mathrm{e}(\underline{\mathbf{R}}',\omega)\times\boldsymbol{\nabla}' G_{\sigma_\mathrm{e}}(\underline{\mathbf{R}}-\underline{\mathbf{R}}',\omega)\;\mathrm{d}S' \\ & +\frac{\mathrm{j}}{\omega\mu}\;\underline{\mathbf{n}}'\cdot\oiint_{S_{\sigma_\mathrm{e}}} [\boldsymbol{\nabla}'\cdot\underline{\mathbf{K}}_\mathrm{m}(\underline{\mathbf{R}}',\omega)]\;\boldsymbol{\nabla}' G_{\sigma_\mathrm{e}}(\underline{\mathbf{R}}-\underline{\mathbf{R}}',\omega)\;\mathrm{d}S' \\ & =-\sigma_\mathrm{e}\;\underline{\mathbf{n}}'\cdot\oiint_{S_{\sigma_\mathrm{e}}} \underline{\mathbf{K}}_\mathrm{m}(\underline{\mathbf{R}}',\omega)\; G_{\sigma_\mathrm{e}}(\underline{\mathbf{R}}-\underline{\mathbf{R}}',\omega)\;\mathrm{d}S'\,. \end{aligned} \tag{5.56}$$

5.3.2.2 MFIE for Non-conducting Region

Inserting the transition conditions (5.40)-(5.47) in Eq. (5.37) results

$$\begin{aligned}\underline{\mathbf{H}}_0(\underline{\mathbf{R}},\omega) = \;\underline{\mathbf{H}}^{\mathrm{imp}}(\underline{\mathbf{R}},\omega) \;-\; & \oiint_{S_{\sigma_\mathrm{e}}} \frac{\mathrm{j}}{\omega\mu}\boldsymbol{\nabla}'\cdot\underline{\mathbf{K}}_\mathrm{m}(\underline{\mathbf{R}}',\omega)\;\boldsymbol{\nabla}' G_{\mathrm{ms}}(\underline{\mathbf{R}}-\underline{\mathbf{R}}')\;\mathrm{d}S' \\ & +\oiint_{S_{\sigma_\mathrm{e}}} \underline{\mathbf{K}}_\mathrm{e}(\underline{\mathbf{R}}',\omega)\times\boldsymbol{\nabla}' G_{\mathrm{ms}}(\underline{\mathbf{R}}-\underline{\mathbf{R}}')\;\mathrm{d}S'\,. \end{aligned} \tag{5.57}$$

We perform the operation $\underline{\mathbf{n}}'\times$ on both sides of Eq. (5.57) and use the transition condition Eq. (5.40) to obtain

$$-\underline{\mathbf{K}}_{\mathrm{e}}(\underline{\mathbf{R}},\omega) \;+\; \frac{\mathrm{j}}{\omega\mu}\,\underline{\mathbf{n}}'\times\oiint_{S_{\sigma_{\mathrm{e}}}}\boldsymbol{\nabla}'\cdot\underline{\mathbf{K}}_{\mathrm{m}}(\underline{\mathbf{R}}',\omega)\;\boldsymbol{\nabla}'G_{\mathrm{ms}}(\underline{\mathbf{R}}-\underline{\mathbf{R}}')\;\mathrm{d}S'$$

$$-\;\underline{\mathbf{n}}'\times\oiint_{S_{\sigma_{\mathrm{e}}}}\underline{\mathbf{K}}_{\mathrm{e}}(\underline{\mathbf{R}}',\omega)\times\boldsymbol{\nabla}'G_{\mathrm{ms}}(\underline{\mathbf{R}}-\underline{\mathbf{R}}')\;\mathrm{d}S' \;=\; \underline{\mathbf{n}}'\times\underline{\mathbf{H}}^{\mathrm{imp}}(\underline{\mathbf{R}},\omega)\,. \tag{5.58}$$

Performing the operation $(\underline{\mathbf{n}}'\cdot\,)$ on both sides of Eq. (5.54) and using the transition conditions Eq. (5.44) yields

$$-\frac{\mathrm{j}}{\omega\mu}\boldsymbol{\nabla}\cdot\underline{\mathbf{K}}_{\mathrm{m}}(\underline{\mathbf{R}},\omega) \;+\; \frac{\mathrm{j}}{\omega\mu}\,\underline{\mathbf{n}}'\cdot\oiint_{S_{\sigma_{\mathrm{e}}}}\boldsymbol{\nabla}'\cdot\underline{\mathbf{K}}_{\mathrm{m}}(\underline{\mathbf{R}}',\omega)\;\boldsymbol{\nabla}'G_{\mathrm{ms}}(\underline{\mathbf{R}}-\underline{\mathbf{R}}')\;\mathrm{d}S'$$

$$-\;\underline{\mathbf{n}}'\cdot\oiint_{S_{\sigma_{\mathrm{e}}}}\underline{\mathbf{K}}_{\mathrm{e}}(\underline{\mathbf{R}}',\omega)\times\boldsymbol{\nabla}'G_{\mathrm{ms}}(\underline{\mathbf{R}}-\underline{\mathbf{R}}')\;\mathrm{d}S' \;=\; \underline{\mathbf{n}}'\cdot\underline{\mathbf{H}}^{\mathrm{imp}}(\underline{\mathbf{R}},\omega)\,. \tag{5.59}$$

The surface field quantities are defined by the MFIE for the conducting and the non-conducting region. The MFIE represents a Fredholm integral equation of the second kind for the magnetic field quantities only and therefore, this formulation has the same disadvantages as the EFIE formulation.

5.4 Boundary Element Discretization and Formulation of the System of Equations

Good results are obtained by using a mixed formulation, where the unknown surface quantities are defined by EFIE for the conducting region and by MFIE for the non-conducting region. For example, the so-called KHJ-formulation (*Rucker et al.*, 1995) is constructed with the EFIE for the conducting region Eq. (5.49) for $\underline{\mathbf{K}}_{\mathrm{m}}(\underline{\mathbf{R}},\omega)$, the MFIE for the conducting region Eq. (5.56) for $\underline{\mathbf{H}}_{0n}(\underline{\mathbf{R}},\omega)$ and the MFIE for non-conducting region Eq. (5.58) for $\underline{\mathbf{K}}_{\mathrm{e}}(\underline{\mathbf{R}},\omega)$ where

$$\underline{\mathbf{H}}_{0n}(\underline{\mathbf{R}},\omega) = -\frac{\mathrm{j}}{\omega\mu}\;\boldsymbol{\nabla}\cdot\underline{\mathbf{K}}_{\mathrm{m}}(\underline{\mathbf{R}},\omega)\,. \tag{5.60}$$

The normal component of the electric field outside the conductive region can be calculated with Eq. (5.53) in a second step.

Theoretically, BEM is a combination of the classical boundary integral equation method and the discretization technique originated from FEM, and therefore, the most important step to solve a magnetoquasistatic problem by BEM is to derive the integral equation formulation of the governing equation that we have discussed earlier. In order to apply the boundary element method (BEM) the surface of the conducting region is discretized into so called boundary elements. Numerical solutions with high accuracy are obtained by using boundary elements of higher order, e. g. eight-noded quadrilateral isoparametric elements using second order shape functions $N_k(\alpha,\beta)$ (*Rucker & Richter*, 1990).

$$\underline{\mathbf{r}}(\zeta_1,\zeta_2) = \sum_{k=1}^{8} N_k(\zeta_1,\zeta_2)\;\underline{\mathbf{r}}_k\,, \tag{5.61}$$

where (ζ_1, ζ_2) is the local coordinate system, defined for each boundary element and the position of the k-th node is given by $\underline{\mathbf{r}}_k$. We define two orthogonal tangential unit vectors $\underline{\mathbf{u}}$ and $\underline{\mathbf{v}}$ as

$$\underline{\mathbf{n}} = \underline{\mathbf{u}} \times \underline{\mathbf{v}} \tag{5.62}$$

in the surface nodes for the description of the surface fields. In the local coordinate system of the considered element the tangential vectors are given by

$$\underline{\mathbf{u}}(\zeta_1, \zeta_2) = \frac{\partial \underline{\mathbf{r}}(\zeta_1, \zeta_2)/\partial \zeta_1}{|\partial \underline{\mathbf{r}}(\zeta_1, \zeta_2)/\partial \zeta_1|} \tag{5.63}$$

$$\underline{\mathbf{v}}(\zeta_1, \zeta_2) = \frac{\partial \underline{\mathbf{r}}(\zeta_1, \zeta_2)/\partial \zeta_2}{|\partial \underline{\mathbf{r}}(\zeta_1, \zeta_2)/\partial \zeta_2|} \ . \tag{5.64}$$

Thus we obtain the orthogonal tangential vectors in the nodes of the global coordinate system as following:

$$\underline{\mathbf{u}}_k = \alpha_k \ \underline{\mathbf{u}}(\zeta_1, \zeta_2) + \beta_k \underline{\mathbf{u}}(\zeta_1, \zeta_2) \tag{5.65}$$

$$\underline{\mathbf{v}}_k = \gamma_k \ \underline{\mathbf{u}}(\zeta_1, \zeta_2) + \delta_k \underline{\mathbf{u}}(\zeta_1, \zeta_2) \, . \tag{5.66}$$

As for example, the tangential component of the electric field is given by $\underline{\mathbf{K}}_\mathrm{m}$ according to Eq. (5.41) and is computed as

$$\underline{\mathbf{K}}_\mathrm{m}(\zeta_1, \zeta_2) = \sum_{k=1}^{8} N_k(\zeta_1, \zeta_2) \left[K_{uk} \underline{\mathbf{u}}_k + K_{vk} \underline{\mathbf{v}}_k \right] . \tag{5.67}$$

The discretization of the boundary integral equations lead for the KHJ formulation to the following equation system:

$$\begin{bmatrix} H_{uu} & H_{uv} & 0 & \mathrm{j}\,\omega\mu G_{uu} & \mathrm{j}\,\omega\mu G_{uv} \\ H_{vu} & H_{vv} & 0 & \mathrm{j}\,\omega\mu G_{vu} & \mathrm{j}\,\omega\mu G_{vv} \\ \sigma_\mathrm{e} G_{nu} & \sigma_\mathrm{e} G_{nv} & H_{nn} & H_{nu} & H_{nv} \\ 0 & 0 & H_{un} & H_{uu} & H_{uv} \\ 0 & 0 & H_{vn} & H_{vu} & H_{vv} \end{bmatrix} \begin{Bmatrix} K_\mathrm{mu} \\ K_\mathrm{mv} \\ H_{0n} \\ K_{eu} \\ K_{ev} \end{Bmatrix} = \begin{Bmatrix} 0 \\ 0 \\ 0 \\ -K_{eu}^\mathrm{imp} \\ -K_{ev}^\mathrm{imp} \end{Bmatrix} . \tag{5.68}$$

The matrix elements in Eq. (5.68) are $N \times N$ sub-matrices where N is the total number of nodes on the closed surface S_{σ_e}. The coefficients of the element matrices $[\mathbf{H}]$ are listed below

$$h_{uu}^k = -\left(\underline{\mathbf{v}} \times \underline{\mathbf{u}}_k\right) \iint\limits_{S_{\sigma_\mathrm{e}}} N_k \boldsymbol{\nabla}' G(\underline{\mathbf{R}}, \underline{\mathbf{R}}') \ \mathrm{d}S \ \pm \frac{1}{2}\delta_{ij} \tag{5.69}$$

$$h_{uv}^k = -\left(\underline{\mathbf{v}} \times \underline{\mathbf{v}}_k\right) \iint\limits_{S_{\sigma_\mathrm{e}}} N_k \boldsymbol{\nabla}' G(\underline{\mathbf{R}}, \underline{\mathbf{R}}') \ \mathrm{d}S \tag{5.70}$$

$$h_{vu}^k = \left(\underline{\mathbf{u}} \times \underline{\mathbf{u}}_k\right) \iint\limits_{S_{\sigma_\mathrm{e}}} N_k \boldsymbol{\nabla}' G(\underline{\mathbf{R}}, \underline{\mathbf{R}}') \ \mathrm{d}S \tag{5.71}$$

$$h_{vv}^k = \left(\underline{\mathbf{u}} \times \underline{\mathbf{v}}_k\right) \iint\limits_{S_{\sigma_\mathrm{e}}} N_k \boldsymbol{\nabla}' G(\underline{\mathbf{R}}, \underline{\mathbf{R}}') \ \mathrm{d}S \ \pm \frac{1}{2}\delta_{ij} \tag{5.72}$$

$$h^k_{nu} = \quad (\underline{\mathbf{n}} \times \underline{\mathbf{u}}_k) \iint\limits_{S_{\sigma_e}} N_k \boldsymbol{\nabla}' G(\underline{\mathbf{R}}, \underline{\mathbf{R}}') \, \mathrm{d}S \tag{5.73}$$

$$h^k_{nv} = \quad (\underline{\mathbf{n}} \times \underline{\mathbf{v}}_k) \iint\limits_{S_{\sigma_e}} N_k \boldsymbol{\nabla}' G(\underline{\mathbf{R}}, \underline{\mathbf{R}}') \, \mathrm{d}S \tag{5.74}$$

$$h^k_{un} = -\underline{\mathbf{v}} \iint\limits_{S_{\sigma_e}} N_k \boldsymbol{\nabla}' G(\underline{\mathbf{R}}, \underline{\mathbf{R}}') \, \mathrm{d}S \tag{5.75}$$

$$h^k_{vn} = \quad \underline{\mathbf{u}} \iint\limits_{S_{\sigma_e}} N_k \boldsymbol{\nabla}' G(\underline{\mathbf{R}}, \underline{\mathbf{R}}') \, \mathrm{d}S \tag{5.76}$$

$$h^k_{nn} = -\underline{\mathbf{n}} \iint\limits_{S_{\sigma_e}} N_k \boldsymbol{\nabla}' G(\underline{\mathbf{R}}, \underline{\mathbf{R}}') \, \mathrm{d}S \pm \frac{1}{2}\delta_{ij} \tag{5.77}$$

and the coefficients of the element matrices $[\mathbf{G}]$ are given by

$$g^k_{uu} = \quad (\underline{\mathbf{v}} \cdot \underline{\mathbf{u}}_k) \iint\limits_{S_{\sigma_e}} N_k \boldsymbol{\nabla}' G(\underline{\mathbf{R}}, \underline{\mathbf{R}}') \, \mathrm{d}S \; \pm \frac{1}{2}\delta_{ij} \tag{5.78}$$

$$g^k_{uv} = \quad (\underline{\mathbf{v}} \cdot \underline{\mathbf{v}}_k) \iint\limits_{S_{\sigma_e}} N_k \boldsymbol{\nabla}' G(\underline{\mathbf{R}}, \underline{\mathbf{R}}') \, \mathrm{d}S \tag{5.79}$$

$$g^k_{vu} = -\,(\underline{\mathbf{u}} \cdot \underline{\mathbf{u}}_k) \iint\limits_{S_{\sigma_e}} N_k \boldsymbol{\nabla}' G(\underline{\mathbf{R}}, \underline{\mathbf{R}}') \, \mathrm{d}S \tag{5.80}$$

$$g^k_{vv} = -\,(\underline{\mathbf{u}} \cdot \underline{\mathbf{v}}_k) \iint\limits_{S_{\sigma_e}} N_k \boldsymbol{\nabla}' G(\underline{\mathbf{R}}, \underline{\mathbf{R}}') \, \mathrm{d}S \; \pm \frac{1}{2}\delta_{ij} \tag{5.81}$$

$$g^k_{nu} = \quad (\underline{\mathbf{n}} \cdot \underline{\mathbf{u}}_k) \iint\limits_{S_{\sigma_e}} N_k \boldsymbol{\nabla}' G(\underline{\mathbf{R}}, \underline{\mathbf{R}}') \, \mathrm{d}S \tag{5.82}$$

$$g^k_{nv} = \quad (\underline{\mathbf{n}} \cdot \underline{\mathbf{v}}_k) \iint\limits_{S_{\sigma_e}} N_k \boldsymbol{\nabla}' G(\underline{\mathbf{R}}, \underline{\mathbf{R}}') \, \mathrm{d}S \,. \tag{5.83}$$

In general, Eq. (5.68) is written as

$$[\mathbf{H}] \; \{\mathbf{K}\} = \{\mathbf{J}\} \quad , \tag{5.84}$$

which is a linear matrix equation. A suitable linear matrix solver, such as, the conjugate gradient (CG) method (*Press et al.*, 2007) or the generalized modified residual (GMRES) method (*Meister*, 2008) is used to solve this equation by determining the unknown values of $\{\mathbf{K}\}$.

Chapter 6

Analytical Solution of an Eddy Current Problem

Numerical modeling of eddy current problems plays an important role in nondestructive evaluation. The results obtained using different numerical techniques should be compared to the analytical results to prove the accuracy and consistency of the numerical methods. As the first step, a simple geometry is chosen for this comparison and then the analytical solution is computed.

6.1 Geometry of a Typical Eddy Current Problem

The most common geometries of interest involve excitation coils near plane or cylindrical surfaces. A typical example is shown in Fig. 6.1 where a current coil resides over a conducting half-space. Due to the excitation in the current coil, an eddy current will be induced on the metal surface. The eddy current field is perturbed by variations in the dimensions or properties (e.g. permeability μ and electric conductivity σ_e) of the metal and by the presence of defects (*Hower et al.*, 1984). These perturbations, in turn, produce changes in the electromagnetic fields near the metal surface which can be detected as changes in the impedance of the eddy current excitation (or search) coil. Theoretical calculations typically

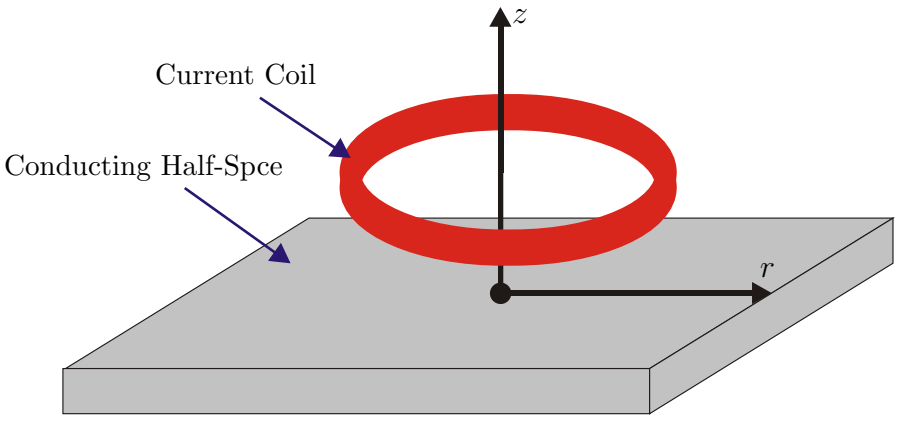

Figure 6.1: A circular coil over a conducting half-space.

involve a full numerical solution of the field equations using finite integration technique (FIT), finite element method (FEM) or method of moments (MoM). Such a problem can

also be solved analytically by evaluating the integral expressions, obtained by solving the appropriate boundary value problem. Specifically, we consider here a circular coil above and parallel to the surface of a homogeneous conducting half-space (see Fig. 6.1). The case of a multiple-turn coil of rectangular cross-section has been presented by *Dodd & Deeds* (1984). The cross-section of such a coil is shown in Fig. 6.2.

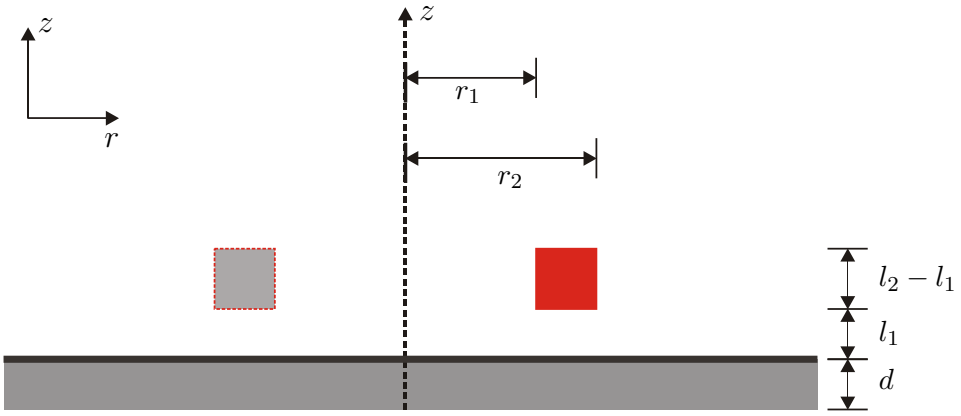

Figure 6.2: Cross section of a circular coil over a conducting half-space. Parameter: r_1 =inner radius, r_2 =outer radius, l_1 =distance between coil to conducting half-space and $l_2 - l_1$ = coil height.

6.2 Analytical Expressions

The expressions of the electric field strength $\underline{\mathbf{E}}$ and magnetic field strength $\underline{\mathbf{H}}$ for the typical eddy current problem, shown in Fig. 6.2, need to be computed in cylindrical coordinate system. The axis of the coil shows the z-axis and the air-metal interface located at $z = 0$. As mentioned in the previous chapters, we compute the magnetic vector potential $\underline{\mathbf{A}}$ to solve an eddy current problem. The geometry is located in rz-plane and therefore, the φ component of the magnetic vector potential A_φ has to be computed. We can write the expression of A_φ for the conducting half-space as

$$\begin{aligned} E_\varphi(r,z) &= -\,\mathrm{j}\,\omega A_\varphi(r,z) \\ &= -\,\mathrm{j}\,\omega\mu K \int_{\alpha=0}^{\infty} \mathrm{J}_1(\alpha r)\, F_a(\alpha r_2, \alpha r_1)\, F_b(\alpha, z)\, \mathrm{d}\alpha \end{aligned} \tag{6.1}$$

$$\Rightarrow A_\varphi(r,z) = \mu K \int_{\alpha=0}^{\infty} \mathrm{J}_1(\alpha r)\, F_a(\alpha r_2, \alpha r_1)\, F_b(\alpha, z)\, \mathrm{d}\alpha \ , \tag{6.2}$$

where

$$K = \frac{N I_\mathrm{e}}{(r_2 - r_1)(l_2 - l_1)} \tag{6.3}$$

$$F_a(\alpha r_2, \alpha r_1) = \int_{x=\alpha r_1}^{\alpha r_2} \mathrm{J}_1(x)\, \mathrm{d}x \tag{6.4}$$

$$F_b(\alpha, z) = \frac{\left(\mathrm{e}^{-\alpha l_1} - \mathrm{e}^{-\alpha l_2}\right) \mathrm{e}^{\sqrt{\alpha^2 + \mathrm{j}\,\omega\mu\sigma_\mathrm{e}}\, z}}{\alpha^2 (\alpha + \sqrt{\alpha^2 + \mathrm{j}\,\omega\mu\sigma_\mathrm{e}})} \,. \tag{6.5}$$

Here N is the number of turns on the coil, I_e is the electric current in the coil, ω is the angular frequency and σ_e is the electric conductivity of the conducting half-space. Furthermore, J_1 represents Bessel function of the first kind and of first order. At the surface of the conducting half-space Eq. (6.5) can be rewritten as

$$\begin{aligned} F_b(\alpha, z=0) &= \frac{\mathrm{e}^{-\alpha l_1} - \mathrm{e}^{-\alpha l_2}}{\alpha^2(\alpha + \sqrt{\alpha^2 + \mathrm{j}\,\omega\mu\sigma_\mathrm{e}})} \\ &= \frac{\mathrm{e}^{-\alpha l_1}}{\alpha^2(\alpha + \sqrt{\alpha^2 + \mathrm{j}\,\omega\mu\sigma_\mathrm{e}})} - \frac{\mathrm{e}^{-\alpha l_2}}{\alpha^2(\alpha + \sqrt{\alpha^2 + \mathrm{j}\,\omega\mu\sigma_\mathrm{e}})}\,. \end{aligned} \tag{6.6}$$

The right side of Eq. (6.2) contains integrals which need to be computed numerically to determine the value of A_φ. One of the following methods can be implemented for this purpose:

- Trapezoidal rule
- Simpson's rule
- Romberg integration
- Gauss quadrature

The first three involve equally spaced samples of the integrand but differ in the method of approximating intermediate values, which causes incorrect results in case of inherent oscillation of the integrand, e.g., in Bessel function. Such an integration requires a relatively small step size and has the difficulty in deciding when to terminate the integration. Gauss quadrature rule can be used to overcome this difficulty. However, it has several approaches, such as

- Gauss-Laguerre quadrature
- Gauss-Lagendre quadrature
- Chebyshev-Gauss quadrature
- Gauss-Kronrod quadrature
- Lobatto quadrature etc.

The definite integral in Eq. (6.4) is solved by Gauss-Kronrod quadrature, which attempts to approximate the integral of a scalar-valued function fun from a to b using high-order global adaptive quadrature. Furthermore, Gauss-Laguerre quadrature rules are designed to approximate integrals on semi-infinite intervals, like $[0, \infty)$, and therefore, are suitable to determine the integration of Eq. (6.2).

6.3 Gauss-Laguerre Quadrature

Gauss-Laguerre quadrature deals with a Gaussian quadrature with an interval $[0, \infty)$ with weighting function $w(x) = \mathrm{e}^{-x}$ (see *Abramowitz & Stegun* (1972)). If there exists an integral of the form

$$\int_{x=0}^{\infty} \mathrm{e}^{-x} f(x)\,\mathrm{d}x\ ,$$

then it can be computed as

$$\int_{x=0}^{\infty} \mathrm{e}^{-x} f(x)\, \mathrm{d}x = \sum_{i=1}^{n} w_i f(x_i) \ , \tag{6.7}$$

where

$$w_i = \frac{1}{x_i \left[\frac{\mathrm{d}}{\mathrm{d}x} L_n(x_i)\right]^2} \ . \tag{6.8}$$

Here $L_n(x_i)$ are the roots of the Laguerre polynomial of n-th order. A higher value of n should be selected while integrating an oscillating function.

6.4 Gauss-Kronrod Quadrature

As mentioned earlier, Gauss-Kronrod quadrature is suitable for definite integrals where the intervals can be typically mentioned as $[a, b]$. If there exists a definite integral of the form

$$\int_{x=a}^{b} f(x)\, \mathrm{d}x \ ,$$

then it can be approximated by n-points Gaussian quadrature as

$$\int_{x=a}^{b} \mathrm{d}x \ \approx \ \sum_{i=1}^{n} w_i f(x_i) \ , \tag{6.9}$$

where w_i and x_i are the weights and points at which to evaluate the function $f(x)$. If the interval $[a, b]$ is subdivided, the Gauss evaluation points of the new subintervals never coincide with the previous evaluation points (except at zero for odd numbers) and thus the integrand must be evaluated at every point. Gauss-Kronrod formulas are extensions of Gauss quadrature formulas generated by adding $n + 1$ points to an n-point rule in such a way that the resulting rule is of order $3n + 1$. This allows for computing higher-order estimates while reusing the function values of a lower-order estimate.

6.5 Computation of the Integrals

Inserting Eq. (6.6) into Eq. (6.2) yields,

$$\begin{aligned} A_\varphi(r, z) \ = \ & \mu K \int_{\alpha=0}^{\infty} \mathrm{e}^{-\alpha l_1} \, \frac{\mathrm{J}_1(\alpha r)\, F_a(\alpha r_2, \alpha r_1)}{\alpha^2(\alpha + \sqrt{\alpha^2 + \mathrm{j}\,\omega\mu\sigma_\mathrm{e}})} \, \mathrm{d}\alpha \\ & - \mu K \int_{\alpha=0}^{\infty} \mathrm{e}^{-\alpha l_2} \, \frac{\mathrm{J}_1(\alpha r)\, F_a(\alpha r_2, \alpha r_1)}{\alpha^2(\alpha + \sqrt{\alpha^2 + \mathrm{j}\,\omega\mu\sigma_\mathrm{e}})} \, \mathrm{d}\alpha \ . \end{aligned} \tag{6.10}$$

We have to substitute αl_1 with α' to compute the first integral as

$$\begin{aligned} \alpha' = \alpha\, l_1 \qquad & \Rightarrow \ \alpha = \frac{\alpha'}{l_1} \\ \Rightarrow \ \mathrm{d}\alpha = \frac{1}{l_1} \, \mathrm{d}\alpha' \ . & \end{aligned} \tag{6.11}$$

Using this substitution the first integral of Eq. (6.10) can be rewritten as

$$\int_{\alpha=0}^{\infty} \mathrm{e}^{-\alpha l_1} \frac{\mathrm{J}_1(\alpha r)\, F_a(\alpha r_2, \alpha r_1)}{\alpha^2(\alpha + \sqrt{\alpha^2 + \mathrm{j}\,\omega\mu\sigma_\mathrm{e}})}\, \mathrm{d}\alpha$$

$$= \frac{1}{l_1} \int_{\alpha'=0}^{\infty} \mathrm{e}^{-\alpha'} \frac{\mathrm{J}_1\left(\frac{\alpha'}{l_1} r\right)\, F_a\left(\frac{\alpha'}{l_1} r_2, \frac{\alpha'}{l_1} r_1\right)}{\left(\frac{\alpha'}{l_1}\right)^2 \left(\frac{\alpha'}{l_1} + \sqrt{\left(\frac{\alpha'}{l_1}\right)^2 + \mathrm{j}\,\omega\mu\sigma_\mathrm{e}}\right)}\, \mathrm{d}\alpha' \tag{6.12}$$

$$= \frac{1}{l_1} \int_{\alpha'=0}^{\infty} \mathrm{e}^{-\alpha'} f(\alpha')\, \mathrm{d}\alpha' \ , \tag{6.13}$$

where

$$f(\alpha') = \frac{\mathrm{J}_1\left(\frac{\alpha'}{l_1} r\right)\, F_a\left(\frac{\alpha'}{l_1} r_2, \frac{\alpha'}{l_1} r_1\right)}{\left(\frac{\alpha'}{l_1}\right)^2 \left(\frac{\alpha'}{l_1} + \sqrt{\left(\frac{\alpha'}{l_1}\right)^2 + \mathrm{j}\,\omega\mu\sigma_\mathrm{e}}\right)}\, \mathrm{d}\alpha' \ . \tag{6.14}$$

Applying Eq. (6.7) we can compute the integral as

$$\frac{1}{l_1} \int_{\alpha'=0}^{\infty} \mathrm{e}^{-\alpha'} f(\alpha')\, \mathrm{d}\alpha' \ = \ \sum_{i=1}^{n} w_i f(\alpha_i') \,. \tag{6.15}$$

In order to compute the second integral of Eq. (6.10) we have to substitute αl_2 with α'' as

$$\alpha'' = \alpha\, l_2 \qquad \Rightarrow \ \alpha = \frac{\alpha''}{l_2}$$

$$\Rightarrow \mathrm{d}\alpha = \frac{1}{l_2}\, \mathrm{d}\alpha'' \ . \tag{6.16}$$

Using this substitution the second integral can be computed in the same way as the first one.

$$\int_{\alpha=0}^{\infty} \mathrm{e}^{-\alpha l_2} \frac{\mathrm{J}_1(\alpha r)\, F_a(\alpha r_2, \alpha r_1)}{\alpha^2(\alpha + \sqrt{\alpha^2 + \mathrm{j}\,\omega\mu\sigma_\mathrm{e}})}\, \mathrm{d}\alpha$$

$$= \frac{1}{l_2} \int_{\alpha''=0}^{\infty} \mathrm{e}^{-\alpha''} \frac{\mathrm{J}_1\left(\frac{\alpha''}{l_2} r\right)\, F_a\left(\frac{\alpha''}{l_2} r_2, \frac{\alpha''}{l_2} r_1\right)}{\left(\frac{\alpha''}{l_2}\right)^2 \left(\frac{\alpha''}{l_2} + \sqrt{\left(\frac{\alpha''}{l_2}\right)^2 + \mathrm{j}\,\omega\mu\sigma_\mathrm{e}}\right)}\, \mathrm{d}\alpha'' \tag{6.17}$$

$$= \frac{1}{l_2} \int_{\alpha''=0}^{\infty} \mathrm{e}^{-\alpha''} f(\alpha'') \mathrm{d}\alpha'' \ , \tag{6.18}$$

$$= \sum_{i=1}^{n} w_i f(\alpha_i'') \,. \tag{6.19}$$

Inserting Eq. (6.15) and Eq. (6.19) into Eq. (6.10) yields

$$A_\varphi(r,z) = \mu K \sum_{i=1}^{n} w_i f(\alpha_i') - \mu K \sum_{i=1}^{n} w_i f(\alpha_i'')$$

$$= \mu K \left[\sum_{i=1}^{n} w_i f(\alpha_i') - \sum_{i=1}^{n} w_i f(\alpha_i'') \right] . \tag{6.20}$$

6.6 Analytical Results

The coil is described by number of turns $N = 200$, inner radius $r_1 = 12$ mm, outer radius $r_2 = 16$ mm, distance from conducting half-space $l_1 = 4$ mm, height of the coil $l_2 - l_1 = 4$ mm, electric current $I_\mathrm{e} = 1$ A and angular excitation frequency $\omega = 4.295 \times 10^4$ s^{-1}. The conducting half space has the thickness $d = 5$ mm and the electric conductivity of $\sigma_\mathrm{e} = 2.46 \times 10^7$ A/Vm. The whole simulation region is considered to have the permeability $\mu = \mu_0$, where μ_0 is the permeability of free space. The magnetic vector potential A_φ at the

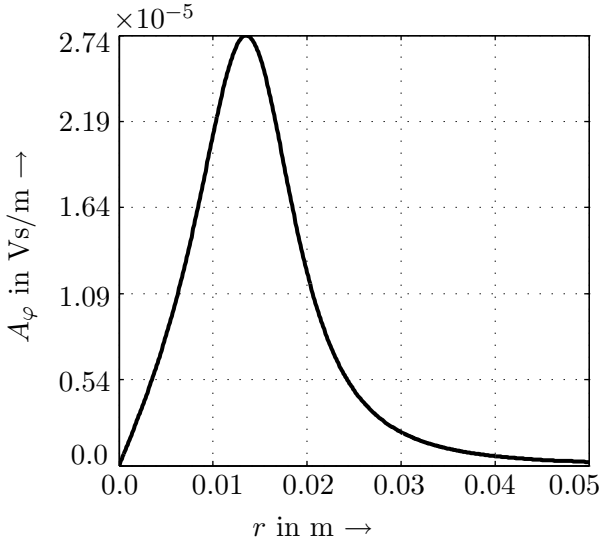

Figure 6.3: Analytic result: magnitude of A_φ at $z = 0$. Parameter: $N = 200$, $r_1 = 12$ mm, $r_2 = 16$ mm, $l_1 = 4$ mm, $l_2 - l_1 = 4$ mm, $d = 5$ mm, $I_\mathrm{e} = 1$ A, $\omega = 4.295 \times 10^4$ s^{-1}, $\sigma_\mathrm{e} = 2.46 \times 10^7$ A/Vm and $\mu = \mu_0$.

upper surface of the conducting half-space is then computed using Eq. (6.20). Some control of the oscillations of the integrands can be exerted by proper selection of the order n for the Gauss-Laguerre quadrature. Fig. 6.3 shows the computed A_φ at $z = 0$ for $n = 300$.

6.7 Comparison with Numerical Results

The eddy current problem mentioned in Sec. 6.1 can also be solved using numerical techniques, such as, the finite integration technique (FIT), the finite element method (FEM) and the boundary element method (BEM).

6.7.1 FIT Results

A 3-D eddy current problem can be reduced to a 2-D problem using rotational symmetry in cylindrical coordinates, and therefore, it is enough to simulate the right half of Fig. 6.2, as shown in Fig. 6.4. The simulation region is discretized by $N_r \times N_z = 200 \times 200$ cells,

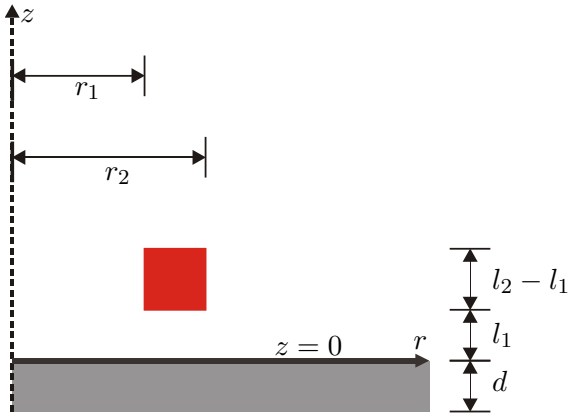

Figure 6.4: Geometry for FIT and FEM using rotational symmetry. Parameter: r_1 =inner radius, r_2 =outer radius, l_1 =distance between coil to conducting half-space and $l_2 - l_1$ = coil height.

where the width of each cell $\Delta = 0.25$ mm. The excitation coil is fed with an electric current density of $J_e = 38.875\text{kA/m}^2$, which is equivalent to the electric current of $I_e = 1$ A in the conductors. The perfectly electric conducting (PEC) boundary conditions are implemented

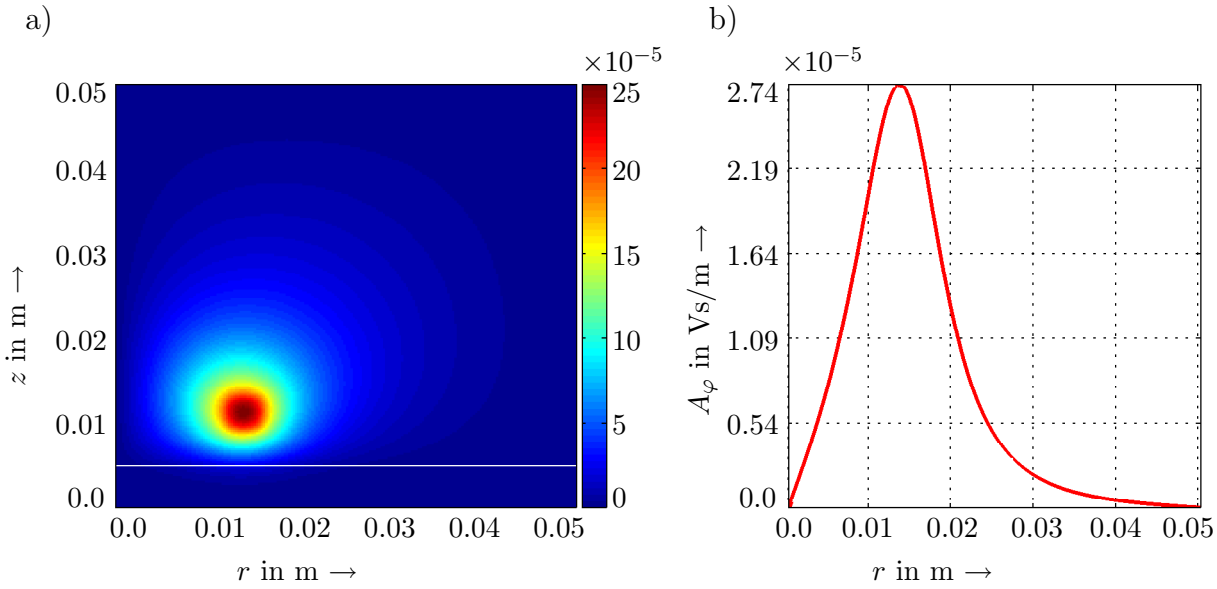

Figure 6.5: FIT result: a) A_φ distribution in rz-plane and b) A_φ at $z = 0$. Parameter: $N_r = 200$, $N_z = 200$, $\Delta = \Delta x = \Delta z = 0.25$ mm, $J_e = 38.875$ kA/m^2, $\omega = 4.295 \times 10^4$ s^{-1}, $\sigma_e = 2.46 \times 10^7$ A/Vm and $\mu = \mu_0$.

on all sides of the simulation plane. The computed magnitude of A_φ is shown in Fig. 6.5a, where the while line indicates the upper surface of the conducting half-space. A_φ at this surface is shown in Fig. 6.5b.

6.7.2 FEM Results

The reduced 2-D problem is simulated here using FEM where the rz-plane is discretized by $N_e = 18000$ triangular elements. The excitation coil is supplied with an electric current density of $J_\mathrm{e} = 38.875\ \mathrm{kA/m^2}$. Similar to FIT, the PEC boundary condition is implemented

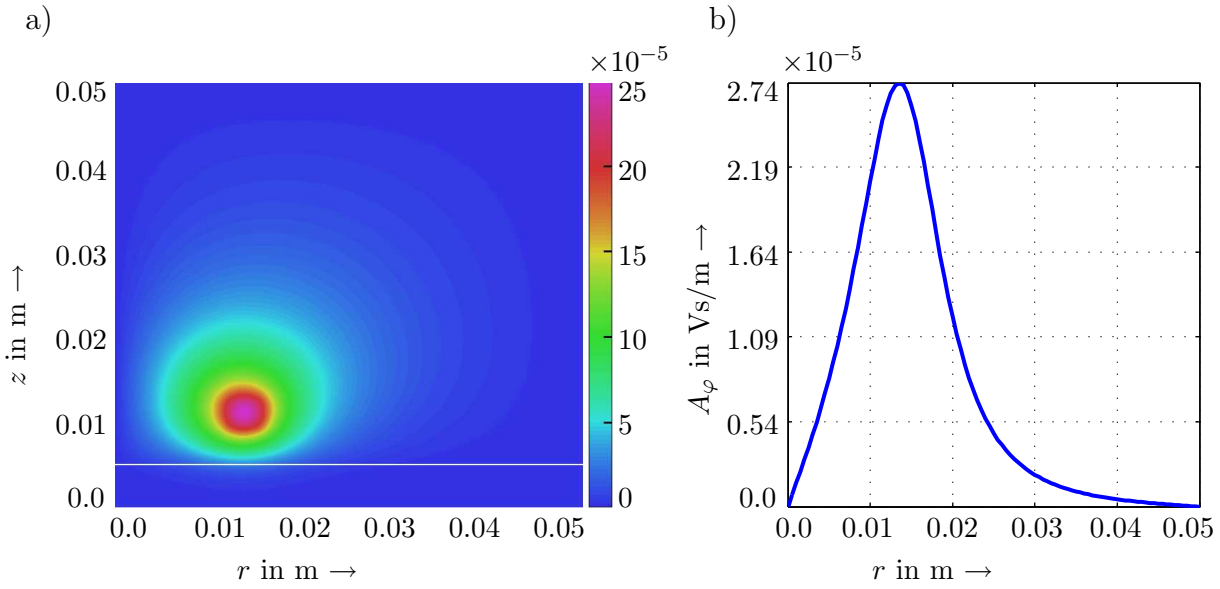

Figure 6.6: FEM result: a) A_φ distribution in rz-plane and b) A_φ at $z = 0$. Parameter: $N_e = 18000$, $J_\mathrm{e} = 38.875\ \mathrm{kA/m^2}$, $\omega = 4.295 \times 10^4\ \mathrm{s^{-1}}$, $\sigma_\mathrm{e} = 2.46 \times 10^7\ \mathrm{A/Vm}$ and $\mu = \mu_0$.

here on all sides of the simulation plane. The computed A_φ is shown in Fig. 6.6a, whereas A_φ at $z = 0$ is shown in Fig. 6.6b.

6.7.3 BEM Results

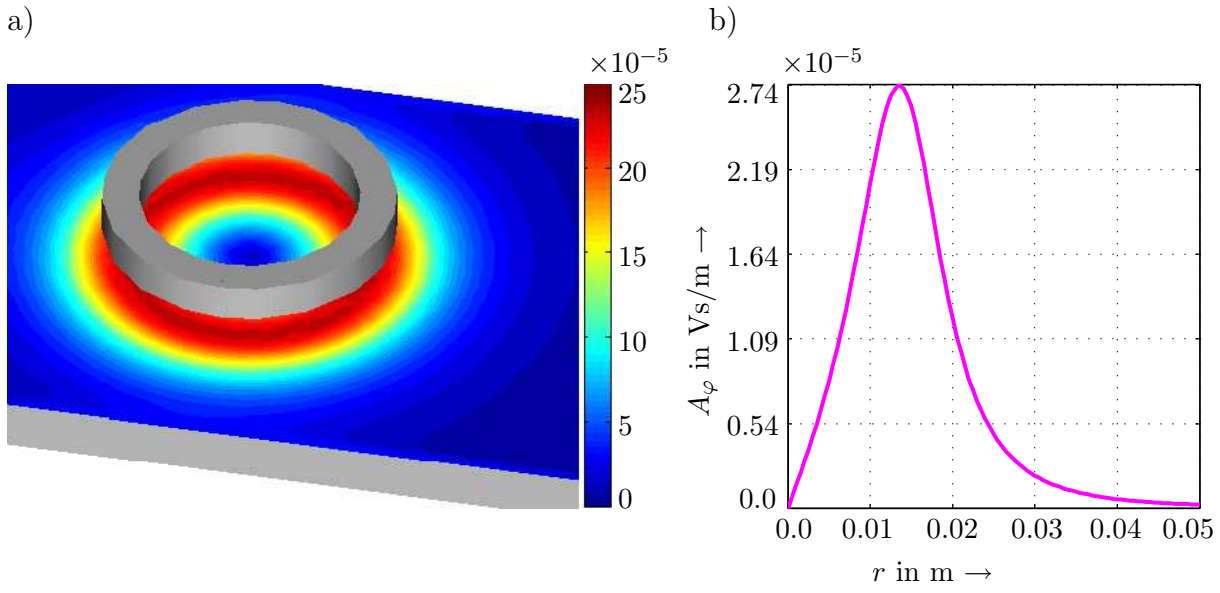

Figure 6.7: BEM result: a) A_φ distribution on the surface of the conducting half-space and b) A_φ at $z = 0$. Parameter: $N_e = 5000$, $NI = 622$ A-T, $\omega = 4.295 \times 10^4\ \mathrm{s^{-1}}$, $\sigma_\mathrm{e} = 2.46 \times 10^7\ \mathrm{A/Vm}$ and $\mu = \mu_0$.

A 3-D eddy current problem is solved here using BEM by discretizing the surface of the conducting half space with $N_e = 5000$ triangular elements. The excitation of the coil is defined by the volume current, i.e., by assigning $NI_e = 622$ A-T. Fig. 6.7 shows the simulated A_φ distribution at the surface of the conducting half-space.

6.7.4 Comparison

A direct comparison between all the methods is shown in Fig. 6.8, where the analytical, FIT, FEM and BEM results are shown in black, red, blue and magenta, respectively. All the results agree perfectly to each other, which proves the accuracy and consistency of the numerical methods. Although we obtain accurate results using all the three techniques, the major

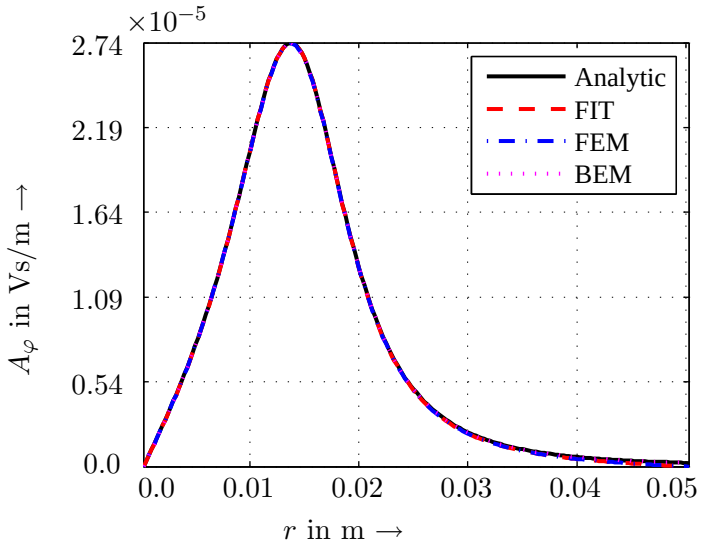

Figure 6.8: Comparison of results obtained from different techniques.

point of consideration is the computation time. Here we have solved the magnetoquasistatic problem with the finite integration technique for 40000 unknowns in 2 minutes, whereas a finite element method based software package Opera (*Opera*, 10.5) requires the same time for 20000 unknowns and a boundary element based software tool Faraday (*Faraday*, 6.1) requires 120 minutes for 5000 unknowns. Due to the large computational time 3-D simulations will be performed only for the models which cannot be simulated in 2-D, such as, for point coil sensors.

Chapter 7

Simulation Results

In this chapter we discuss the results of different eddy current sensors developed during the INCOSTEEL project, which is an EU research project and is performed by the University of Kassel in collaboration with Tecnatom (*Tecnatom*, S.A.), TU Freiberg (*TU Freiberg*, FB) and Sidenor (*Sidenor*, S.A.). At first, a traditional encircling coil will be discussed. Such a sensor is typically used to detect the transversal cracks. Secondly, we shall discuss about the modified encircling coil sensor. In the next part, the point core sensors, suitable to detect the longitudinal cracks, will be reported. At the end, we shall make a velocity analysis to simulate the effect of the velocity of the hot wire on the detection process.

7.1 Simulation Results of Encircling Coil Sensors

Two types of encircling coils have been analyzed in this section.

- Encircling coil sensor without ferrite core
- Encircling coil sensor with ferrite core

We simulate the following simulations with the sensors mentioned above:

- Encircling coil sensor without ferrite core to simulate a transversal crack
- Encircling coil sensor with ferrite core to simulate a transversal crack
- Encircling coil sensor without ferrite core to simulate a longitudinal crack

7.1.1 Encircling Coil Sensor without Ferrite Core to Simulate a Transversal Crack

In this section the modeling of the detection of a transversal crack with an encircling coil sensor without ferrite core is reported. Such a sensor is typically used in the rolling mills to detect the surface defects. This prototype is built according to the design of the encircling coil sensor which is in operation in Sidenor (*Sidenor*, S.A.). The modeling of this first generation sensor need to be performed to understand and determine the ways to modify it.

7.1.1.1 Geometry of an Encircling Coil Sensor without Ferrite Core

The schematic view of an encircling coil sensor is shown in Fig. 7.1. Such a sensor consists of four coils, where the two outer coils (red colored in Fig. 7.1b) operate as excitation coils and the two inner coils (blue colored in Fig. 7.1b) operate as receiving coils. Each of the excitation coils has the height of 3 mm and consists of 140 turns of copper wire and each of the receiving coils is constructed of 180 turns of copper wire.

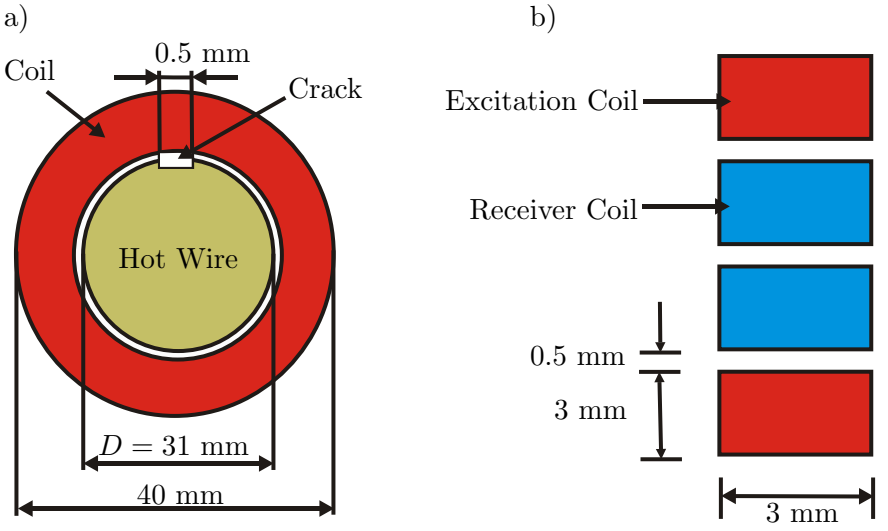

Figure 7.1: a) Cross section of the encircling coil sensor with steel wire inside and b) detailed view of the cross section of the sensor coils.

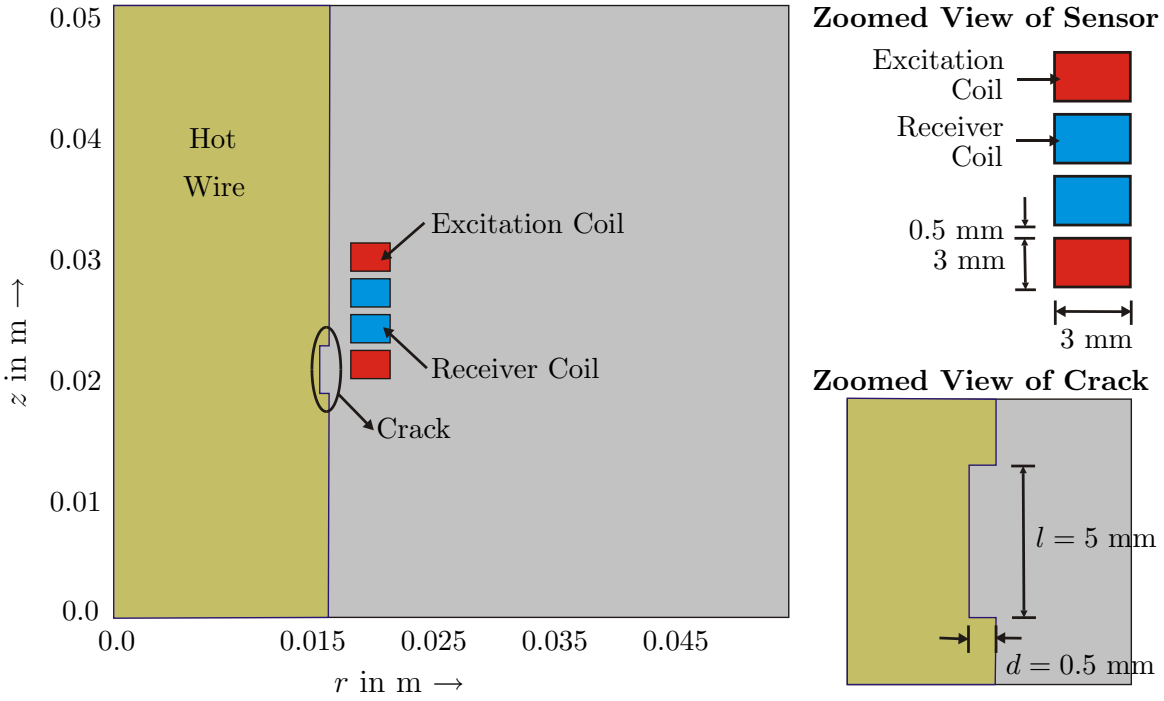

Figure 7.2: Schematic view of the geometry of the hot wire steel with a crack at $z = 20$ mm embedded in free-space and a sketch of an encircling coil sensor, electric conductivity of hot wire $\sigma_e = 1.4 \times 10^6$ A/Vm and magnetic permeability $\mu = \mu_0$.

The applied voltage at the driving circuit of the excitation coils is $V = 1.14142$ V (rms) which results a current density $\underline{\mathbf{J}}_{\mathrm{e}}^{\mathrm{imp}}(\underline{\mathbf{R}}, \omega) = 2.4 \times 10^4$ A/m^2 in the excitation coil. The obtained voltages in the receiver coils are recorded and plotted to determine the response of the sensor when a crack crosses the sensor. The size of the crack is length $l = 5$ mm and depth $d = 0.5$ mm.

7.1.1.2 Numerical Technique to Simulate an Encircling Coil Sensor without Ferrite Core

The simulations are performed by finite integration technique (FIT) with the help of MQSFIT (*Marklein*, 2002). The geometry shown in Fig. 7.2 lies in rz-plane and is discretized by $500 \times 500 = 250000$ rectangular elements. The resulting linear matrix equation is iteratively by bi-congugate gradient (BCG) method (*Shewchuk et al.*, 1994; *Press et al.*, 2007) with a relative tolerance of 1×10^{-8}. An excitation frequency of $f = 50$ kHz is used and the resulting radial component of the magnetic flux density is displayed in Fig. 7.3, the real part of A_φ is displayed on the left and the imaginary part on the right.

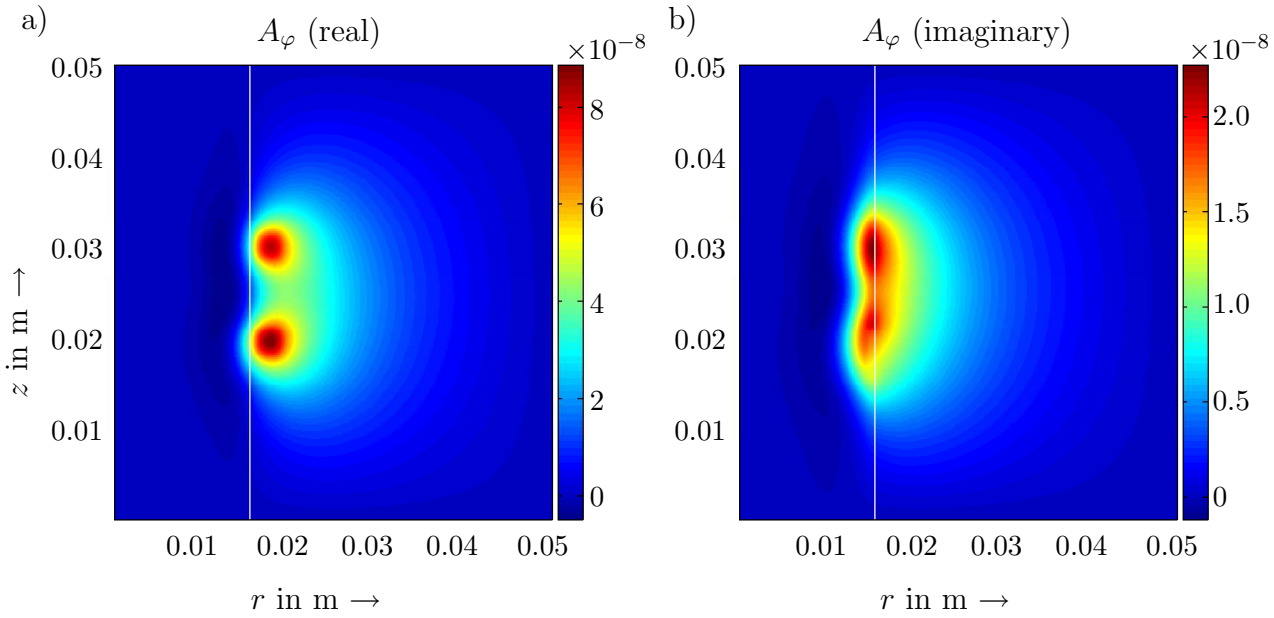

Figure 7.3: Simulation result using MQSFIT: a) real part and b) imaginary part of A_φ distribution in hot wire. Parameter: $N_r = 500$, $N_z = 500$, $\Delta = \Delta x = \Delta z = 0.1$ mm, $f = 50$ kHz, $\sigma_{\mathrm{e}} = 1.4 \times 10^6$ A/Vm and $\mu = \mu_0$.

7.1.1.3 Modeling of the Receiving Coils

The cross section of a receiving coil is shown in Fig. 7.4a. However, a coil consists of copper wires and cannot be realized as a block of copper. Fig. 7.4b shows an approximated view of the cross section of the receiving coil, where the cross sections of the copper wires are drawn as blue circles and $\Delta = \Delta r = \Delta z$. We compute A_φ for each of the node which resides inside the coil using MQSFIT. The electric field strength $\underline{\mathbf{E}}(\underline{\mathbf{R}}, \omega)$ is then computed in the second step by

$$E_\varphi(\underline{\mathbf{R}}, \omega) = \mathrm{j}\,\omega A_\varphi(\underline{\mathbf{R}}, \omega)\,. \tag{7.1}$$

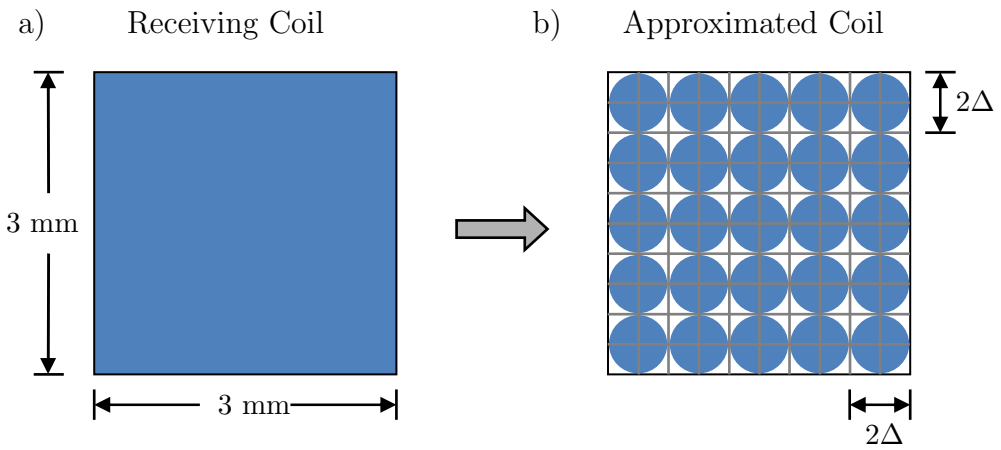

Figure 7.4: a) cross section of a receiving coil and b) the approximated geometry of the coil; $\Delta = \Delta r = \Delta z$.

The φ component of the electric field strength $E_\varphi(\underline{\mathbf{R}}, \omega)$ at the center of each conductor is determined by Eq. (7.1). We assume that inside each conductor $E_\varphi(\underline{\mathbf{R}}, \omega)$ remains constant and therefore, the induced electric voltage $V_\mathrm{e}(\omega)$ for each conductor of the receiving coil is calculated by

$$V_\mathrm{e}(\omega) = \oint \underline{\mathbf{E}}(\underline{\mathbf{R}}, \omega) \cdot \underline{\mathbf{dR}} = 2\pi R^{\mathrm{con}}\ E_\varphi(\underline{\mathbf{R}}, \omega)\,, \tag{7.2}$$

where R^{con} is the radius of the considered conductor. The total induced electric voltage of the receiving coil is then computed as

$$V_\mathrm{e}^{\mathrm{tot}}(\omega) = N_t\ V_\mathrm{e}(\omega)\,, \tag{7.3}$$

where the receiving coil consists of N_t turns of copper wire.

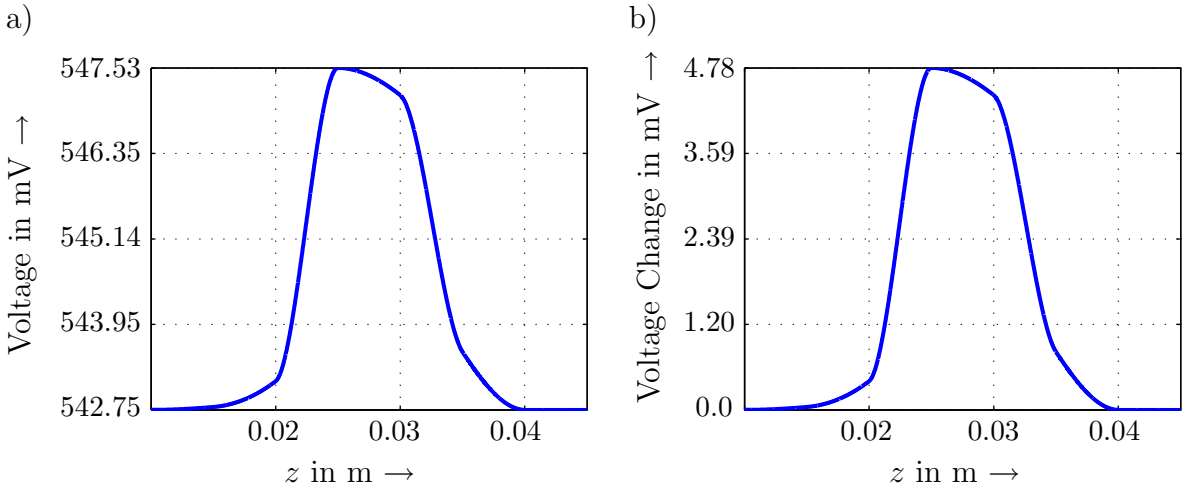

Figure 7.5: Simulation result using MQSFIT: a) Induced electric voltages of an encircling coil sensor as a function of crack position and b) change of induced electric voltages with the presence of a crack as a function of crack position.

7.1.1.4 Results and Performance Analysis of an Encircling Coil Sensor without Ferrite Core

A plot of the induced electric voltages recorded at the sensor coil as a function of crack position is given in Fig. 7.5a (*Rahman & Marklein*, 2006). The induced electric voltage at the receiver coils without any crack is 542.75 mV. Taking this voltage as an offset, the change of the induced voltage with the presence of a crack is plotted in Fig. 7.5b. If we take a close look of the magnetic flux distribution in Fig. 7.3, we find that measures can be taken to focus the magnetic flux density towards the steel surface, which will increase the induced electrical voltage at the sensor coil and will ensure better detection. The outcome of the modeling results lead to the development of a modified version of the encircling coil sensor which is later manufactured by Messtechnik, University of Kassel (*Messtechnik*, KS) and is presented in the next section.

7.1.2 Encircling Coil Sensor with Ferrite Core to Simulate a Transversal Crack

An encircling coil sensor with ferrite core, developed by the University of Kassel, is a modified version of an encircling coil. The simulation of the detection process with the presence of a transversal crack will be discussed here.

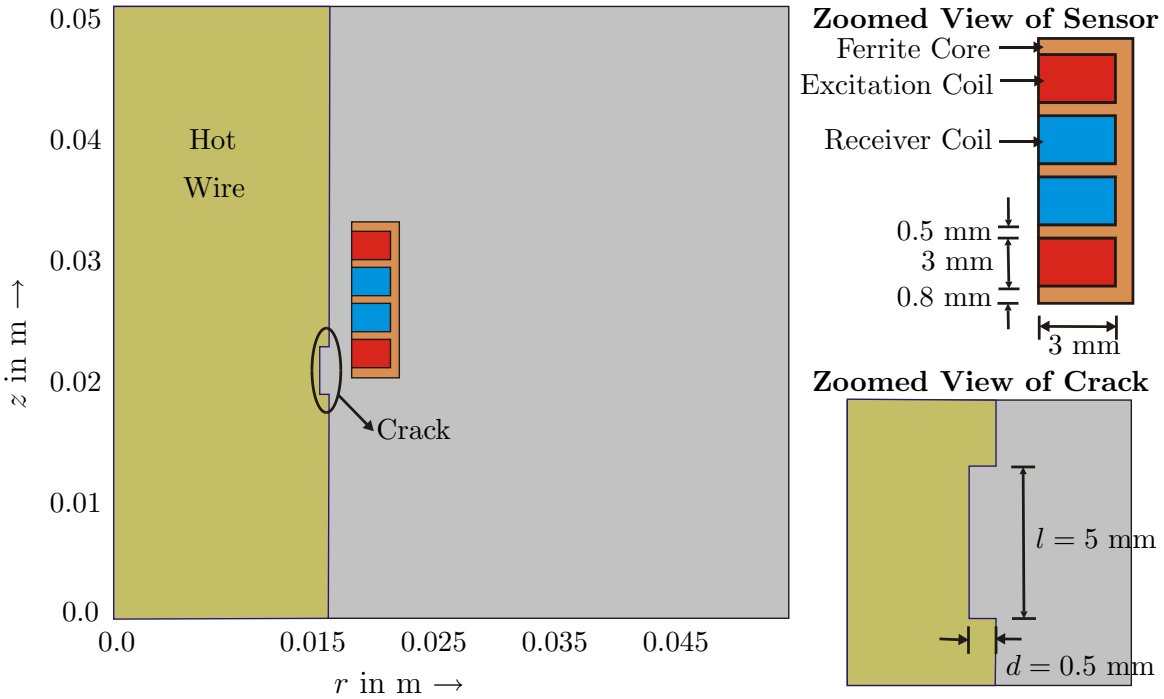

Figure 7.6: Schematic view of the geometry of the hot wire steel with a crack at $z = 20$ mm embedded in free-space and a sketch of an encircling coil sensor with ferrite core.

7.1.2.1 Geometry of an Encircling Coil Sensor with Ferrite Core

An encircling coil sensor with ferrite core has been shown in Fig. 7.6. The excitations coils are marked as red and the receiving coils are marked as blue. The ferrite core of the thickness of 0.8 mm resides in and around the sensor coils. A so called T38 type ferrite material is used here which posses a high magnetic permeability $\mu_r = 5000$ and therefore, it is suitable for guiding magnetic flux towards the steel wire. The other geometric details are the same as the encircling coil sensor without ferrite.

7.1.2.2 Numerical Technique to Simulate an Encircling Coil Sensor with Ferrite Core

The simulations are performed in cylindrical coordinates by finite element method (FEM) with the help of the steady-state AC module of Opera-2d (*Opera*, 10.5). We have used $e = 20000$ elements to discretize the simulation domain, which resides in rz-plane. The radial component of the magnetic flux density B_r is displayed in Fig. 7.7. As the magnetic flux lines are focused towards the steel bar with the help of the ferrite core, we observe here higher flux concentration and hence, higher induced voltage than in the case without ferrite core (see Fig. 7.8).

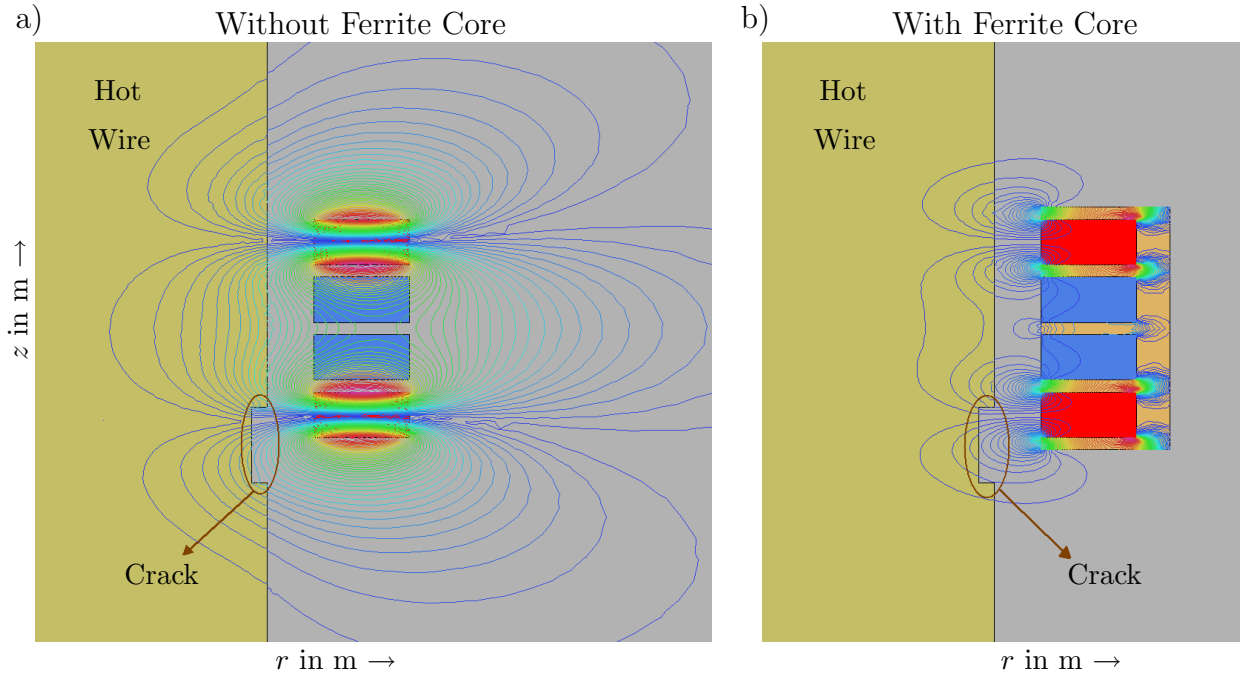

Figure 7.7: Field distribution of the radial component of the magnetic flux density of an encircling coil sensor system: a) without with ferrite core and b) with ferrite core. Parameter: no. of triangular elements $N_e = 20000$, $\sigma_e = 1.4 \times 10^6$ A/Vm, $\mu = \mu_0$.

7.1.2.3 Results and Performance Analysis of an Encircling Coil Sensor with Ferrite Core

A comparison of the induced electric voltages recorded at the sensor coil of the modified encircling coil sensor system with that of a traditional encircling coil sensor system is given in Fig. 7.8, where we find that the modified encircling coil sensor with ferrite core shows a higher sensitivity than a traditional one (*Rahman & Marklein*, 2009). Fig. 7.9 shows a

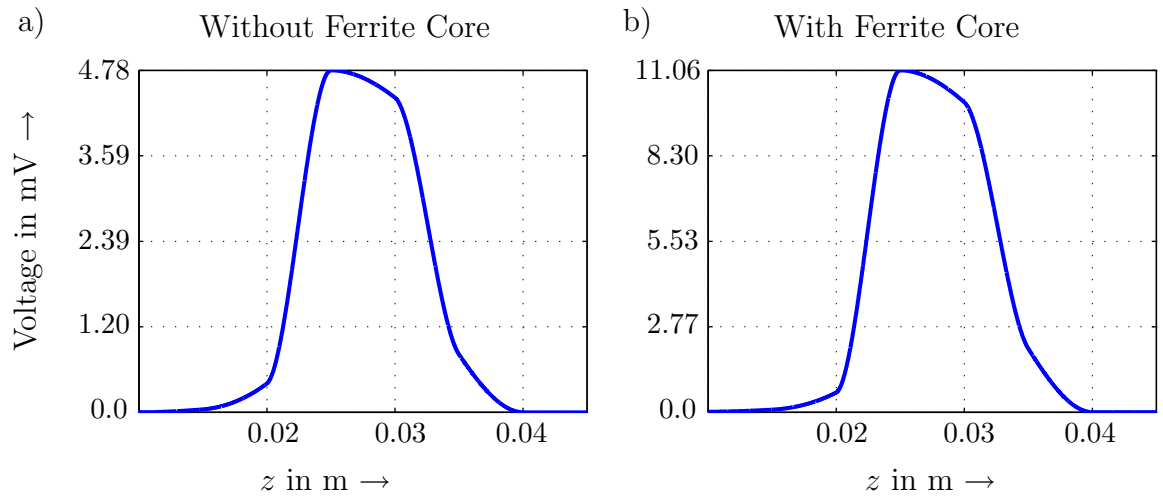

Figure 7.8: Change of induced electric voltages with the presence of a crack as a function of crack position obtained from a) an encircling coil sensor system without ferrite core and b) with ferrite core.

comparison of the synthetic A-scan to the measured A-scan, where the synthetic A-scan is shown on the right and the simulated A-scan on the right.

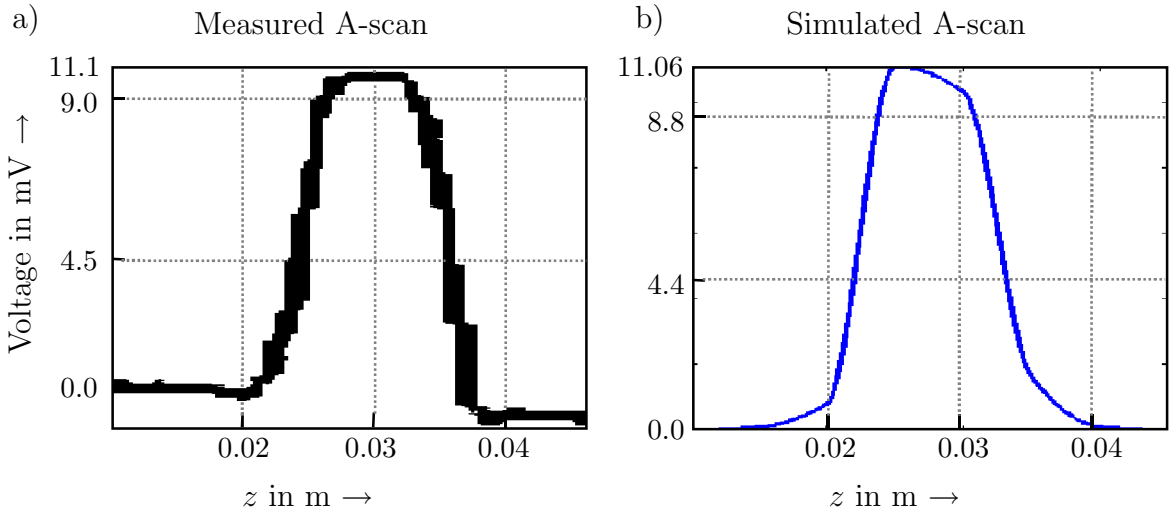

Figure 7.9: Eddy current testing of hot wire with an encircling coil with ferrite core: a) measured A-scan and b) simulated A-scan.

7.1.3 Encircling Coil Sensor without Ferrite Core to Simulate a Longitudinal Crack

The detection of the transversal cracks is not enough to meet the goals of the INCOSTEEL project. Depending on the production process, the presence of the longitudinal cracks at the upper surface of hot wire is quite usual and therefore, the encircling coil sensors need to be tested whether they are capable of detecting such cracks. In this section we report the modeling of the detection of a longitudinal crack with an encircling coil sensor without ferrite core.

7.1.3.1 Geometry of an Encircling Coil Sensor without Ferrite Core

The geometry of the encircling coil sensor without ferrite core is already discussed in Sec. 7.1.1.1 (see Fig. 7.2). The two outer coils of the sensor work as excitation coils , while the inner two marked as R1 and R2 in Fig. 7.10, function as receiver coils. The dimension of the crack is length $l = 20$ mm, depth $d = 0.5$ mm and width $w = 0.5$ mm. A steel wire of the length $L = 50$ mm and a diameter $D = 12$ mm is tested here.

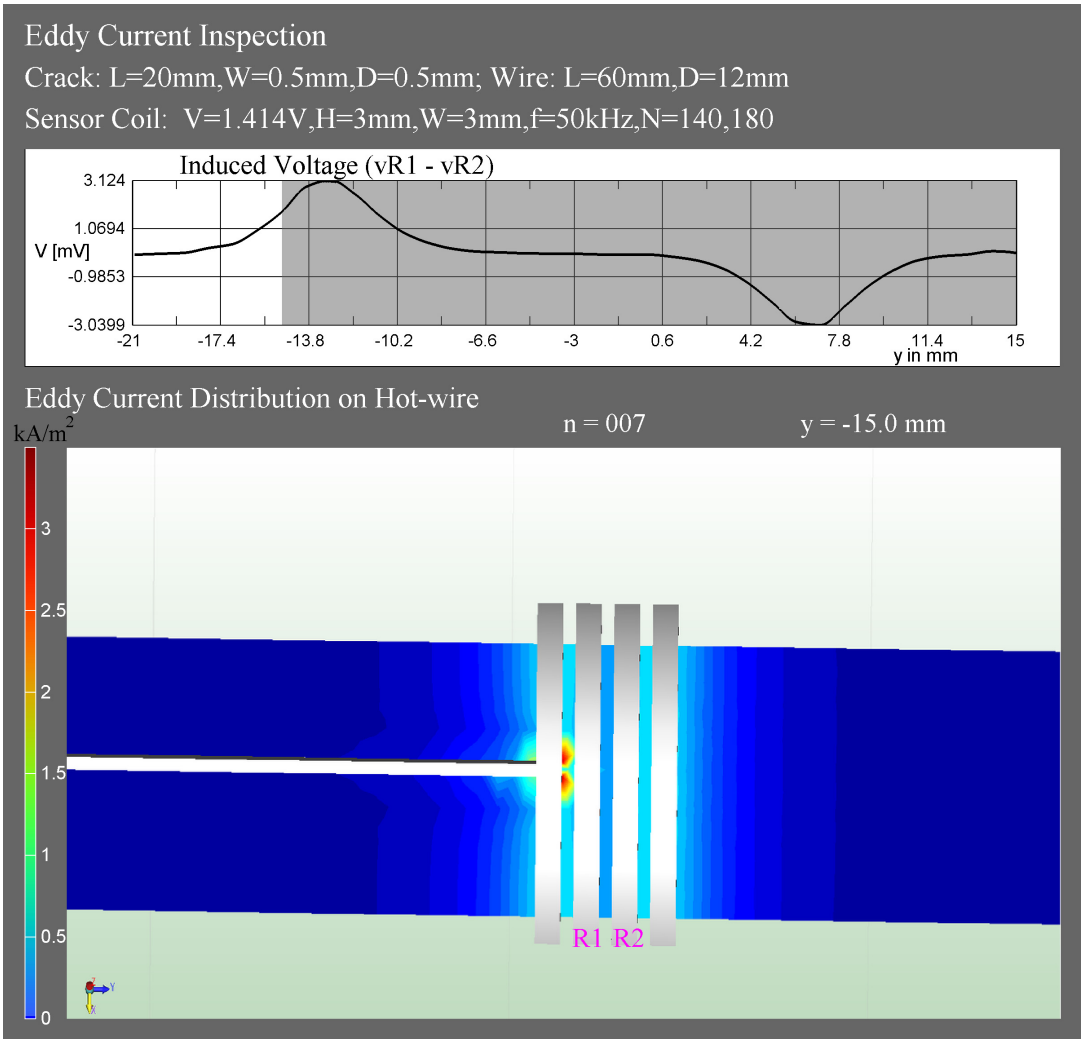

Figure 7.10: A snapshot of the hot wire inspection with a longitudinal crack. Geometry of Crack: $l = 20$ mm, $d = 0.5$ mm, $w = 0.5$ mm, Parameter: $f = 50$ kHz, $\sigma_e = 1.4 \times 10^6$ A/Vm and $\mu = \mu_0$.

7.1.3.2 Numerical Technique to Simulate an Encircling Coil Sensor without Ferrite Core

It is not possible to simulate a longitudinal crack using rotational symmetry and hence, we have to perform a 3-D modeling in this case. The simulations are accomplished by boundary element method (BEM) with the help of Faraday 6.1 (*Faraday*, 6.1). Fig. 7.10 shows a snapshot of the detection process where the eddy current distribution on the steel surface is

displayed in the bottom and the obtained differential signal (vR1−vR2) from the receiver coils is plotted on the top.

7.1.3.3 Results and Performance Analysis of an Encircling Coil Sensor without Ferrite Core

A plot of the induced electric voltages recorded at the sensor coil as a function of crack position is given in Fig. 7.11. The first peak indicates the beginning of the crack, while the second peak indicates the end. Such a sensor detects only the edges of the cracks and does not give continuous response while a longitudinal crack is crossing the sensor coils. Theoretically, it is possible to detect a longitudinal crack with an encircling coil sensor, as

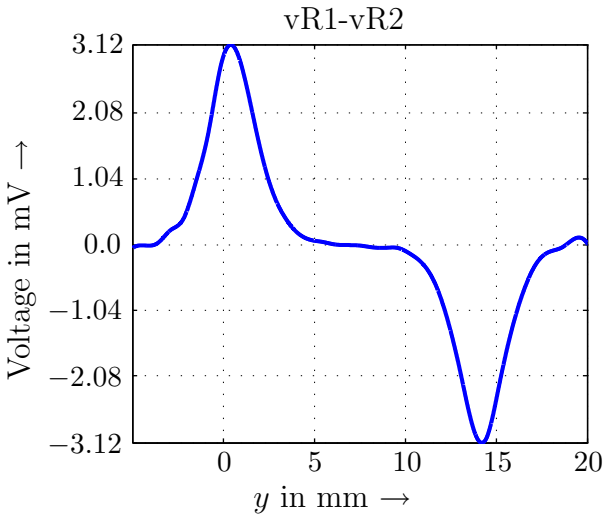

Figure 7.11: Differential signal vR1−vR2 obtained from an encircling coil sensor without ferrite core in presence of a longitudinal crack.

we have seen in the simulation results. Practically, in a rolling mill where more than one cracks can occur at the same time, it is almost impossible to detect the beginning and end of each longitudinal cracks with an encircling coil sensor. As a result, new sensors need to be developed which will not only detect the beginning and end of the crack, but also produce continuous response while the longitudinal cracks are passing by.

7.1.3.4 Innovative Ideas to Detect Longitudinal Cracks

The modeling results in the previous section show that a new kind of eddy current sensor has to be developed to detect the longitudinal cracks. As we observe from Fig. 7.10 that an encircling coil sensor produces a eddy current distribution which is parallel to the sensor coils and therefore, a longitudinal crack weekly influences such a distribution. As a result, an encircling coil sensor can only detect the crack tips and no continuous response can be obtained. To solve this problem we need to produce such an eddy current distribution which is more sensitive to the longitudinal one, i.e., a distribution which is not in the perpendicular direction to the length of the longitudinal crack. A circular uniform distribution on the steel surface is a suitable option in this sense but to produce such a distribution we require point coils. Based on this theoretical background the first point coil sensor, also known as a 3-coils sensor is suggested by Tecnatom (*Tecnatom*, S.A.). However, the inspection technique needs

to be modeled before manufacturing such a sensor system. Furthermore, the behaviour of the point coil sensor system in array mode also need to be studied.

7.2 Simulation Results of Point Coil Sensors

A number of point coil sensors are developed in INCOSTEEL (*INCOSTEEL*, 2004) project to detect the longitudinal cracks. We shall discuss in this section the following types of point coil sensors:

- 3-coils sensor in unitary mode
- 3-coils sensor in array mode
- D-coils sensor
- 4-coils sensor
- Pot core sensor

7.2.1 A 3-Coils Sensor in Unitary Mode

A 3-coils sensor consists of three small elementary coils (see Fig. 7.12a) where one of the coils operates as the excitation coil and the other two coils operate as the receiving coils. For test purpose this type of sensor is first operated in unitary mode.

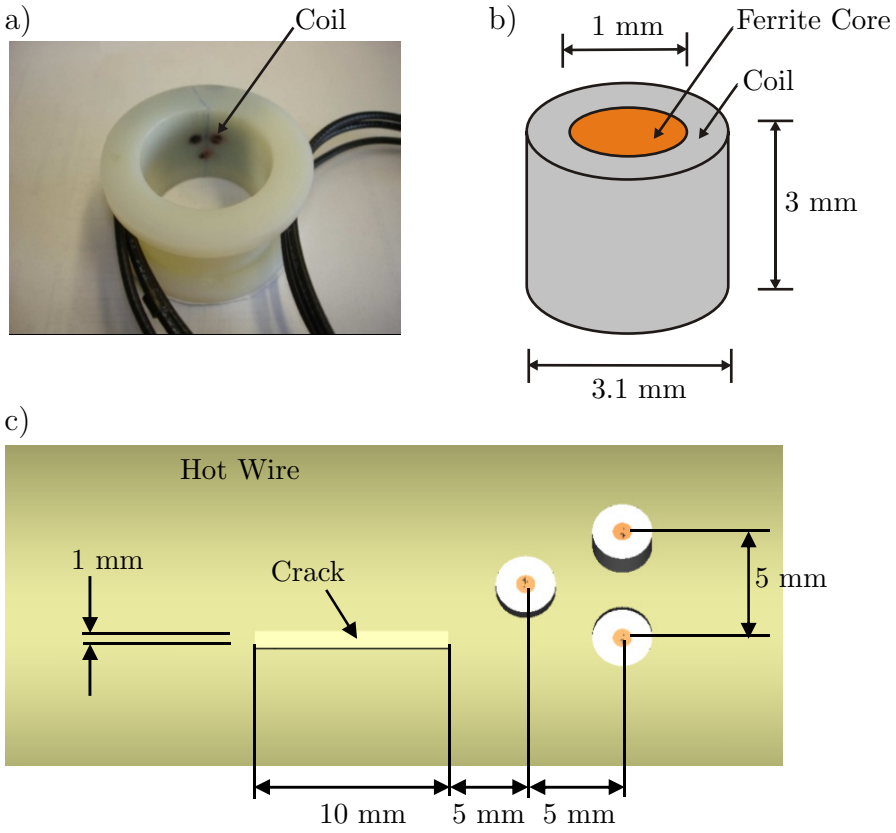

Figure 7.12: a) Photo of a 3-coils sensor, b) geometric detail of a single element of a 3-coils sensor and c) test setup using a 3-coils sensor.

7.2.1.1 Geometry of a 3-Coils Sensor in Unitary Mode

Each element of a 3-coils sensor has the height of 3 mm and the diameter of 3.1 mm (see Fig. 7.12b). 260 turns of copper wire is wound over a ferrite core to form a single element. In Fig. 7.12c the elements marked as R1 and R2 work as the receiving coils. The other lone element works as the excitation coil, which posses a current density of $\mathbf{J}_{\mathrm{e}}^{\mathrm{imp}}(\underline{\mathbf{R}}, \omega) = 2.337 \times 10^7$ A/m^2, where a monochromatic frequency of $f = 74$ kHz is used. The coils reside 0.5 mm above the steel surface and 5 mm apart from each other (see Fig. 7.12c).

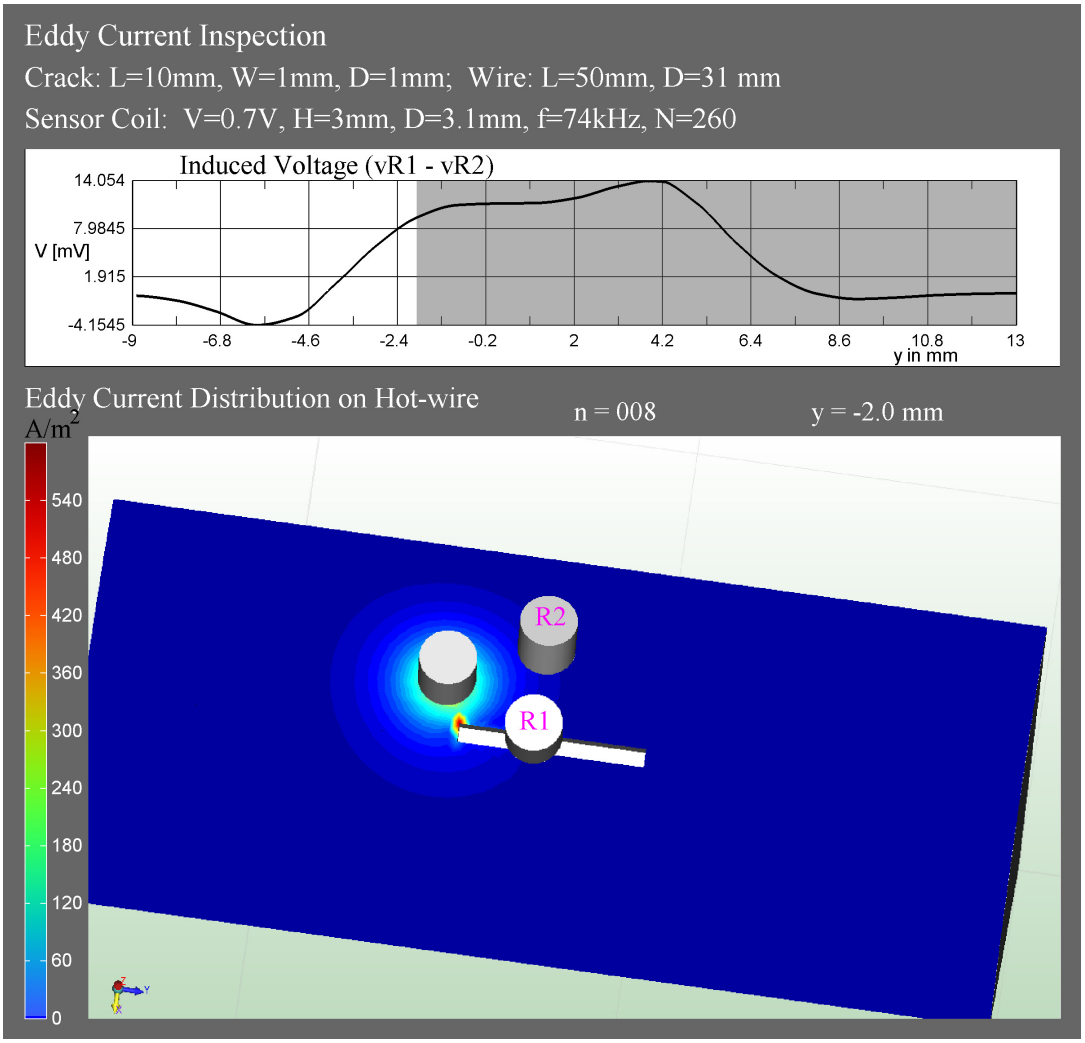

Figure 7.13: A snapshot of the detection process; top: induced voltage in the receiving coils, bottom: eddy current distribution on the hot wire.

7.2.1.2 Numerical Technique to Simulate a 3-Coils Sensor in Unitary Mode

The 3-coils sensor system is simulated boundary element method (BEM) with the help of Faraday 6.1 (*Faraday*, 6.1). To discretize the geometry the eddy current skin depth of the hot wire steel is calculated as

$$\chi = \frac{1}{\sqrt{\pi f \mu \sigma_{\mathrm{e}}}} = 1.55 \text{ mm}, \tag{7.4}$$

where relative permittivity of hot wire steel $\mu = \mu_0$ above the Courie point and the electric conductivity $\sigma_{\mathrm{e}} = 1.4 \times 10^6$ A/Vm. The length of a side of each triangular element should

be less than the skin depth and therefore, triangles having the area of 0.21 mm^2 have been chosen. A total number of $N_e = 6000$ triangular elements are used to discretize the steel surface, whereas each of the ferrite core is discretized using 308 triangular elements. The obtained linear matrix equation has been solved using generalized minimal residual (GMRES) method (*Meister*, 2008). Fig. 7.13 shows a snapshot of the detection process. $L = 50$ mm of a steel wire of the diameter $D = 31$ mm has been simulated here. The size of the crack is: length $l = 10$ mm, width $w = 1$ mm and depth $d = 1$ mm. The eddy current distribution on the steel surface is displayed in the bottom of Fig. 7.13, where an excitation frequency of $f = 74$ kHz is used. The obtained voltages in the sensor coils are recorded and the differential signal is plotted on the top of Fig. 7.13 to determine the response of the sensor when a crack crosses the sensor.

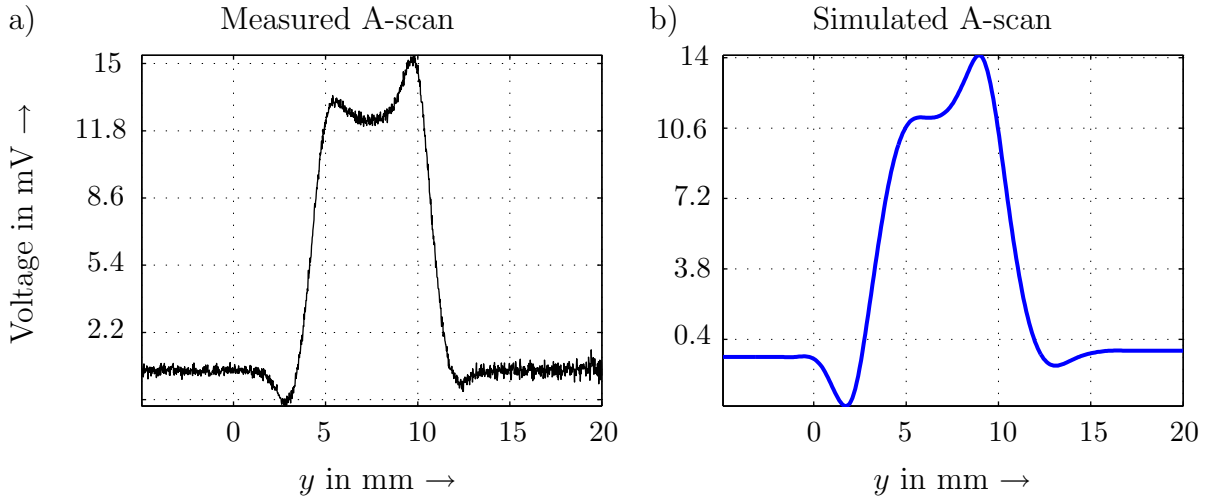

Figure 7.14: Hot wire testing with a 3-coils sensor: a) measured A-scan and b) simulated A-scan.

7.2.1.3 Results and Performance Analysis of a 3-Coils Sensor in Unitary Mode

The synthetic A-scan, obtained from the simulation, is validated against the measured A-scan in Fig. 7.14. The comparison shows satisfactory results and proves the accuracy of the simulation (*Rahman & Marklein*, 2008; *Ricken et al.*, 2008). The modeling of the inspection technique shows good detection of the longitudinal cracks with a 3-coils sensor. This leads to the manufacturing of the prototype of this sensor and testing in the industrial environment in TU Freiberg (*TU Freiberg*, FB). A 3-coils sensor shows good results to detect the longitudinal cracks in laboratory as well as industrial environment. However, this sensor shows a major drawback when any longitudinal crack resides direct beneath the excitation coil. In this case, both the excitation coils show the same voltages, and hence no differential signal can be obtained. A modification needs to be performed to overcome this difficulty. Furthermore, for successful testing of the hot wire we have to operate a 3-coils sensor in array mode and hence, more simulations need to be performed to evaluate the array mode of such a sensor.

7.2.2 A 3-Coils Sensor in Array Mode

The use of an array of sensors shows better performance in detecting the cracks than a single sensor. That's why it is important to study the performance of sensors when they work in an array.

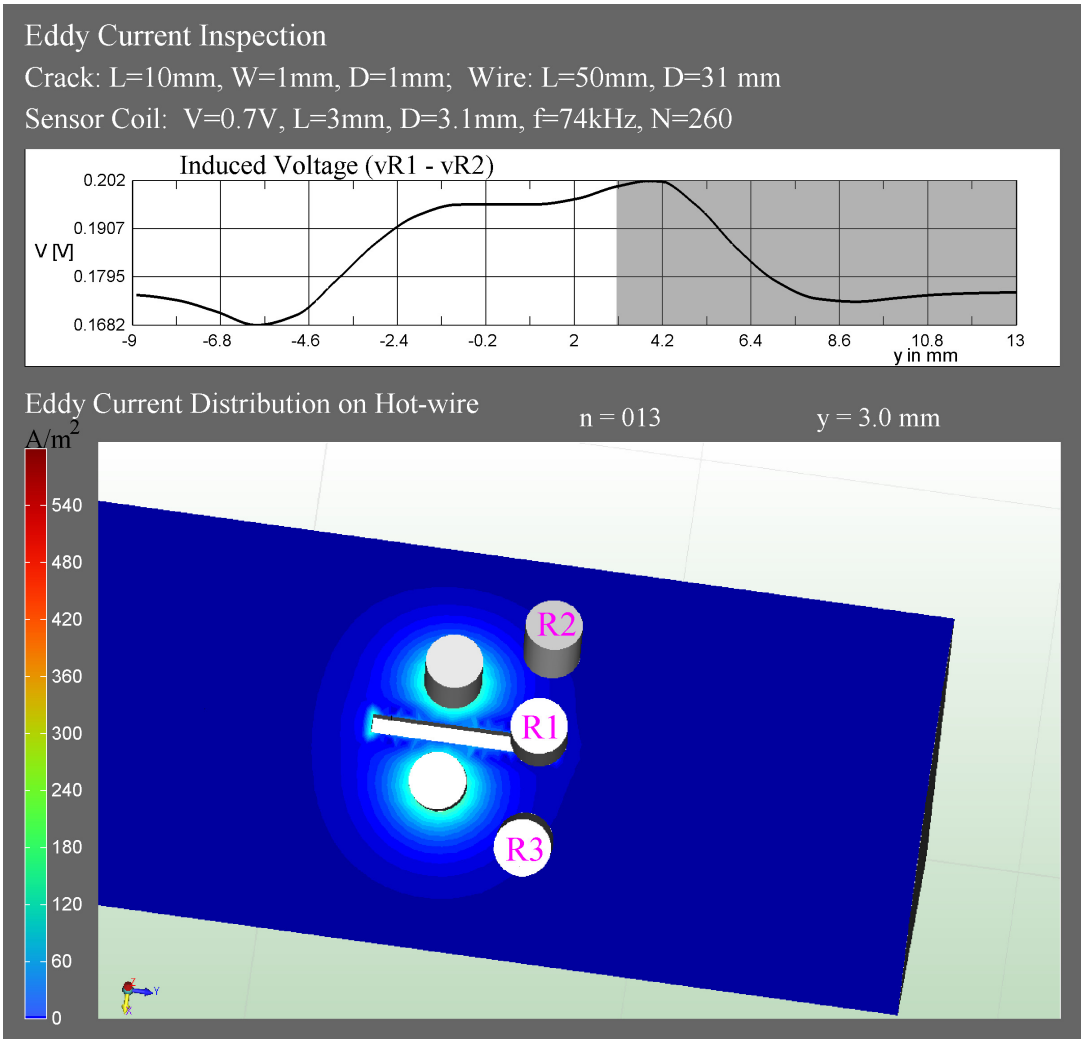

Figure 7.15: A snapshot of the detection process with an array of 3-coils sensor consists of 2 excitation coils and 3 receiver coils; top: induced voltage in the receiving coils and bottom: eddy current distribution on the hot steel wire.

7.2.2.1 Geometry and Numerical Technique to Simulate a 3-Coils Sensor in Array Mode

A sensor array consisting 2 excitation coils and 3 receiver coils is simulated in Fig. 7.15. The differential signal obtained from the receiver elements R1 and R2 is shown on top. On the bottom the eddy current distribution on the hot wire is shown. The simulated crack has the length of $l = 10$ mm and the depth of $d = 1$ mm. The excitation is performed using a current density $\underline{\mathbf{J}}_{\mathrm{e}}^{\mathrm{imp}}(\underline{\mathbf{R}}, \omega) = 2.337 \times 10^7$ A/m^2 in the excitation coils where a frequency of $f = 74$ kHz is used. The shadowed bar of the A-scan indicates the induced voltage at the particular crack position. As this type of sensor is an edge-detected one, we observe the change in the induced voltage only at the beginning and end of the crack.

7.2.2.2 Simulation Results and Performance Analysis of a 3-Coils Sensor in Array Mode

The voltages obtained from the receiver coils R1, R2 and R3 are plotted in Fig. 7.16. The calculated difference signals vR1−vR2 and vR1−vR3 are shown in Fig. 7.17. Comparing

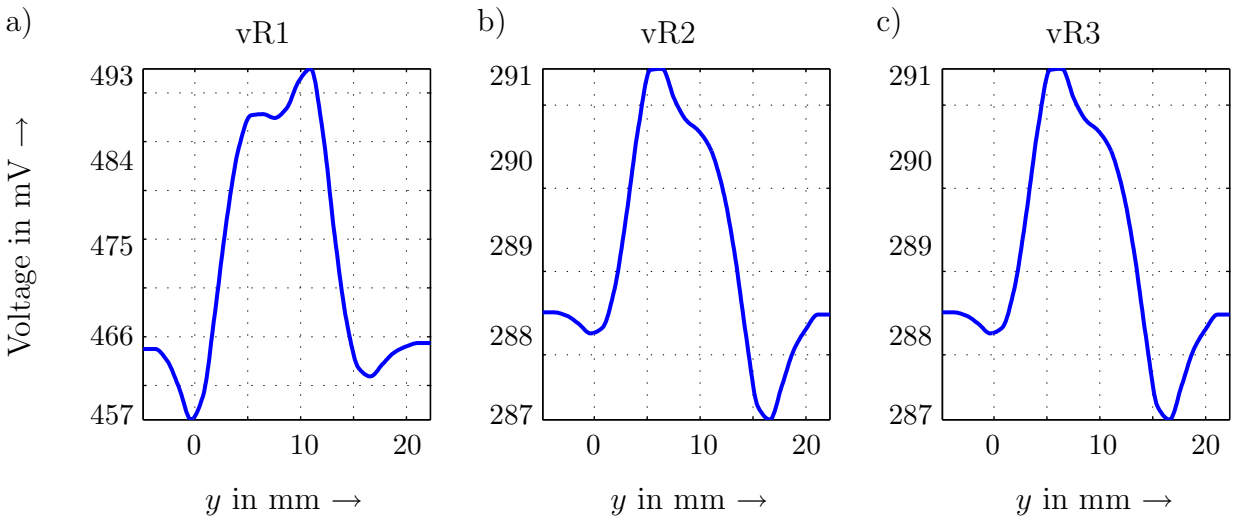

Figure 7.16: Induced voltages at a) receiver 1 (vR1), b) receiver 2 (vR2) and c) receiver 3 (vR3).

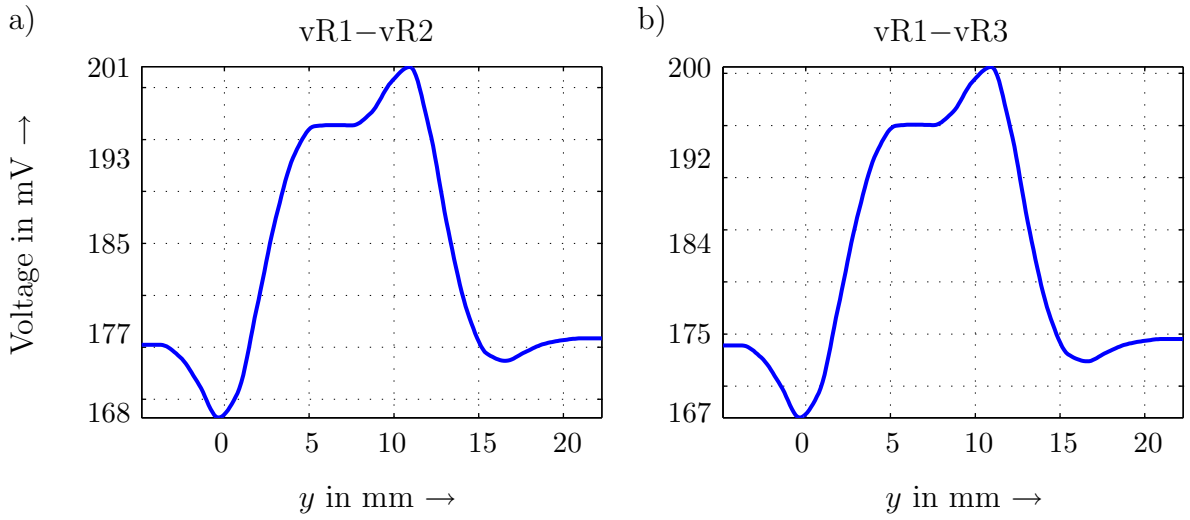

Figure 7.17: Differential signal obtained from a 3-coils sensor in array mode: a) vR1-vR2 and b) vR1-vR3.

Fig. 7.17 to Fig. 7.13 we find that the induced voltage obtained from a 3-coils sensor in array mode is higher than that in unitary mode, which proves, a 3-coils sensor shows better sensitivity in array mode than in unitary mode. However, it is difficult to manufacture such arrays because of the angular displacement between the rings of excitation and receiver coils. To overcome this difficulty a 4-coils sensor is developed which has simpler geometry and also better sensitivity.

7.2.3 Simulation Results of a D-coils Sensor

University of Kassel has developed several designs of surface probe coils throughout the project. The aim of this design was the detection of longitudinal defects, although other defect orientations were also detected.

7.2.3.1 Geometry of a D-coils Sensor

A D-coils sensor consists of an oval shaped excitation coil (see Fig. 7.18a), which resides around the receiving coils. The receiving coils are developed inside the pot formed ferrite

cores (see Fig. 7.18b). The excitation coil is built of 150 turns of copper wire and each of the receiving coils is formed of 40 turns of copper wire. The efficiency of the prototype has to be determined through numerical modeling before fabricating it for industrial test.

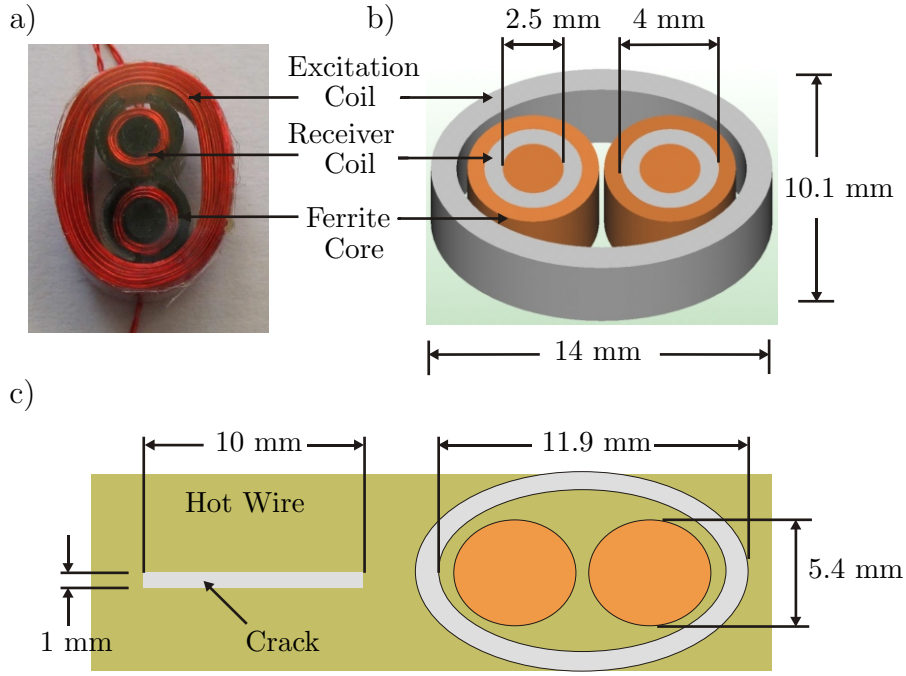

Figure 7.18: a) Photo of a D-coils core sensor, b) ferrite core of the receiver coils of the sensor and c) top view of test setup using a d-coils sensor.

7.2.3.2 Numerical Technique to Simulate a D-coils Sensor

Fig. 7.19 shows a snapshot of the detection process using a D-coils sensor. 50 mm of a steel wire of the diameter $D = 12$ mm has been simulated here. The size of the crack is: length $l = 10$ mm, width $w = 1$ mm and depth $d = 1$ mm. An excitation frequency of $f = 400$ kHz is used and the eddy current distribution on the steel surface is displayed in the bottom of Fig. 7.19. The obtained voltages in the sensor coils are recorded and the differential signal is plotted on the top of Fig. 7.19 to determine the response of the sensor when a crack crosses the sensor. The simulation is performed using the boundary element method (BEM) with the help of Faraday 6.1 (*Faraday*, 6.1).

7.2.3.3 Simulation Results and Performance Analysis of a D-coils Sensor

The induced voltages in the receiver coils R1 and R2 are plotted in Fig. 7.20a and Fig. 7.20b respectively, whereas the differential signal vR1−vR2 is plotted in Fig. 7.20c. There are some major cons of the D-coils sensor. As this sensor is larger than the steel wire of the diameter of $D = 12$ mm, it fails to produce a uniform eddy current distribution on the steel surface and therefore, offers poor sensitivity. Furthermore, the receiver coils are oriented along the axis of the steel wire, which causes difficulties in determining the position and size of the longitudinal cracks (see Fig. 7.20c). Due to these drawbacks we conclude from numerical modeling that this prototype is not suitable in detecting longitudinal cracks and therefore, modifications need to be performed to overcomes these problems.

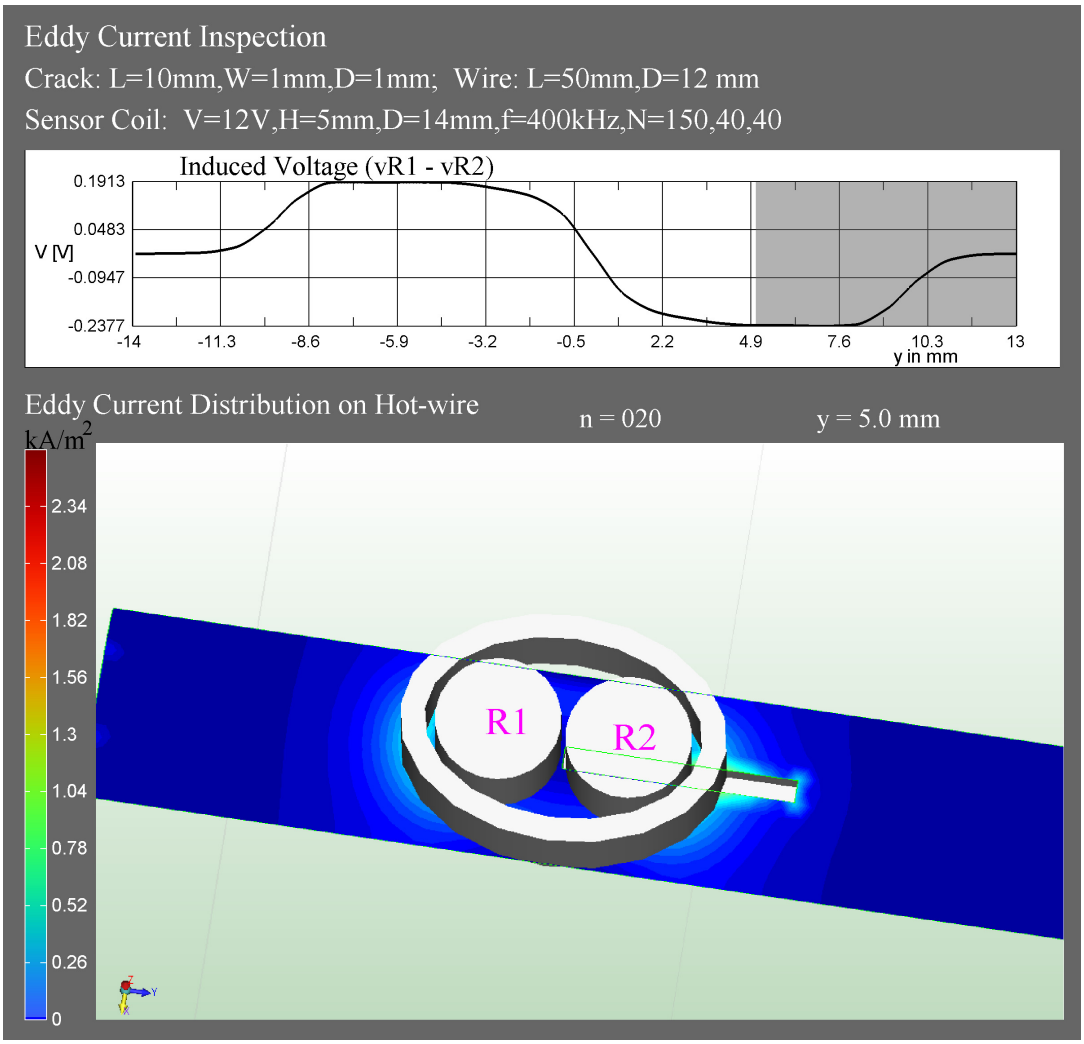

Figure 7.19: Hot wire testing using a d-coils sensor; top: induced voltage in the receiving coils, bottom: eddy current distribution on the hot wire.

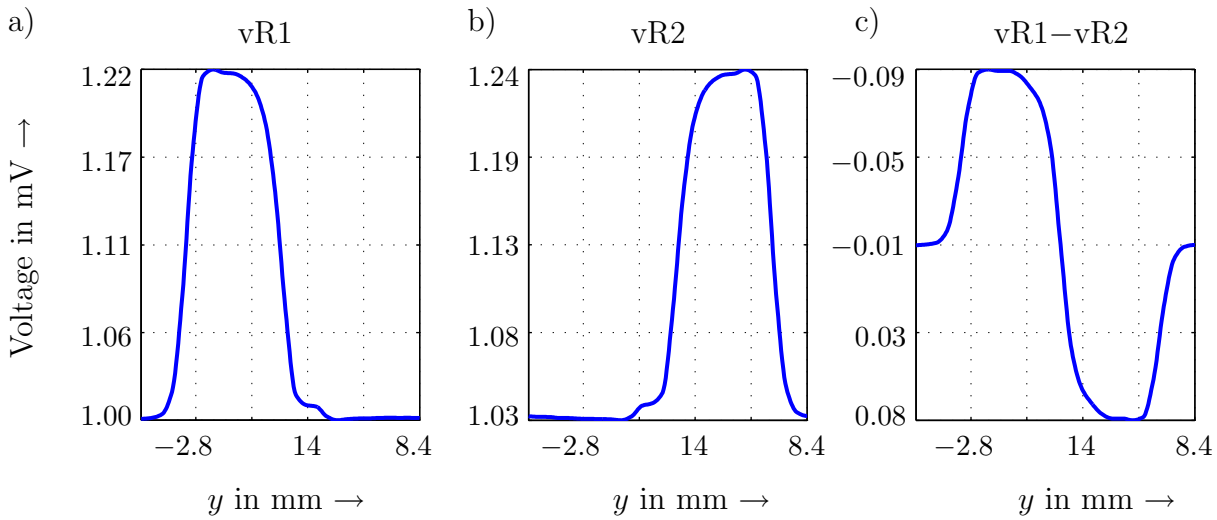

Figure 7.20: Induced voltages at a) receiver 1 (vR1), b) receiver 2 (vR2) and c) differential signal (vR1−vR2).

One idea to modify this sensor is to reduce the size of the pot shaped ferrite cores of the receiving coils and to redesign the excitation coils. The second idea is to use same type of excitation coils as the receiving coils. These two ideas lead to the development of the pot coil sensor which will be discussed later.

7.2.4 Simulation Results of a 4-Coils Sensor

The 4-coils sensor, a modified version of the 3-coils sensor, is developed by Tecnatom in order to overcome the difficulties of a 3-coils sensor. However, the initial prototype needs to be verified and optimized through numerical simulations to develop the final prototype. After the numerical evaluation of the first prototype we have executed a parameter study to find the optimum distance between the coils.

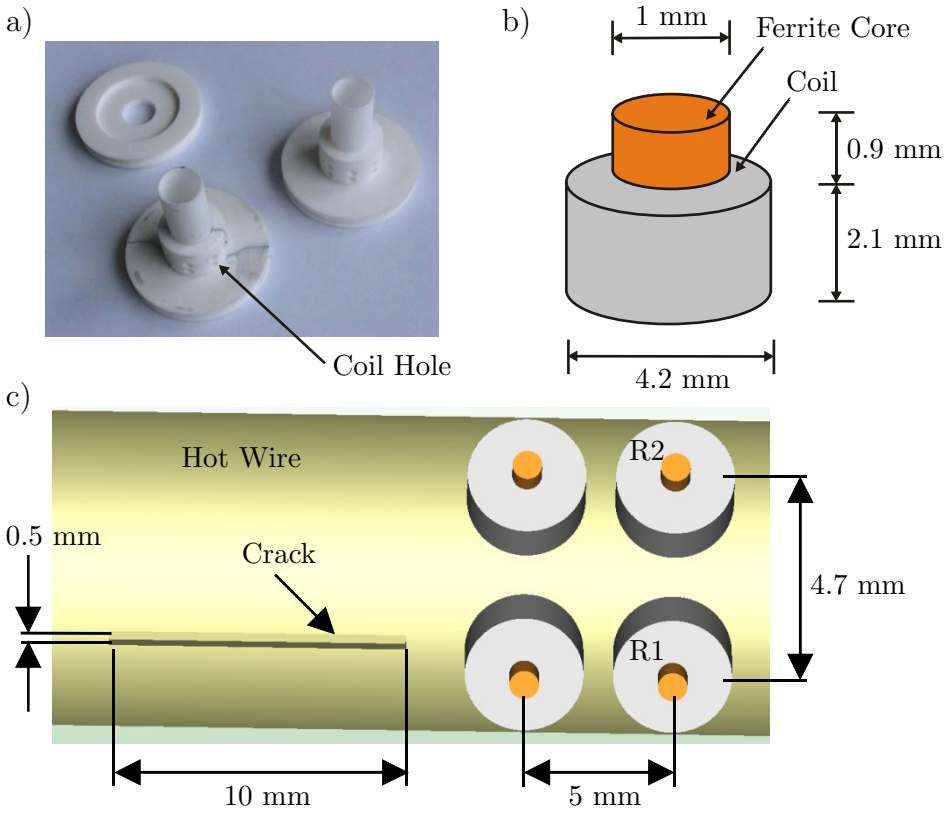

Figure 7.21: a) Photo of a 4-coils sensor, b) geometry of a single element of a 4-coils sensor and c) top view of test setup using a 4-coils sensor.

7.2.4.1 Geometry of a 4-Coils Sensor

A 4-coils sensor consists of four coils, where two of them operate as excitation coils and the other two (marked as R1 and R2 in Fig. 7.21c) operate as receiving coils. 260 turns of copper wire is wound over a ferrite core of the height of 3 mm and the width of 1mm (see Fig. 7.21b). Two rings of sensor coils are used here, where each ring contains eight coils. The optimum distance between an excitation and a receiving coil is 6 mm which is determined by a parametric analysis.

7.2.4.2 Numerical Technique to Simulate a 4-Coils Sensor

A surface crack of the length $l = 10$ mm, width $w = 0.5$ mm and depth $d = 0.5$ mm is detected using a 4-coils sensor system in Fig. 7.22. The tested steel wire has a length of $L = 50$ mm and a diameter $D = 12$ mm. The excitation coils are fed with a current density of $\underline{\mathbf{J}}_{\mathrm{e}}^{\mathrm{imp}}(\underline{\mathbf{R}}, \omega) = 5.26 \times 10^7$ A/m^2 with a frequency of $f = 200$ kHz. The resulting eddy current distribution on the steel surface is displayed in the bottom of Fig. 7.22. The

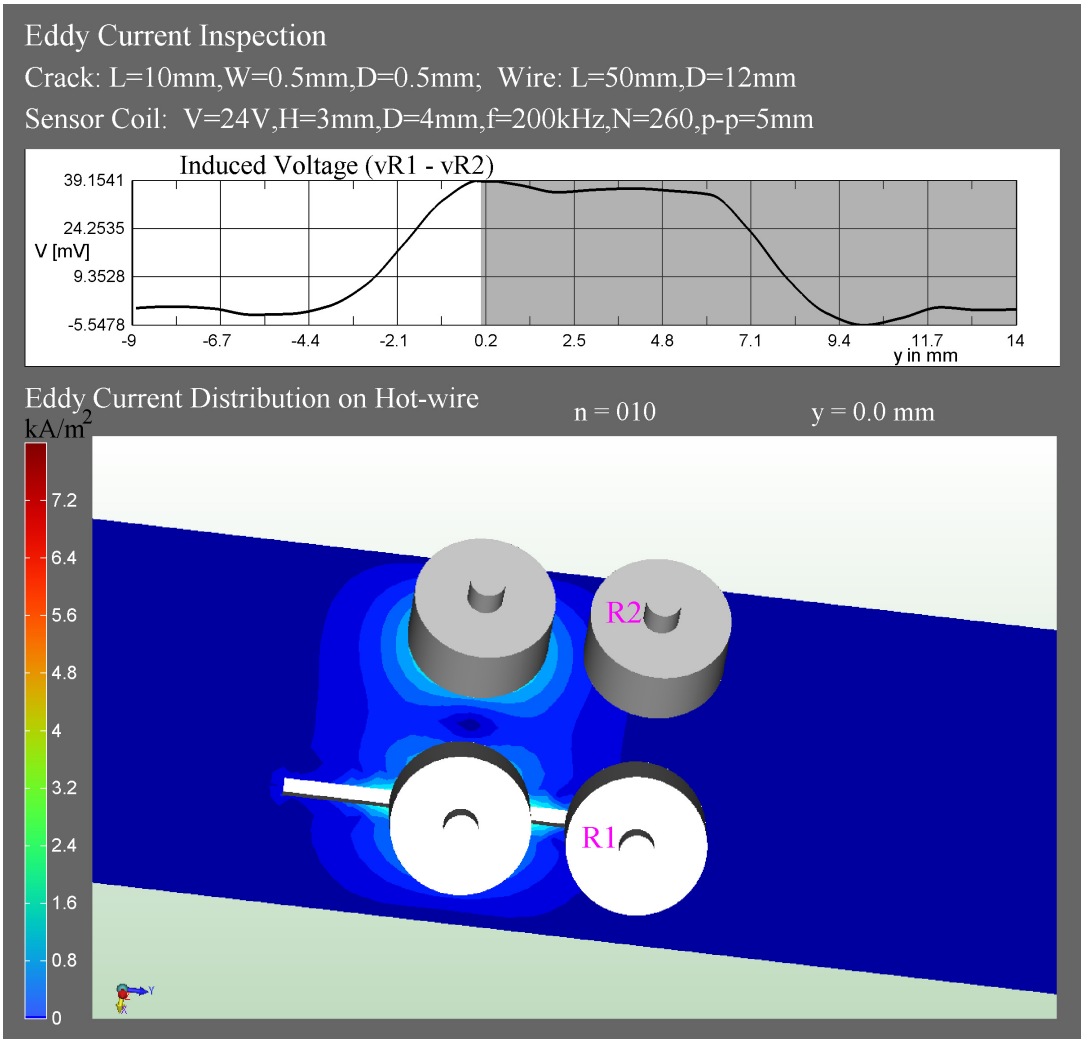

Figure 7.22: A snapshot of the detection process using a 4-coils sensor; top: induced voltage in the receiving coils, bottom: eddy current distribution on the hot wire.

obtained voltages in the sensor coils are recorded and the differential signal is plotted on the top of Fig. 7.22 to determine the response of the sensor. The boundary element method (BEM) is implemented here to model this eddy current problem with the help of Faraday 6.1 (*Faraday*, 6.1). Induced voltages at different receiving points have been shown in Fig. 7.23. The receiver 1 shows higher induced voltage than that of receiver 2 because it resides over the crack (*Rahman & Marklein*, 2009). A differential signal vR1−vR2 is plotted on the left side of Fig. 7.24.

7.2.4.3 Simulation Results and Performance Analysis of a 4-Coils Sensor

Like its predecessor a 4-coils sensor also shows good performance in detecting longitudinal cracks. Comparing the results of a 3-coils sensor with that of a 4-coils sensor reveals that a 4-coils sensor shows higher sensitivity in presence of a crack (see Fig. 7.14 and Fig. 7.24). Furthermore, unlike a 3-coils sensor this sensor system does not show a blind zone when a crack resides direct beneath the excitation coils. The modeling results show that a 4-coils sensor posses high sensitivity and better performance and hence, is suitable for final prototype. This leads to the manufacturing of the final prototype of a 4-coils sensor, which has shown very good performance in laboratory tests as well as in the rolling mills in TU Freiberg.

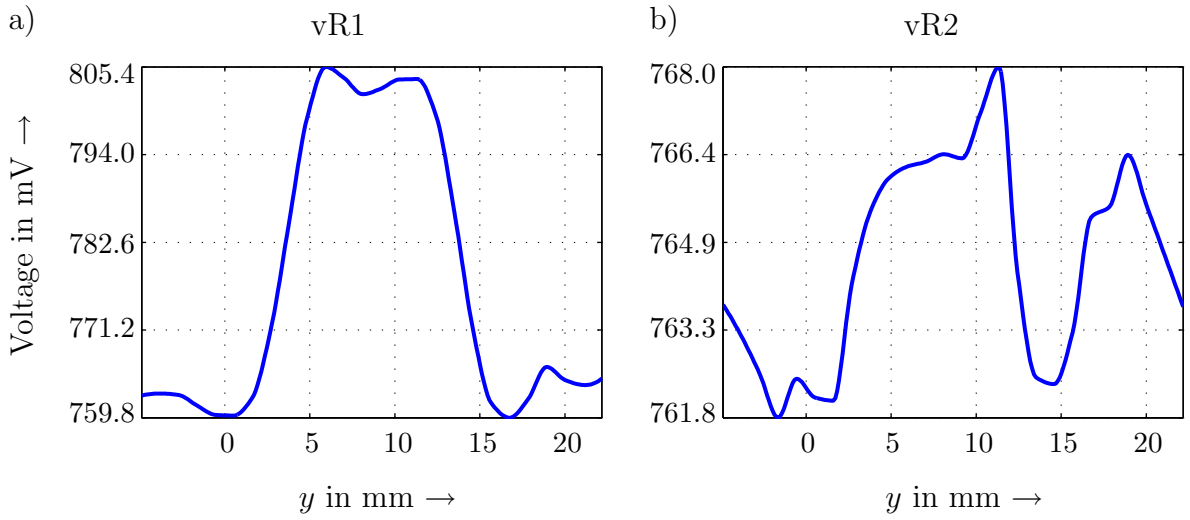

Figure 7.23: Induced voltages at a) receiver 1 (vR1) and b) receiver 2 (vR2).

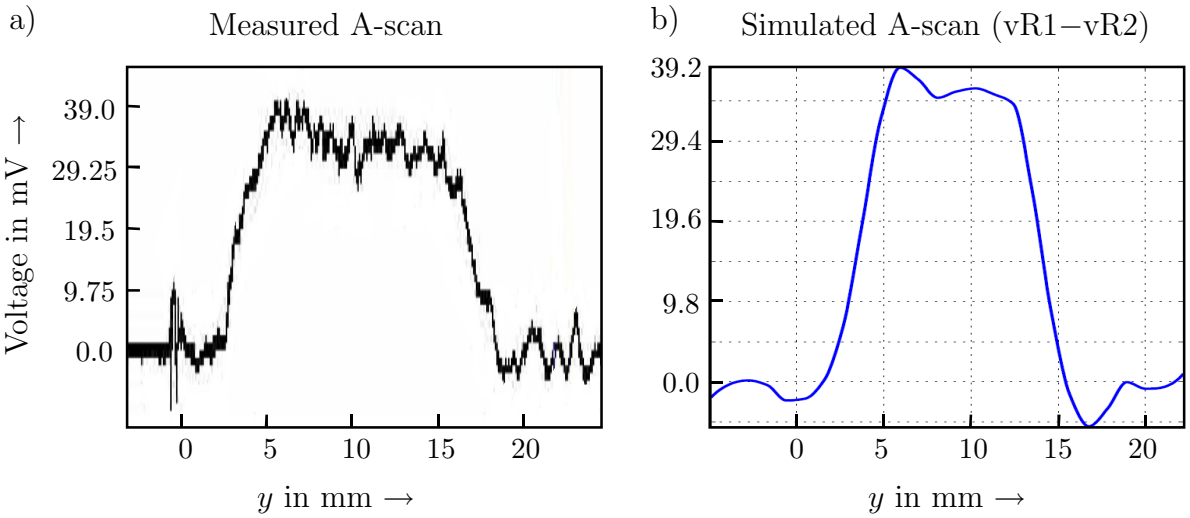

Figure 7.24: Hot wire testing with a 4-coils sensor: a) measured A-scan and b) simulated A-scan (vR1−vR2).

7.2.4.4 Effect of the Length of a Crack on Sensor Performance

The effect of the length of a crack on the performance of a 4-coils sensor need to be determined before final test in Sidenor (*Sidenor*, S.A.). Numerical modeling is obviously the best way

for such an evaluation. In our previous simulations, we have used a crack length of $l = 10$ mm. A hot wire steel with a surface crack of the length $l = 15$ mm, width $w = 0.5$ mm and depth $d = 0.5$ mm is inspected using a 4-coils sensor system in Fig. 7.25. The geometrical details of the sensor and the hot wire remain unchanged.

Fig. 7.26 shows a comparison between the differential signals for a crack of the length $l = 10$

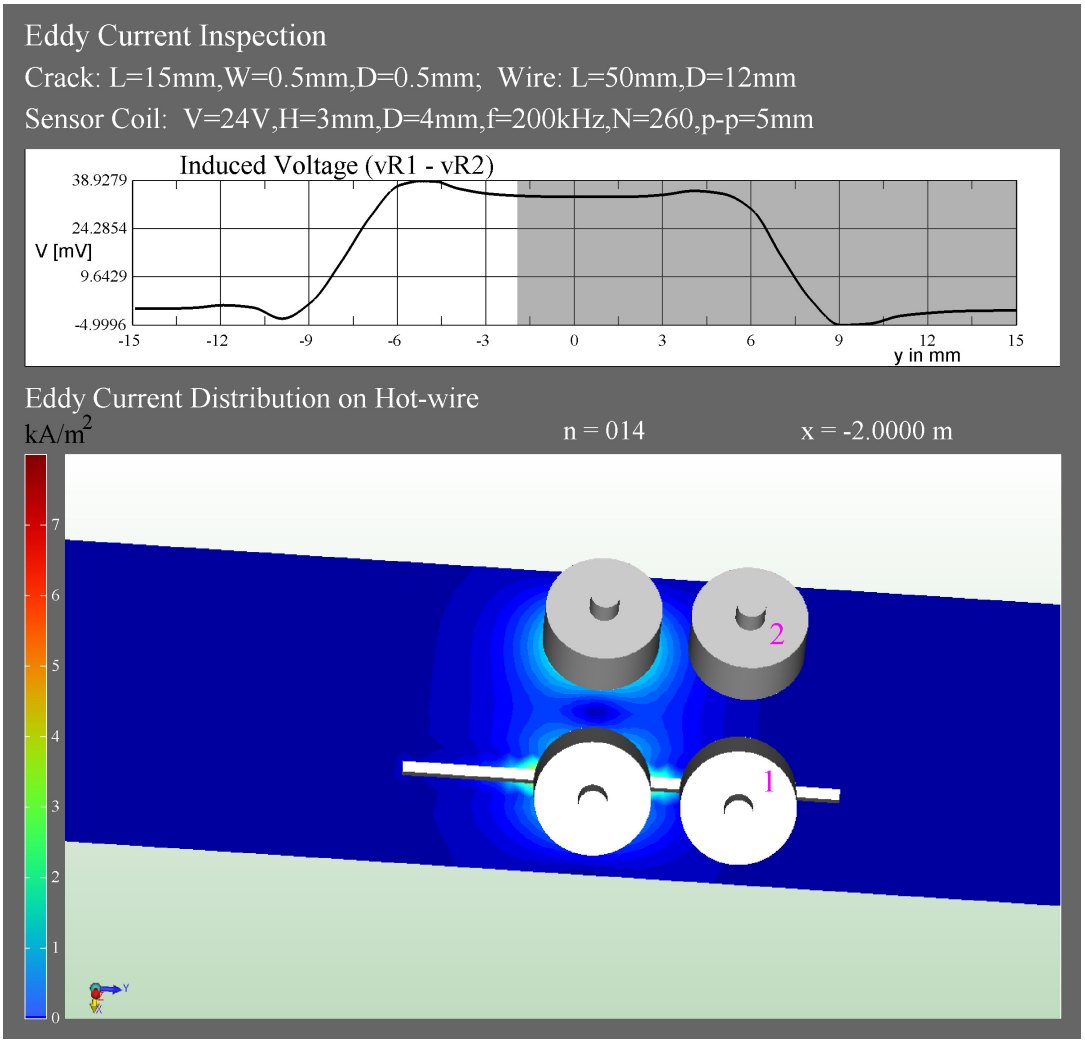

Figure 7.25: A snapshot of the detection process using a 4-coils sensor with a crack of the length $l = 15$ mm; top: induced voltage in the receiving coils, bottom: eddy current distribution on the hot wire.

mm and that of a crack of the length $l = 15$ mm. In case of $l = 10$ mm (see Fig. 7.26a) we observe higher oscillation at the beginning and at the end of the voltage peak, whereas, in case of $l = 15$ mm (see Fig. 7.26b) the voltage rise to the peak level is relatively smooth. Furthermore, this comparison shows that a 4-coils sensor gives continuous response as long as the crack is there and therefore, is suitable to detect longitudinal cracks of any length in hot wire steel.

Because of good performance in all the the numerical evaluations, a 4-coils sensor is accepted for the final design and later used to produce a combined sensor system.

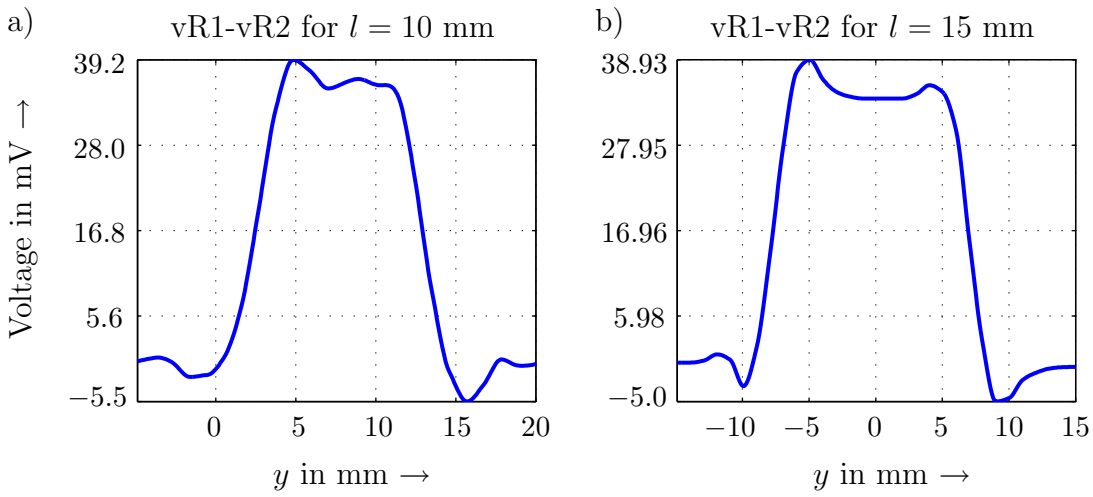

Figure 7.26: Hot wire testing with a 4-coils sensor with a crack of the length a) $l = 10$ mm and b) $l = 15$ mm.

7.2.5 Simulation Results of a Pot Core Sensor

A pot core sensor is a modified version of a D-coils sensor and is developed by Messtechnik, University of Kassel (*Messtechnik*, KS). The aim of this design is to apply the ideas, obtained from the numerical modeling of the D-coils sensor and thus develop a new sensor as an alternative to the 4-coils sensor for the detection of longitudinal cracks. We have tested a number of different orientation of the coils of a pot core sensor by numerical modeling and have found the geometry shown in Fig. 7.27d as the best one.

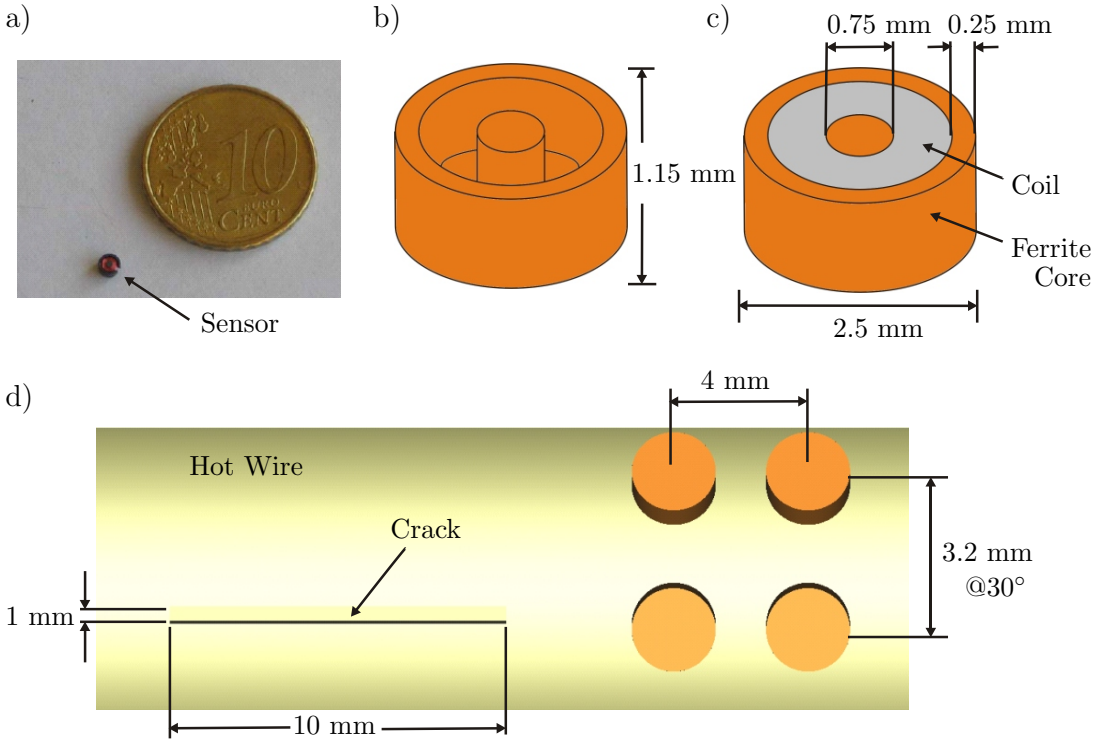

Figure 7.27: a) Photo of a pot core sensor, b) pot shaped ferrite core of the sensor, c) pot core with coil inside and d) top view of test setup using a pot core sensor.

7.2.5.1 Geometry of a Pot Core Sensor

The formation of a pot core sensor system is similar to a 4-coils sensor system. It also consists of four coils, where two of them operate as excitation coils and the other two as receiving coils. Each coil has its own pot formed ferrite core (see Fig. 7.27b), which operates as a magnetic shield from the neighboring coils and a guide for the magnetic flux towards the steel surface. 140 turns of copper wire is wound inside a ferrite core to form a coil, which has the height of 1.15 mm and the outer diameter of 2.5 mm (see Fig. 7.27c). To illustrate the size of a pot core, a 10 cent coin is shown by the side of a pot core in Fig. 7.27a. Twelve coils are positioned with an angular coil to coil distance of 30° to form a ring and two such rings are used in this sensor system - one for the excitation coils and the other one for the receiver coils.

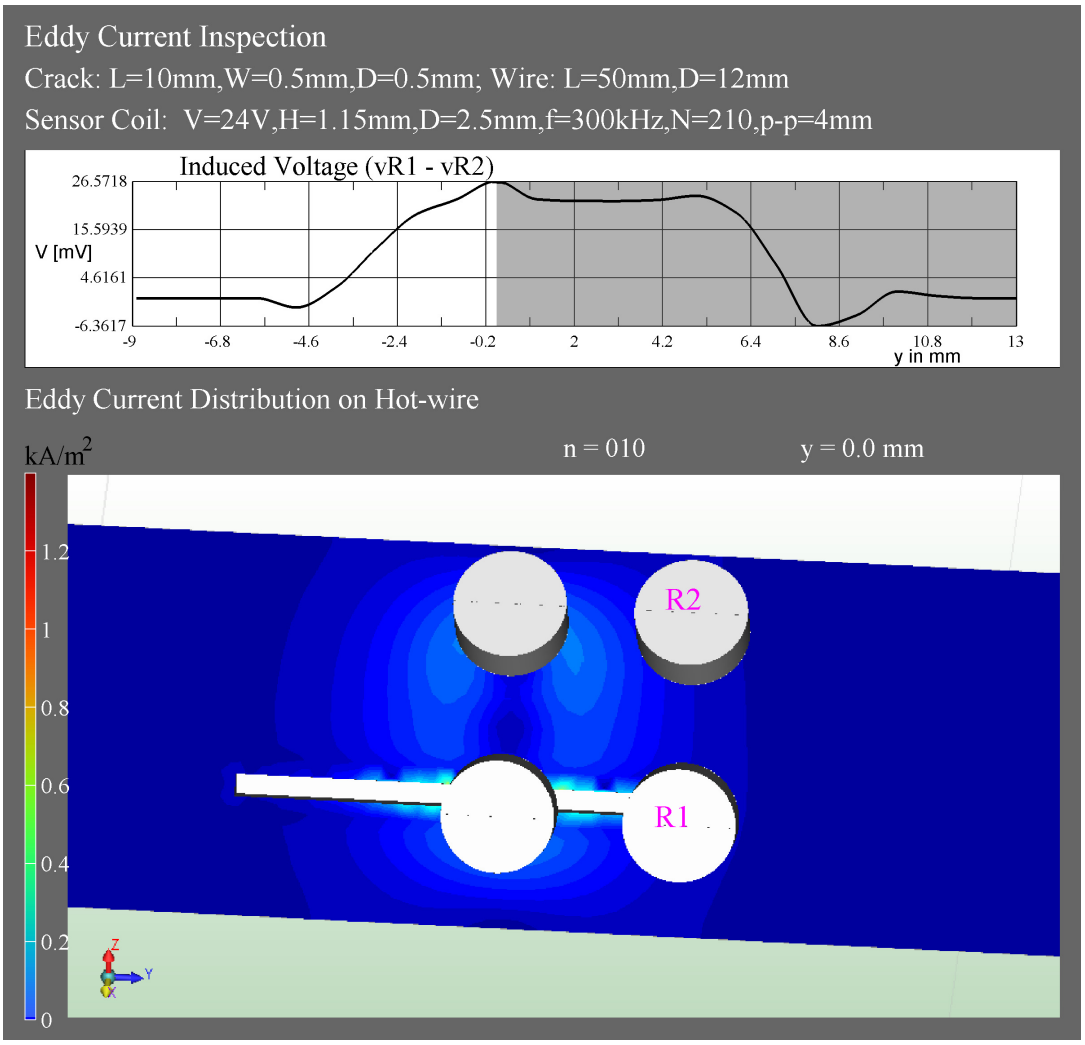

Figure 7.28: Hot wire testing using a pot core sensor; top: induced voltage in the receiving coils, bottom: eddy current distribution on the hot wire.

7.2.5.2 Numerical Technique to Simulate a Pot Core Sensor

A snapshot of the detection process using a pot core sensor is shown in Fig. 7.28. The detection process is simulated using the boundary element method (BEM). The size of the

crack is: length $l = 10$ mm, width $w = 1$ mm and depth $d = 1$ mm. An excitation frequency of $f = 300$ kHz is used and the eddy current distribution on the steel surface is displayed in the bottom of Fig. 7.28. We apply a current density $\underline{\mathbf{J}}_{\mathrm{e}}^{\mathrm{imp}}(\underline{\mathbf{R}}, \omega) = 1.19 \times 10^7$ A/m^2 in the excitation coil and the resulting induced electric voltages in the receiver coils vR1 and vR2 are recorded and the differential signal vR1−vR2 is plotted in Fig. 7.29.

7.2.5.3 Simulation Results and Performance Analysis of a Pot Core Sensor

Due to the pot formed ferrite core, this sensor system shows less sensitivity than a 4-coils sensor system. We conclude from Fig. 7.22 and Fig. 7.29 that a pot core sensor shows a peak of 26.34 mV at the presence of a crack whereas, a 4-coils sensor shows a 39.2 mV peak. However, the compactness of the pot core sensor is its major advantage over the other sensor systems. As a result, a higher number of coils can be positioned around the hot wire to cover the entire circumference. In snapshot Fig. 7.28 the coils are positioned at 30° angular distance and thus, an array of 12 coils are used for excitation or reception. On the other hand, in case of the previous point coil sensors, such as a 4-coils sensor or a 3-coils sensor we have used an angular displacement of 45° to position the coils, which means, only 8 coils can be positioned in an array. The use of higher number of elements in excitation

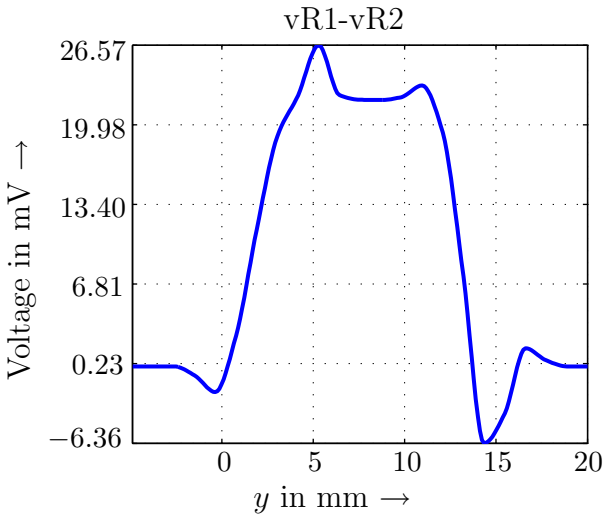

Figure 7.29: Induced voltages at a) receiver 1 (vR1) and b) receiver 2 (vR2) of a pot core sensor.

and reception array results less blind zones and ensures better detection and hence, a pot core sensor is also a good choice for hot wire steel inspection. According to the numerical results we conclude that a pot core sensor is also a suitable candidate for final design and therefore, such a sensor is also used in the combined EC sensor system.

7.3 Selection of Eddy Current Sensors for the Final Prototype

We have discussed different encircling coil and point coil sensors in the previous sections. The advantages and disadvantages of each of the developed sensors need to be considered in order to select suitable sensors for final prototype.

- **Encircling coil without ferrite core:**
  + Good performance for detecting transversal cracks
  − Poor detection of longitudinal cracks

- **Encircling coil with ferrite core:**
  + Modified version of an encircling coil without ferrite core
  + Very Good detection of transversal cracks
  − Poor performance in detecting longitudinal cracks

- **3-coils sensor:**
  + Designed to detect the longitudinal cracks
  − Problems exist due to blind zones and geometric difficulty

- **D-coils sensor:**
  − Poor detection of the cracks due to large size and orientations of the coils

- **4-coils sensor:**
  + Modified version of the 3-coils sensor
  + Offers the highest sensitivity
  + Very good detection of the longitudinal cracks

- **Pot core sensor:**
  + Modified version of the D-coils sensor
  + Due to very small size higher number of elements can be used in the array which ensures less blind zones
  + Good detection of the longitudinal cracks

The analysis of the modeled sensors, given above, shows that an encircling coil sensor with ferrite core is suitable for detecting the transversal cracks, whereas a 4-coils sensor and a pot core sensor shows good results in detecting longitudinal cracks. As a result, a mixed sensor system: an encircling coil and a 4-coils sensor or an encircling coil and a pot core sensor are the suitable options to fulfill our goal.

7.4 Velocity Analysis

The linear velocity of the hot wire influences magnetic flux distribution and thus causes change in the induced voltage in the sensor coils. The effect of velocity on the performance of the sensor system is discussed in this section. As mentioned before, the eddy current problem in case of a moving conductor is solved by determining the magnetic vector potential $\underline{\mathbf{A}}_{\mathrm{m}}(\underline{\mathbf{R}}, \omega)$ using Eq. (2.146). Here we simulate the hot wire inspection process with the help of the Linear Motion (LM) module of Opera-2d (*Opera*, 10.5) to determine the velocity effect. The LM module is a Transient Eddy Current Solver, extended to include the effects of motion. The simulated model has a rotational symmetry, where the motion is in z-direction. The output time points are selected first and at these time points, the transient value of the induced voltages are recorded. The applied voltage at the driving circuit of the excitation coils is $V = 1.4142$ V (rms). The construction of the simulated eddy current sensor is similar to the encircling coil sensor, described in Sec. 7.1.

7.4.1 Simulation Results for Different Velocities

The simulated crack has the length $l = 5$ mm and the depth $d = 0.5$ mm. At time $t = 0$, the crack lies between $z = 15$ mm and $z = 20$ mm zone of the steel wire (see Fig. 7.30a). The steel wire moves in the positive z-direction at a linear velocity $\underline{\mathbf{v}}_\mathrm{c}$. Fig. 7.30b shows the

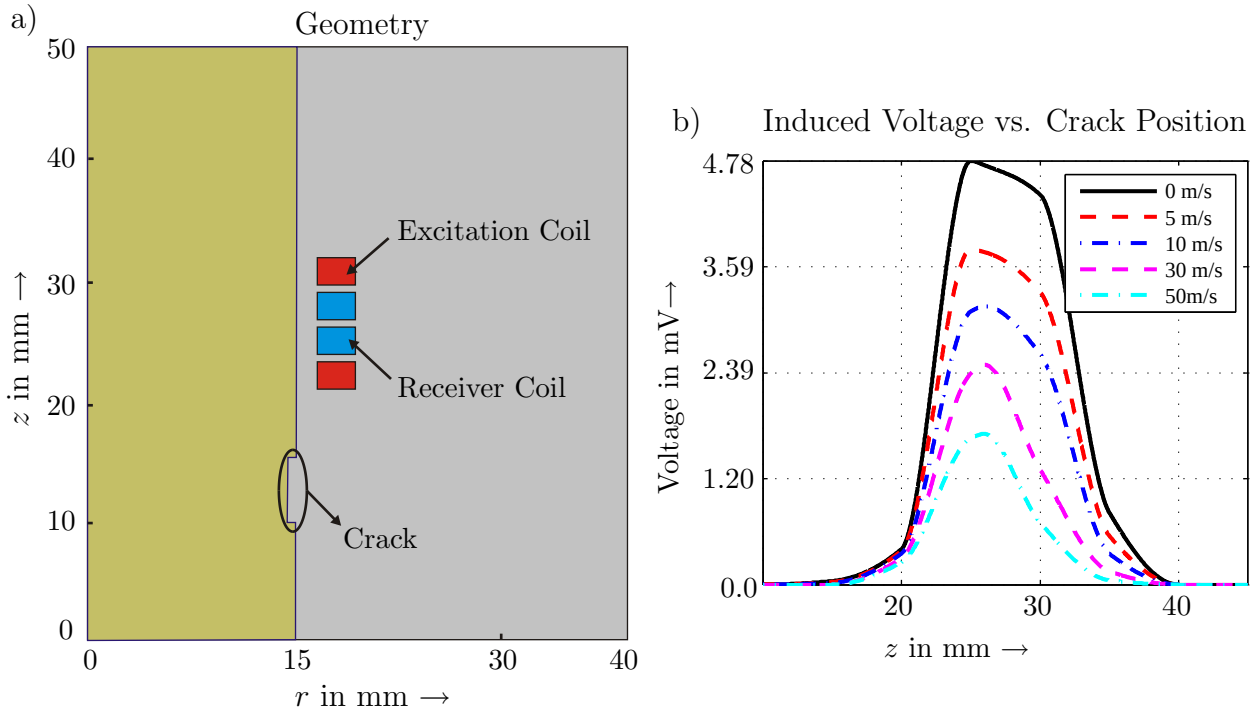

Figure 7.30: a) Geometry of the experimental setup for velocity analysis and b) induced electric voltages at different velocities: $\underline{\mathbf{v}}_\mathrm{c} = 0$ m/s (black), 5 m/s (red), 10 m/s (blue), 30 m/s (magenta) and 50 m/s (cyan).

comparison of the received voltages at the velocity of $\underline{\mathbf{v}}_\mathrm{c} = 5,\ 10,\ 20,\ 30,\ 50$ m/s of the hot wire. The effect of the increasing velocity is explained by recalling Eq. (2.146) as

$$\Delta\underline{\mathbf{A}}_\mathrm{m}(\underline{\mathbf{R}},\omega) + \mu\sigma_\mathrm{e}(\underline{\mathbf{R}})\left[\mathrm{j}\,\omega\ \underline{\mathbf{A}}_\mathrm{m}(\underline{\mathbf{R}},\omega) + \underline{\mathbf{v}}_\mathrm{c} \times \boldsymbol{\nabla}\times\underline{\mathbf{A}}_\mathrm{m}(\underline{\mathbf{R}},\omega) - \boldsymbol{\nabla}\Phi_\mathrm{e}(\underline{\mathbf{R}},\omega)\right] = -\mu\underline{\mathbf{J}}_\mathrm{e}^\mathrm{imp}(\underline{\mathbf{R}},\omega) \tag{7.5}$$

and the electric field strength $\underline{\mathbf{E}}(\underline{\mathbf{R}},\omega)$ is then computed from the magnetic vector potential $\underline{\mathbf{A}}_\mathrm{m}(\underline{\mathbf{R}},\omega)$ by

$$\underline{\mathbf{E}}(\underline{\mathbf{R}},\omega) = \mathrm{j}\,\omega\underline{\mathbf{A}}_\mathrm{m}(\underline{\mathbf{R}},\omega) + \underline{\mathbf{v}}_\mathrm{c} \times \boldsymbol{\nabla}\times\underline{\mathbf{A}}_\mathrm{m}(\underline{\mathbf{R}},\omega) - \boldsymbol{\nabla}\Phi_\mathrm{e}(\underline{\mathbf{R}},\omega)\,, \tag{7.6}$$

which is written in time-domain as

$$\frac{\partial\underline{\mathbf{E}}(\underline{\mathbf{R}},t)}{\partial t} = -\frac{\partial\underline{\mathbf{A}}_\mathrm{m}(\underline{\mathbf{R}},t)}{\partial t} + \underline{\mathbf{v}}_\mathrm{c}(\underline{\mathbf{R}},t) \times \boldsymbol{\nabla}\times\underline{\mathbf{A}}_\mathrm{m}(\underline{\mathbf{R}},t) - \boldsymbol{\nabla}\Phi_\mathrm{e}(\underline{\mathbf{R}},t)\,. \tag{7.7}$$

The addition of the velocity term $\underline{\mathbf{v}}_\mathrm{c}(\underline{\mathbf{R}},t) \times \boldsymbol{\nabla}\times\underline{\mathbf{A}}_\mathrm{m}(\underline{\mathbf{R}},t)$ causes a negative effect in the induced voltage which is shown by Eq. (7.7) mathematically and is also visible in Fig. 7.30b.

7.4.2 Validation of the Simulation Results

A validation of the velocity analysis is important to examine the results of the simulation. As no measurements have been performed with velocity, this validation has been done against

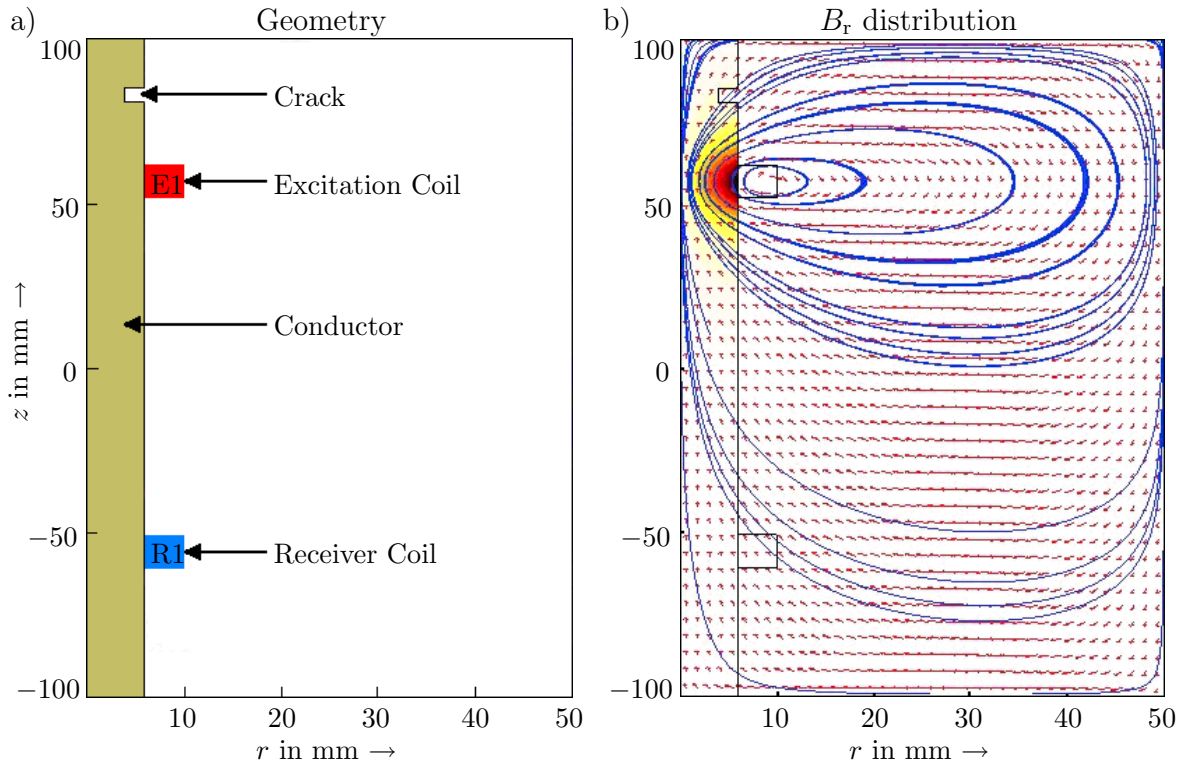

Figure 7.31: a) Geometry of the experimental setup for validation of the results and b) distribution of the radial component of the magnetic flux B_r.

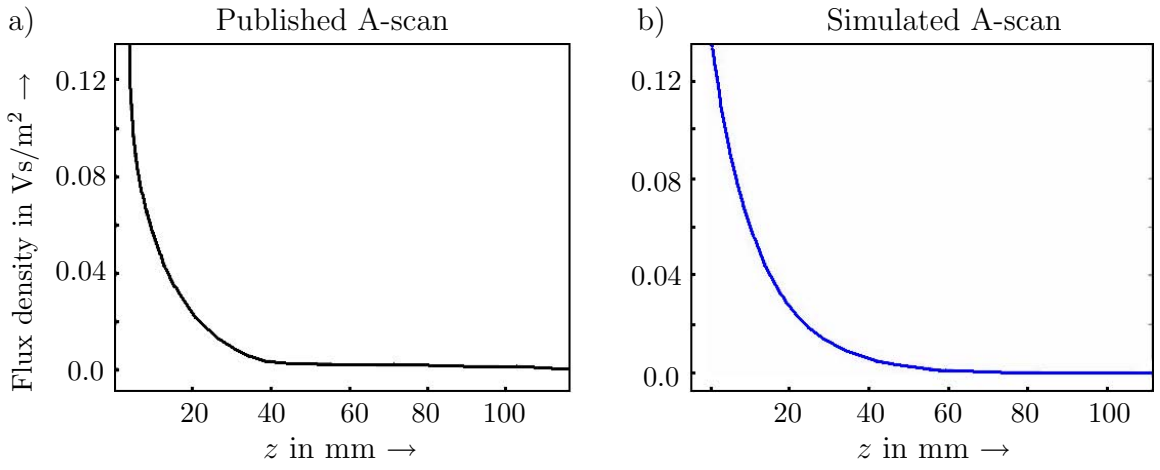

Figure 7.32: a) Published flux density and b) simulated flux density.

the results published by *Yu et al.* (1998). The geometry of the experimental setup is shown in Fig. 7.31a. On the left part is the conductor which has a crack on the top. The length of the crack is $l = 4$ mm and the depth $d = 2$ mm. The conductor is moving in the z-direction with the velocity of $v_c = 50$ m/s. There are two coils in this figure, mentioned as E1 and R1. Here E1 is the excitation coil and R1 is the receiving coil. The distribution of the radial component of the magnetic flux density B_r is shown in Fig. 7.31b. The flux density at the upper surface of the conductor is plotted as a function of distance in Fig. 7.32, where the flux density from the published paper (*Yu et al.*, 1998) is plotted on the left and the simulated result on the right (*Ebby*, 2007). The comparison shows that the simulated result is identical to the published one what proves the accuracy of velocity modeling.

Conclusions

The eddy current (EC) problem is modeled by solving the magnetic diffusion problem described by the magnetoquasistatic governing equation. A proper numerical method need to be chosen to solve the underlying differential as well as integral equation accurately. For the eddy current modeling we apply the finite integration technique (FIT), the finite element method (FEM) and the boundary element method (BEM). Two commercial software packages – Opera and Faraday based on FEM and BEM are used to model the problem. However, a specific software tool with built-in geometry is always the best option to solve a particular eddy current problem. The commercial tools have generalized structures and suffer from major drawbacks, such as, difficulty with choosing the type of excitation for the excitation coils, complex procedure for reading data from the output files and also very slow computation. As a solution to these problems a software tool named as MQSFIT, based on the finite integration technique (FIT), is developed for deep understanding of numerical approach and proper modeling of the eddy current problem. The results obtained from MQSFIT are compared with the measured A-scan and also validated against analytical results.

The reliability and accuracy of the numerical methods need to be determined before using them for sensor optimization and feedback modeling. This can be performed by validating the numerical results against the analytic one. As the first step for such a validation we have defined a typical eddy current problem and have discussed the analytical solution of this problem. In the second step, we have computed numerical solutions using FIT, FEM and BEM. A comparison of the results to the analytical results is performed and the advantages and disadvantages of each method are discussed to find a suitable one.

The modeling results play an important role in optimization and validation of eddy current sensors. Numerical modeling ensures deep physical understanding by analyzing the influence of different parameters and thus facilitates the development of EC sensors to meet the goals of INCOSTEEL project. The initial modeling, performed with a standard encircling coil, shows us the drawbacks of such a sensor and also the ways to modify it for better performance. The result is the encircling coil sensor with ferrite core, which offers better detection of transversal cracks. However, the simulation results show that this modification is not enough and the problem with a longitudinal crack cannot be solved. As an initial solution a 3-point sensor is proposed by Tecnatom, which obviously need to be modeled to validate the design. This opens the door for further modification and innovative ideas to develop new sensors to meet the goals. Based on the numerical computations we have developed, modified and optimized two encircling coils and four point coil sensors. The numerical techniques, modeling details, simulation results and performance analysis are discussed for each sensor type. The inspection techniques have been modeled and the results are shared with the other groups (measurement and testing). The simulated results are compared and validated against the measured results. At the end, the results obtained from different sensors have

been compared to choose optimum candidates to fulfill the goal of INCOSTEEL project.

Considering the pros and cons of different sensor systems, three of them have been selected for final prototypes. An encircling coil sensor with ferrite core is suitable for detecting the transversal cracks, whereas a 4-coils sensor and a pot core sensor show good results in case of detecting longitudinal cracks. As a result, a mixed sensor system: an encircling coil and a 4-coils sensor or an encircling coil and a pot core sensor are suggested. Both of the mixed sensor systems show good results in laboratory, as well as in rolling mill tests. The project results are accepted by the EU scientific commission, which brings up the successful conclusion of the INCOSTEEL project.

The results obtained from this thesis opens the door for future research. The computation time required for 3-D modeling is a serious issue which needs to be studied further. As for example, the developed MQSFIT tool is tested with a 2-D magnetoquasistatic problem with 250000 unknowns, which is solved in 25 minutes with an AMD X2 Processor (2x2.1 GHZ). The FEM based software package Opera is able to solve a problem with maximum 20000 unknowns because of memory allocation problem, where it requires 2 minutes with the same processor. Furthermore, the BEM based software tool Faraday 6.1 requires 2 hours to solve a 3-D magnetoquasistatic problem with 5000 unknowns, which need to be improved using a better technique.

As a solution to this problem the discontinuous Galerkin finite element (DGFEM) method (*Hesthaven & Warburton*, 2008) can be proposed. Although DGFEM is a state of art numerical method to solve a 3-D magnetoquasistatic problem with high speed and accuracy, the FIT based MQSFIT is a suitable option for solving 2-D problems for its simplicity and accuracy.

Bibliography

Abramowitz, M. and Stegun, I. A.: *Handbook of Mathematical Functions*. U.S. Goverment Printing Office, Washington, D.C., 1972. 79

Akcakoca, U.: *The Finite Element Method in Electromagnetics in Time and Frequency Domain*. Master Thesis, Computational Electronics and Photonics, University of Kassel, 2009. (in German) 58

Dodd, C. V. and Deeds, W. E.: Analytical Solutions to Eddy-Current Probe-Coil Problems. *Journal of Applied Physics*, Vol. 39, No. 6, pp. 2829-2838, 1968. 78

Ebby, W. T.: *Numerical Calculation of Eddy Current in Moving Conductors*. Master Thesis, Department of Electromagnetic Theory, University of Kassel, 2007. (in German) 112

Fachgebiet Messtechnik, University of Kassel, Wilhelmshöher Allee 71, 34121 Kassel, Germany (http://cms.uni-kassel.de/unicms/index.php?id=24447). 91, 107

Faraday, Version 6.1, 2005, Integrated Engineering Software, Manitoba, Canada (http://www.integratedsoft.com). 5, 85, 94, 97, 101, 104

Gibson, W. C.: *The Method of Moments in Electromagnetics*. Chapman & Hall/CRC, Boca Raton, FL 33487, USA, 2007. 63

Harrington, R. F.: *Field Computation by Moment Methods*. Wiley/IEEE Press, New York, USA, 1993. 63

Haus, H. A. and Melcher, J. R.: *Electromagnetic Fields and Energy*. Prentice Hall, Englewood Cliffs, NJ, (online version at MIT: http://web.mit.edu/6.013_book/www/), 1989. 20

Hesthaven, J. S. and Warburton, T.: *Nodal Discontinuous Galerkin Methods - Algorithms, Analysis, and Applications*. Springer, New York, USA, 2008. 114

Hower, G. L., Philipp, L. D., Abtahi, A. and Rupe, R. W.: Some Computational Considerations in Eddy-Current NDE. *Journal of Nondestructive Evaluation*, Vol. 4, No. 1, pp. 39-42, 1984. 77

Ida, N.: *Numerical Modeling for Electromagnetic Non-Destructive Evaluation*. Springer, New York, USA, 1995. 49, 55, 56

INCOSTEEL: *In-line Quality Control of Hot Wire steel - Towards Innovative Contactless Solutions and Data Fusion*, http://projects.tecnatom.es/incosteel/index.htm. 96

Jin, J.: *The Finite Element Method in Electromagnetics*. John Wiley & Sons, 2nd ed., USA, 2002. 47, 56, 61

Kost, A.: *Numerische Methoden in der Berechnung elektromagnetischer Felder*. Springer-Verlag, Berlin, 1994. (in German) 47

Langenberg, K.-J.: *Theory of Electromagnetic Waves*. Manuskript, Universität Kassel, Kassel, 2002. (in German) 7, 9, 15

Marklein, R.: *Numerical Methods for the Modeling of Acoustic, Electromagnetic, Elastic and Piezoelectric Wave Propagation Problems in the Time Domain Based on the Finite Integration Technique*. Shaker Verlag, Aachen, Germany, 1997. (in German) 25

Marklein, R.: The Finite Integration Technique as a General Tool to Compute Acoustic, Electromagnetic, Elastodynamic, and Coupled Wave Fields. In: *Review of Radio Science: 1999-2002 URSI*, pp. 201-244, W. R. Stone (ed.), IEEE Press/John Wiley and Sons, Piscataway/New York, 2002. 5, 25, 89

Marklein, R.: *Electromagnetic Field Theory I (EFT I)*, Manuscript, Department of Computational Electronics and Photonics, University of Kassel, Kassel, 2009. 10

Marklein, R.: *Electromagnetic Field Theory II (EFT II)*, Manuscript, Department of Computational Electronics and Photonics, University of Kassel, Kassel, 2009. 9

Meister, A.: *Numerik Linearer Gleichungssysteme*. 3rd ed., Vieweg & Sohn Verlag, Wiesbaden, 2008. (in German) 75, 98

Opera-2d, Version 10.5, 2005, Software for Electromagnetic Design, Vector Fields Limited, Oxford, England (http://www.vectorfields.com). 5, 85, 92, 110

Poljak, D. and Brebbia, C. A.: *Boundary Element Methods for Electrical Engineers*. WIT Press, Southampton, UK, 2005. 23, 63

Press, W. H., Teukolsky, S. A., Vetterling, W. T. and Flannery, B. P.: *Numerical Recipies: The Art of Scientific Computing*. 3rd ed., Cambridge University Press, NY, USA, 2007. 75, 89

Rahman, M.-U. and Marklein, R.: Advanced Techniques for Modelling and Detection of Cracks in Hot Wire Steel - Part 1. *Proceedings on the 9th European Conference on NDT (ECNDT)*, CD-ROM, Berlin, 2006. 91

Rahman, M.-U. and Marklein, R.: Advanced Techniques for Modelling and Detection of Cracks in Hot Wire Steel - Part 2. *International Magnetics Conference (INTERMAG)*, Madrid, 2008. 98

Rahman, M.-U. and Marklein, R.: Numerische Modellierung und Optimierung von Wirbelstromsensoren zur Online-Heißdrahtprüfung. *DGZfP-Jahrestagung 2009*, Münster, 2009. (in German) 92, 104

Ricken, W., Hartmann, K., Becker, W.-J., Perez, C. and Gonzalo, L.: Optimierung von Wirbelstromspulen. Verbesserte Fehlerdetektion bei der Heißdrahtprüfung. *Technisches Messen*, Vol. 75, No. 9, pp. 501-507, 2008. (in German) 98

Rothwell, E. J. and Cloud, M. J.: *Electromagnetics*. CRC Press, Boca Raton, FL, 2001. 7, 23

Rucker, W. M. and Richter, K. R.: A BEM Code for 3-D Eddy Current Calculations. *IEEE Transactions on Magnetics*, Vol. 26, No. 2, pp. 462-465, March 1990. 73

Rucker, W. M., Hoschek, R. and Richter, K. R.: Various BEM Formulations For Calculating Eddy Currents In Terms Of Field Variables. *IEEE Transactions on Magnetics*, Vol. 31, No. 3, pp. 1336-1341, May 1995. 71, 73

Shewchuk, J. R.: *An Introduction to the Conjugate Gradient Method Without the Agonizing Pain*. Ed. $1\frac{1}{4}$, School of Computer Science, Carnegie Mellon University, PA, 1994. 89

Sidenor Investigacin y Desarrollo, S.A., Barrio Ugarte S/N, Apartado de Correos 152 ES-48970 Basauri (Vizcaya), Spain (http://www.sidenor.com/). 87, 105

Silvester, P. P. and Ferrari, R. L.: *Finite Elements for Electrical Engineers*. Cambridge University Press, Cambridge, 1983. 51

Tai, C.-T.: *Generalized Vector and Dyadic Analysis*. Artech House, Norwood, MA, 1997. 23

Tecnatom, S.A., Avda. Montes de Oca, 1, 28709-San Sebastián de los Reyes, Madrid, Spain (http://www.tecnatom.es). 87, 95

TU Bergakademie Freiberg, Akademiestraße 6, 09596 Freiberg, Germany (http://tu-freiberg.de/index.en.html). 87, 98

Volakis, J. L., Chatterjee, A. and Kempel, L. C.: *Finite Element Method for Electromagnetics: Antennas, Microwave Circuits, and Scattering Applications*. IEEE Press, NY, 1998. 51

Weiland, T.: A Discretization Method for the Solution of Maxwell‘s Equations for Six-Component Fields. *Electronics and Communications*, Vol. 31, No. 3, pp. 116-120, 1977. 25

Yu, H., Shao, K. R., Lavers, J. D. and Shen, J.: A Mathematical Model for Computing Moving Conductor Problems. *IEEE Transactions on Magnetics*, Vol. 34, No. 5, pp. 2570-2572, September 1998. 112

Zhang, D.: Three-Dimensional Eddy Current Analysis by the Boundary Element Method. *IEEE Transactions on Magnetics*, Vol. 33, No. 2, pp. 1354-1357, March 1997. 63, 69

List of Publications

- M.-U. Rahman, R. Marklein: Time-Domain Techniques for Computation and Reconstruction of One-Dimensional Profiles, *Advances in Radio Science*, Vol. 3, pp. 219-225, 2005.

- M.-U. Rahman, R. Marklein: Advanced Techniques for Modelling and Detection of Cracks in Hot Wire Steel - Part 1. *Proceedings on the 9th European Conference on NDT (ECNDT)*, CD-ROM, Berlin, 2006.

- R. Marklein, J. Miao, M.-U. Rahman, K.-J. Langenberg: Inverse Scattering and Imaging in Non-Destructive Testing: Recent Applications and Advances. *Proceedings on the 9th European Conference on NDT (ECNDT)*, CD-ROM, Berlin, 2006.

- M.-U. Rahman, R. Marklein: Advanced Techniques for Modelling and Detection of Cracks in Hot Wire Steel - Part 2. *International Magnetics Conference (INTERMAG)*, Madrid, 2008.

- M.-U. Rahman, R. Marklein: Permittivity and Electric Conductivity Profile Reconstruction Technique in the Time Domain. Presented in: *XXIX General Assembly of the International Union of Radio Science (URSI)*, Chicago, USA, 2008.

- M.-U. Rahman, R. Marklein: Numerische Modellierung und Optimierung von Wirbelstromsensoren zur Online-Heißdrahtprüfung. *DGZfP-Jahrestagung 2009*, Münster, 2009. (in German)

- M.-U. Rahman, R. Marklein: Modellierung und Inversion von eindimensionalen Profilen im Zeitbereich: Theorie und Anwendung. *DGZfP-Jahrestagung 2009*, Münster, 2009. (in German)

- M.-U. Rahman, R. Marklein: Modeling and inversion of 1-D profiles in time-domain. *COMPEL: The International Journal for Computation and Mathematics in Electrical and Electronic Engineering*, Vol. 28, issue 5, pp. 1349-1361, 2009.

- R. Marklein, M.-U. Rahman, C. Bommaraju: Numerical Modeling and Inverse Profiling in Non-Destructive Testing. *IEEE Applied Electromagnetics Conference (AEMC)*, Kolkata, India, 2009.

- R. Marklein, M.-U. Rahman, J. Miao: Applied Modeling and Inverse Profiling in Electromagnetic Non-Destructive Evaluation. *International Symposium on Electromagnetic Theory (EMTS 2010)*, Berlin, Germany, 2010.

ISBN 978-3-86219-168-0